Mixture Preparation Behavior in Port Fuel Injected Spark Ignition Engines during Transient Operation

by

Jim S. Cowart

S.M. Mechanical Engineering
Massachusetts Institute of Technology, 1990

B.S. Mechanical Engineering
University of California, Davis, 1988

SUBMITTED TO THE DEPARTMENT OF MECHANICAL ENGINEERING IN PARTIAL FULLFILLMENT OF THE REQUIRMENTS FOR THE DEGREE OF

DOCTOR OF PHILOSOPHY
AT THE
MASSACHUSETTS INSTITUTE OF TECHNOLOGY

September 2000

Signature of Author:_____
Department of Mechanical Engineering
September 2000

Certified by:_____
Wai K. Cheng
Professor of Mechanical Engineering
Thesis Supervisor

Accepted by:_____
Ain A. Sonin
Chairman, Departmental Graduate Committee

Mixture Preparation Behavior in Port Fuel Injected Spark Ignition Engines during Transient Operation

by

Jim S. Cowart

Submitted to the Department of Mechanical Engineering
on August 18, 2000 in partial fulfillment of the requirements
for the Degree of Doctor of Philosophy

ABSTRACT

Improving Port Fuel Injected (PFI) Spark Ignition engine performance requires understanding the transport of port injected fuel into the combustion chamber. This thesis addresses the issue of actual fuel delivery to the engine's combustion chamber during transient operation. A fast in-cylinder diagnostic, the Fast Flame Ionization Detector was used to observe in-cylinder fuel behavior during throttle and cranking transients. Both empirical and physical models were applied to provide further insights into the generation of in-cylinder fuel vapor from port injected fuel.

Throttle transients of various throttle rates were investigated. Experiments (both with and without transient fueling compensation) showed that in-cylinder fuel behavior across all studied throttle rates very closely followed predictions by the conventional x-τ model calibrated with slow uncompensated throttle openings. Despite excellent model-data agreement, fuel control during fast transients was still not ideal. The source of poor fuel control was due to errors in transient air mass determination.

Engine cranking-startup experiments were performed to elucidate the effects of initial engine position, first and second cycle fueling, engine temperature and spark timing on fuel delivery to the combustion chamber and the associated IMEPg. The most important effect of the piston starting position is on the first firing cycle's engine speed, which influences the IMEPg through combustion phasing. Due to low speeds for the first cycle, combustion is usually too advanced with typical production engine ignition timing. For all three starting temperatures studied (0 C to 90 C), the threshold for firing is at an in-cylinder relative air-fuel ratio of 1.1. Increased fueling delivered diminishing in-cylinder fuel vapor levels. Open valve injection (OVI) is detrimental to the mixture preparation process because it causes mixture non-uniformity with high levels of engine-out hydrocarbons. For ambient and cold engine cranking OVI misfiring resulted.

A physically based crank mixture preparation model was developed to provide insights into the fuel vapor generation process. The modeling work showed for increasing engine temperatures an increased importance in individual fuel component distillation with a corresponding reduction in convective mass transfer. Additionally, the modeling work suggests that fuel pooling is occurring at rich fueling levels.

Thesis Supervisor: Wai Cheng
Title: Professor of Mechanical Engineering

Acknowledgements

I am sincerely grateful to many people. As I am a bit older than the 'average' graduate student, I have more people to thank, and thus I take the liberty of making this section longer than normal.

I am indebted to my PhD Thesis Advisor, Wai Cheng, for his outstanding technical direction. Wai was always available for consultation. He would immediately halt his work to assist in my project direction, data analysis and technical problems. Thankyou.

I am extremely grateful for John Heywood's support. John was my Master's Advisor, and continued as a key advisor to me both during my years at Ford Motor Company and as a member on my PhD committee. His sage advice both technical and personal will always be appreciated.

Thanks to Jim Keck. Professor Keck was my Master's Co-Advisor and an essential PhD Committee Member. I will forever acknowledge him as the source of my strong approach to physical analysis. I can correctly analyze problems now because of him.

I owe all of my Heat and Mass Transfer knowledge to Bora Mikic. Bora was a wonderful teacher and PhD Committee Member. Thankyou for all of your help and encouragement.

My final PhD Committee Member, Tom Kenney of Ford Motor Company, was crucial in keeping us all grounded to 'real' engineering. He has been a solid resource to me for over 12 years through both my S.M. and PhD efforts. I am grateful.

Eric Curtis of Ford Motor Company was an outstanding teacher in the art and science of modeling. I greatly appreciate time spent with him, both at Ford and on the telephone. His work was an inspiration for much of my modeling efforts.

Much of this work was funded by the Ford Motor Company. Rod Tabaczynski, Nizar Trigui, George Davis and Don Reeck were all great supports. Additional support for this project was provided by the MIT Engine and Fuels Consortium. Insights and direction from numerous consortium members was critical for my success.

I could not have selfishly pursued this further education without the incalculable support from my beautiful wife, Amy. She is my source of earthly light and best friend.

My parents, Jim and Ann Cowart, have always taught me that learning is life long. As I finish this PhD, I realize that I am just beginning to understand Mechanical Engineering. I will forever be a student. My love and passion of learning is from them. They are best friends and counselors. I could not have succeeded without them.

My other parents, Bill and Barb Wiersma have been a source of endless support as well. Their faith and love are amazing. Thankyou.

My sister Karen and brother-in-law, David are great friends and encouragers. Breaks from MIT to their home in Seattle and European 'Flats' were essential respites. Also, my nieces, Christina and Elizabeth, frequently remind me what life is all about.

My other siblings-in-law, Ryan and Janna Wiersma were wonderful friends during this pursuit. While far away, we were blessed to strengthen our relationships.

Our dearest friends, Jeff and Maria Harshe, Kurt and Tammy Amolsch, Phil and Carter Weeber were the greatest of encouragers. Additionally, Dave and Lisa Allen, Christopher Wenk, Justin

and Bernie Wu and Steve Melander are dear friends. I will always be grateful for their love and support.

I was blessed to be able to Consult with Litex Corporation and ADL-Combustion during the past two years. It was a pleasure to work for Jack Ekchian. Additionally, the time with Eric Balles, Bouke Nordzij, Peter Palmer, Pete Menard, J.R. Linna and Mark Sztenderowicz was more enjoyable than work. It was a great learning experience to pursue these efforts.

Once again, Karla Stryker has been a great friend and help over these years. It has been a joy to renew this friendship over the past 3 years. I trust it will continue.

The Sloan Lab would've been ineffective without Nancy Cook and Susan Lutin. They both were continuously pleasant, supportive and helpful in my academic endeavors.

My experimental work would not have been so smooth without the help of Brian Corkum. He is sorely missed in the Laboratory, both for his technical expertise and friendship. Additionally, Pete Menard, John Baron and Thane DeWitt were selfless in their assistance to my project. Thanks also to our Lab Manager, Victor Wong.

Leslie Regan for my 12 years affiliated with MIT has been a saint in the administrative beaurocracy of MIT. She shelters us from the hassles that would otherwise exist. Leslie truly deserves commendation for making the lives of many hundreds of Grad-Students (at one time – many thousands over the years!) easy, including mine.

My office mates have made the Lab feel a little like home. Matt Rublewski often provided for lively discussions. I relish those debates. Young-Chul has given me enlightening technical discusses that 'wet the appetite' for research. Thanks to Young-Chul for some FORTRAN properties' subroutines.

The qualifier experience was made manageable because of wonderful collaborations with James Moran, Micha Wiegel, Benoist Thirouard and Ertan Yilmaz.

Many Labmates over the past three years have brought joy and fun to the long hours at the Sloan Lab. Just mentioning them is not sufficient, but since I'm running out of room here goes: Carlos Herrera, Mark Dawson, Cornelius O'Sullivan, Connor McNally, Ertan Yilmaz, Brad VanDerWege, Benoist Thirouard, Robert Meyer, Chris O'Brien, Gary Landsberg, Brian Hallgren, Ioannis Kitsopanidis, Ferran Ayala, David Schmidt, Rik Waero, Martin Kosto, Rolf Karlsson, Dave Kayes and Brigitte Castaing – it was a pleasure to collaborate with her during the cranking experiments.

Finally my Grandmother Odie and Aunt Dot will forever bring me joy. My late Grandfather (and Grandmother) Heytens I owe my love of engines. I think of him often, and wish he could be with me today. My Uncle George, who gave me my first engine, is equally due the thanks for helping discover and encourage my passion.

Lastly, I Thank the Lord God Almighty. My Faith in God was the strength through so many days. I end with Proverbs 3:5, which brought me so much peace. "Trust in the Lord with all your heart, and lean not on your own understanding. In all your ways acknowledge Him, and he will make your path straight."

Jim S. Cowart, Cambridge, MA, August 18, 2000.

Table of Contents

List of Symbols and Abbreviations

A, B, C, D, E	Initial Engine Positions
ABC	After Bottom Center
ATC	After Top Center
A/F	Air-Fuel ratio
BCC	Bottom Center Compression
BDC	Bottom Dead Center
BTC	Before Top Center
C	Celsius
CA	Crank Angle
cadeg	crank angle degrees
CAP2	CAlifornia Phase II fuel
cf	coefficient of friction
CFI	Central Fuel Injection
C.I.	Confidence Interval
CO	Carbon Monoxide
CP	Constant Pressure
CVI	Closed Valve Injection
degC	degrees Celsius
DOHC	Dual OverHead Camshaft
ECT	Engine Coolant Temperature
EEC	Electronic Engine Controller
EGO	Exhaust Gas Oxygen sensor
EGR	Exhaust Gas Recirculation
EOHC	Engine Out HydroCarbons
EOI	End Of Injection
f	friction factor
F/A	Fuel-Air ratio
FFID	Fast Flame Ionization Detector
FID	Flame Ionization Detector
FPW	Fuel Pulse Width
HC	Hydrocarbons
IMEPg	Indicated Mean Effective Pressure (gross)
IVC	Inlet Valve Closing
IVO	Inlet Valve Opening
LIF	Laser Induced Fluorescence
m	mass, fuel vapor mass in cylinder
M	mass, liquid fuel mass in puddle
MAF	Mass Air Flow
MAFS	Mass Air Flow Sensor
MAP	Manifold Absolute Pressure
MBT	Maximum Brake Torque
MW	Molecular Weight
NOx	Oxides of Nitrogen
OVI	Open Valve Injection

PCV	Positive Crankcase Ventilation
PFI	Port Fuel Injection
p_i	intake manifold pressure
ppm	parts per million
ppmC1	parts per million – single carbon
R	Radius
R_{arc}	puddle arc radius
Re	Reynold's No.
rpm	engine speed – revolutions per second
Sc	Schmidt No.
Sh	Sherwood No.
SI	Spark Ignition
SMD	Sauter Mean Diameter
T	Temperature
TCC	Top Center Compression
TDC	Top Dead Center
TFC	Transient Fuel Compensation
UEGO	Universal Exhaust Gas Oxygen sensor
V_{FFID}	Voltage from FFID
$V_{manifold}$	intake manifold volume
W_a	Molecular Weight of air
W_f	Molecular Weight of fuel
W_r	Molecular Weight of residual
WOT	Wide Open Throttle
x	fraction of injected fuel into the puddle
$x_{i,f}$	liquid mole fraction of specie 'i'
$x_{i,g}$	vapor mole fraction of specie 'i'
x_r	residual mass fraction
y_f	mole fraction of fuel

ε	relative roughness
λ	relative air-fuel ratio
σ	standard deviation
τ	time constant

Chapter 1:
Introduction

1.1 Background and Motivation

One of the major challenges in optimizing port-fuel-injected (PFI) spark-ignition (SI) engine operation is the generation of fuel vapor out of liquid fuel. Beyond creating vapor out of liquid fuel, the fuel vapor must also appropriately mix with chemically correct proportions of air in order to achieve a combustible mixture. This area of engine research is commonly referred to as mixture preparation.

Several factors contribute to the complexity of the mixture preparation process. There are significant variations in operational conditions in conventional automotive engines. Engine coolant temperatures range from ambient conditions to over 100 C, with individual engine components experiencing even higher temperatures. Throughout these temperature variations engines are also required to change torque and power levels within fractions of a second based on driver demand. Wide variations in engine speeds are also necessary. Thus, the intake and combustion chamber systems in which a combustible mixture must be formed are constantly changing in state (temperatures and pressures) which directly affects the mixture preparation process.

Another important factor in the mixture preparation process is the multi-component nature of fuel. Conventional automotive SI gasolines are typically composed of many hundreds of hydrocarbon (HC) compounds from light HCs (C4-butane base) to heavy HCs (C10-decane base) with multiple chemical variations of each compound. The source of the crude oil and the specific refining processes can produce different fuel 'mixtures'. These HC fuel 'mixtures' are then varied regionally by oil companies throughout the year in order to ensure adequate engine performance during the different seasonal conditions. Each of these hundreds of species has unique physical properties, which additionally makes comprehension of real engine mixture preparation a daunting task.

The nature of PFI SI engine design strongly affects mixture preparation processes [1.1, 1.2]. In PFI engines, liquid fuel is injected into the intake port towards the intake valve. It is generally accepted that most of the injected fuel impacts either the intake valve head or the lower intake port to form a liquid film. Fuel evaporation and boiling processes can then take place at the liquid film on the port surfaces; direct evaporation from the droplets is relatively minor. Thus efforts to create a fine quality spray often show no performance improvement over low cost injectors (relatively large droplets) in PFI engines. Even with fine sprays, their initial momentum carries the injected droplets to intake wall surfaces. With most of the injected fuel impacting intake system surfaces, the liquid fuel effect has once again become dominant.

After fuel injection is complete, depending on the intake port and valve temperatures, some of the lighter fuel components may have boiled off creating some fuel vapor in the intake port. However, a significant portion of the fuel still resides as liquid on the intake port surface until the vigorous convective action of the intake stroke enhances fuel mass transfer into the engine's combustion chamber. Yet, even after the intake valve is closed for the current cycle, significant amounts of residual fuel still remains in the intake port, and contributes to the mixture preparation process of the next cycle. The residual intake port fuel levels have been seen to be strong function of fuel type and engine operating conditions. It is this variable residual intake port fuel behavior from cycle to cycle that makes the mixture preparation process challenging.

A further complication results during engine transients (load and thermal). In these situations, residual intake port fuel levels change. Under certain engine transients (e.g. cranking and throttle opening) the residual intake port fuel mass increases, while under other transients (e.g. engine turned off or throttle closings) the residual fuel mass can decrease. Thus this residual port fuel can trap or release fuel mass to the combustion chamber beyond what was injected on a given engine cycle. In practice, this effect again makes precise fuel control difficult to achieve.

Because of the above complexity, fuel-air management in the powertrain development process is strongly empirically based. Engine calibration development is currently as much art as science. Successful engine calibrators, who set up the fuel control algorithms in production engine controllers, often must 'sense' if injected fuel is delayed upon entering the combustion chamber. If they are correct, additional commanded injected fuel is necessary in order to obtain an appropriate combustible mixture inside the engine. If they are wrong, often engine stumbles/stalls and high emission rates result.

One additional note on terminology is necessary. Residual intake port fuel is more commonly referred to as a 'puddle' of fuel [1.3]. This is an idealization. In reality, a single fuel puddle is unlikely. Visual observations of intake port fuel behavior indicate that residual port fuel can be widely distributed around the intake port region and is not necessarily a well-defined puddle. In the following, the term 'puddle' will be frequently used for the sake of semantic brevity. In all of the following discussions of actual engine behavior, 'puddle' will more precisely refer to residual intake port fuel mass.

1.2 Objectives

In light of the above mentioned empirical nature of engine fuel control, this work seeks to develop an improved quantitative physical description relating the preparation of a combustible charge to the injected fuel during engine transients. A key tool for achieving this objective is the cycle-resolved measurement of the in-cylinder (combustion chamber) fuel vapor mass levels. Physically based models that connect this data to the injected fuel levels will be used to enhance understanding of the mixture preparation process.

Specifically, two topics in transient engine operation were chosen for this study: throttle transients and cranking transients.

Within the area of throttle transients, the following broad objectives were laid forth:

- to establish the injected fuel mass disposition using in-cylinder Fast Flame Ionization Detector (FFID) measurements
- to characterize the port puddle adjustment in throttle transients
- to recognize key parameters in the process
- to improve Transient Fuel Control (TFC)

Within the area of cranking transients, the following broad objectives were laid forth:

- to characterize in-cylinder fuel behavior during engine cranking/starting as a function of initial starting position, crank rpm, Engine Coolant Temperature (ECT), fueling and ignition behavior
- to develop a physically based model to describe the first engine cycle mixture preparation behavior
- to improve practical engine cranking processes

1.3 Thesis Framework

This thesis comprises two main sections (of multiple chapters each): the throttle transient work, and the cranking transient work. Each section will contain an introductory chapter that includes a discussion of the current state of research on the topic, and a description of the current industry practices towards controlling the specific transient engine operation. Each introductory section will then describe issues and motivations surrounding that topic.

Following each introductory chapter will be a chapter of experimental results, interpretation and discussion. A separate chapter for the first cycle of crank modeling work will follow the cranking experimental data chapter.

Finally, a comprehensive Conclusion chapter will attempt to summarize the significant results from this work.

Chapter 1 References:

[1.1] Shin, Y., Min, K. and Cheng, W.K., "Visualization of Mixture Preparation in a Port Fuel Injection Engine during Engine Warm-up", SAE#952481, 1995.

[1.2] Shin, Y., Cheng, W.K. and Heywood, J.B.,"Liquid Gasoline Behavior in the Engine Cylinder of a SI Engine", SAE#941872, 1994.

[1.3] Aquino, C.F., "Transient A/F Control Characteristics of the 5 Liter Central Fuel Injection Engine", SAE#810494, 1981.

(This page was intentionally left blank)

Chapter 2:
Experimental Apparatus and Procedures

2.1 Experimental Apparatus

2.1.1 Engine-dynamometer

The engine used in this study was a Ford 4-cylinder (I4) 2.0L Zetec DOHC (16-valve), which has a 9.6 compression ratio, 84.8 mm bore, 88 mm stroke, and was equipped with PFI. This engine was connected to a Froude Consine AG80 eddy-current dynamometer with a Digalog (1022A) controller on a test bed. The engine used its production starter motor and battery for cranking/startup, since this dynamometer is of the absorbing only type. Once the engine was running, the engine's alternator then charged the battery. The dynamometer rotor inertia is ~23% that of the engine flywheel; therefore the crank-start process is not materially different from an actual engine with the transmission disengaged.

The engine was installed on the test bed with most of its production vehicle hardware intact with the following exceptions. The engine's front-end accessories were removed (A/C compressor and power steering pump) except for the alternator. The EGR valve was also removed. The lack of an EGR valve and EGR flow was not considered important for the start-up experiments since EGR is not used in this case. For the throttle transient experiments, EGR was not used due to FFID calibration complexity. Finally, the thermostat was also removed for the cranking experiments, to allow for maximum cooling rates when the engine was shut down.

The engine control was via a production EEC (Electronic Engine Controller) unit with a switching-type Exhaust Gas Oxygen (EGO) sensor, except when cylinder #4 was

controlled by a PC based system (described below). Production vehicle calibration was used for fuel metering. The strategy provided for nominal steady-state stoichiometric operation over most speeds and loads with the exception of cold start and Wide-Open-Throttle (WOT) operations at which excess fuel was injected. The spark control (firing order 1-3-4-2) was calibrated for MBT operation over most of the operating range except at heavy load conditions where spark retard was used for knock control.

The engine possesses a return type fuel system with a fuel pressure regulator that keeps the pressure difference across the PFI fuel injector at approximately 267 kPa (40 psi). A Bosch fuel-pump and accumulator assembly was used in place of the production Ford (in-tank) fuel pump. An evaluation was performed to ensure that the fuel pressure regulator could respond quickly to the fast throttle openings. California Phase II (CAP2) summer reformulated fuel was used throughout the experiments. Fuel properties are located in the crank modeling section (Chapter 7 – Figure 7.1).

The engine cooling system has multiple cooling paths depending on the testing requirements. One option closely simulates an actual vehicle so as to represent production vehicle warm-up characteristics. Included in this cooling path are the vehicle's radiator, heater core, bypass line and thermostat. The other cooling option uses an external heat exchanger with plant water to cool the engine's coolant. The hoses to/from the radiator were modified with 3-way valves to provide a means to divert the coolant to the external heat exchanger if desired. An external water pump was included in the later circuit such that engine coolant flow could be generated without the engine running.

2.1.2 PC Controller for fuel and spark

Two Cyber Research DAS1202 A/D I/O boards installed in a 486-based PC were used for fuel and ignition control for cylinder #4 when specialized operation was required (uncompensated throttle transients and crank). Numerous inputs to the A/D boards were used, including two BEI shaft encoders. A BEI H25 incremental optical encoder with BDC pulse and 360° resolution/revolution was connected to the crankshaft. Another BEI absolute shaft encoder with a resolution of 256 bits/revolution was applied to the camshaft (for the cranking experiments). Engine operational variables, engine rpm and MAP, were also input to the A/D boards as variable voltages from sensors. These voltages were then converted to physical units in the PC for calculation of injected fuel mass. Fuel and ignition controls were accomplished through a 'C' program that would interface with the A/D boards. See Appendix A for an example of the 'C' code for fuel and spark control operation.

The second A/D board was primarily used for timing purposes. An internal 10 μsec clock was used for controlling the duration of FPW. Additionally, a counter of crank angles triggered from a BCC pulse (Bottom Center Compression-signal conditioned from the crankshaft encoder's BDC signals to eliminate the bottom center exhaust pulse) allowed for controlling fuel injection timing and spark timing during non-cranking engine operation. The absolute shaft encoder was always used for the first two or three engine cycles during crank.

2.1.3 Diagnostics

2.1.3.1 FFID and Probe

A Fast response Flame Ionization Detector (FFID) manufactured by Cambustion (HFR 400) was used to measure both in-cylinder and exhaust hydrocarbon (HC) mole fractions. A Flame Ionization Detector (FID) is basically a carbon counter. A gaseous sample

containing hydrocarbons (HCs) that is introduced to the flame chamber (hydrogen-air flame) of a FID produces ions in proportion to the amount of carbon atoms burned [2.1]. These HC based ions are then collected by an electrode negatively biased at ~200 V with respect to the burner. The ion current is converted to an output voltage. Thus the FFID output is proportional to both sample mass flow rate and HC concentration. The FFID has a time response on the order of 1 msec. For a detailed description of the FFID and its operational characteristics refer to reference [2.2].

The in-cylinder FFID probe was approximately 7 cm long. It was placed in the back end of the engine in cylinder #4 (see **Figure 1**), and protruded into the combustion chamber 2 mm in order to draw in combustion chamber gases representative of the bulk charge. The sample tube's inner diameter was 0.2032 mm (0.008"). This was surrounded by a ceramic tube and encased by an outside stainless steel tube (O.D. 2.11 mm or 0.083"). Both heated and unheated versions were used. For most of the data analysis, this point measurement is assumed to represent the bulk in-cylinder fuel vapor behavior. During cranking, due to the relatively slow cycle times, the FFID signal was used to give qualitative indications of in-cylinder air-fuel inhomogeneity.

The in-cylinder FFID was operated at flame temperatures in the range of 300-350° C (this was controlled by adjusting the hydrogen and air feed pressures to the FID). Atmospheric CP chamber pressure was found best suited to all of the in-cylinder experiments. FID chamber vacuum was approximately 75 mmHg. Bench tests with the FFID and probe connected to a sample test chamber flowing span gas were conducted to ensure that a constant mass flow rate, and thus constant FFID output voltage were achieved despite variable span gas pressures.

The exhaust FFID probe was approximately 20 cm long and placed 5 cm from the exhaust valves in the exhaust port. It used an internal sample tube of I.D. 0.66 mm (0.026"). The FFID's CP chamber was operated at ~75 mmHg vacuum, with the FID

chamber ~75 mmHg below the CP chamber. Calibration span gas with 1500 ppmC3 = 4500 ppmC1 was used.

2.1.3.2 UEGO

A Horiba MEXA-110λ AFR analyzer was used for exhaust gas A/F ratio analysis. This Universal Exhaust Gas Oxygen (UEGO) sensor was placed in cylinder #4's isolated exhaust runner approximately 10 cm from the exhaust valves. The accuracy of this UEGO is listed at +/- 1% at λ=1. Various studies have characterized the UEGO's time response from 100 msec to 300 msec. From the author's discussions with Horiba personnel, at best they advertise a 100 msec response. In the following Chapter 4, in this application, a time response of ~200 msec was observed. Very little detailed operation information is available on UEGOs. One published study [2.3] provides some insights; however, it is far from complete.

2.1.3.3 MAP sensor

A Data Instruments Model SA 25 pressure transducer was used in the intake manifold plenum of the engine. This transducer has a range of 0-25psia, and a fast response (bandwidth = 80 Hz). The transducer was bench calibrated (statically) using an OMEGA PX605 vacuum transducer with a DP205-E pressure gauge (see reference [2.4] for response details).

2.1.3.4 Fuel Injector #4

The production Ford fuel injector was used (21 LB/hr, 9.55 kg/hr max flow). This conventional pintle type fuel injector has a splitter cap on its tip to direct fuel into both intake ports in each cylinder. The fuel injector in port/cylinder #4 was graviametrically calibrated by weighing the injected fuel collected in an ice trap over a large number of counted cycles.

2.1.3.5 In-cylinder Pressure

In-cylinder pressure measurements were obtained with a Kistler 6123 piezoelectric transducer coupled to a Charge Amplifier. The transducer gain was bench statically calibrated. Absolute reference was obtained by setting the pressure to the intake manifold pressure at BCC of each engine cycle. (A 30 cadeg average of MAP around BCC was used to reduce possible electrical noise). The transducer surface exposed to the combustion chamber was not coated to reduce thermal shock. As a result, IMEPg levels may be slightly underpredicted.

2.1.4 Throttle Controller

A Pacific Scientific SinMax 1.8° stepper motor with a 5230 indexer/driver was connected via a throttle cable to the engine's throttle body. It takes upwards of 170 steps to move the throttle from fully closed to fully open (WOT). A 486-based PC using a Cyber Research DAS1602 A/D board controlled the driver. At its maximum speed, the throttle controller could open the engine's throttle at 1500rpm in approximately 3 engine cycles (about ¼ second). This 'fast' throttle opening is typical of aggressive accelerations, however even faster throttle 'stomps' can be observed in practice. See reference [2.4] for detailed throttle response information.

2.1.5 Data Acquisition

For the throttle transient work, a 4-channel Global Lab system that output binary files was used. Further data analysis was performed using custom developed Fortran based codes. For the Cranking experiments, a 16-channel National Instruments LabView system was used. Files were output as ASCII files, and then analyzed via Fortran based programs.

2.2 Experiments and Calibration

2.2.1 General FFID Behavior in the Engine Application

An essential quantity to measure in the study of mixture preparation is the air-fuel (A/F) or fuel-air (F/A) ratio of the charge mixture in the combustion chamber. This information is contained in the FFID signal. It should be noted that because of the transport time in the FFID sampling system, there is a delay in the FFID signal responding to the HC concentration changes at the sampling inlet. In the subsequent discussion and in all the data presented in this paper, this delay has been taken out in the data processing.

In each cycle, the FFID signal rises to a plateau level as fresh charge is inducted and falls rapidly to zero when the flame arrives at the sampling inlet. The plateau value represents the HC level of the charge (assuming that the charge is uniform [2.5]), and hence is related to the vaporous fuel mass in the cylinder in the following manner.

Since the FFID measures a sample's HC mole fraction, the output voltage V_{FFID} is a function of the charge fuel/air ratio (F/A) and residual gas mass fraction (x_r). The assumption that x_r is only a function of the intake pressure p_i[1], whence

$$V_{FFID} = f_n(F/A, x_r(p_i)) \tag{2.1}$$

It can be shown that to a good approximation, the RHS (Right Hand Side) of Eq.(2.1) may further be factored as

$$V_{FFID} = F/A\ \alpha(x_r(p_i)) \tag{2.2}$$

where the proportional 'constant' α is only a function of the intake pressure.

[1] In general, x_r is also a function of F/A and combustion phasing. Steady state measurements have shown that these dependencies are weak [2.5].

This approximation is reasonable based on the following analysis. For a unit mass of charge with fuel to air ratio F/A, and with residual mass fraction of x_r, if W_a, W_f and W_r are the molecular weights of air, fuel and residual, the mole fraction of fuel y_f is:

$$y_f = \frac{\dfrac{(1 - x_r)\,F/A}{(1 + F/A)W_f}}{\dfrac{(1 - x_r)}{(1 + F/A)W_a} + \dfrac{(1 - x_r)\,F/A}{(1 + F/A)W_f} + \dfrac{x_r}{W_r}} \qquad (2.3)$$

Ratios of y_f / (F/A) are plotted as a function of x_r in **Figure 2.2** for A/F values of 10,12,14 and 16. To a good approximation (within 2% error), the ratios are independent of F/A and are only a function of x_r; whence the output of the FFID may be factored in the manner of Eq.(2.2).

The procedure was to calibrate Eq.(2.2) at steady state conditions under stoichiometric F/A at different values of p_i so that $\alpha(p_i)$ could be tabulated. Then for the measurements during the transient, the intake pressure for the cycle was determined from a 30° CA averaged value centered at BDC compression. This value was used with the $\alpha(p_i)$ calibration to determine the F/A ratio from Eq.(2.2). To correct for day-to-day drift in the calibration (primarily caused by slight variability in the FFID flame temperature), steady state data before and after the throttle step were used to rescale the look-up table in each throttle transient run.

The fuel mass in the charge per cycle was calculated from the F/A measured by the FFID and the charge air mass. To obtain the latter, the steady-state volumetric efficiencies of the engine were measured at various values of p_i at the selected engine speeds. These values were assumed to be applicable to each cycle during the transient if the instantaneous p_i value for the cycle was used.

2.2.2 Throttle Transient Details

2.2.2.1 Experimental Operating Conditions

For the throttle transient experiments, the engine was operated primarily at 1500 rpm with only a maximum variation of +/- 2% during the transients. Below this speed, dynamometer speed control was poor during a throttle transient. Some transient data was taken at 2000 rpm, but this was the upper limit. Above this speed, the FFID response time relative to cycle times became to great, and the FFID in-cylinder signal did not have adequate time to plateau. The lowest engine load used was 0.4 bar intake pressure. This intake pressure would roughly correspond to an engine-transmission combination operating at idle in drive. At intake pressures below 0.4 bar, the FFID signal would demonstrate erratic behavior – a clear plateau was not evident. The throttle was then jumped/ramped to approximately 0.9 bar intake pressure for most of the throttle transients. This represents an aggressive acceleration. WOT was not chosen as the final high load value due to WOT enrichment (λ~0.9) being applied by the Ford EEC above 0.95 bar loads. Some throttle transients that jumped from 0.4 to 0.65 and from 0.7 to 0.95 were performed to test less severe transient behavior.

The compensated throttle transients were performed with the production Ford EEC (Electronic Engine Controller). Throttle openings were initiated by the PC controlled Throttle controller. The initiation of the transient was not timed to any specific engine event. This was not a factor for slow throttle openings due to the slow ramp rate relative to cycle times. For fast throttle openings, various cycle positions at which the transient began were evaluated. No noticeable effect in initiation position was observed.

The uncompensated throttle transients were performed with the PC-based fuel controller. A speed-density type system was employed, using the MAP sensor. The ideal gas law, coupled with a volumetric efficiency term was used in the calculation of fuel mass (always based on stoichiometric fueling relative to MAP). Steady-state loads were run at

which the volumetric efficiency was determined based upon UEGO feedback. This volumetric efficiency map was then placed in the 'C' code prior to the experimental uncompensated throttle transients. Thus this closed-loop controller would always inject a stoichiometric amount of fuel based on the current MAP reading. No additional fuel was applied during the throttle transient as was the case with the Ford EEC.

For most of the data, the engine was operated at fully stabilized temperatures in a laboratory environment of ~22° C +/- 2° C. Engine-out coolant was maintained at ~90° C +/- 2° C. Limited data was taken at a stabilized coolant temperature of 22° C. In this case, a continual fresh supply of cool plant water was applied to the engine's water pump inlet. Only a few results from these tests will be presented.

2.2.2.2 Calibration Specific Details

As mentioned in 2.2.1, the FFID calibration function $\alpha(p_i)$ was determined at steady-state conditions and applied during the transient. Figure 2.3 shows the results of a calibration load sweep. Plotted on the right axis is the FFID plateau voltage at various engine loads running at stoichiometric fueling conditions. The FFID voltage at a given load is the average from 125 cycles. It can be seen that a positive linear correlation exists between intake pressure and FFID voltage (or $\alpha(p_i, \lambda=1)$). Voltage is seen to increase with load (at constant $\lambda=1$) due to the decreasing presence of residual gas, thus raising the effective overall concentration of fuel relative to the total in-cylinder charge. Ford Motor Company [2.5] residual gas fraction data from the same engine at similar operating conditions is plotted on the left axis. Estimates of residual gas fraction from the solution of Eq. 2.3 are also shown plotted on the left axis. The agreement is excellent.

Due to slow FFID drifts (mainly from slight flame temperature drifts on the scale of minutes), and in order to obtain very accurate in-cylinder data during a throttle transient, a light-load calibration file was taken prior to each throttle transient. Additionally, immediately after each throttle transient another high-load calibration file was taken.

These two points allowed the generation of a calibration curve as in **Figure 2.3**. Then for each engine cycle before, during and after the transient, the calibration $\alpha(p_i)$ was applied to determine the in-cylinder F/A ratio.

2.2.3 Cranking Transient Details

2.2.3.1 Experimental Operating Conditions

The effects of initial engine position, fueling and temperature on cranking/start-up performance were evaluated. For most of the experiments the 1st cycle FPW was delivered shortly after the start of engine rotation (~28°). This is representative of production engines, in which fuel is injected shortly after cranking begins in order to achieve fast starting performance. In all cases the 2nd cycle FPW was delivered around BC of the exhaust stroke, also a common production fuel injection location shortly before the intake valve opens (once fuel synchronization occurs based upon receipt of camshaft signal – generally takes numerous cycles after start to sync-up).

Experiments were performed at three engine temperatures. Hot starting experiments were done at an engine coolant temperature of 90° C +/- 2° C. After each start the engine was run for five minutes. Then injector #4 was disabled, and cylinder #4 was motored for ten seconds before shutting the engine down. This was done to ensure that the intake port was fully drained of fuel. Experiments were performed to evaluate how quickly, the port drained. It was on the order of a couple engine cycles, thus a normal shutdown would've accomplished the same objective.

Ambient starting experiments were performed at 20° C +/- 2° C. Cold starting experiments were performed at 0° C +/- 2° C. For ambient and cold starting experiments, the engine was warmed-up until the coolant temperature stabilized at 80° C. After shut-down the coolant was cooled via the external heat exchanger for one hour. Then a large fan was blown across the engine during the next hour with ambient laboratory air. At this

point the engine temperatures were all at ambient. This equality of engine temperature was confirmed in previous experiments with an extensively instrumented (thermocouple) engine.

2.2.3.2 Calibration Specific Details

Immediately after each engine start, as soon as the intake pressure was pumped down to its stabilized light-load (~0.4 bar pi) and high idle speed (~1200 rpm), a light-load calibration file was taken. The throttle was then opened to approximately 0.9 bar p_i, and a high-load calibration file was taken. Similarly to the throttle transient work, $\alpha(p_i)$ was determined and applied to the second and following engine cycles. This assumes that a stabilized level of residual gas fraction is present.

The first cycle is a bit more complicated. Since a previous combustion cycle is not present, a burned gas residual mass is not present. Rather an air residual amount is contained in the combustion chamber before the first cycle's induction event. This air residual is a result of the engine spinning down when shut off. The residual port fuel is pumped out to the exhaust in a few cycles, and intake system air during the spin down is retained in the cylinder for the next startup. Thus the calibration curve (linear line) for the first cycle is modified assuming extra air exists in the cylinder, thus diluting the fuel further. The modification entails scaling the calibration (representing a HC concentration with residual present) by the product $1+x_r$(0.9bar p_i, ~200rpm). The residual gas fraction x_r(0.9bar p_i, ~200rpm) is estimated by extrapolation of data in reference [2.5] to low engine speeds giving a value of approximately 6%. This new α_{1st} (p_i) is then slightly higher than the stabilized $\alpha(p_i)$, thus effectively requiring a higher FFID signal to achieve a comparable F/A ratio due to the extra air.

Chapter 2 References

[2.1] Heywood, J.B., Internal Combustion Engine Fundamentals, McGraw-Hill, 1988.

[2.2] Cheng, W. K., Summers, T. and Collings, N., "The Fast-Response Flame Ionization Detector", Prog. in Energy and Combustion Science, 24, pg. 89-124, 1998.

[2.3] Yamada, T., Hayakawa, N., Kami, Y. and Kawai, T., "Universal Air-Fuel Ratio Heated Exhaust Gas Oxygen Sensor and Further Applications", SAE#920234, 1992.

[2.4] Tseng, T.C., An Adaptive Approach to Air/Fuel Ratio Control for SI Engines, PhD Thesis, MIT, 1997.

[2.5] Miller, R., Russ, S., Weaver, C., Kaiser, E., Newman, C., Davis, G. and Lavioe, G., "Comparison of Analytically and Experimentally Obtained Residual Fractions and NOx Emissions in SI Engines", SAE#982562, 1998.

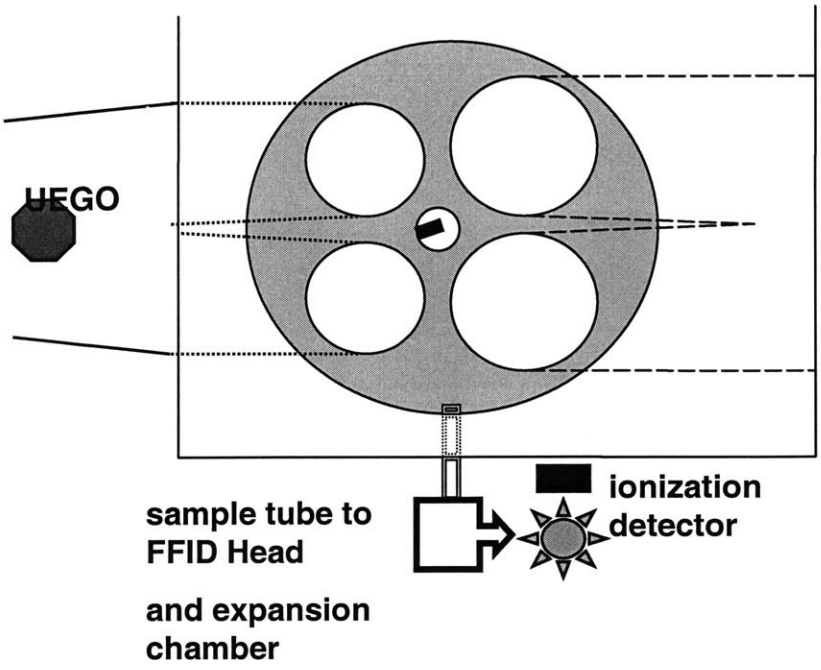

Figure 2.1: In-cylinder probe location at the back end of the engine in cylinder#4 exhaust port is to the left, intake port to the right, FFID located at the bottom

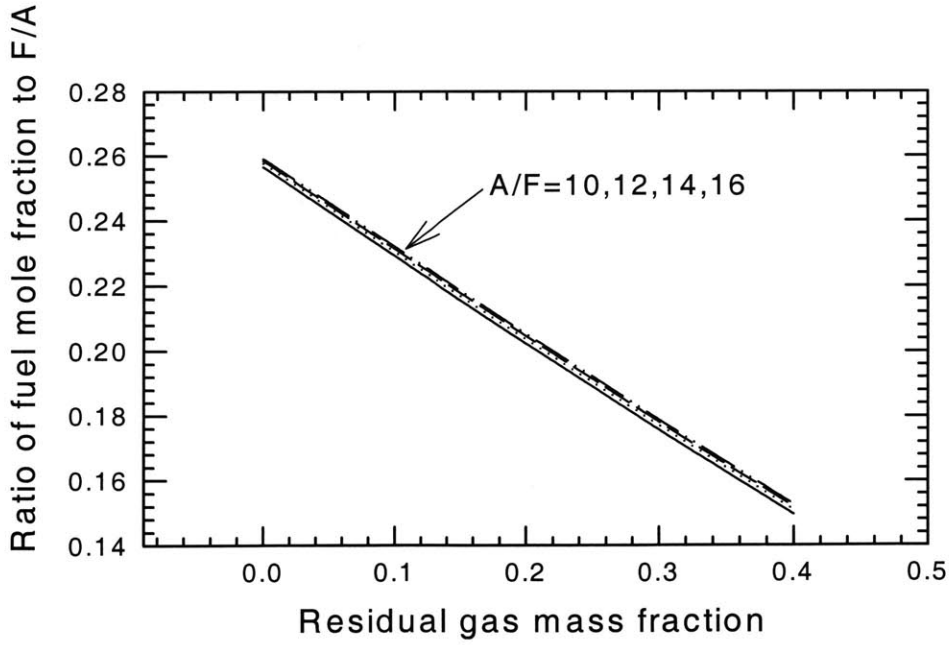

Figure 2.2: Ratio of fuel mole fraction y_r to F/A value as a function of the residual gas fraction x_r at F/A=10, 12, 14,and 16. The ratio is, to a good approximation, independent of F/A.

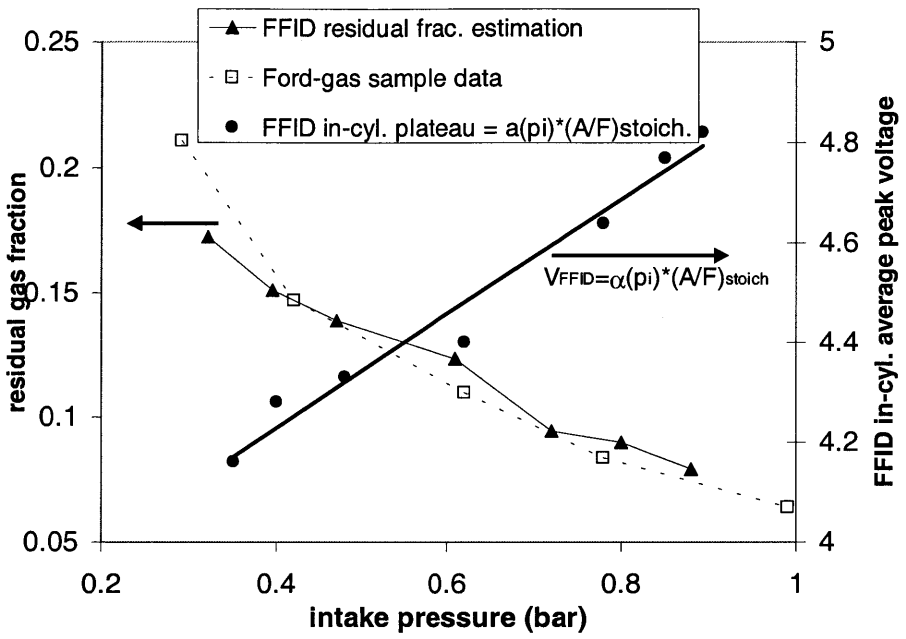

Figure 2.3: FFID calibration shown to be linear function of engine load-intake pressure. Ford residual fraction data and predictions based upon calibration scheme

(This page was intentionally left blank)

Chapter 3:
Throttle Transients Overview

3.1 General Throttle Transient Behavior

3.1.1 Basic Physical Description

Mixture preparation behavior in PFI SI engines during throttle transients is a particularly complex process. Fuel is usually injected with the intake valve closed. Analysis of this injection behavior with its fairly large (~300 μm [3.1]) and fast (~20 m/s) [3.2] droplets shows that only a small amount of the injected fuel spray (less than twenty percent) will become vapor before impacting the intake system surfaces (during stabilized operation) [3.3]. Cold engine operation will additionally result in less injected fuel becoming vapor during the fuel injection process. It is commonly believed that essentially all of the injected fuel in a PFI engine impacts the intake surface walls immediately after injection, and that very little of the original fuel spray is of a small enough diameter (~10 μm) to remain airborne in the intake port.

After the fuel impacts the intake port/valve wall surfaces, depending on the surface temperatures, some of the fuel film components distill or boil into gaseous vapor, while a significant amount continues to reside as a fuel film in the port. As the intake valve opens, a brief but vigorous back-flow period of in-cylinder gases (near atmospheric pressure) occurs into the intake port (with pressures often below atmospheric) [3.4]. This back-flow both forces liquid fuel from the puddle upstream into the intake system while also strip atomizing some of the wall liquid fuel film into small, approximately 50 μm droplets [3.5]. This back flow period is then followed by the main forward flowing intake stroke. This forward flow draws into the combustion chamber fresh intake air along with convected fuel mass from port film surfaces, vaporized fuel from the injection period and back-flow events, and some liquid fuel in the port (especially when the engine is cold) [3.6,3.7]. At the end of the intake process, however, there is still residual liquid fuel remaining in the intake port [3.8]. This liquid fuel will contribute to the fuel delivery

process in future cycles. Thus, the fuel delivered to the cylinder in a given cycle is partly due to the fuel injected for that cycle and partly due to the fuel residing in the port from the previous cycles.

As the throttle is opened, more fuel starts to flow (in the form on longer fuel pulse widths (FPWs). This has a tendency to create a larger puddle (discussed in 3.1.2). The higher fuel flow rates lower metal surface temperatures by increasing the evaporated liquid fuel mass, and by convection from the film flow into the cylinder [3.9]. The lower intake port and valve metal surface temperatures allow for more retained intake port residual fuel since lower boiling point species will remain in the liquid phase. In addition to the fuel dynamics, as the Manifold Absolute Pressure (MAP) rises due to the opening throttle, the strength of the backflow event (both velocity and duration) upon intake valve open is significantly diminished. This effect tends to reduce the redistribution of the puddle into the upstream intake port at high engine loads.

The trapping and releasing of the injected fuel in the intake port puddle is commonly referred to as fuel lag or fuel delay. The effect of the delay manifests as driveability problems in throttle transients; the problem is especially prominent when the engine is cold, and when large load transients are experienced. In practice, significantly more fuel (relative to the stoichiometric requirement according to the airflow) is injected during transients in order to ensure that enough fuel mass is delivered to the cylinder to create a combustible mixture.

The fuel lag problem is illustrated in **Figure 3.1** (lower ½); an engine's throttle is opened and the fuel flow is increased to match the increasing airflow so that a constant injected air-fuel ratio (approx. 11:1 here) is delivered. The measured air-fuel ratio is seen to be greater than intended during the throttle opening (air-fuel ratio greater than the injected 11:1), and less than intended (air-fuel ratio less than injected) during the throttle closing. The deviations from the intended value are usually referred to as the lean and rich spikes, although in absolute terms, the air- fuel ratio may be above or below stoichiometric. The lean spike affects the driveability of the vehicle and results in NOx spiking, while the rich

spike affects the HC and CO emissions. With high mileage aged catalytic converter systems, emissions spiking can result in emissions breakthrough to the tailpipe.

3.1.2 Steady-State Residual Intake Port Fuel Behavior

Fuel wall wetting in the intake port has been made apparent by visual studies that use high-speed cameras to observe intake port behavior [3.10,3.11]. Additionally, from the author's experience at Ford Motor Company, where high speed cameras were also used in the intake port, fuel films around the intake valve were evident throughout all observed operating regimes: temperature, speed and load. It is the fuel film dynamics that are responsible for the fuel lag problem.

At first thought, it is surprising that fuel films can exist in a hot, warmed-up engine. But upon examination of a distillation curve for a common automotive gasoline, it becomes apparent that roughly the upper half of the distillation curve exists above ~100 C. Thus the residual intake port fuel puddle is not comprised of fuel components that are identical to the injected fuel, but rather heavier fuel components. The puddle composition is a strong function of the intake system temperatures, with average puddle molecular weight increasing with increasing engine surface temperatures. This increasing puddle molecular weight with increasing temperature results in the puddle mass decreasing as the engine warms up. From modeling work (performed at Ford Motor Co.) it is estimated that for a stabilized engine (coolant temperature ~ 90 C) that the average puddle molecular weight is approximately 130-140, depending on load. The average molecular weight for gasoline is approximately ~105-110.

From the author's work at Ford Motor Co., a characterization of intake port residual fuel was made for a 3.0L V-6 2V engine in a Taurus vehicle (using a technique similar to that described in reference [3.21]). **Figure 3.2** shows the estimated residual port fuel for as a function of engine load (normalized: 0.8~WOT) and temperature for one intake port. It is evident that load changes at low temperatures results in massive intake port puddle

increases. Also at stabilized engine temperatures, the increase in the puddle with load in significant.

This puddle map (**Figure 3.2**) is for a fixed engine speed at ~1500 rpm. A simple linear puddle mass increase with increasing engine speed was then used to account for higher speeds. The stabilized puddle mass is often predicted to be a product of calibrated scalars x and τ and fuel flow rate (x and τ will be described below). As engine speed increases, fuel flow rate increases tending to increase the puddle mass. However, as seen in **Table 3.2**, it is generally accepted that both x and τ decrease with increasing engine speed. These effects would tend to reduce the puddle. For this Taurus engine, the net result appeared to be a slow increase in puddle mass with increasing engine speed. This simple modification provided for acceptable driveability, but was not optimized for lowest transient engine-out emissions.

Due to the importance of the residual intake port fuel, much research work has been directed towards understanding the behavior better. However, with the complex distributed (around the intake port) nature of the fuel films, and the difficulty in intake port access to an operating engine, progress in this area has been slow.

Residual port fuel mass has been measured by Toyota [3.12]. They developed a specialized engine with solenoid-operated valves and an intake port that can be closed off. At various points during engine operation, they shut off injected fuel to the port while immediately closing off the port and deactivating the valves. Next, by pumping into the sealed intake port hot air to vaporize all of the residual port fuel, and then drawing out port gases through a FID, they were able to determine puddle mass levels.

Another approach to quantify absolute intake port fuel levels is through the use of injector cut-off. Measurement of in-cylinder and/or exhaust HCs with a FFID after the injector is shut off, and the engine motored (thus pumping out the puddles), can provide an estimate of both intake port and in-cylinder residual fuel levels. Some results from this technique will be discussed in the following chapter. Unfortuneately, this technique

cannot distinguish between port and in-cylinder puddle masses. While lost fuel to the sump can underestimate puddle levels, FFID calibration at low HC levels can also be a concern.

Beyond the above two experimental, characterization of absolute residual port fuel levels must then reside with modeling efforts. Models with various levels of physically based sophistication [3.13-3.3.16] have all shown the puddle to increase with engine load, and decrease with increasing temperature.

Unfortunately, puddle mass is not sufficient to fully understand the dynamic behavior of the puddle. In order to estimate liquid puddle flow (shear driven flow), puddle height must be known. Additionally, in order to estimate heat and mass transfer effects, puddle area must be known. Thus, an effective puddle geometry is necessary to predict specific behaviors. Towards this end, a number of researchers [3.17-3.19] have used LIF measurements in order to characterize the absolute and changing puddle thickness at a given point in the intake port. While the data is only for an isolated point, it nonetheless provides some clues to puddle behavior. Puddle area is more difficult to quantify. As discussed at the outset, a single well-defined puddle is not reality. The visual studies mentioned above show that the puddle can in fact be distributed around the intake port into many smaller puddles. Needless to say, this area of engine behavior is poorly understood.

3.1.3 Throttle Transient Behavior

In light of the fact that the intake port puddle mass increases with increasing engine load, the question arises as to the processes involved leading to increased residual intake port fuel. What is the 'path' or history of the puddle as the engine's load is increased? Knowledge of the intake port fuel mass disposition is essential in order to appropriately compensate with injected fuel, such that a desired in-cylinder air-fuel ratio is achieved during the engine transient.

Since the early days of throttle body fuel injection (CFI-Central Fuel Injection), researchers [3.20,3.21] found that treating the intake port puddle as a first order system worked nicely. This model, commonly referred to as the x- τ model, has been widely used since then, including in PFI engines.

In research and in practice, x and τ (wall wetting model constants at a given operating condition-details to be given in the next section) have been principally characterized using a UEGO sensor as its fundamental diagnostic while measuring an uncompensated transient response. For a given engine and fuel, characterization of x and τ is performed across a wide range of operating conditions. Three groups of characterization techniques have emerged. Firstly, those using slow throttle opening rates (over the period of one second) in order to minimize the errors involved with in-cylinder air mass determination [3.20-3.22]. Secondly, those using very fast throttle openings (less than one engine cycle) in which both anticipated fueling requirements as well as automatic uncompensated controller response were used [3.23-3.25]. Lastly, step fuel perturbations at a fixed speed and load were used to infer transient fueling response [3.26]. Clearly, much disagreement exists over the appropriate characterization method, and the results appear to be different. This thesis will also address this issue.

Beyond the UEGO, alternative diagnostic techniques have emerged which seek to characterize the in-cylinder air-fuel ratio during throttle transients. As discussed earlier, the UEGO possesses a time constant, which can be greater than an engine cycle time scale. This effectively leads to filtering of the true in-cylinder behavior. Thus, two in-cylinder approaches have been used allowing for cycle-by-cycle resolution. Firstly, a catalytic hot wire sonic nozzle probe was used [3.27]. Secondly, one research group used an in-cylinder FFID to characterize fast throttle openings [3.28, 3.29]. This thesis will employ the later method, a FFID diagnostic, in all of its experiments.

3.2 Approaches used in Production Engine Controllers to Compensate for Wall Wetting Changes

3.2.1 The x- τ model

Over the last 15 years, both the automotive industry and engine researchers have approached the fuel lag issue by using a model in which residual intake port fuel mass exists in the intake system. By treating this intake port residual fuel (puddle) as a first order system that is filled upon increased fueling, and drained during decreased fueling, a modeled uncompensated in-cylinder fuel response similar to that shown in Figure 1 can be generated using 2 parameters. This approach is referred to as the x- τ model, where 'x' is the fraction of the injected fuel in the current cycle that is trapped in the intake port puddle for future cycles, and 'τ' is the relaxation time for the release of the puddle mass into the cylinder. By using this open-loop x- τ model coupled to the base closed-loop fuel control system, compensation schemes that provide additional fuel enrichment during transient throttle openings, and reduced fueling during throttle closings may be devised to reduce air- fuel ratio spikes.

The x-τ model in the continuous form is described by [3.20]:

$$\dot{m} = (1 - x)\,\dot{f} + M/\tau \tag{3.1}$$

$$\dot{M} = x\dot{f} - M/\tau \tag{3.2}$$

where m is the mass of fuel delivered to the cylinder, f is the injected fuel mass; M is the fuel mass in the puddle. The parameters x and τ are the fraction of the injected fuel that is retained in the port and the time constant for the release of the port fuel. Integrating the equations over one cycle, the discrete form of the x-τ model is:

$$m_i = (1-x)\, f_i + M_i / (\tau / \Delta t) \tag{3.3}$$

$$M_{i+1} = M_i + x\, f_i - M_i / (\tau / \Delta t) \tag{3.4}$$

Where Δt is the time for one cycle and i is the cycle index. At steady state, the puddle

mass is

$$M(s.s.) = x\,(\tau/\Delta t)\,f(s.s.) \qquad (3.5)$$

For a given value of x and τ, and injection sequence f_i, the fuel delivery m_i and the puddle mass M_i can be calculated from equations (3.3) and (3.4).

3.2.2 x-τ Model Simulation and Actual Implementation in a Production Controller

From 4-cylinder Zetec Engine Transient Fuel Compensation (TFC) characterization work done at Ford Motor Company, at 1500 rpm, x and τ were found to equal 0.3, 0.4 sec. **Figure 3.3** shows injected fuel x-τ model simulations using the above x and τ values for a fast (3 cycles ~ ¼ sec), medium (7 cycles ~ ½ sec) and slow (13 cycles ~ 1sec) throttle opening ramp. This simulation assumes that an in-cylinder λ=1.0 exists for every cycle, and then calculates the necessary injection. Thus, over-fueling in order to fill the puddle is evident. **Figure 3.4** shows actual production controller behavior (with an imbedded open-loop x-τ model using the above values for x and τ) for similar throttle ramps. In comparing **Figures 3.3 and 3.4** it appears that the production engine controller is behaving as the simulation predicts.

In using the x-τ model during transients to determine the wall wetted compensated fuel injection amount, the model will calculate an injected fuel amount that is more than stoichiometrically required (~20% extra for the fast opening, ~5% extra for the slow opening) to account for intake-port puddle filling. Then after the throttle transient is complete, the first order model reduces TFC 'over-fueling' until a steady-state stoichiometric fueling (based on air-flow) is achieved. Corresponding to throttle rate is the rate at which the puddle is filled; quickly for fast throttles, slow filling for slow throttles. This is the model -predicted behavior, but is it physically based? Should the same x and τ value be used for all throttle rates?

It is true that in fast throttle openings, fuel flow rates increase quickly, tending to fill the puddle quickly. However, in fast throttle openings, the Manifold Absolute Pressure (MAP) also rises quickly, thus few of the engine cycles during the transient have low MAPs. With few low MAP cycles, very little fuel redistribution upstream in the intake port is allowed to occur at intake valve opening. At lower intake pressures, studies have shown significant backflow of in-cylinder gases occurring when the intake valve first opens [3.4]. This vigorous backflow has been seen to create large droplets (~ 50 μm) that are forced upstream into the intake port [3.1]. This effect (as with injector flash boiling) tends to more widely distribute a fuel film in the port, effectively increasing the wall wetting fuel delay (x and τ get larger). Thus the 'path' or puddle history might be different for fast and slow throttle openings since fast throttle openings do not experience numerous low MAP cycles during the transient which redistribute intake port residual fuel.

3.3 Practical Issues and Motivation

3.3.1 x- τ Model Behavior in Practice

In practice, even after characterizing a given engine on a specific fuel across a range of transient operating conditions (x and τ are strong functions of ECT, rpm, injector behavior and port geometry), fuel control is still observed to be imperfect. This is evidenced by deviations in the desired stoichiometric behavior as indicated by either a UEGO, in-cylinder FFID, or engine-out emissions. Additionally, a closed-loop fuel controller can show deviations from ideal behavior. In all these cases, the in-cylinder relative air-fuel ratio, which is targeted for λ=1, deviates either rich or lean during and after transients, despite attempts to account for intake port fuel lag.

The lower half of **Figure 3.5** shows a calibrated FFID signal from the exhaust port of a Zetec engine (used in this study) running a production engine calibration during a fast

throttle opening at 1500 rpm. Transient Fuel Compensation (TFC: calibrated x- τ model embedded into engine controller) was developed at Ford in an effort to keep the in-cylinder λ~1. However, it is clear that for a couple engine cycles during the transient, the in-cylinder λ (in the upper half of **Figure 3.5** as measured by the FFID) is very rich. This consequently leads to cycles with significantly higher HCs than would be attained at the same steady-state condition. It is expected that CO emissions also, during this transient, would be abnormally high. Since the TFC x and τ calibration was developed for a one second, slow throttle opening and is applied equally to all throttle rate events, the question exists as to applicability of the same calibrated x and τ for especially fast throttle openings. Additionally, questions exist as to the physical basis of the x and τ model's first order puddle behavior assumption for fast-throttle openings.

When one observes a production engine controller's internal operation during and after a throttle transient, evidences of non-ideal behavior can become apparent. **Figure 3.6** shows internal EEC (Electronic Engine Controller –Ford acronym) signals during a throttle transient. Shown are engine load, transient fuel compensation and the closed-loop lambda controller. Normally, the lambda controller ramps the injected fuel slightly rich (beyond the nominal stoichiometric level based on the Mass AirFlow Sensor: MAFS) when the Exhaust Gas Oxygen (EGO) sensor reads lean. Then, when the EGO sensor switches rich (due to the slight overfueling and transport delay through the engine), the controller jumps back near stoichiometric and ramps injected fuel lean until the EGO switches lean. This closed-loop fuel lambda limit cycle process is then repeated. Thus, while injected fuel is controlled nominally around λ=1, in production controller practice, the fuel is actually cycled around λ=1 with deviations both rich and lean of approximately 3-4% (conventional automotive 3-way catalysts are designed for this mode of operation). Under normal steady-state operation the lambda controller limit cycle frequency is on the order of 1 Hz (this limit cycle frequency is a strong function of the transport delay of injected fuel through the engine to the EGO sensor-this delay is reduced as engine speed increases).

This normal control is observed before the transient occurs (in the first few seconds of **Figure 3.6**). However, as evidenced by the lambda controller's operation after the throttle opening, an excursion (lambda controller steadily ramps since the EGO sensor does not experience a stoichiometric switch) exists for many seconds. This lean excursion indicates that too much 'extra' fuel was incorrectly added during the transient, and now the lambda controller must adjust for the overfueling by reducing FPW (increasing λ) over the next few seconds until a stable intake port puddle is achieved. After the throttle closing, again a significant lean excursion exists, indicating that not enough injected fuel was reduced to account for the puddle draining into the cylinder. In both cases, especially with aged catalytic converter systems, emissions breakthrough to the tailpipe can occur.

In addition to the changing operational behavior of engines, the nature of fuel changes with the seasons. In winter, a high volatility fuel is needed to start the engine, while in summer, a reduction in vapor pressure is necessary to achieve hot engine starting acceptability. Unfortunately, engine controllers do not know what type of fuel is in the tank, thus a compromised engine fuel control calibration must be implemented for production which satisfies many environmental conditions. Unfortuneately this leads to non-optimized performance most of the time.

The approach taken by the author while an engine calibrator at Ford Motor Company was to calibrate x and τ's at lower Engine Coolant Temperatures (ECTs $< \sim 15$ degC) with a high volatility fuel representative of winter grade fuels. For engine temperatures above this point (which also corresponds to the temperature range of Federal Emissions Testing) a summer grade fuel was used for calibration purposes. This led to reasonably good transient fuel control for emissions testing, and stabilized summer driving. During winter months, due to the high volatility fuel, when the engine was operating at stabilized temperatures, overfueling during transients would generally result, due to lower puddle masses with relatively more fuel entering the combustion chamber as compared to stabilized operation with summer fuel. Overfueling is safer from a performance perspective, thus this behavior was necessarily tolerated. However, again, PFI operation

is not optimized, thus catalytic converter performance can be diminished. References [3.21] and [3.23] show the above mentioned fuel effects on x-τ calibration results.

Beyond fuel type, fuel temperature can also affect TFC performance. This is a relatively new discovery just a few years ago by Aquino [3.30] at Ford Motor Company. It was believed since fuel injection was developed that port fuel sprays behave in the actual operating engine intake port as they do on a bench testing rig – well behaved cone angle. However, visual studies in the intake port showed that at warmer fuel temperatures (>~30 degC) and lower intake pressures, a transition to flash boiling can occur. With injector flash boiling, a significantly increased surface area for wall wetting occurs. This lead too greater fuel lags, e.g. x and τ's increase. If not accounted for, lean excursions and stumbles as if no TFC were applied can result.

Finally, one additional unknown in calibrating TFC occurs during the first minute of operation after the engine is started. From experience it is known that TFC levels must be increased by up to many factors depending on engine temperature in order to keep the engine from stalling during a throttle opening. The calibration of an internal EEC table similar to **Table 3.1** is solely empirically based. As seen in **Table 3.1**, a TFC multiplier based on time since engine start and engine coolant temperature can strongly affect TFC. This EEC table is loosely based on the fact that the intake valve temperature is changing rapidly during an engine warm-up (see reference 3.9) on the time scale of a minute. After the intake valve achieves a quasi-steady temperature, engine coolant temperature can be used to appropriately compensate for the wall wetting fuel lag.

3.3.2 Key Variables- Variations amongst Different Studies

There appears to be anomalies with the x- τ model. Only limited agreement exists among engine researchers as to the dependencies of x and τ upon operating conditions; see **Table 3.2**, which displays the trends in x and τ with operating conditions. Additionally, estimates of residual port fuel mass amongst various researchers vary substantially. Obviously, some engine differences exist among the studies that may play a role in the

disparate results. However, the basic engine geometry is not all that different, and many physical mechanisms should be identical amongst the different studies so that it is difficult to reconcile the diverging trends. In some cases, the empirically observed trend is contrary to the physical premise of the model — for example, some engine calibrations have τ increasing with a rise in engine temperature; this trend does not fit the concept of τ being the puddle evaporation time. Thus while the concept of the x- τ model is plausible, there are significant details in the fuel delivery process that are not well understood.

As discussed in Section 3.1.3, comparison of transient fueling studies reveal differences in experimental technique that could contribute to the disparate results. For example, some researchers characterize the transient fueling behavior using fuel perturbations in order to simulate the increase in fuel flow [3.26]. However, this technique neglects the increase in intake system pressure and air flow velocity that is associated with real throttle transients; these phenomena have a major impact on the fuel transport process. Many researchers thus use a one-second-duration throttle ramp in order to characterize the behavior [3.20-3.22], while still others use very fast throttle opening times [3.23-3.25]. Lastly, the technique of using a wide-range exhaust gas sensor (Universal Exhaust Gas Sensor, UEGO) almost exclusively in the many studies to infer in-cylinder fueling behavior might possess some limitations because of the sensor response (both inherent to the sensor and due to gas mixing processes in the exhaust system). Thus, what is the best approach?

3.4 The Direction of this Study

The case of fuel delivery behavior in rapid throttle movement is of particular interest. In practice, 'real world' driving often includes rapid throttle movements. Many of the engines in use today were calibrated by using a slow ramp transient (~ 1 second). Field tests of vehicles show good fuel compensation under mild accelerations, as indicated by a close to stoichiometric exhaust λ reading throughout the transient. Under rapid acceleration, however, the calibration often over-delivers fuel into the engine and results

in considerable enrichment for a number of engine cycles. This behavior increases engine out emissions of hydrocarbons and carbon monoxide.

Thus, this study will observe throttle transient behavior for various rates of throttle openings, from fast throttles (~ 200 msec) to slow throttles (~ 1+ sec). A fast in-cylinder diagnostic (FFID) will be used in order to capture the true in-cylinder fuel behavior on a cycle-by-cycle basis. This data will be compared against the relatively slow UEGO response, which effectively filters in-cylinder behavior. Due to response limitations of the FFID in-cylinder, only lower engine speed throttle transients will be performed across various load increases. Further, fuel control actions both with and without compensation will be observed in order to evaluate the effect. Chapter 4 discusses these results.

Chapter 3 References:

[3.1] Whelan, D.E., Kelly-Zion, P.L., Lee, C.F., Peters, J.E. and White, R.A., "Back-Flow Atomization in the Intake Port of Spark Ignition Engines", SAE#972988, 1997.

[3.2] Bauer, W., Balun, P., and Heywood, J. B., "Heat Transfer and Mixture Vaporization in Intake Port of SI Engine", SAE#972983, 1997.

[3.3] Chen, G., Vincent, M.T. and Gutermuth, T.R., "The Behavior of Multiphase Fuel-Flow in the Intake Port", SAE#940445, 1994.

[3.4] Cheng, C.O., Cheng, W.K. and Heywood, J.B., "Intake Port Phenomena in a Spark Ignition Engine at Part Load", SAE#912401, 1991.

[3.5] same as [3.1].

[3.6] Dawson, M. and Hochgreb, S., "Liquid Fuel Visualization Using Laser Induced Fluorescence", SAE#982466, 1998.

[3.7] Shin, Y., Cheng, W.K. and Heywood, J.B.,"Liquid Gasoline Behavior in the Engine Cylinder of a SI Engine", SAE#941872, 1994.

[3.8] Imatake, N., Saito, K., Morishima, S., Kudo, S. and Ohhata, A., "Quantitative Analysis of Fuel Behavior in Port Injected Gasoline Engine", SAE#971639, 1997.

[3.9] J. Cowart, W.K. Cheng, "Intake Valve Thermal Behavior During Steady-State and Transient Engine Operation," SAE Paper 1999-01-3643, 1999.

[3.10] Shin, Y., Min, K. and Cheng, W.K., "Visualization of Mixture Preparation in a Port Fuel Injection Engine during Engine Warm-up", SAE#952481, 1995.

[3.11] Saito, K, Sekiguchi, K. Imatake, N., Takeda, K. and Yaegashi, T., "A New Method to Analyze Fuel Behavior in a SI Engine", SAE#950044, 1995.

[3.12] Imatake, N., Saito, K., Morishima, S., Kudo, S., and Ohhata, A., "Quantitative Analysis of Fuel Behavior in Port-Injection Gasoline Engines", SAE#971639, 1997.

[3.13] Servati, H. B. and Yuen, W.W., "Deposition of Fuel Droplets in Horizontal Intake Manifolds and the Behavior of Fuel Film Flow on its Walls", SAE#840239, 1984.

[3.14] Servati, H. B. and Herman, E.W., "Spray/Wall Interactions Simulation", SAE#890566, 1989.

[3.15] Benyettou, F.M. and Thelliez, M., "Modeling of Unsteady Multiphase Flow in the Intake Manifold of SI Engines", SAE#910392, 1991.

[3.16] Chen, G., Vincent, M.T. and Gutermuth, T.R., "The Behavior of Multiphase Fuel-Flow in the Intake Port", SAE#940445, 1994.

[3.17] Almkvist, G., Denbratt, I., Josefsson, G. and Magnusson, I., "Measurements of Fuel Film Thickness in the Inlet Port of an SI Engine by LIF", SAE#952483, 1995.

[3.18] Coste, T.L. and Evers, L.W., "An Optical Sensor for Measuring Fuel Film Dynamics of a Port-Injected Engine", SAE#970869, 1997.

[3.19] Senda, J, Ohnishi, M., Takahashi, T., Fujimoto, H., Utsunomiya, A., Wakatabe, M., "Measurement and Modeling on Wall Wetted Fuel Film Profile and Mixture Preparation in Intake Port of SI Engine", SAE#99010798, 1999.

[3.20] Aquino, C.F., "Transient A/F Control Characteristics of the 5 Liter Central Fuel Injection Engine", SAE#810494, 1981.

[3.21] Fozo, S.R. and Aquino, C.F., "Transient A/F Characteristics for Cold Operation of a 1.6 Liter Engine with Sequential Fuel Injection", SAE#880691, 1988.

[3.22] Aquino, C.F. and Fozo, H.B., "Steady-State Transient A/F Control Requirements for Cold Operation of a 1.6 Liter Engine with Single Point Injection", SAE#850509, 1985.

[3.23] Almkvist, G. and Eriksson, "An Analysis for Air to Fuel Ratio Response in a Multi Point Fuel Injected Engine Under Transient Conditions", SAE#932753, 1993.

[3.24] Hendricks, E., Vesterholm, T. Kaidantzis, Rasmussen, P. and Jensen, M.,"Nonlinear Transient Film Compensation", SAE#930767, 1993.

[3.25] Bossert, J.C., Shin, Y. and Cheng, W.K., "Fuel Effects on Throttle Transient in PFI SI Engines", SAE#971613, 1997.

[3.26] Shayler, P.J., Teo, Y.C. and Scarisbrick, A., "Fuel Transport Characteristics of SI Engines for Transient Fuel Compensation", SAE#950067, 1995.

[3.27] Li, C.F., Duan, Q.C., Marateaux, F. and Murat, M., "Time-Resolved Measurement of Fuel Transient Behavior and Cycle to Cycle Variation of Local Fuel-Air Ratio in Gasoline Engine", SAE# 940989 ,1994

[3.28] Rose, D., Ladommatos, N. and Stone, R., "In-Cylinder Mixture Excursions in a Port-Injected Engine During Fast Throttle Opening", SAE#940382, 1994.

[3.29] Ladommatos, N. and Rose, D.W.,"On the Causes of In-Cylinder A/F Ratio Excursions during Load and Fueling Transients in PFI SI Engines", SAE#960466. 1996.

[3.30] Aquino, C.F., Plensdorf, W, Lavoie, G. and Curtis, E., "The Occurrence of Flash Boiling in a Port Injected Gasoline Engine", SAE#982522, 1998.

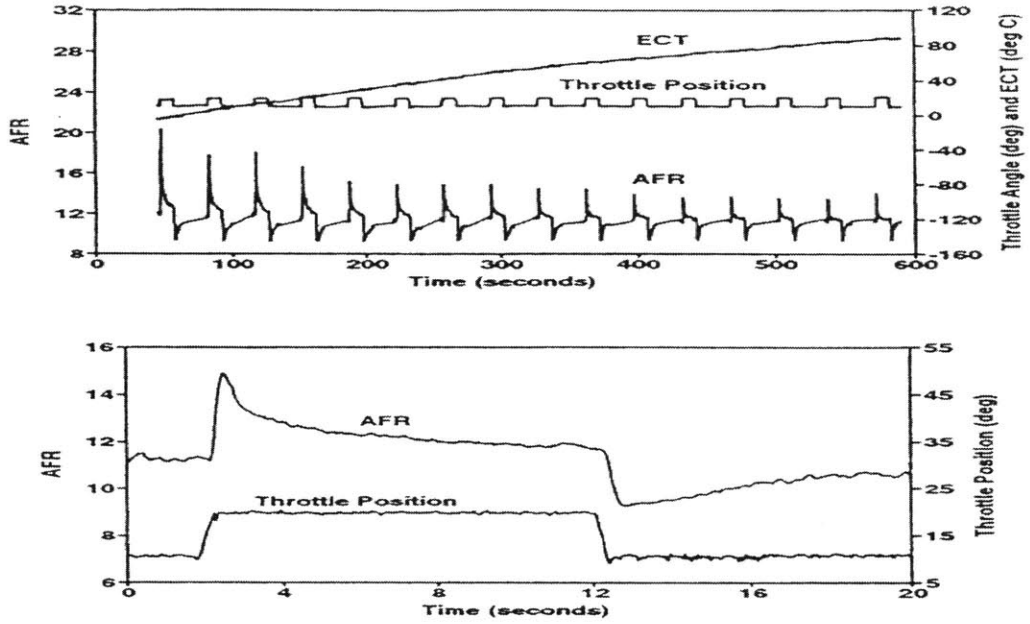

Figure 3.1: An uncompensated throttle transient response
From: Shayler, SAE#950067. Used without permission.

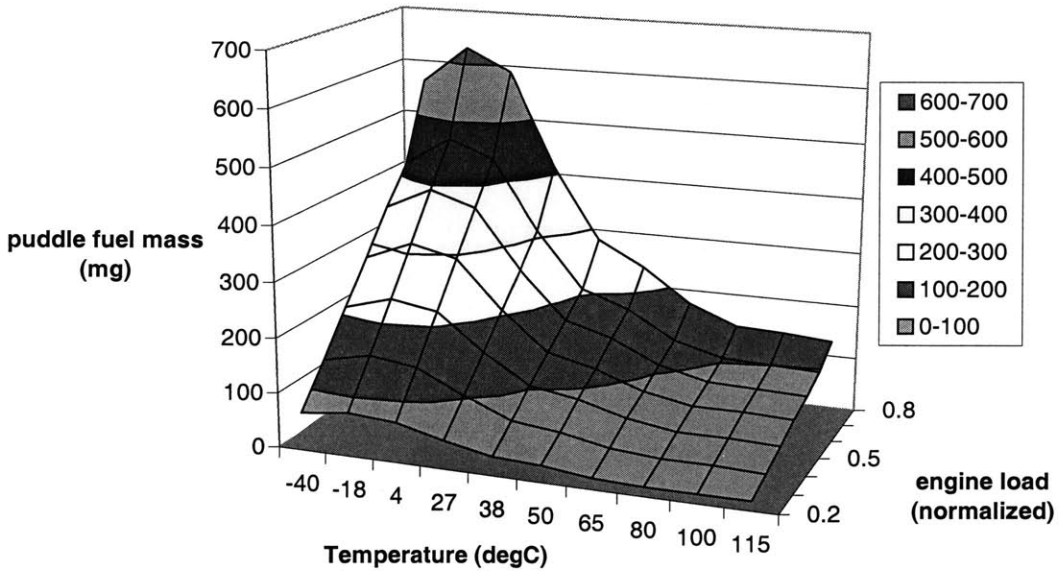

Figure 3.2: Residual intake port fuel (mg) as a function of engine coolant temperature (ECT) and normalized engine load (WOT~0.8)

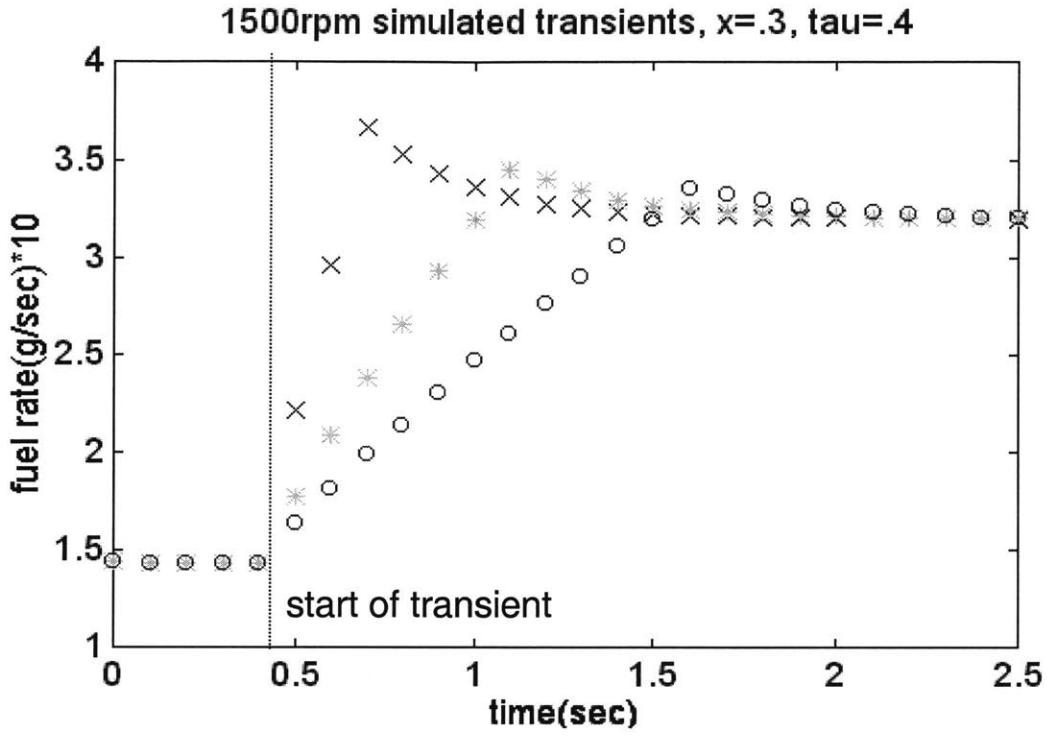

Figure 3.3: x-tau model prediction of injection history in order to maintain an in-cylinder stoichiometric charge mass for fast/medium/slow throttle ramps.

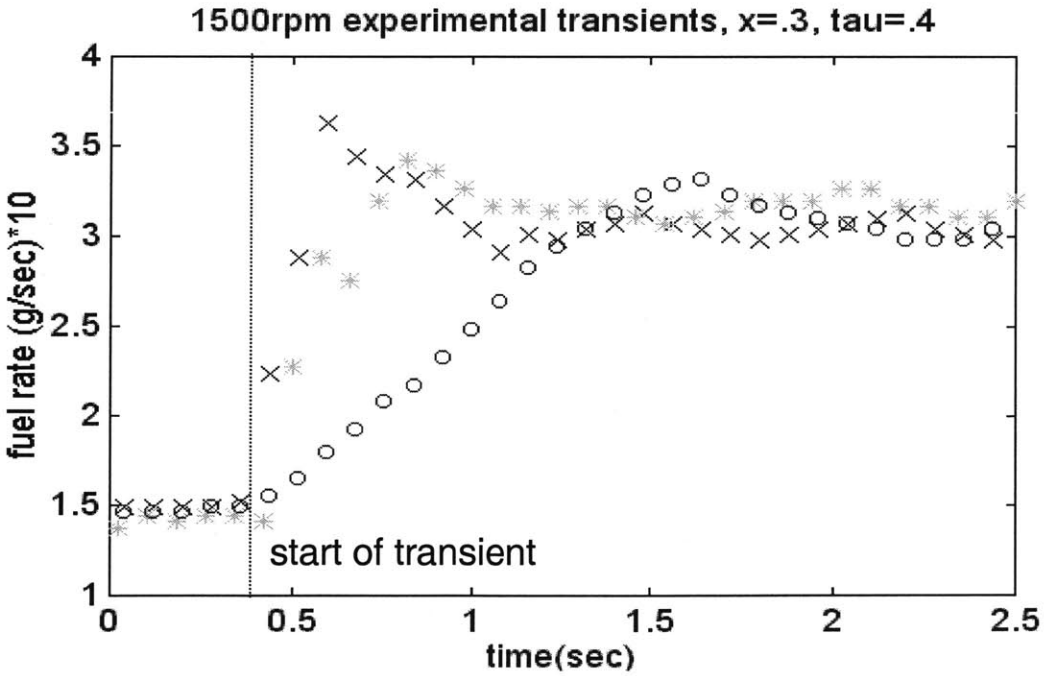

Figure 3.4: production x-tau model actual injection history calibrated in an effort to maintain an in-cylinder stoichiometric charge mass.

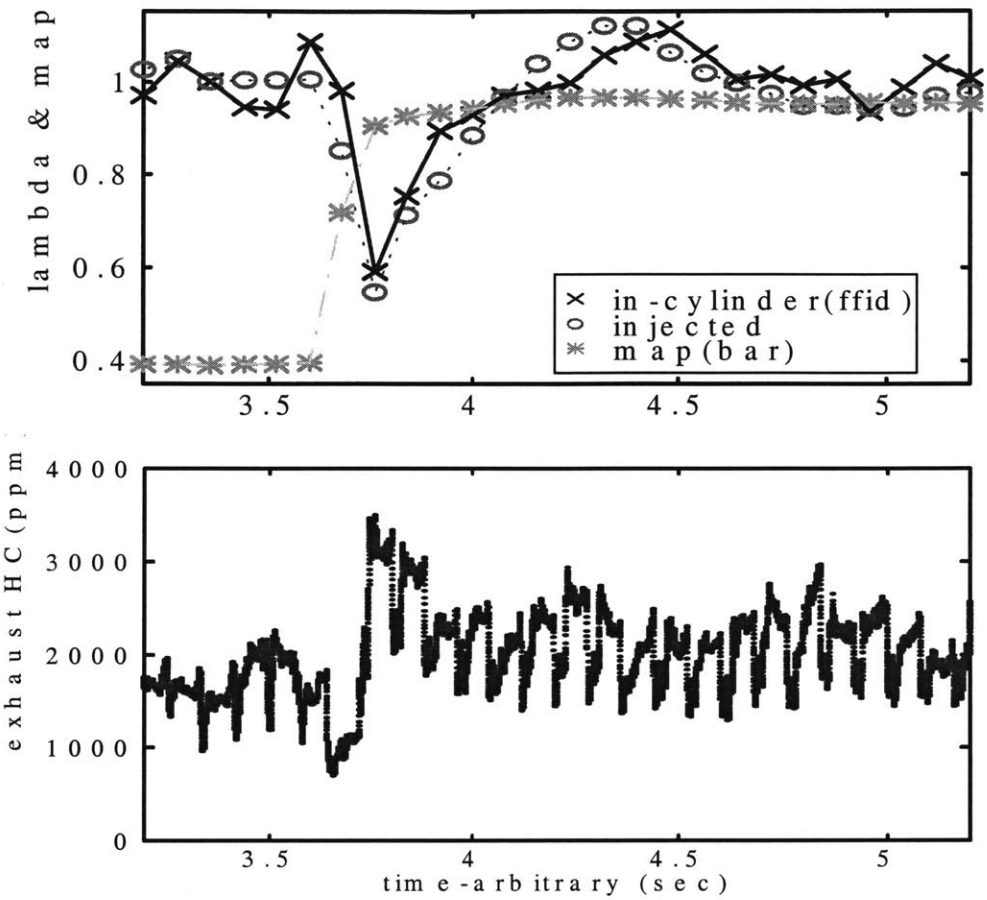

Figure 3.5: Compensated Zetec Engine fast throttle opening, 1500rpm

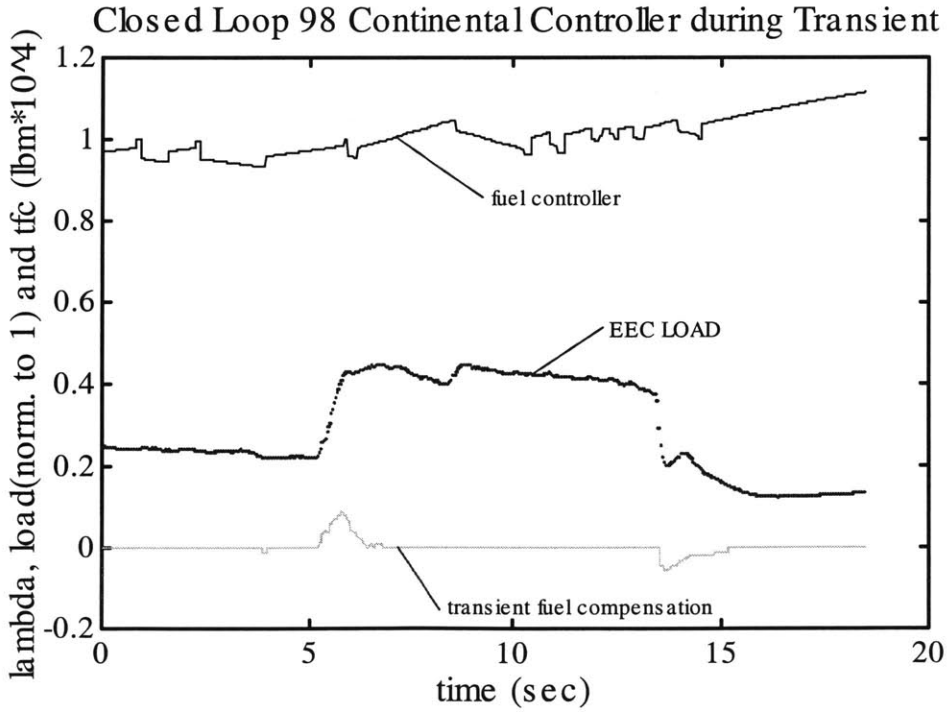

Figure 3.6: Production Lambda Controller during throttle opening and closing

time since start (sec)	engine coolant temp (degC) -20	10	40	70	100
60	1.75	1.5	1	1	1
40	2.5	2.25	1.5	1	1
20	3.5	3	2	1.25	1
0	4	3.5	2.25	1.5	1.25

Table 3.1: Transient Fuel Compensation (TFC) Multiplier versus time since start and engine coolant temperature

Comparison of Transient Fuel-Wall Wetting X-up and Tau (for a given variable increase)

0	x (load)	x (ECT)	x (rpm)	x (RVP)	tau (load)	tau (ECT)	tau (rpm)	tau (RVP)	
Cowart '96-Taurus	⇧	⇩⇩	⇩	⇩	⇩	⇧		⇩	2V - 1sec throttle ramps
Shayler SAE#950067	—	⇩	⇩	n/a	—	⇩⇩	⇩⇩	n/a	4V - step fuel pertabation
Aquino SAE#880691	⇧	⇩⇩	n/a	⇨	⇩	⇧⇧/⇩	⇩⇩	⇨	2V - 1sec throttle ramps
Almkvist SAE#932753	⇧⇧	⇩⇩	⇩	⇨	⇩⇩	n/a	⇩	⇨	4V - 50ms step throttle

All engines equipped w/ SEFI. All characterizations used a UEGO. A double arrow represents a > factor of two effect over the operating range. X-indolene > X-iC8H18. Tau-up is strong function of injection timing. . ..Aquino

Table 3.2: x and t trends with operating conditions as characterized by various researchers

Chapter 4
Throttle Transient Experiments

4.1 Introduction to the Experimental Work and Analysis

In the previous chapter, it was discussed that the effects of throttle rate on transient fueling behavior are unknown. Studies have looked exclusively at either very fast throttle openings, or slow throttle transients. Practical industry experience (from the author's engine calibration experience) has additionally suggested that unique fueling requirements as a function of throttle rate might be necessary in order to achieve stoichiometric in-cylinder fueling during a transient. Observation of production engine fuel control during load transients (Chapter 3.3) shows significant deviations from stoichiometric operation. Current transient fuel control (TFC) is not optimized, and a greater understanding of transient fuel behavior is necessary for improved engine performance and reduced emissions. Thus the effects of throttle rate are observed.

For this thesis, an experimental program was pursued to evaluate if throttle-opening rate affects the in-cylinder fuel transport. Specifically this work will evaluate if the conventional x-τ model with coefficients derived from a slow uncompensated throttle transient is also appropriate for faster throttle openings.

The approach used here will be to perform throttle transient experiments, both with and without wall wetting compensation for the transient, across a wide range of throttle rates. During these experiments in-cylinder air-fuel ratio data will be collected with a FFID. Injected fuel will also be simultaneously observed. This measured injection history will then be applied to the x-τ model (using the x and τ values from a slow throttle characterization) on a cycle-by-cycle basis. The outputs from the model predict both an in-cylinder fuel mass and changing puddle behavior. These outputs will be compared to the measured in-cylinder fuel mass, and the inferred puddle change behavior in order to

evaluated the fitness of the model as throttle rates increase. This analysis will aid in the determination of the source of air-fuel deviations during transient operation.

The organization of this chapter is as follows:

Accurate in-cylinder air-fuel ratio data cycle-by-cycle is essential. This is made especially difficult due to changing in-cylinder fueling behavior during transients. **Section 4.2** looks first at why the popular and widely used UEGO is inappropriate for fast throttle experiments. The in-cylinder FFID, while significantly more difficult to use, is necessary for giving a true indication of in-cylinder fueling behavior.

Next, in order to obtain an accurate fuel injection history during transient operation (for application to the x-τ model), it is imperative to initially study the effects of dynamic fueling on in-cylinder fuel transport. It is common in production controllers to apply an extra injection pulse during the intake valve open period in an attempt to 'keep up' with increasing air flow as the throttle is opening. Unfortunately, UEGOs are used to determine the latest possible location for dynamic pulses. It is believed that these pulses reach the combustion chamber on the current cycle, but do they really? Thus, experiments were performed that simulate this dynamic pulse. The in-cylinder response was measured so as to characterize the effectiveness of the dynamic fuel pulse in reaching the combustion chamber on the current engine cycle (**Section 4.3**).

One more initial section lays the groundwork for the throttle transient experiments. As discussed in Chapter 3, fuel cut-off experiments can be used to indicate absolute residual fuel levels. In **Section 4.4**, fuel cut-off experiments were performed at steady-state operating conditions, 1500 rpm, both at 0.4 bar and 0.9 bar p_i. The majority of the throttle transient experiments were performed at this speed with the MAP initially at 0.4 bar p_i and increased to 0.9 bar p_i. The fuel cut-off data will indicate both the absolute starting and ending residual port fuel levels for the actual throttle transients, as well as the change in puddle mass that must occur during a transient. It will be useful to compare

this data with the residual port fuel change inferred from experimental throttle transient data.

Finally, the throttle transient experimental data is presented in **Section 4.5**. The measured injection histories are applied to the x-τ model for comparison with the measured data.

The x-τ model provides fuel compensation in addition to stoichiometric fueling requirements based on in-cylinder air-flow. The implications of incorrect air-flow estimates will be discussed in relation to the above observed transient fueling behavior in **Section 4.6**.

The x-τ model behavior is lastly tested at various load changes, and at another speed (**Section 4.7**). It is additionally tested upon two single component fuels (**Section 4.8**).

Finally, a brief look at cold engine transients is presented in **Section 4.9**.

4.2 Production Compensated Controller Fast Throttle UEGO Response

A/F ratio measurements using the FFID and UEGO were taken simultaneously and compared during transient operation. The UEGO was placed 10 cm downstream of the exhaust valves in the isolated exhaust manifold of cylinder #4. The results are plotted in **Figure 4.1** for a fast throttle opening. During the first cycle of the transient (cycle #42) both the FFID and the UEGO show a lean excursion of similar magnitude. Then on the next cycle, the in-cylinder signal ('x' symbols) shows that the combustion chamber relative air-fuel ratio went very rich (λ~0.55). While the UEGO signal also registered a rich excursion, it severely underestimated the magnitude because of its slow time response. When a 200 msec (which is approximately the time response of the UEGO sensor [4.5]) first order low pass filter was applied to the FFID signal, the resulting λ matched up with the UEGO signal. The reverse process of compensating for the UEGO

signal involves differentiating the signal and is prone to noise. Thus, 'backing out' the appropriate in-cylinder behavior from the UEGO signal would be very difficult.

The agreement between the filtered FFID signal and the UEGO signal lends support to the validity of the FFID measurement method. It should also be pointed out that because of the slow UEGO response, using the UEGO measured λ as the basis for calibrating the x-τ values for fast throttle (and step fuel changes, as discussed above) could lead to a substantial error. Finally, comparison of the FFID signal and the UEGO for slow throttle transients, where significant cycle-by-cycle variations do not occur, showed excellent agreement.

4.3 Investigation of the Dynamic Pulse

4.3.1 Experimental Simulation of Dynamic Pulse

When one observes the fuel injection behavior of a production controller during transient operation, an extra injection pulse can be seen during the intake event. This extra pulse or dynamic pulse is to compensate for the increasing rate of airflow into the engine. This section evaluates the effectiveness of the dynamic pulse in reaching the combustion chamber on the cycle in which it is injected, and for which it is intended. It is essential to know whether the dynamic pulse enters the combustion chamber on its injected cycle so that an accurate fuel injection history is known and may be correctly applied to the model.

Most automakers make estimates of in-cylinder air mass (with either a Mass AirFlow Sensor-MAFS or MAP-speed density system) almost one complete cycle before the intake valve opens. Then fuel injection is scheduled so that the End of Injection (EOI) is shortly before the intake valve opens. This very early calculation of air mass is necessary in the case of high speed/load operation, in which the fuel injectors are on almost continuously. Unfortunately, with such an early air mass calculation, throttle demands

can and do change. Thus, it is essential to try and update fuel injection during a transient, if possible.

In the case of cylinder #4 on this four-cylinder Zetec, the MAFS signal is integrated for one-half of an engine revolution approximately one cycle before the air and fuel are to be inducted into the cylinder (#4). Fuel injection is then scheduled prior to the next intake-valve-open event (#4). However, before cylinder #4 has its next intake event, cylinder #2, then cylinder #1 and then cylinder #3 (firing order 1-3-4-2) will all integrate the MAFS for a half-revolution and schedule their own fueling. If a significant change is observed in the integrated air mass for cylinders 2, 3 or 1, before the intake valve has closed on cylinder #4, then the controller will attempt to make up the difference in increasing air mass by delivering a dynamic pulse during the intake event to cylinder #4.

Figure 4.2 shows a dynamic pulse occurring during a fast throttle opening in the Zetec controller. This dynamic pulse is in addition to the base closed-valve injection fuel pulse. The EOI of the dynamic pulse is 50 BBC (pulse duration ~ 30 cadeg). The intake valve closes at 50 ABC. From measurements of Wolf Bauer [4.4], scaled to the Zetec port geometry (injector to intake valve = 10 cm), at 1500 rpm the transport time for the injector tip to the intake valve is ~ 50 crank angle degrees (~6 msec, thus apparent average fuel velocity ~17 m/s). It seems plausible that the dynamic pulse should arrive into the cylinder, but does it?

Step fuel experiments were done at steady-state low load (0.4 bar intake pressure) in order to simulate experimentally the dynamic pulse occurring early in a throttle transient. Cylinder #4 was operated with the PC controller running approximately 10-20% (λ=1.1-1.2) lean before the dynamic pulse was applied. With the addition of a 30 cadeg dynamic pulse in the same location as the Ford controller 640-670 cadeg (0 deg=BCC) the final steady-state relative air-fuel ratio was approximately 25% rich (λ=0.75).

Figure 4.3 shows the experimental results. The dynamic pulse is added in cycle number 24 (arbitrary for each test). Cycles 23 and earlier contain only a single fuel pulse each

engine cycle. Cycles 24 and later contain both the base pulse and the dynamic pulse each engine cycle. However, the in-cylinder fuel measurement (from the FFID: 'x' symbols) for cycle #24 has not responded to the extra fuel at all, it still measures a lean in-cylinder fuel level (λ~1.2). It is not until cycle #25 that slightly over half of the extra fuel is seen. Then a few cycles later the steady-state value is reached. Thus, with the currently positioned dynamic pulse, essentially none of the fuel reaches the combustion chamber on the current cycle. Despite OVI, most of the injected fuel must impact the intake port and valve surfaces first, thus leading to wall wetting surface fuel delays. Since this dynamic pulse is in the later half of the intake valve open period, intake port air velocities have reduced significantly since the piston is approaching bottom dead center. This effect strongly reduces the convective mass transfer effect of the fluid films into the combustion chamber.

A sweep of dynamic pulse locations was performed in order to see if earlier dynamic pulse locations would allow for induction of fuel into the combustion chamber on the current cycle. **Figure 4.4** shows the results from that sweep at 1500 rpm. It is seen that for EOI locations before ~600 cadeg, most of the extra dynamic fuel enters the combustion chamber on the current cycle. However, for the later half of the intake event period very little of the dynamic pulse enters. Scheduling of the dynamic pulse thus must occur before mid-intake stoke. At higher engine speeds this timing will need to be further advanced.

Since the production controller dynamic fuel pulse does not enter the cylinder on the current cycle, in the following analysis this dynamic pulse fuel mass will be applied to the analysis as if it were delivered/injected in the following-next cycle. For some transients, multiple dynamic pulses can occur. In each case, the dynamic injected fuel pulse is applied to the next cycle.

The difference in injection history is substantial whether the dynamic pulse is considered to enter the current or following cycle. **Figure 4.5** shows a comparison of the injection history during a fast throttle opening with the dynamic pulse applied both to the current

cycle, and the next cycle. Cycle #52 is the first cycle of the transient. With the dynamic pulse applied to the next cycle it is seen that the first cycle of the transient receives the same fueling as the stabilized light load cycles. This is very plausible due to computational and transport delays. Then in cycle #53 the dynamic pulse is added to the normal injection amount leading to a high second cycle of transient fueling for the carried over dynamic pulse.

4.3.2 Closed Valve Step Fuel Experiments

Figure 4.6 shows results from one of the above dynamic step fuel experiments in which the second dynamic pulse was added while the intake valve was still closed. This experiment is very similar to a step fuel experiment where at some point (closed valve) the FPW is increased by a significant factor and the A/F response is evaluated.

The additional closed valve dynamic pulse was added in cycle #23 for this run (the cycle number for the fueling change is arbitrary). It can be seen in **Figure 4.6** that almost all of the dynamic pulse entered the combustion chamber on the current cycle as evidenced by the in-cylinder FFID response immediately changing from λ=1.13 to λ=0.77 on cycle #23 which received the extra injected fuel. The response for a similar closed intake-valve step-fuel experiment (FPW lengthened instead of 2nd pulse on the same cycle) was very similar.

Another interesting result of this experiment is the UEGO response. On the first cycle with the extra-injected fuel, the exhaust based UEGO analysis for cycle #23, only indicated that an in-cylinder λ=0.9 was achieved. Using this step fuel method to characterize 'x' for the x-τ model results in x=0.5. However, the slow throttle uncompensated technique showed that x=0.3. Using the FFID signal with the step experiment, x=0.15.

Thus, the step fuel UEGO response is characteristic more of its time delay constant (~200 msec) rather than puddle dynamics. It is clear that using Fuel Step methods with a

UEGO for characterizing puddle dynamics is not a prudent approach. But what about the value of 'x' generated by the FFID step fuel response? This will be answered shortly.

4.4 Absolute Port Fuel Levels

It is generally agreed that intake port fuel levels increase with engine load at a given engine coolant temperature. Throttle transient experiments are able to quantify a residual fuel mass change, but absolute fuel mass levels cannot be established with this technique. In an effort to both verify the puddle mass increase amount, and to understand the initial starting and ending absolute equilibrium fuel masses, experiments were performed to estimate these residual fuel levels and how they change with load.

The engine was run at steady-state operating conditions at both light and high loads. The injector to cylinder #4 (with the FFID in-cylinder) was disabled while data was being acquired. The other 3 cylinders continued to operate, and thus the residual fuel in intake port (and cylinder) #4 was 'pumped out'. The resulting signal with the engine run at 0.4 bar p_i is shown in **Figure 4.7**. It is seen that for the first cycle without fuel injection the signal drops to approximately 1/3 the stabilized level with fuel injection. Following cycles show an asymptotic decay towards zero. In this case the PCV system was vented to the exhaust trench. If the PCV system were still connected to the intake manifold, the signal would not decay to zero after injector disablement, but would continue to show FFID peaks at 5-10% of the injection FFID level.

The voltage decay behavior for the first ten cycles following injector disablement at both 0.4 and 0.9 bar pi are shown in **Figure 4.8**. At each engine load, ten draining experiments were performed. The error bars represent +/- two standard deviations in the data. It is evident that the higher engine load clearly possesses more residual fuel.

A calibration file was taken prior to each injector disablement with the engine running at λ=1. This was used to quantify the mass of fuel passing through the cylinder for each

cycle following disablement. The sum of these fuel masses led to an estimation of total intake port residual fuel. It should be pointed out that the FFID calibration is taken at λ=1.0. These stabilized engine (engine coolant ~90 C) draining cycles have very high-lean λs (λ>2), thus the calibration could be in error for such very lean cycles.

Estimates of residual intake port fuel at 1500rpm at 0.4 and 0.9 bar p_i indicate that approximately 5 mg of fuel resides in the intake port at the light load and 32 mg of fuel resides in the intake port at high load. Thus a change of approximately 27 mg of fuel occurs during a throttle opening from 0.4 to 0.9 bar p_i. This corresponds to roughly one extra high load injection unit.

A few experiments were performed in order to elucidate how quickly this change occurs during the throttle transient. **Figure 4.9** shows the estimated fuel mass per cycle (after injector disablement) for disablement that occurs immediately after a fast throttle opening (once the high load is achieved), and for disablement that occurs approximately 1.5 seconds (~20 engine cycles) after the high load is achieved. Again, each condition was repeated ten times, and the error bars are indicated. At the 95% confidence interval (C.I.), there appears to be no difference between the two cases. The averages, however, indicate that slightly less fuel was in the intake port when disablement occurred immediately after the throttle opened. Regardless, it appears that for fast throttle openings, the intake port residual fuel level has reached its stabilized level in the time frame of the transient itself.

4.5 Throttle Rate Effect

4.5.1 Data for slow and fast throttle openings (compensated and uncompensated)

The fueling behavior at 1500 rpm for a slow throttle ramp rate is shown in **Figure 4.10**. The intake pressure was raised from 0.4 to 0.9 bar in approximately one second (~13 cycles). For the data in **Figure 4.10**, transient fuel compensation was not used. The

amount of injected fuel for each cycle was determined by the speed-density method with a pre-calibrated volumetric efficiency and the desired λ at stoichiometric (in the compensated case the desired λ is less than one in order to account for puddle filling). In this slow throttle transient, the in-cylinder fuel mass frequently slightly lagged the injected mass (**Figure 4.10a**-top graph in **Figure 4.10**). With no transient compensation applied, the in-cylinder charge equivalence ratio λ drifted towards 1.1 for many cycles during the transient (**Figure 14.10b**-below **14.10a**). The puddle increment per cycle (**Figure 14.10c**) was calculated from the difference of the cycle injected fuel mass f_i and the in-cylinder fuel mass m_I, which was obtained from the FFID signal. The filling of the puddle which was a result of the slight difference in the values of f_i and m_i in each cycle, was a gradual process (**Figures 14.10c, d**) with an increment of less than 3 mg per cycle. It should be noted that In calculating the cumulative puddle increment, any slight offset error of the FFID signal is cumulative. Therefore the absolute level of the cumulative puddle increment may not be precise.

The fueling data for the same slow throttle ramp, but with transient fuel compensation, are shown in **Figure 4.11**. The amount of compensation was small so that injected fuel was not very different from the uncompensated case. Yet during the transient, the in-cylinder relative air-fuel ratio stayed closer to 1 than in the uncompensated case.

The fueling behavior for an uncompensated fast throttle ramp is shown in **Figure 4.12**. The intake pressure was ramped from 0.4 to 0.9 bar in approximately 0.25 sec. (3 cycles). No transient compensation was used: the injected fuel was equal to the stoichiometric fuel air ratio times the air inducted. Because the fuel delivered into the cylinder was less than the fuel injected, the mixture experienced a lean spike for two cycles (**Figure 4.12b**).

When the production EEC transient compensation was applied, the response is shown in **Figure 4.13**. The in-cylinder mixture exhibited a one-cycle lean spike at the first cycle of the transient, and then in the next cycle, it went substantially rich (λ~0.7) before relaxing back to stoichiometric.

For the data in **Figure 4.13**, the record of the injector pulses indicated that for the first

cycle (cycle 52 in the figure) of the fast ramp, the base injection had the same pulse width as the previous cycle (which was before the throttle movement). Then a dynamic pulse was added. This pulse started at 640° CA and ended at 670° CA. (All crank angles are referenced to BDC of compression stroke of the cycle. The timing for the intake period was IVO at 540°; IVC at 770°). For cycle 52, however, the FFID measurement showed that the fuel delivered to the cylinder was the same as the previous cycle: i.e., very little of the fuel supplied by the dynamic pulse during open-valve injection actually went into the cylinder. This effect is consistent with the above described step-fuel experiments. Thus, as with the case in the step-fuel experiments, very little of the fuel went into the intended cycle and the dynamic pulse fuel was retained in the port for the next cycle. Therefore in the fuel accounting procedure, this dynamic pulse fuel was added to the fuel for the next cycle (Cycle 53; see top graph of **Figure 4.13**). Thus the lean spike in **Figure 4.13** occurred because effectively the injected fuel had not responded to the increase of air charge in the rapid throttle transient. The rich spike in the next cycle was partly due to the addition of the fuel of the dynamic pulse to that cycle.

The fueling behavior at a medium-fast throttle ramp rate (0.4 second or 5 cycle ramp) using EEC control is shown in **Figure 4.14**. The ramp from 0.4 bar to 0.9 bar MAP started from cycle 68. No lean spike was observed. There were two rich cycles (69 and 70) at λ ~0.8. For this ramp, there was a dynamic pulse each on cycles 68 and 69. The associated fuel had been shifted by one cycle as discussed in the previous paragraph.
The fueling behavior of a medium-slow throttle ramp rate (0.8 second or 10 cycle ramp) under EEC control is shown in **Figure 4.15**. The in-cylinder mixture stayed stoichiometric with no significant λ excursions.

Finally, a summary of fast and slow throttle transients both with and without compensation is shown in **Figures 4.16 and 4.17**. For the same data in each of these two figures, on the ordinate is displayed the actual puddle increment per cycle and the

fraction of injected fuel that goes into the puddle per cycle for **Figures 4.16 and 4.17**, respectively. The abscissa shows MAP. Each symbol represents a specific engine cycle. Before the transient at 0.4 bar pi steady state, approximately fifty data points are shown for each of the four cases. The variation of approximately +/- 1mg (+/- 7% injected fuel into the puddle is reflective of steady-state fluctuations in puddle behavior. At the high load, after the transients, approximately +/- 2mg of fuel per cycle (again approximately +/- 7% of injected fuel) is observed.

In **Figure 4.16** it is seen that a general trend of increasing puddle increment with increasing MAP is seen for all cases. However as MAP increases, so does FPW. So, the data was normalized to the current cycles injected fuel mass. This is shown in **Figure 4.17**, and is described next.

As the throttle transients occur (MAP changing from 0.4 bar pi to ~0.9 bar pi), the fraction of injected fuel that stays in the puddle is shown for the four cases. It is seen that for the fast and slow compensated cases along with the fast uncompensated case, the fraction of injected fuel is approximately stable during the transient at a nominal value of roughly 8%. From cycle to cycle during the transient in these cases, variations of 5 to 14% are observed. This range of variation is also typical of the steady-state conditions as mentioned above.

The case of the uncompensated slow transient is interesting. Some slow uncompensated transients demonstrate this behavior, while others are very similar to the slow compensated case. In this slow uncompensated transient, the fraction of injected fuel to the puddle cycles from 0% to 12% from cycle to cycle, with an average that roughly behaves as the above cases. It is possible that for a given cycle, after filling the puddle with 12% of the injected fuel, the puddle is overfilled. Then for the next cycle, the quasi-stable level of the puddle is already satisfied until the load incrementally increases again on the following cycle.

With this approximate constant fraction of injected fuel staying in the port as MAP

increases, regardless of throttle rate or fueling strategy, it is evident why the puddle filling rate is roughly proportional to throttle rate. Fast throttles attain their final high MAP level in a couple engine cycles. At high MAPs the absolute increase in puddle per cycle is more than double that of light MAPs. This leads to faster filling of the puddle for fast throttle openings.

4.5.2 Discussion

The above results showed that during fast throttle transients (**Figure 4.13**), the fuel injection as controlled by the production EEC unit tended to deliver to the cylinder a mixture with significant lean and/or rich excursions. A major cause of this behavior was the inability of the dynamic pulse to deliver the fuel to the current cycle. Of interest are the following two questions for the fuel behavior in fast throttle transients:

(a) Given the corrected fuel injection schedule, does the x-τ model predict the in-cylinder value of λ with the x-τ values from the engine calibration?

(b) If the dynamic pulse were able to deliver the fuel to the current cycle, would the transient compensation be correct?

To answer (a), the x-τ model was applied to the record of the injection schedule throughout the throttle ramp. (As discussed before, the fuel supplied by the dynamic pulse was shifted to the subsequent cycle). A single fixed set of values of x and τ was used for all the throttle transient simulations. These values were the ones used by the EEC unit for transient fuel compensation; they were originally obtained by fitting the x-τ model to the exhaust λ for a slow throttle ramp rate (1 second ramp time). The results for the fast throttle transient are shown in **Figure 4.18**. (The horizontal scale had been expanded from the corresponding **Figure 4.15** for clarity.)

The x-τ model predicted the fuel behavior in excellent agreement with the FFID observations. Both the lean and the rich spikes in λ were reproduced.

4.5.3 Application of x-τ model (fast/med/slow throttles)

The comparisons of the observed in-cylinder λ and the values predicted by the x-τ model for the remaining throttle transient experiments are shown in **Figure 4.19**. Data from throttle transients both with and without fuel compensation are included. In all cases, the x-τ model gave excellent agreement with the measured in-cylinder value. Thus, the answer to question (a) is yes; that the x-τ model with constant x and τ values is valid for the throttle transients independent over the range of ramp rates tested.

4.5.4 Application of model to intended fueling strategy

Now that we have established the validity of the x-τ for calculating the fuel delivery to the cylinder for a given injection sequence, the model could be used to address question (b). With the fuel assigned in the dynamic pulse placed back to the cycle for which it was intended, the x-τ model was exercised for the resulting injection sequence. The results are shown as triangle symbols in **Figure 4.20** for the transient with the fast throttle ramp rate. With such an injection schedule, there would be no lean spike, but the first cycle was substantially rich (λ = 0.7). Thus, if the fuel introduced by the dynamic pulse were delivered to the intended cycle, the amount would have significantly over-compensated the fuel lag.

Various calibration strategies have different ways of determining the amount of fuel introduced by the dynamic pulse. They are all based on the latest estimation of the air to be inducted by the cylinder (i.e., the information after the base injection). The estimate may come from calibrated filtering of the throttle body air-flow sensor signal for engines equipped with such sensors, or from extrapolation of the intake pressure signal for engines with MAP sensor and using the speed-density method. These estimates are usually calibrated at a slow ramp rate because the calibrations are usually done with the slow response UEGO sensor. Therefore when the method is applied to fast throttle ramp rates, the air charge estimate may be erred.

4.6 Discussion of Manifold Filling Relationship

This Zetec Engine uses a hot wire Mass Air Flow Sensor (MAFS) for determination of in-cylinder air mass. During steady-state operation (constant engine speed, load and temperature), the calibrated MAFS can accurately indicate in-cylinder air mass. However, during throttle transients, 'filling' of the intake manifold must occur as the throttle is opened and intake manifold pressure increases in order to increase the density of the air in the intake system accordingly. Likewise, during a deceleration, manifold emptying must also occur.

Figure 4.21 shows the production raw MAFS signal during a fast and slow throttle transient from the Zetec engine. Additionally, MAP is shown from the research MAP sensor used on the intake manifold plenum. It is evident that during the throttle opening the MAFS signal has a significant voltage (mass air flow ~ voltage) overshoot. This is a result of the manifold filling effect.

In production applications using a MAFS, appropriate management of this overshoot must be employed in order to achieve accurate in-cylinder air mass estimates. For intake manifold volume to displaced engine volume ratios less than 1, the manifold filling effect is small. With ratios greater than 1, air mass adjustments must be made. Equation 4.1

$$\frac{dm_{cylinder}}{dt} = \frac{dm_{throttle-sensor}}{dt} - \frac{V_{manifold}}{RT} * \frac{dp_i}{dt} \qquad (4.1)$$

(below) is the conservation of mass equation for a control volume around an intake system:

The first term on the RHS of the equation is the changing MAFS signal. The second term on the RHS is the filling/emptying term. Unfortunately p_i is not known, so look-up tables must be used to generate p_i. Inherent in the determination of p_i is the volumetric efficiency (η_v) of the intake system. Volumetric efficiency is a strong function of many

variables [4.6]. It is errors and inaccuracies in this inferred intake pressure determination (e.g. filter constants for the raw MAFS signal during transients) that can lead to errors in air mass determination (LHS of equation 4.1).

From the author's experience at Ford Motor Company, the term $V_{manifold}$ was also used to 'optimize' the air mass estimation process. Frequently values 20% different from the true-physical $V_{manifold}$ would be employed/calibrated in an effort to improve performance (in other words this approach would attempt to correct for errors elsewhere in the calculation). These 'optimized' $V_{manifold}$ values would often show engine speed dependencies, but with a single calibrated value for $V_{manifold}$, a compromise would need to be made.

This study was not intended to focus on engine control algorithms and calibration. The above mentioned basic manifold filling and transient fuel descriptions were given as a simple general introduction to the topic. Much of the details of these control algorithms are proprietary, and thus the author cannot describe in detail here the specifics of their models and implementation. The approach of this study was not intended to directly improve control software, but rather to observe the physical behavior resulting from the use of a production controller calibrated with state-of-the-art industry techniques.

In Section 4.5 it was observed that the x-τ model worked remarkably well across a range of throttle rates with a constant values of x and τ. This result shows that characterization of x and τ from a slow throttle opening (a UEGO in the exhaust can work well here) is also an appropriate characterization of the intake port puddle dynamics for fast throttle openings. In order to develop improved fuel control during the engine development process, follow up work on the manifold filling calibration (performed 1st before TFC work is done) will be necessary after the TFC calibration is developed. In practice, often, modification of the TFC (x and τ values) were used in an effort to tighten A/F control. It is now evident why such an approach was futile.

A more accurate manifold filling calibration is used at 2000 rpm (as shown in next section). At 2000 rpm more filtering of the MAFS signal is occurring leading to more accurate air mass estimations. At 1500 rpm the MAFS signal is not filtered enough. This leads to a higher than actual air mass estimation by the engine controller. This over-estimation of air mass was responsible for the very rich cycles during the fast and medium-fast throttle transients.

4.7 Speed and Load Effects on Transient Fuel Compensation

All of the throttle transients in Section 4.5 were performed at 1500 rpm with the engine load (intake pressure) changing from 0.4 bar to 0.9 bar. In this section some variations in load changes at 1500 rpm and at a higher speed, 2000 rpm, are presented in order to confirm the above observations.

4.7.1 Compensated 1500 rpm ½ Throttle Steps

Figure 4.22 shows a characteristic compensated fast throttle transient at 1500 rpm, with intake pressure jumping from 0.4 bar to 0.65 bar in a few engine cycles. The engine controller is using the same values for x and τ as above (0.3 and 0.4 sec), as well as for the model analysis in the figure. In the first cycle of the transient (cycle #34-**Figure 4.22b**) both the in-cylinder diagnostic (FFID) and the model predicts (from the experimental fueling history) that the in-cylinder λ goes slightly lean. The following cycle shows then both the experimental data and the model proceeding to a rich state (λ~0.8). The puddle increment per cycle (**Figure 4.22c**) is on the same order as the fast full transients (~5mg/cycle) but for a shorter duration of engine cycles. The cumulative puddle increase is slightly less than half that of a full transient. This behavior is very similar to the full transient (0.4 to 0.9 bar p_i) except of smaller magnitude, with excellent agreement by the x-τ model.

Figure 4.23 shows a fast throttle transient from 0.7 to 0.95 bar p_i. Again, as with the previous half throttle opening and the above full throttle openings (Section 4.5) the data and model are in excellent agreement. Thus a constant value of x and τ are good not only across a range of throttle rates, but also show excellent agreement for load increases of various magnitudes.

4.7.2 Compensated 2000 rpm Throttle Openings

Full throttle transients (0.4 to 0.9 bar p_i) were performed at one additional engine speed. At 2000rpm, the FFID's response time was near its upper limit for this application. In this case, the x and τ characterization from Ford were 0.25 and 0.35 sec. **Figures 4.24** and **4.25** show a slow and fast throttle opening, respectively. The slow throttle opening data shows a slight lean drift over the transient, with the model correctly predicting the experimental behavior. The fast transient data shows the characteristic lean spike during the first cycle of the transient. However in this case, the data (and model) move quickly towards stoichiometric operation after the first lean cycle. The significant rich excursions during the mid-transient are not observed as in the fast/medium-fast transients at 1500rpm. The difference is due to a more accurate manifold filling calibration-air mass determination.

The final cumulative puddle increase values at 2000 rpm are very similar to that observed at 1500 rpm for all throttle rates. Using Eqn. 3.5 for the steady-state puddle mass level estimation from the x-τ model, and generating a ratio of puddle mass: M(s.s. @ 1500)/M(s.s @ 2000 rpm)=1.05. This implies that the puddle should be approximately 5% larger at the lower engine speed. While this small difference is difficult to discern from the data, it is nonetheless consistent with the explanation that at higher engine speeds greater connective mass transfer of the puddle exists thus both lowering the retained fuel fraction ('x') and the time constant for puddle draining ('τ').

4.8 Fuel Effects on Compensated Response

Two single component fuels were chosen for additional throttle transient experiments. One very light fuel, iso-pentane reflects the very low end of the distillation curve with a boiling temperature of 35 degC and a molecular weight (MW) of 72. Second, a heavy single component fuel was also chosen to represent the upper end of the distillation curve. This fuel was cumene, C9H20 with a boiling temperature of 140 degC and a MW of 128. Both fuels were chosen due to their good octane ratings. The California Phase II reformulated gasoline used throughout the previous experiments has a T10 of 60 degC, a T90 of 180 degC and an average MW of 103.

For these throttle transients, with both single component fuels, the production controller with its transient compensation active (x=0.3 and τ=0.4, calibrated for gasoline) was used. Thus it is anticipated that the agreement between the in-cylinder data and the model will be in error.

4.8.1 Iso-Pentane Throttle Transients

A slow full throttle transient (0.4 to 0.9 bar pi) is shown in **Figure 4.26**. In part b of the figure, a comparison of in-cylinder FFID measurement is made against the x-τ model prediction. In this case, for the measured experimental fueling, the x-τ model predicts that the in-cylinder λ will stay about 1 during the throttle transient (cycles #33-45) as was the case for operation on gasoline. However, the actual experimental data shows that the in-cylinder λ goes ten percent lean for a few engine cycles. Thus, as was expected a deviation occurs between the model and data.

Some interesting behavior occurs as evidenced in part c and d of **Figure 4.26**. The puddle increment increases during the first half of the transient, and decreases during the second half, so that a net zero change in puddle increment was observed. This behavior was both repeatable, and unexpected.

The behavior is believed to be a result of flash boiling at the injector tip at light engine loads [4.7]. The fuel was run through an ice bath in order to keep its temperature around 20 degC, yet it nonetheless possesses a relatively high vapor pressure, especially at low intake pressures. This property can result in the injected fuel boiling upon exit from the injector tip. With flash boiling, an associated wide fan injector pattern results leading to significant upstream port wall wetting and fuel delay. This is occurring during the first half of the transient. As the intake pressure rises the flash boiling subsides and the injector returns to normal tight cone operation. The upstream port fuel evaporates and provides extra fuel during the later half of the transient (negative puddle increments) allowing the cumulative puddle mass to return near its original level.

Port draining experiments similar to that described in Section 4.4 using iso-pentane fuel showed very little residual intake port fuel. Absolute levels of a few milligrams of fuel were observed at light engine loads with only a few milligram increase at high engine loads. Thus, these results are consistent with the above throttle transient results.

Figure 4.27 shows a fast throttle transient with iso-pentane fuel. Due to the fast transition to high load flash boiling behavior was not observed. In this case, part b of the figure shows the anticipated model rich response for the fast throttle. The actual data, however, shows a significantly greater rich excursion than predicted by the model. This is due to the lack of fuel puddle delay with the volatile iso-pentane as compared to gasoline. Thus, nearly all of the injected fuel is entering the combustion chamber. As expected in part d of the figure, little change in the cumulative puddle is observed.

4.8.2 Cumene Throttle Transients

The heavy cumene fuel was also used for slow and fast throttle transients. **Figure 4.28** shows the slow throttle transient behavior. As with all the previous compensated slow throttle transients the model predicts (part b of the figure) good in-cylinder λ behavior around 1 during the transient. In this case however, due to the low volatility of the fuel, the experimental in-cylinder data shows a significant lean excursion (λ~1.1) throughout

the transient. More fuel is delayed upon entering the combustion chamber as compared to gasoline.

Figure 4.28d shows the cumulative puddle increment. The final puddle increase is observed to be around 40 mg. This level is approximately 10 mg higher than for the similar gasoline throttle transients. This analysis of cumulative puddle increment assumes that no fuel is lost to the sump. It is possible that this level is slightly overstated, since due to the heavy nature of cumene, some of the injected fuel might have been drawn in the combustion chamber and down to the sump as unevaporated liquid.

Curtis' four-puddle transient fuel model [4.8] predicts that the average molecular weight of the puddle changes from approximately 140 at light loads to 125 at high loads. The cumene experiments, with a MW of 128 are in rough agreement with the four-puddle model predictions.

Finally, **Figure 4.29** shows a representative cumene fast throttle transient. In part b of the figure, the experimental data shows a clear strong lean excursion (up to λ=1.3) due to the low volatility fuel. The model, calibrated for gasoline, shows the characteristic lean then rich A/F ratio behavior.

4.9 Cold Engine Throttle Transients

Limited throttle transient experiments were performed on a stabilized-cold engine. In this case, fresh plant water at 20 degC was continuously applied to the engine's water pump inlet. The coolant temperature raised a few degrees as it traveled through the engine leaving the thermostat housing at ~22 degC, where it was then dumped to the trench. Unfortunately, due to this quasi-steady cold engine operation (not characteristic of a true vehicle) it was not exactly clear as to the commanded x-τ model parameters by the production EEC processor so model comparison was not possible. Additionally, due to the cold engine, uncompensated throttle transients were not possible due to engine stumbles and stalls occurring without extra fuel during the throttle openings.

The cold engine transient area continues to be problematic for the automotive industry. Compensation schemes consistently over-fuel in order to be safe and deliver good drive-aways. However, the engine controls are far from optimized, and poor emissions performance, high unburned hydrocarbons and carbon monoxide result.

Figures 4.30 and **4.31** show medium-fast and medium slow stabilized-cold throttle transients. The production controller is seen to provide significant enrichment for long periods. Part of this enrichment is due to the open-loop x-τ model. The longer scale enrichment is most likely due to the closed-loop throttle controller providing additional enrichment due to the lean in-cylinder behavior.

Chapter 4 References

[4.1] Cheng, C.O., Cheng, W.K. and Heywood, J.B., "Intake Port Phenomena in a Spark Ignition Engine at Part Load", SAE#912401, 1991.

[4.2] Same as [4.1]

[4.3] Whelan, D.E., Kelly-Zion, P.L., Lee, C.F., Peters, J.E. and White, R.A., "Back-Flow Atomization in the Intake Port of Spark Ignition Engines", SAE#972988, 1997.

[4.4] Bauer, W., Balun, P., and Heywood, J. B., "Heat Transfer and Mixture Vaporization in Intake Port of SI Engine", SAE#972983, 1997.

[4.5] Yamada, T., Hayakawa, N., Kami, Y. and Kawai, T., "Universal Air-Fuel Ratio Heated Exhaust Gas Oxygen Sensor and Further Applications", SAE#920234, 1992.

[4.6] Heywood, J.B., Internal Combustion Engine Fundamentals, McGraw-Hill, 1988.

[4.7] Aquino, C.F., Plensdorf, W, Lavoie, G. and Curtis, E., "The Occurrence of Flash Boiling in a Port Injected Gasoline Engine", SAE#982522, 1998.

[4.8] Curtis, E.W., Aquino, C.F., Trumpy, D.K and Davis, G.C., "A New Port and Cylinder Wall Wetting Model to Predict Transient A/F Excursions in a PFI Engine", SAE#961186, 1996.

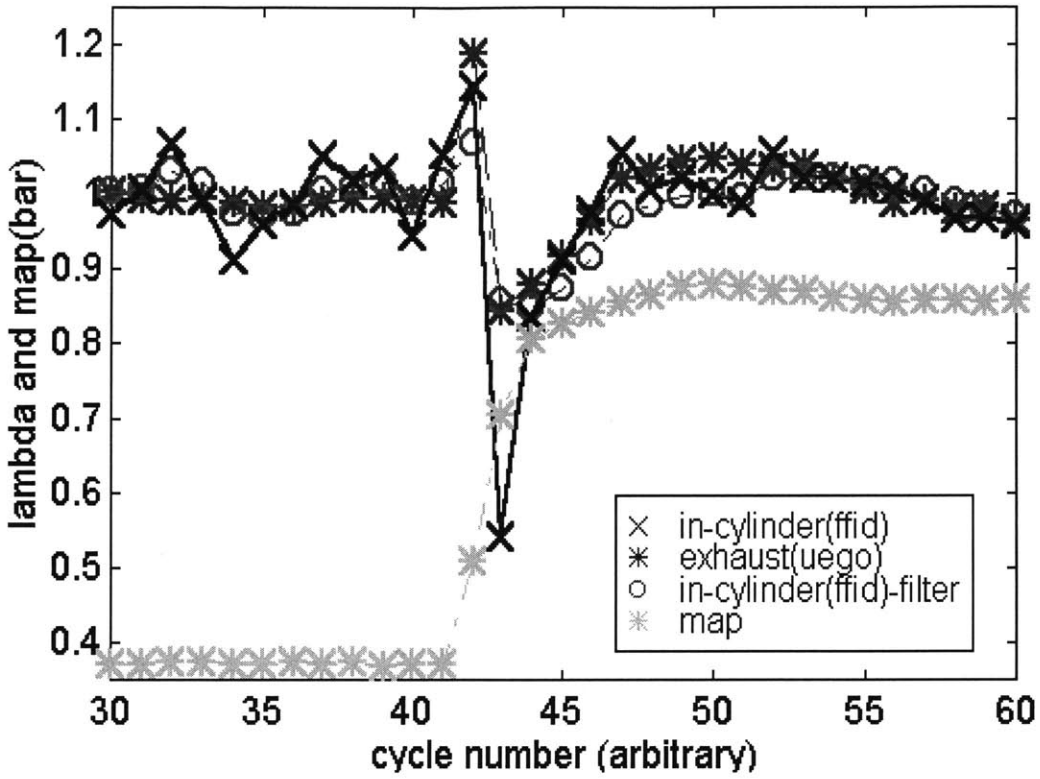

Figure 4.1: Correctly accounted dynamic pulse during production controller transient. Comparison of in-cylinder FFID signal to UEGO.

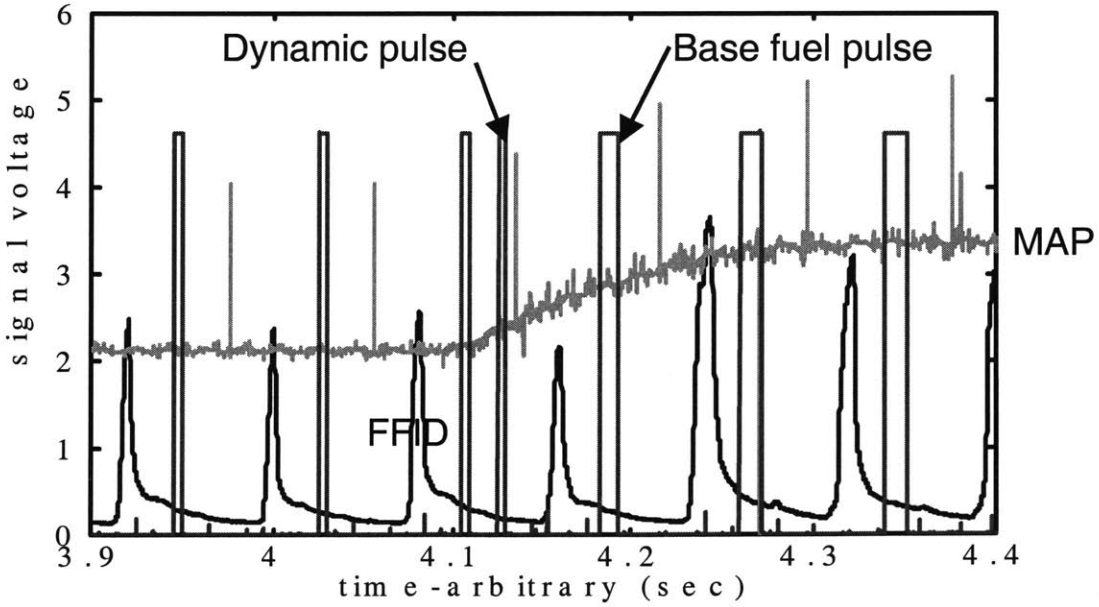

Figure 4.2: Raw fast throttle transient data: FPW, FFID in-cyl. and MAP.

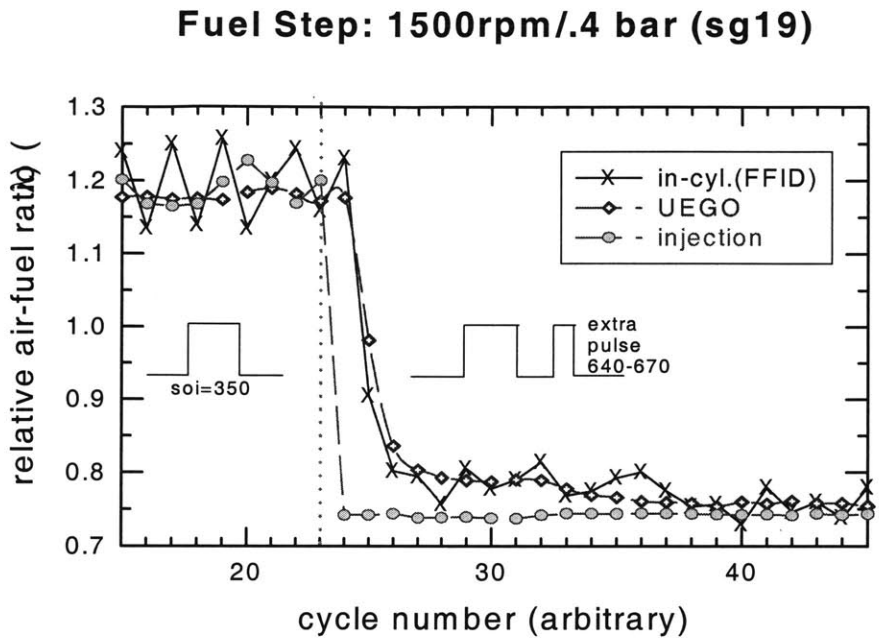

Figure 4.3: Experimental steady-state dynamic pulse during IVO at 1500rpm 0.4 bar pi. The pulse is located in the same location as the Production Controller.

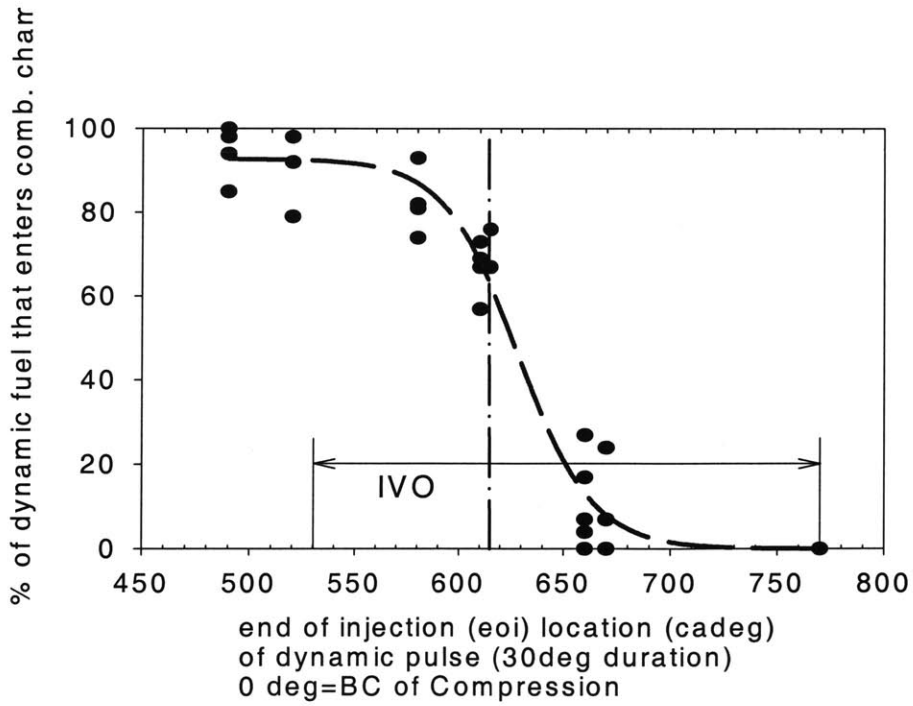

Figure 4.4: Percent of fuel in the dynamic fuel pulse that enters the combustion chamber on the current cycle at various injection timings; 1500 rpm, 0.4 bar pi.

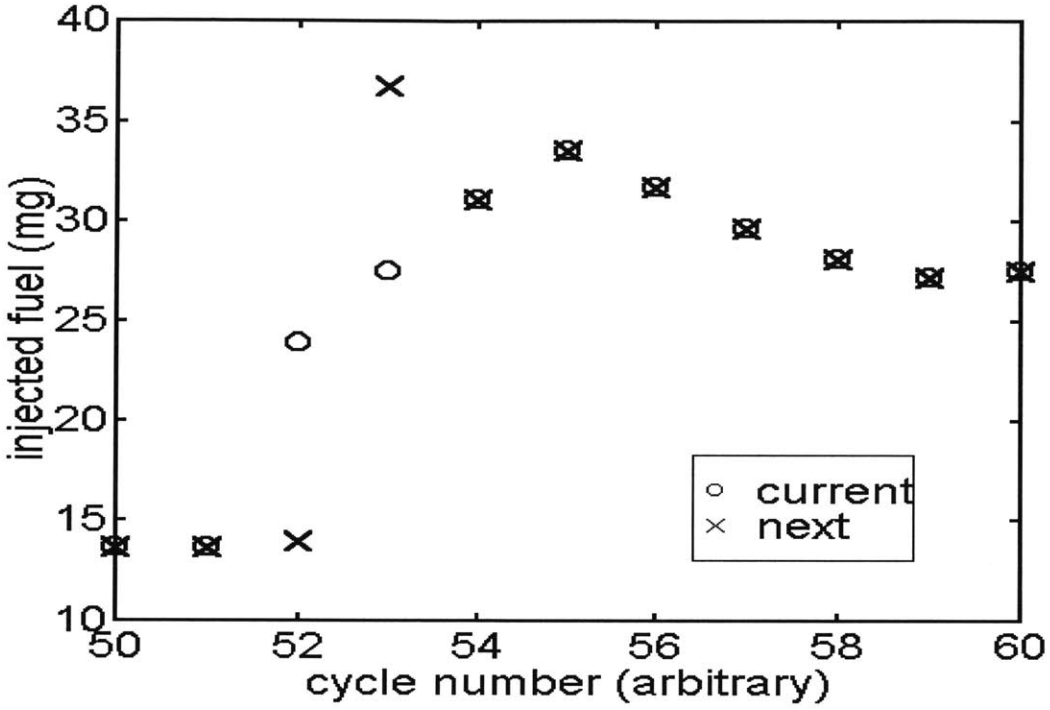

Figure 4.5: Production controller fast transients injection history with dynamic pulse applied to the current cycle and the following cycle.

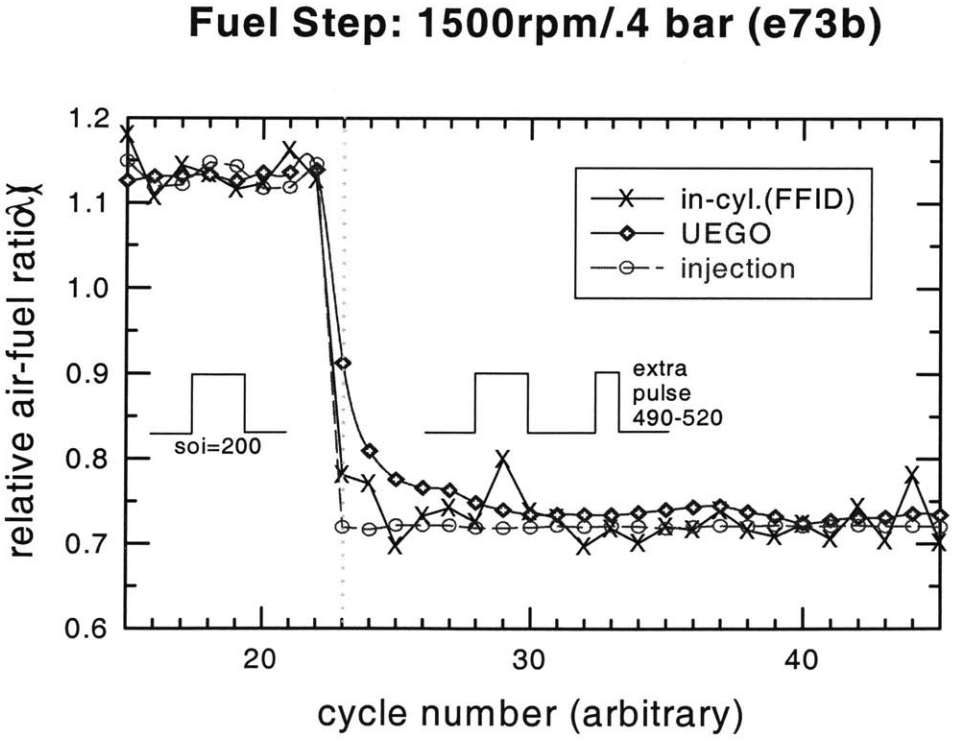

Figure 4.6: Experimental steady-state dynamic pulse during IVC

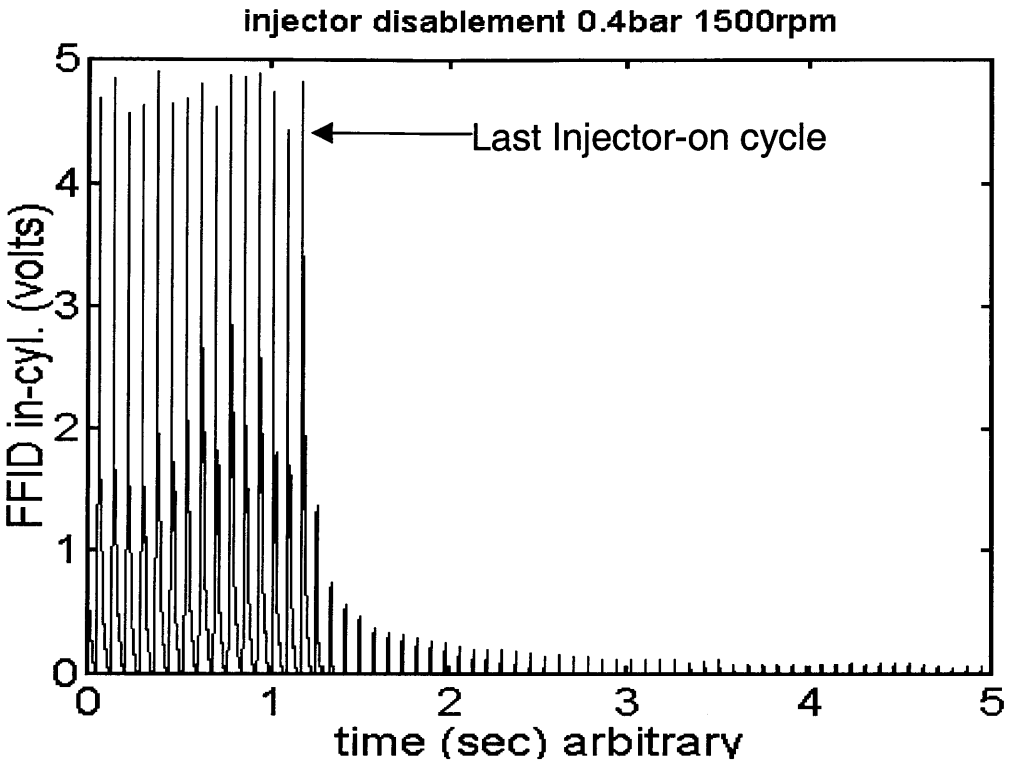

Figure 4.7: Raw FFID voltage decline after injector disablement.

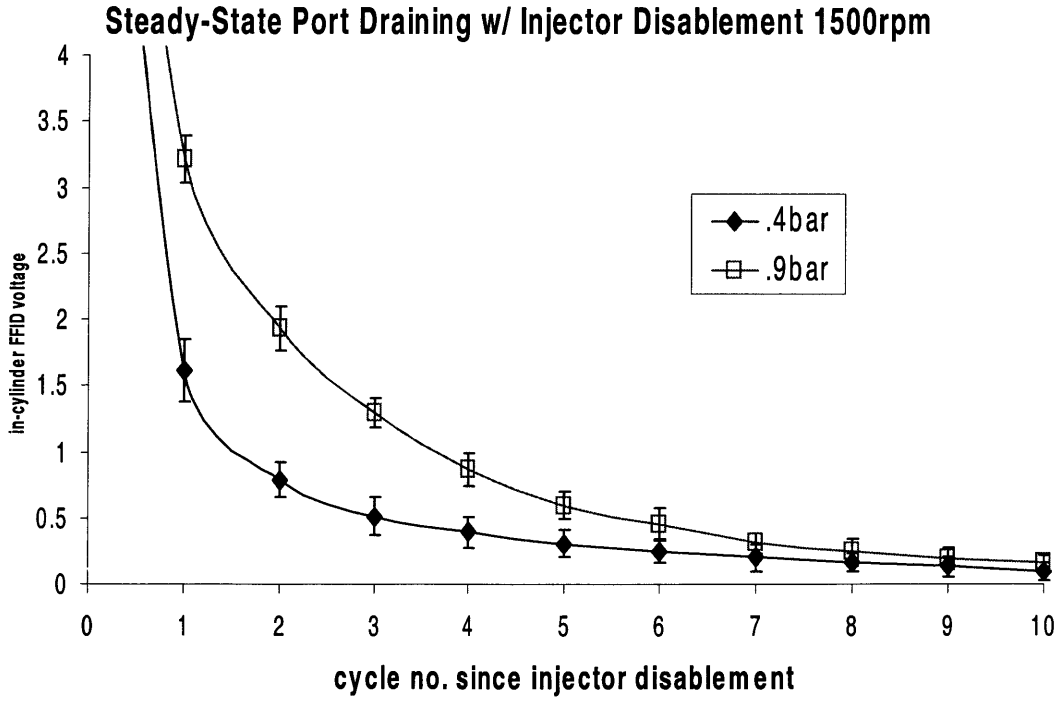

Figure 4.8: In-cylinder FFID voltage decay after injector disablement at 0.4 bar and 0.9 bar pi at 1500rpm. Error bars +/- 2σ (95% C.I.) 10 tests each.

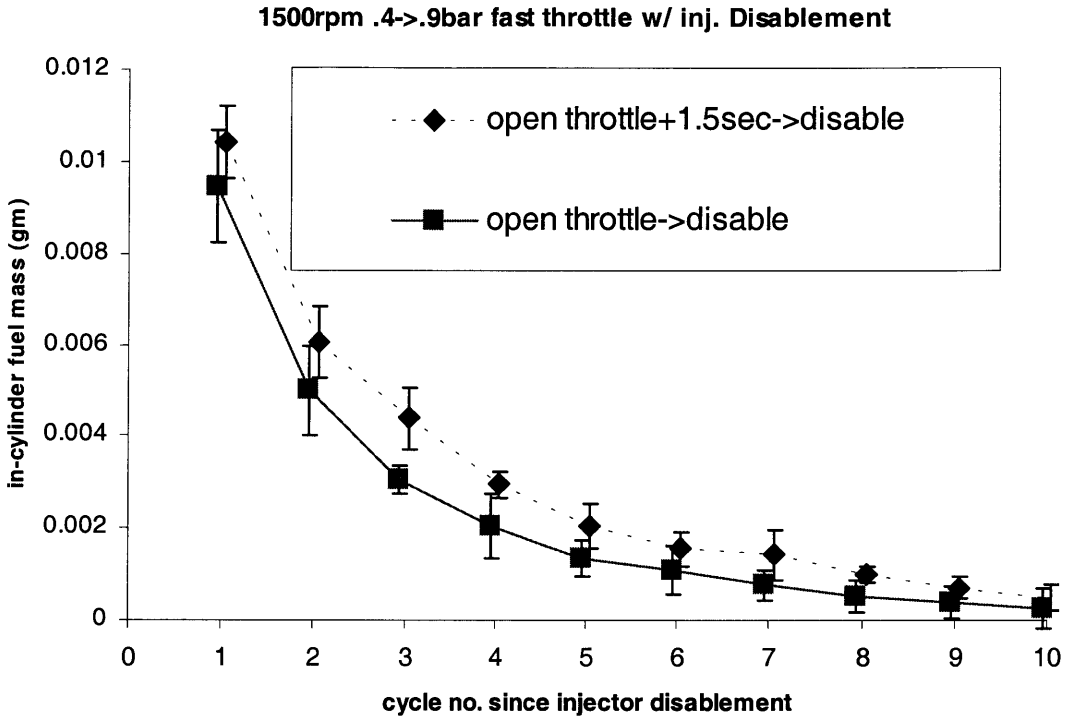

Figure 4.9: Cycle-by-cycle in-cylinder mass after throttle transient and injector disablement (draining). Error bars +/- 2σ (95% C.I.) 10 tests each.

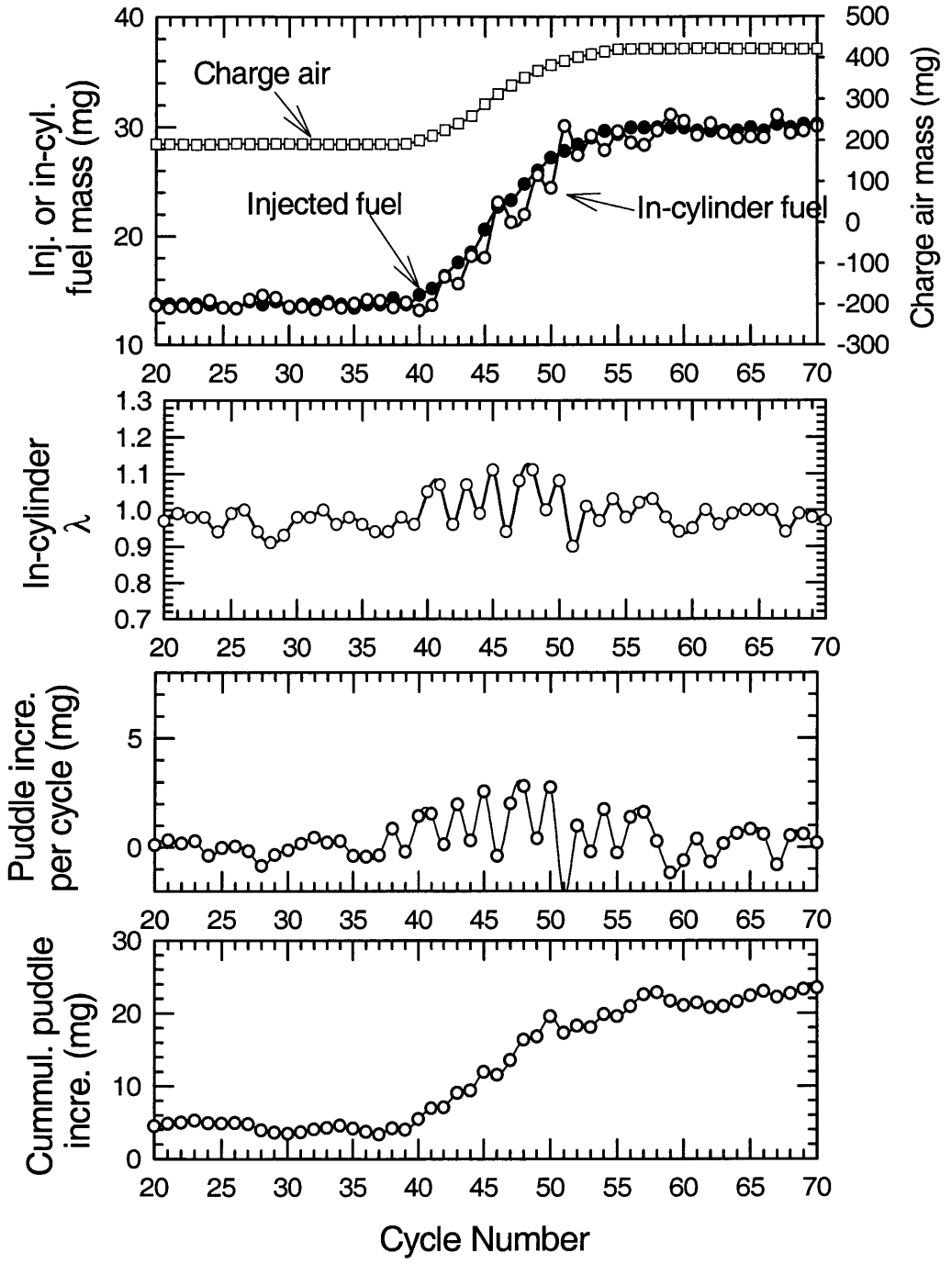

Figure 4.10: Fueling behavior for a slow throttle ramp (1 sec. ramp time). Engine operated at 1500 rpm; no transient fuel compensation was applied.

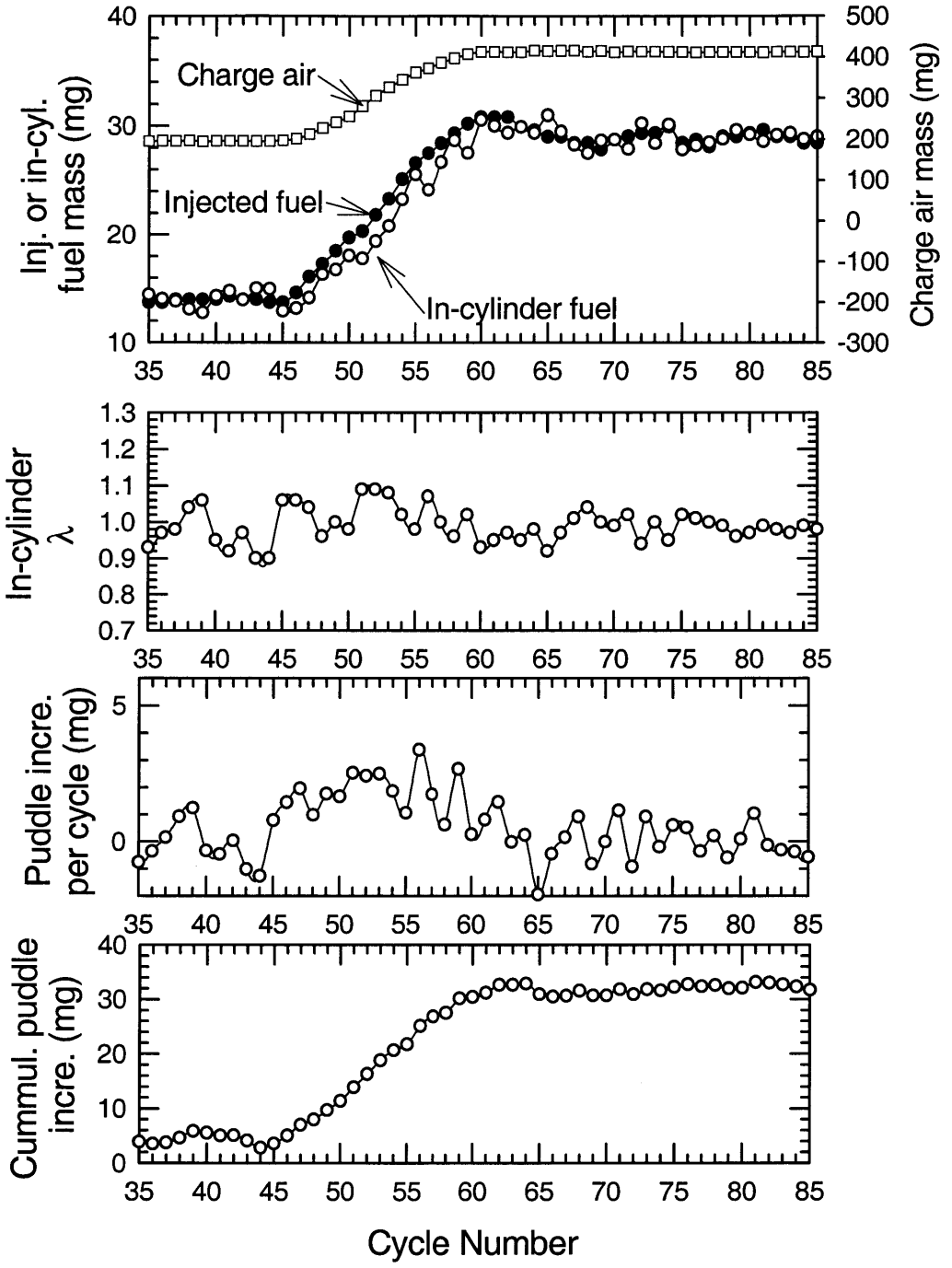

Figure 4.11: Fueling behavior for a slow throttle ramp (1 sec. ramp time). Engine operated at 1500 rpm; transient fuel compensation as controlled by the production EEC was applied.

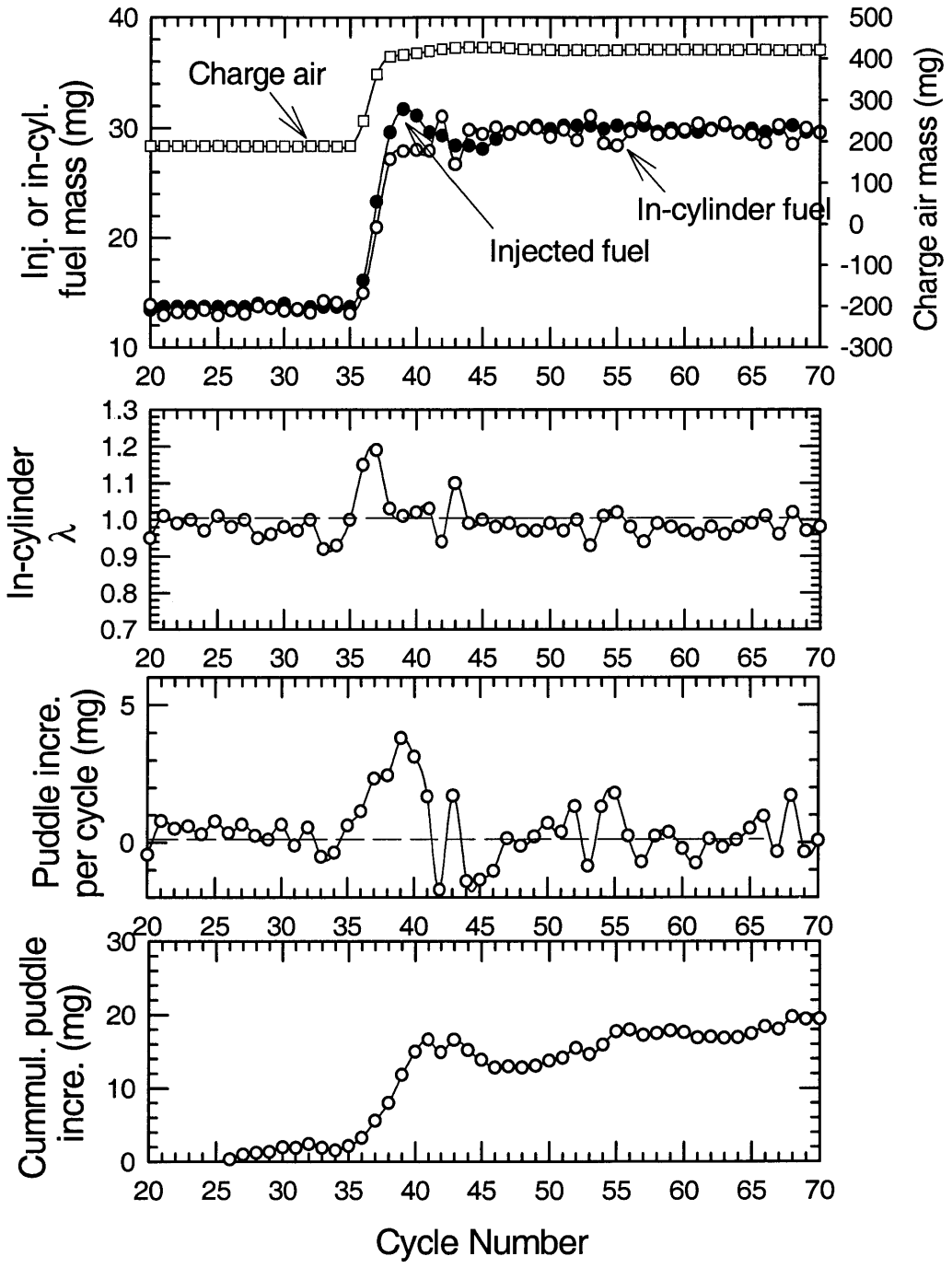

Figure 4.12: Fueling behavior for a rapid throttle ramp (~0.25 sec. ramp time). Engine operated at 1500rpm; no transient fuel compensation applied.

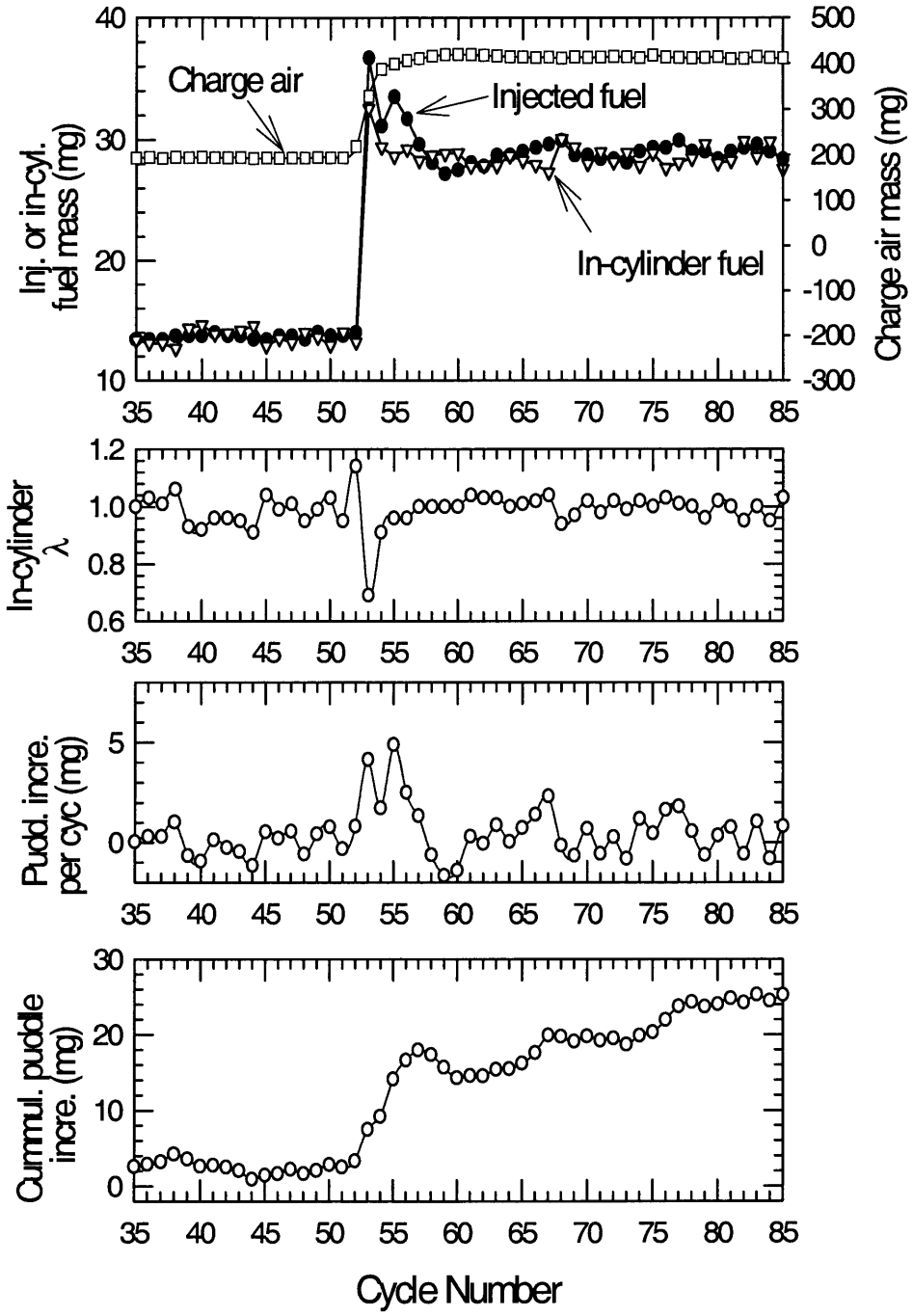

Figure 4.13: Fueling behavior for a fast throttle ramp (~0.25 sec. ramp time). Engine operated at 1500 rpm; transient fuel compensation as controlled by the production EEC was applied.

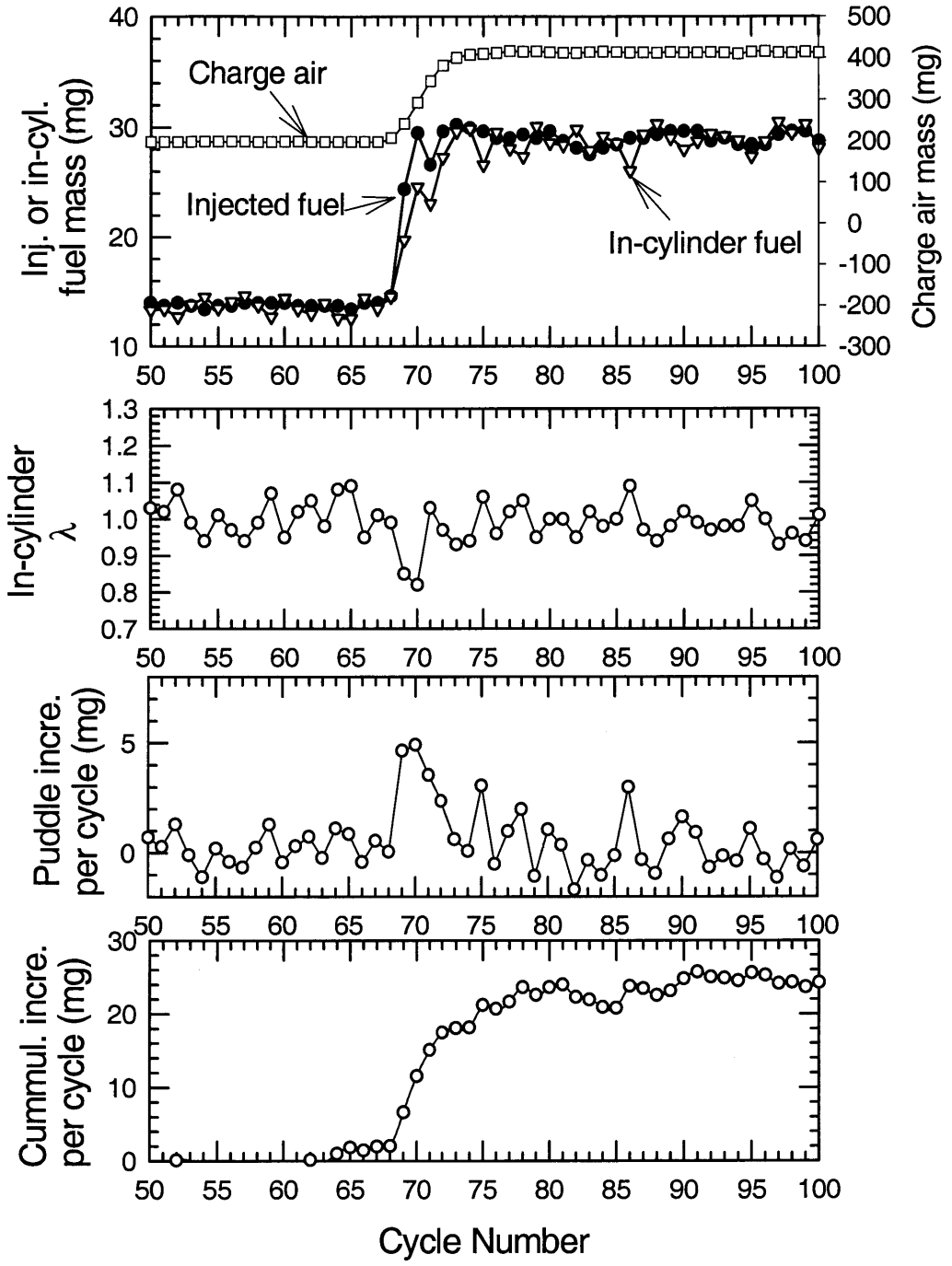

Figure 4.14: Fueling behavior for a medium-fast throttle ramp (~0.4 sec. ramp time). Engine operated at 1500 rpm; transient fuel compensation as controlled by the production EEC was applied.

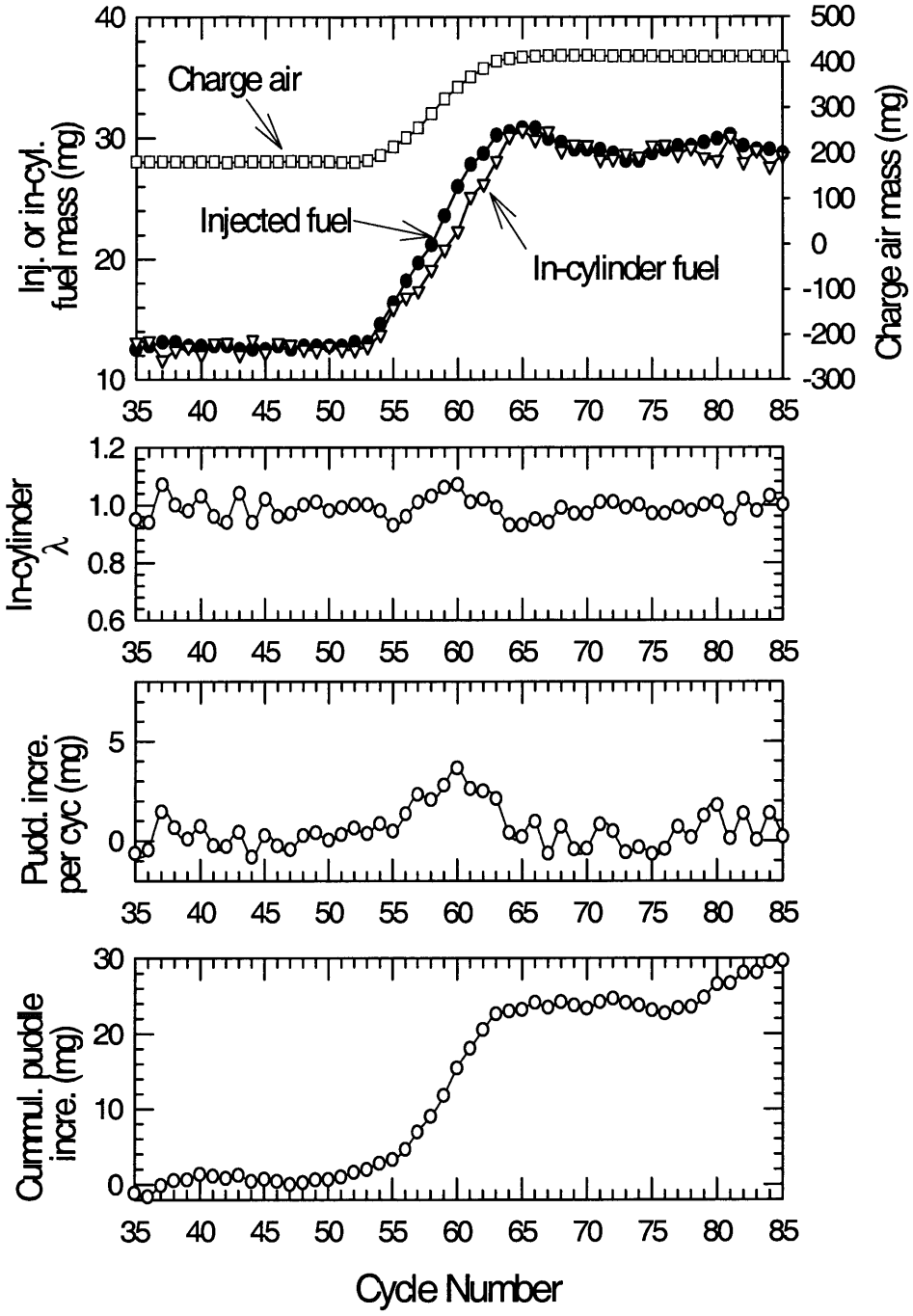

Figure 4.15: Fueling behavior for a medium-slow throttle ramp (~0.8 sec. ramp time). Engine operated at 1500 rpm; transient fuel compensation as controlled by the production EEC was applied.

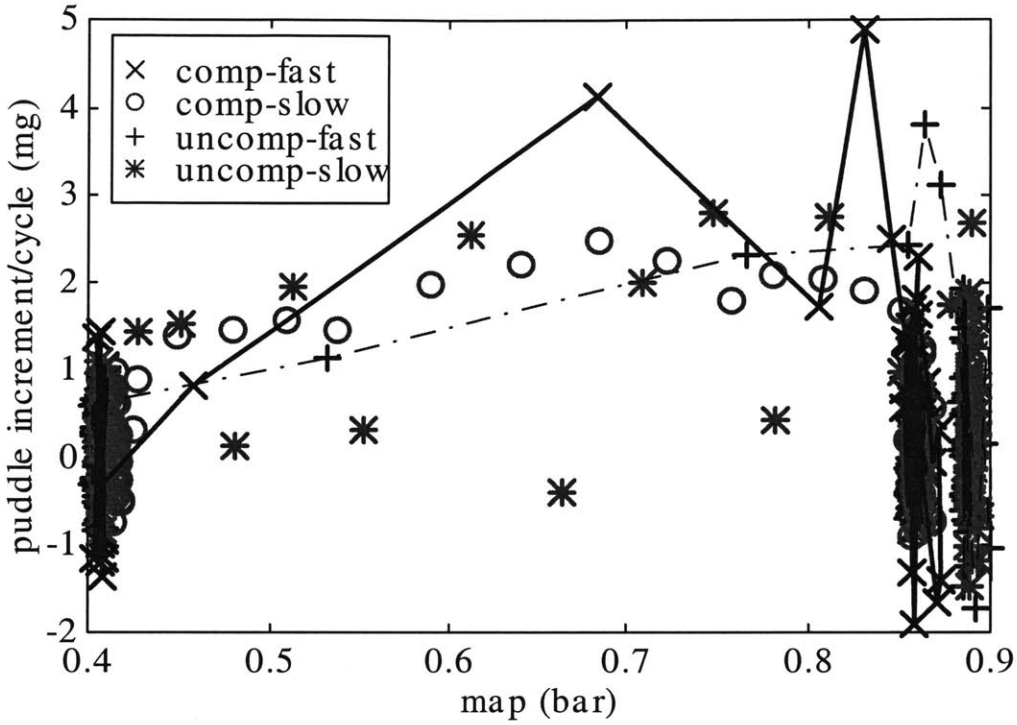

Figure 4.16: Puddle Increment per cycle (mg) for various throttle transients; 1500 rpm, 0.4 to 0.9 bar inlet pressure increase.

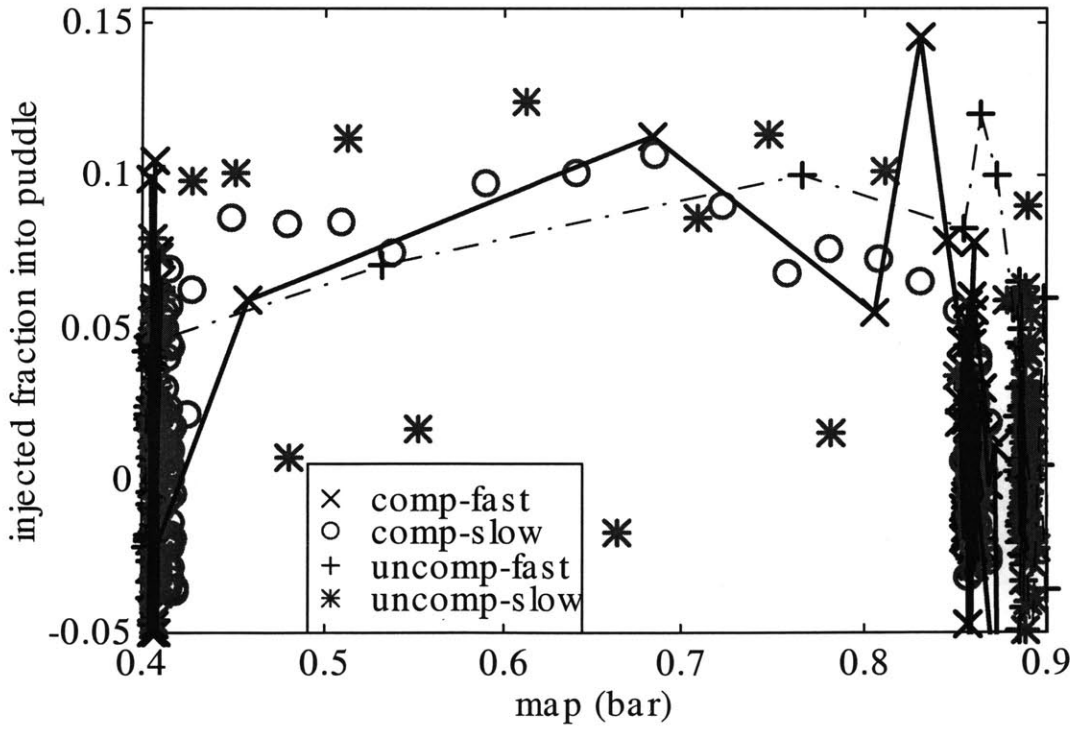

Figure 4.17: Normalized puddle increment per cycle for various throttle transients; 1500 rpm, 0.4 to 0.9 bar inlet pressure increase.

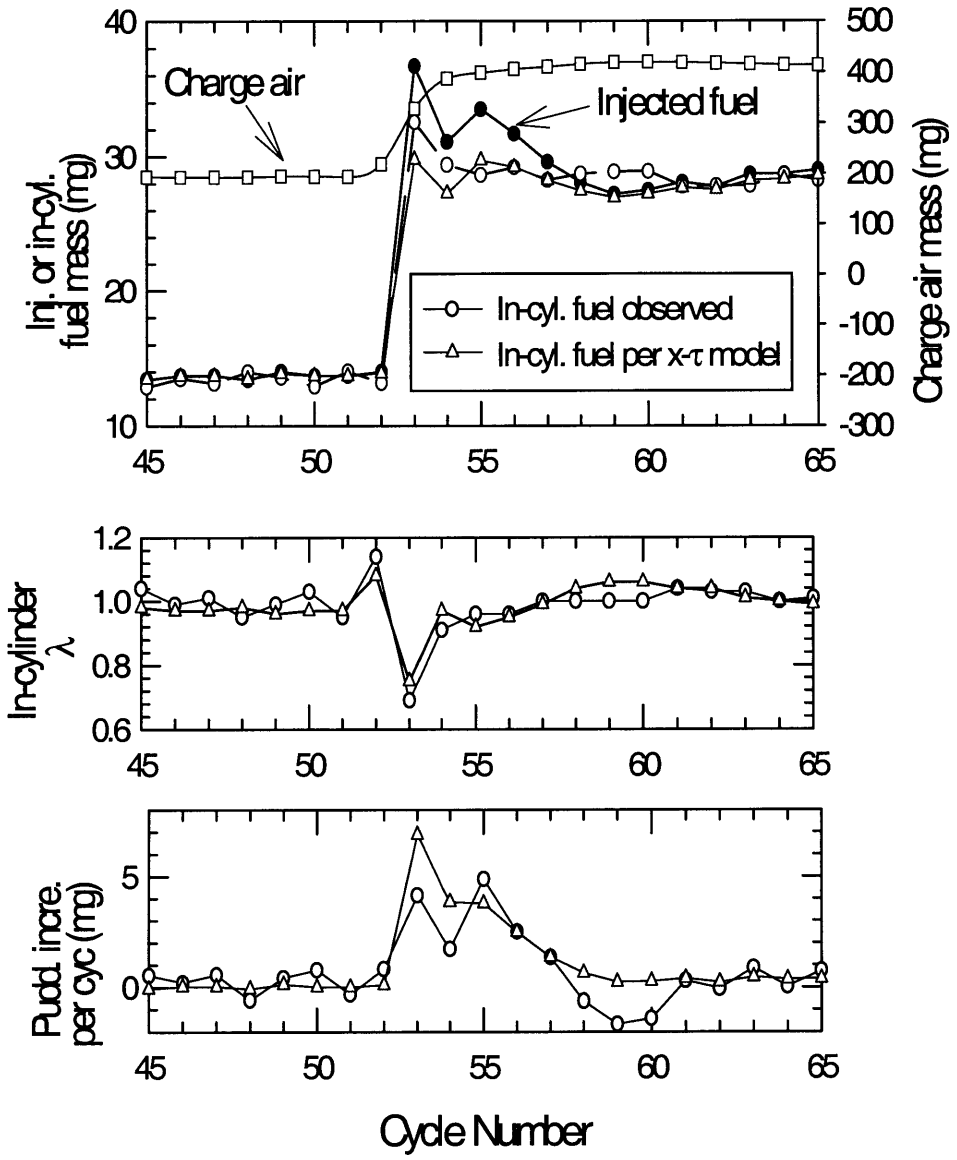

Figure 4.18: Comparison between the observed in-cylinder fuel and that as predicted by the x-tau model. Symbols: circle-observed valvues; triangl-computed values

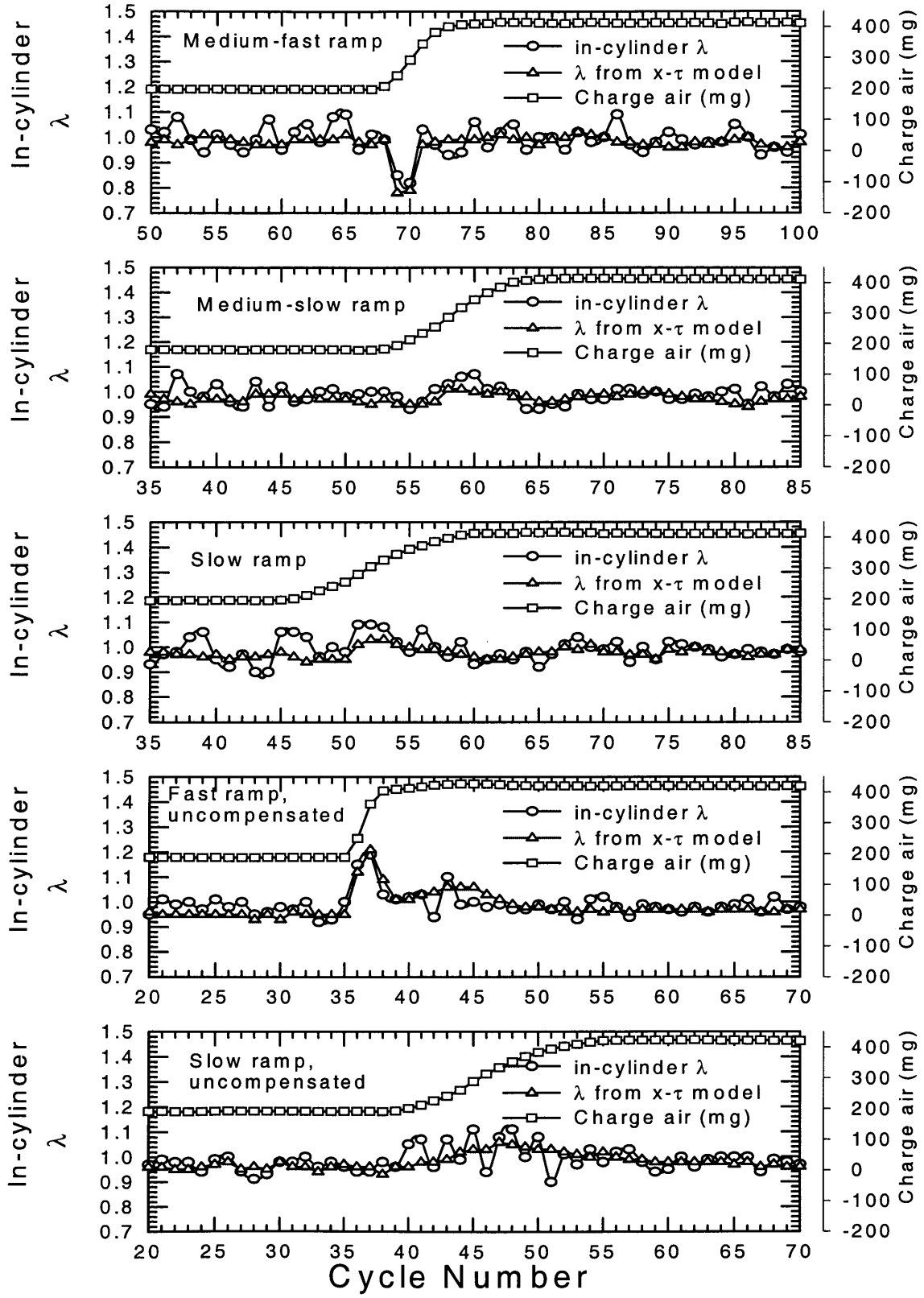

Figure 4.19: Comparisons of measured in-cylinder λ and the predicted values from the injected fuel based on x-τ model at different ramp rates. Data from transients with and without compensation are included.

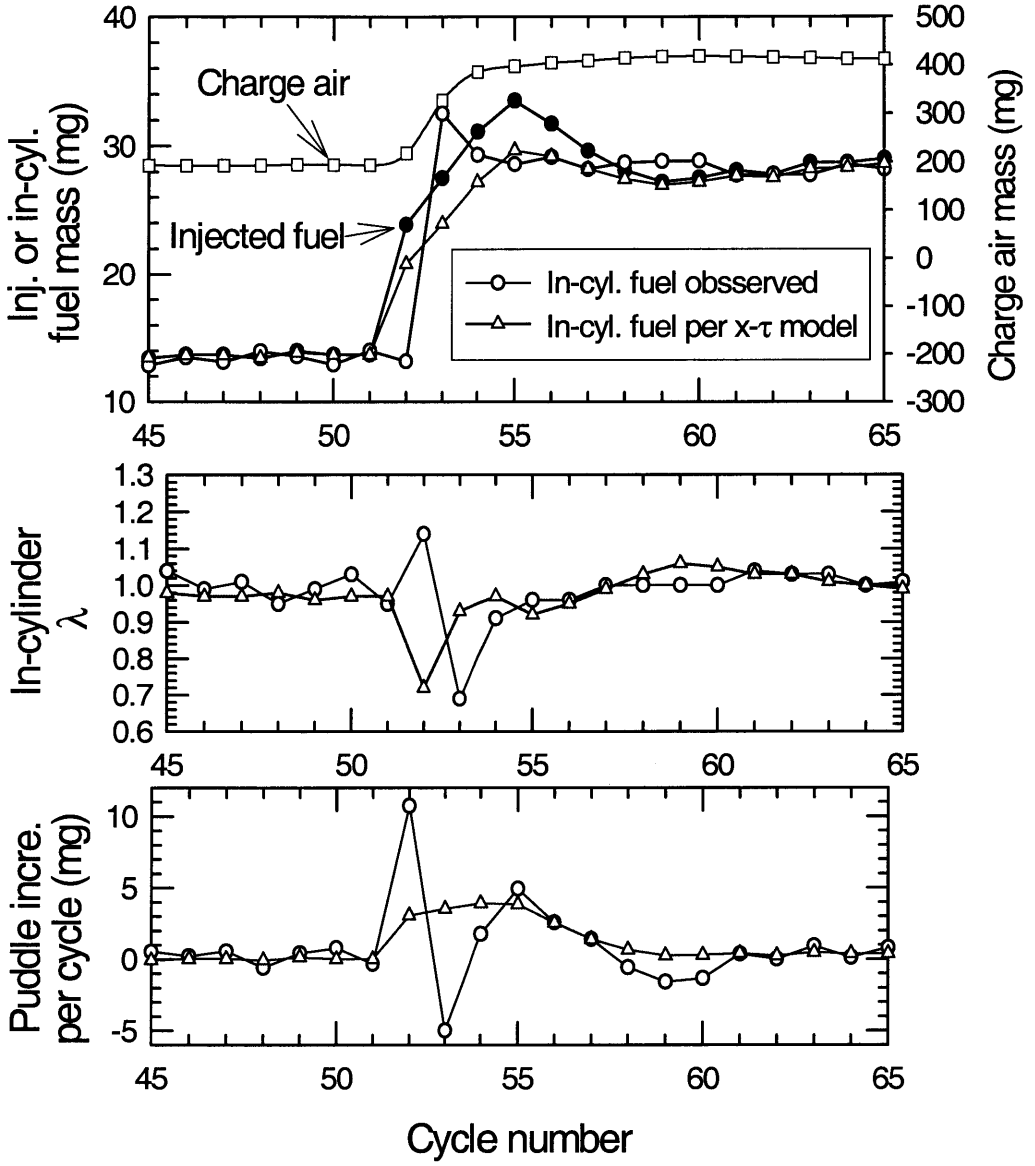

Figure 4.20: Predictions of the x-t model (triangle symbol) with the fuel from the dynamic pulse assigned to the intended cycle.

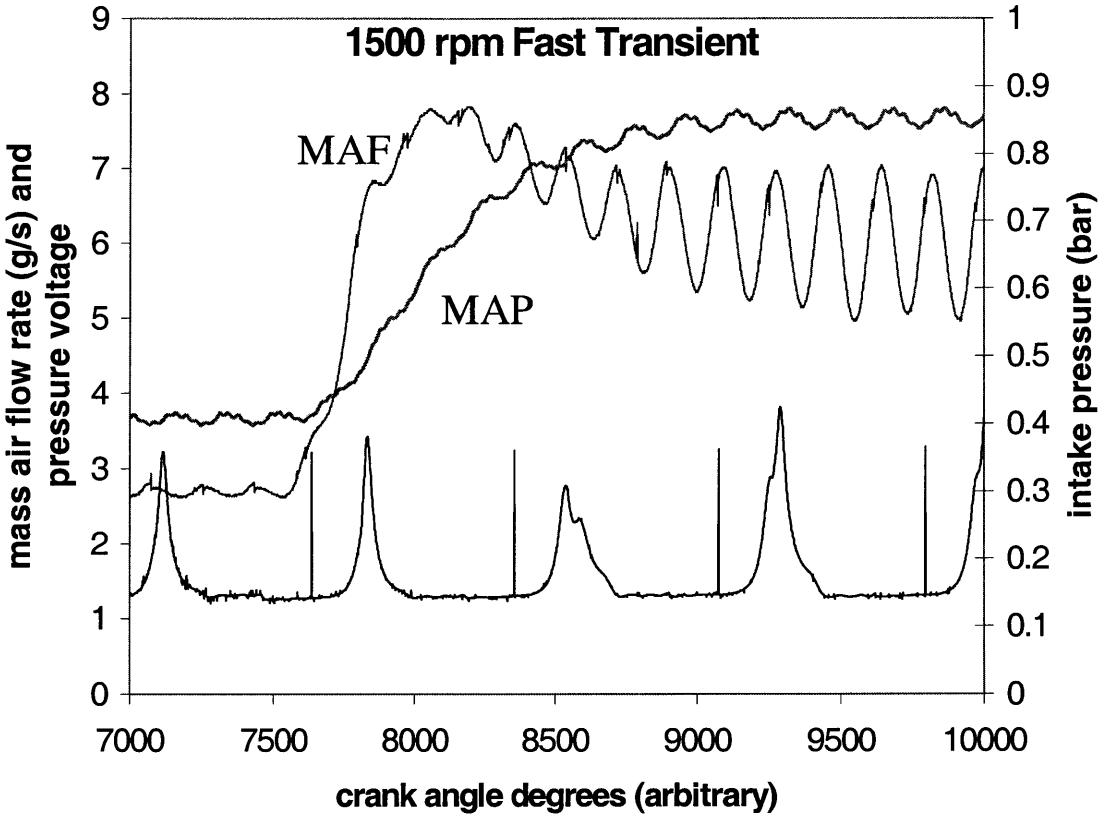

Figure 4.21: Fast Transient Mass Air Flow Signal and MAP signal; 1500 rpm, 0.4 to 0.9 bar pi

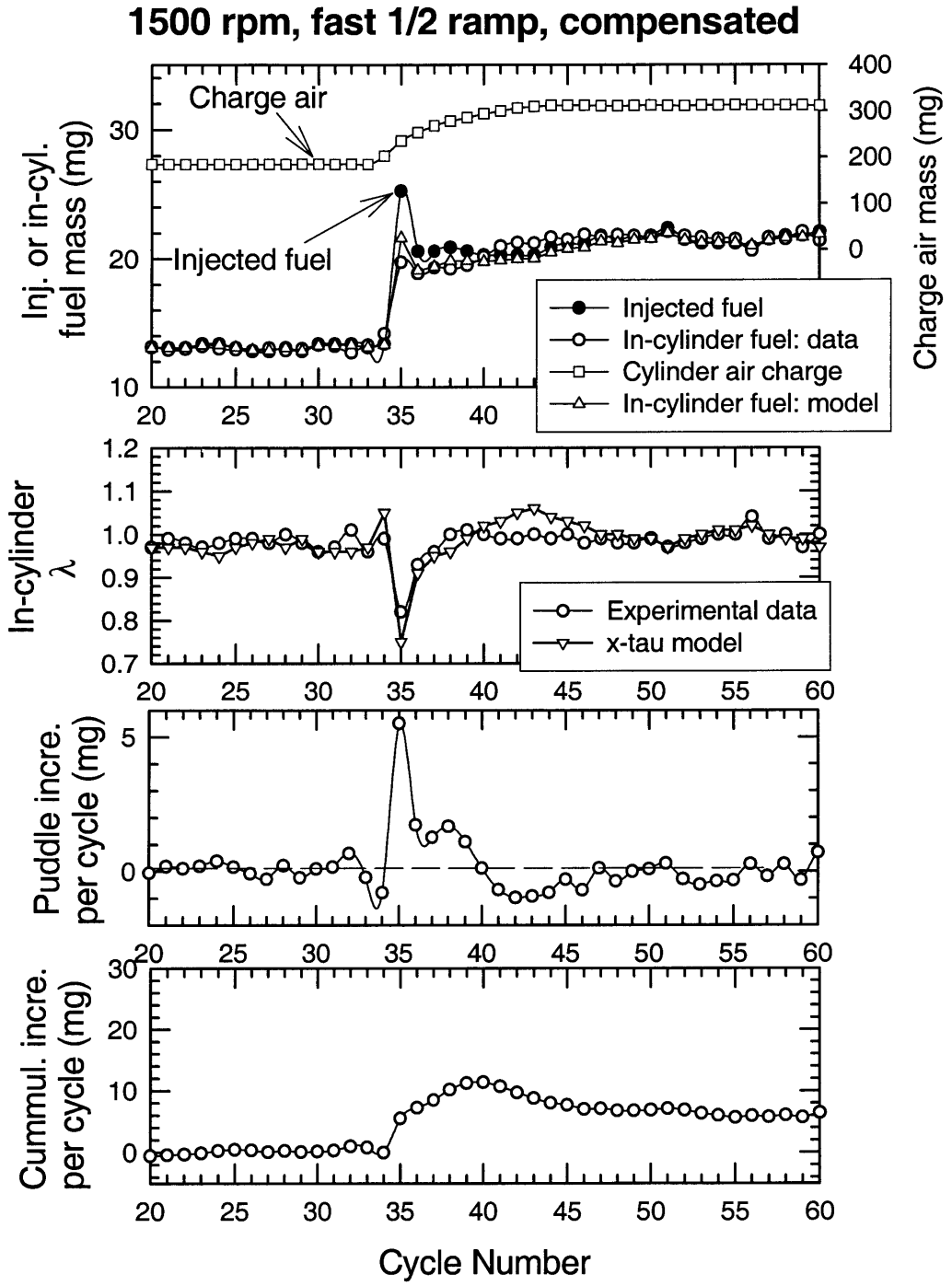

Figure 4.22: Fueling behavior for a fast 1/2 throttle ramp (0.4 bar to 0.65 bar pi). Engine operated at 1500 rpm; transient fuel compensation as controlled by the production EEC was applied.

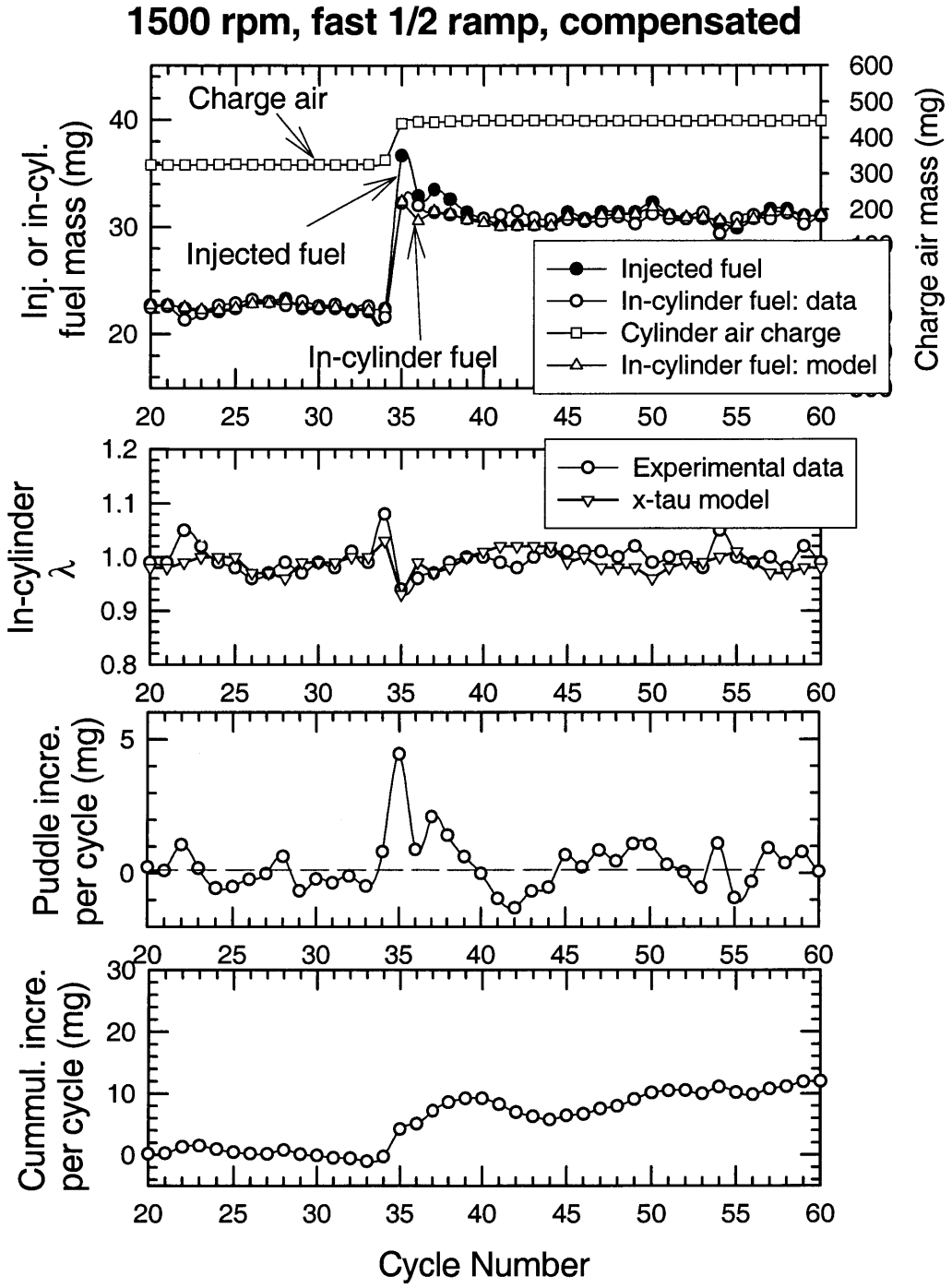

Figure 4.23: Fueling behavior for a fast 1/2 throttle ramp (0.7 bar to 0.95 bar pi). Engine operated at 1500 rpm; transient fuel compensation as controlled by the production EEC was applied.

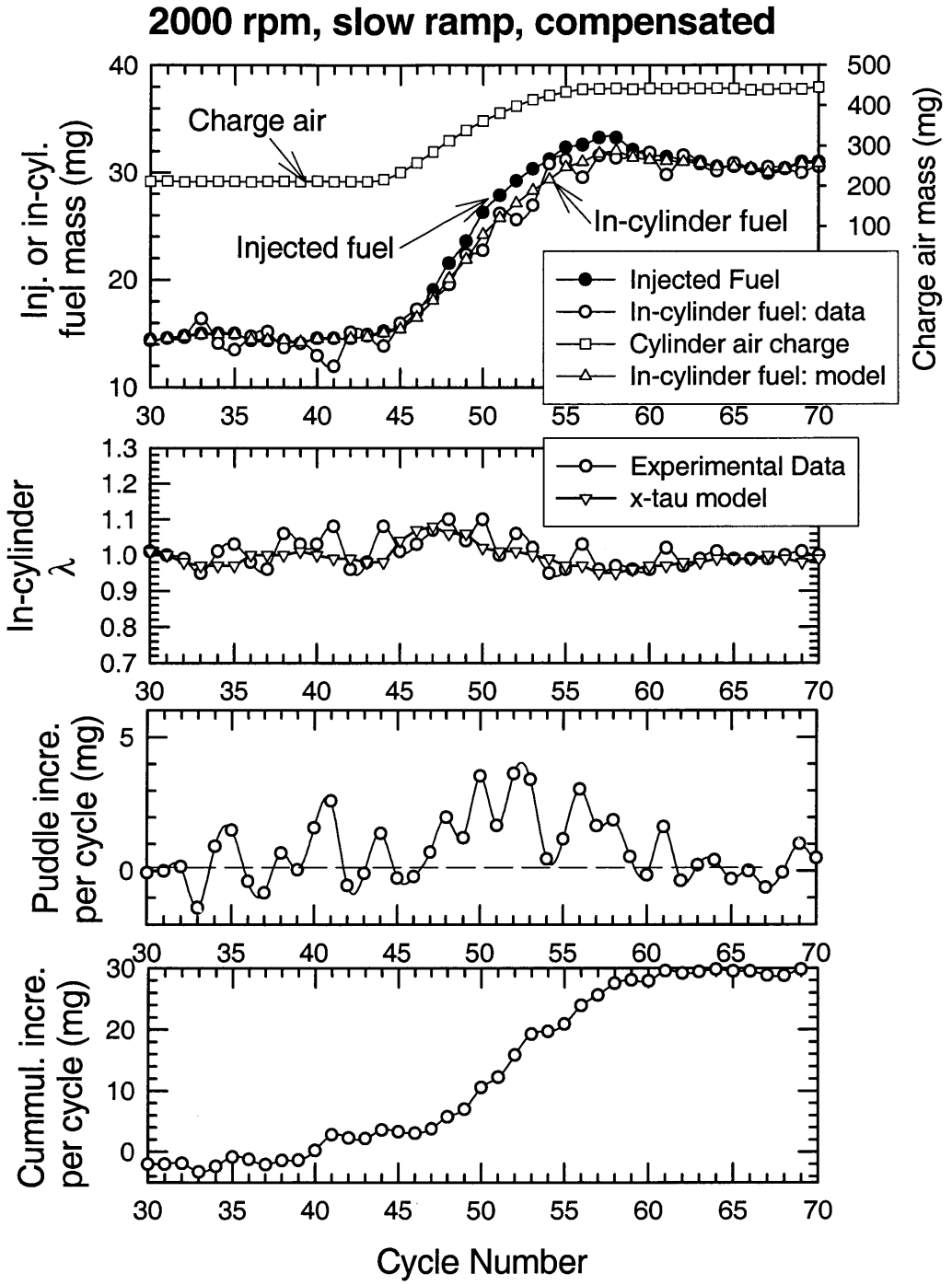

Figure 4.24: Fueling behavior for a slow throttle ramp (1 sec. ramp time). Engine operated at 2000 rpm; transient fuel compensation as controlled by the production EEC was applied.

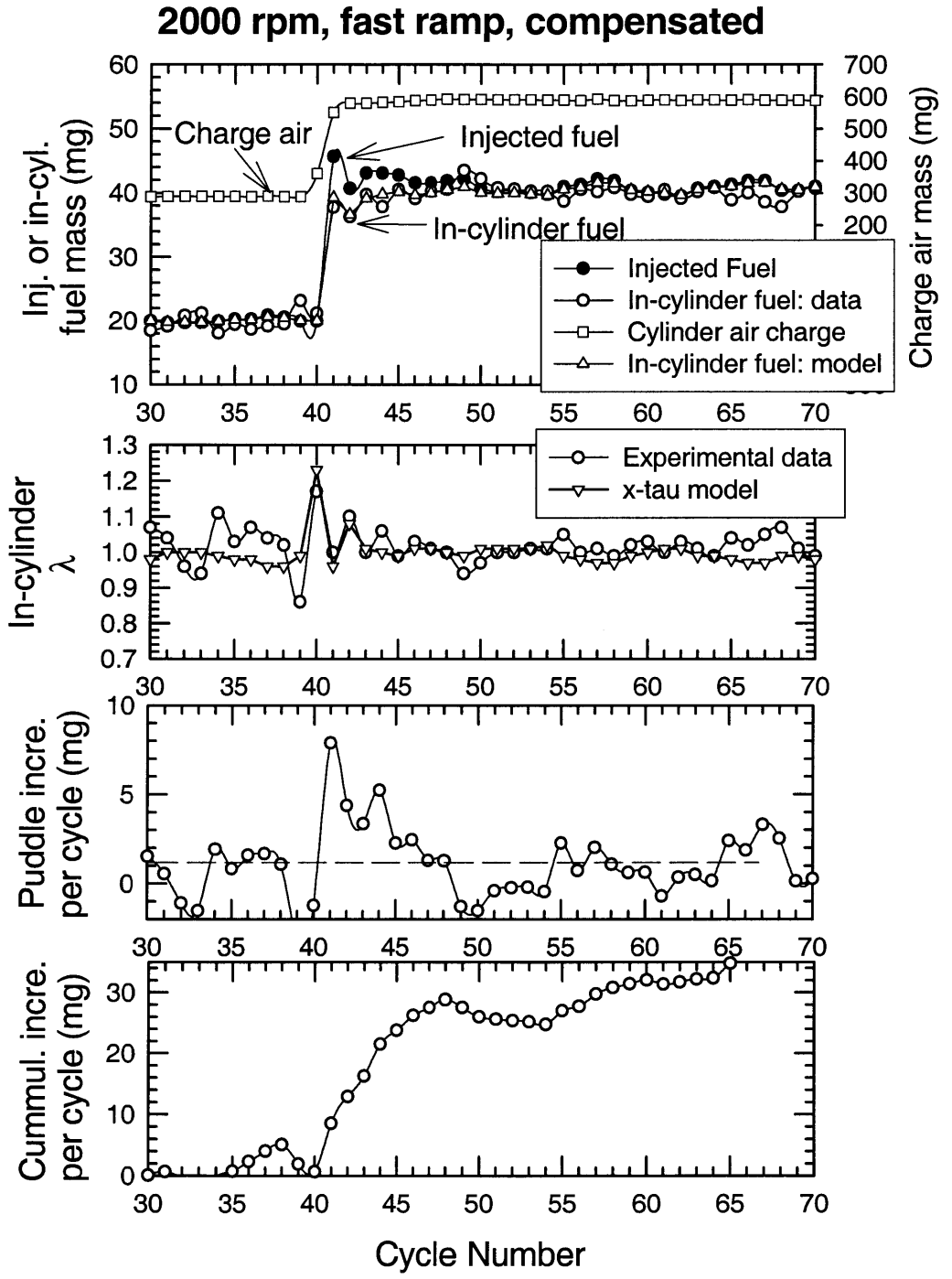

Figure 4.25: Fueling behavior for a fast throttle ramp (0.3 sec. ramp time). Engine operated at 2000 rpm; transient fuel compensation as controlled by the production EEC was applied.

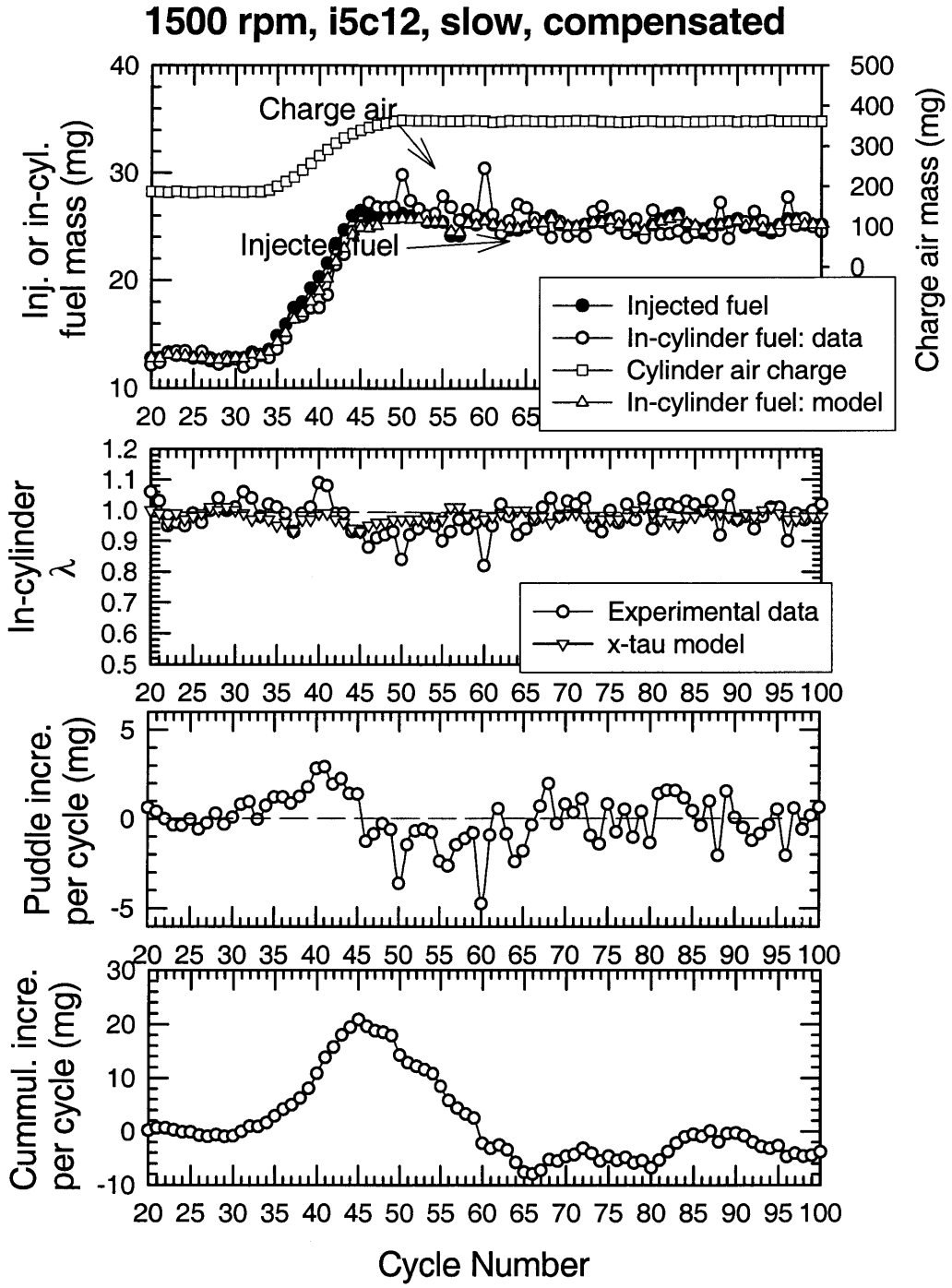

Figure 4.26: Fueling behavior for a slow throttle ramp (1 sec. ramp time). Engine operated at 1500 rpm; transient fuel compensation as controlled by the production EEC was applied. Iso-pentane fuel.

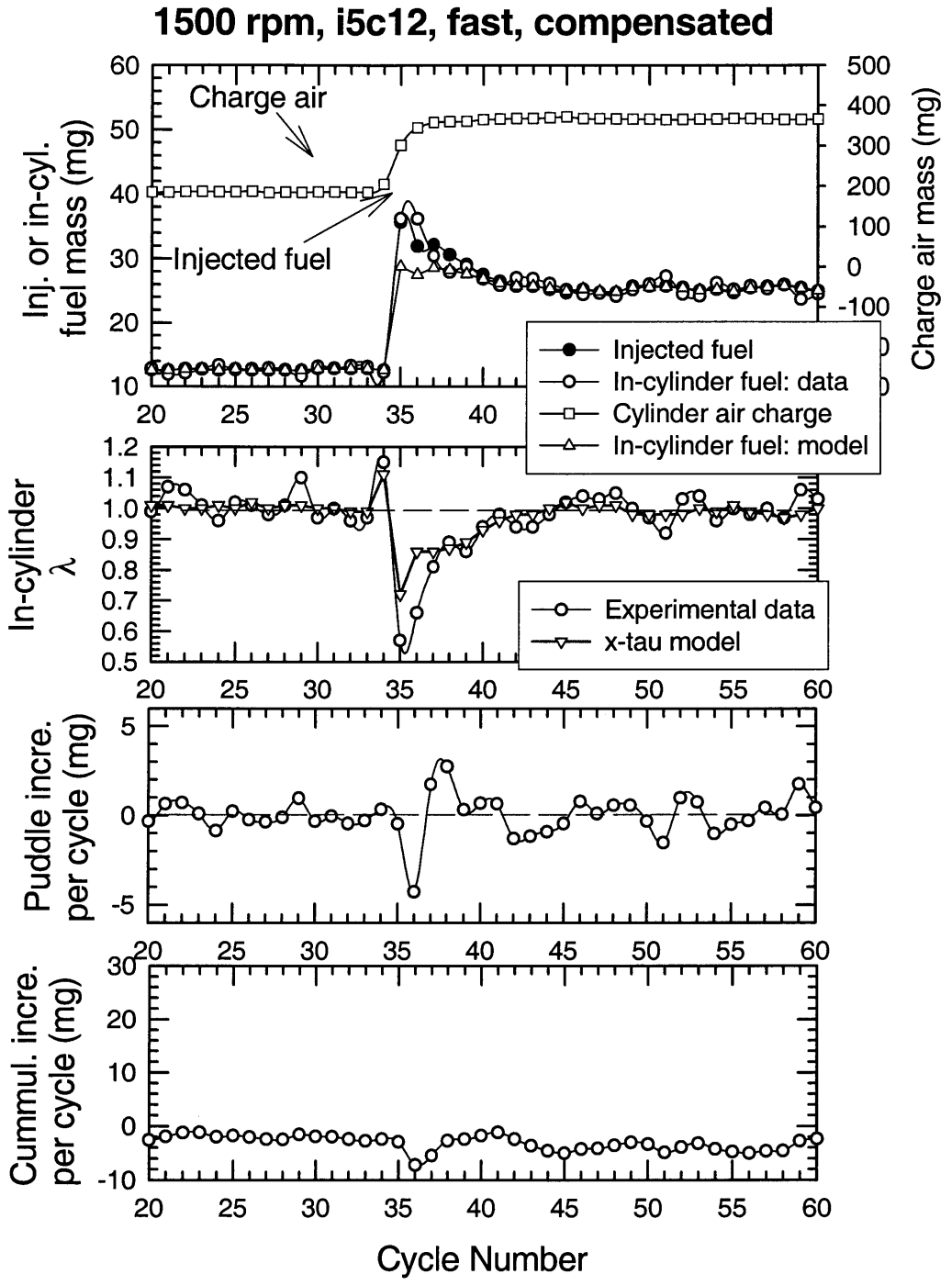

Figure 4.27: Fueling behavior for a fast throttle ramp (0.3 sec. ramp time). Engine operated at 1500 rpm; transient fuel compensation as controlled by the production EEC was applied. Iso-pentane fuel.

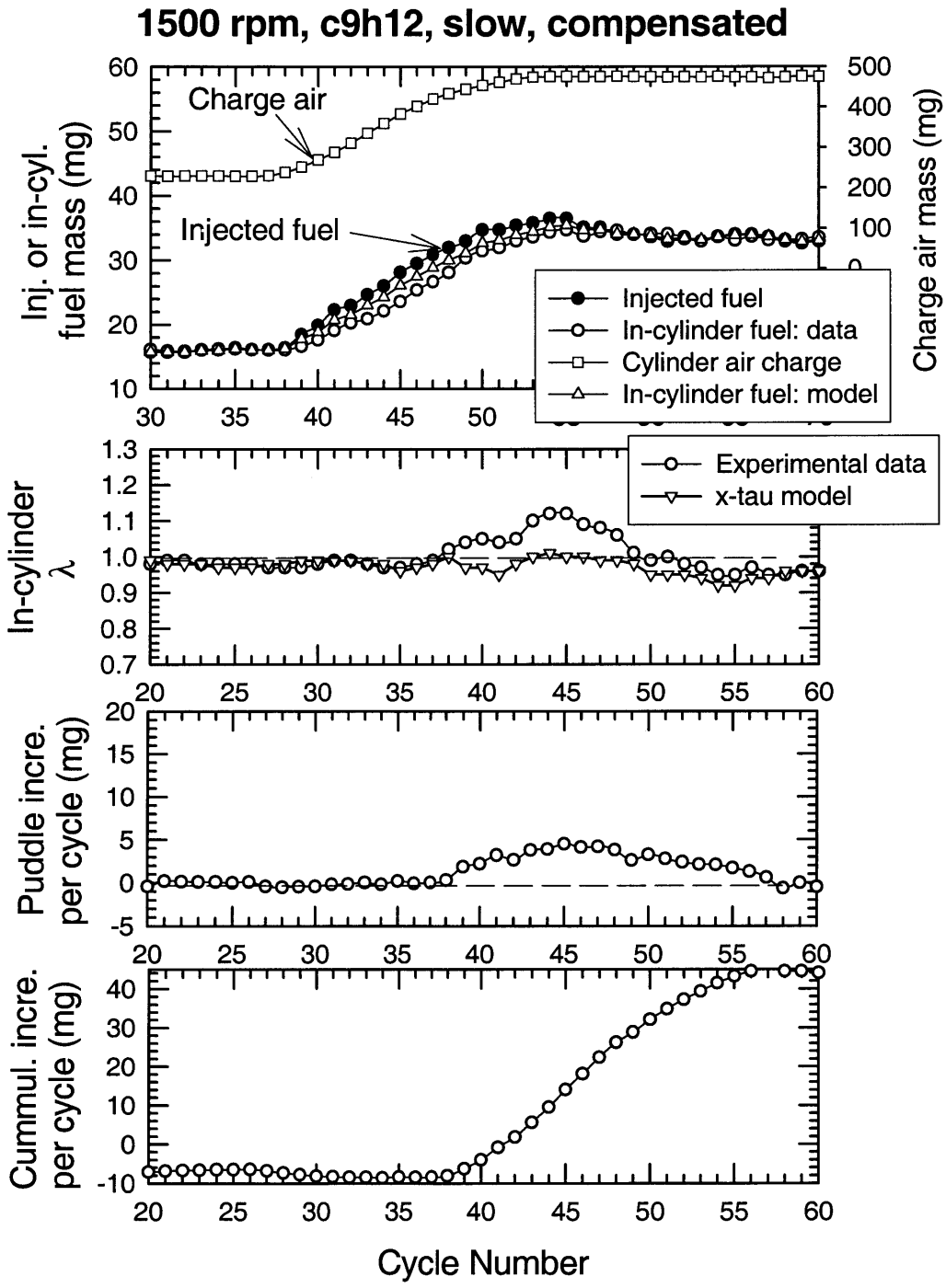

Figure 4.28: Fueling behavior for a slow throttle ramp (1 sec. ramp time). Engine operated at 1500 rpm; transient fuel compensation as controlled by the production EEC was applied. Cumene fuel.

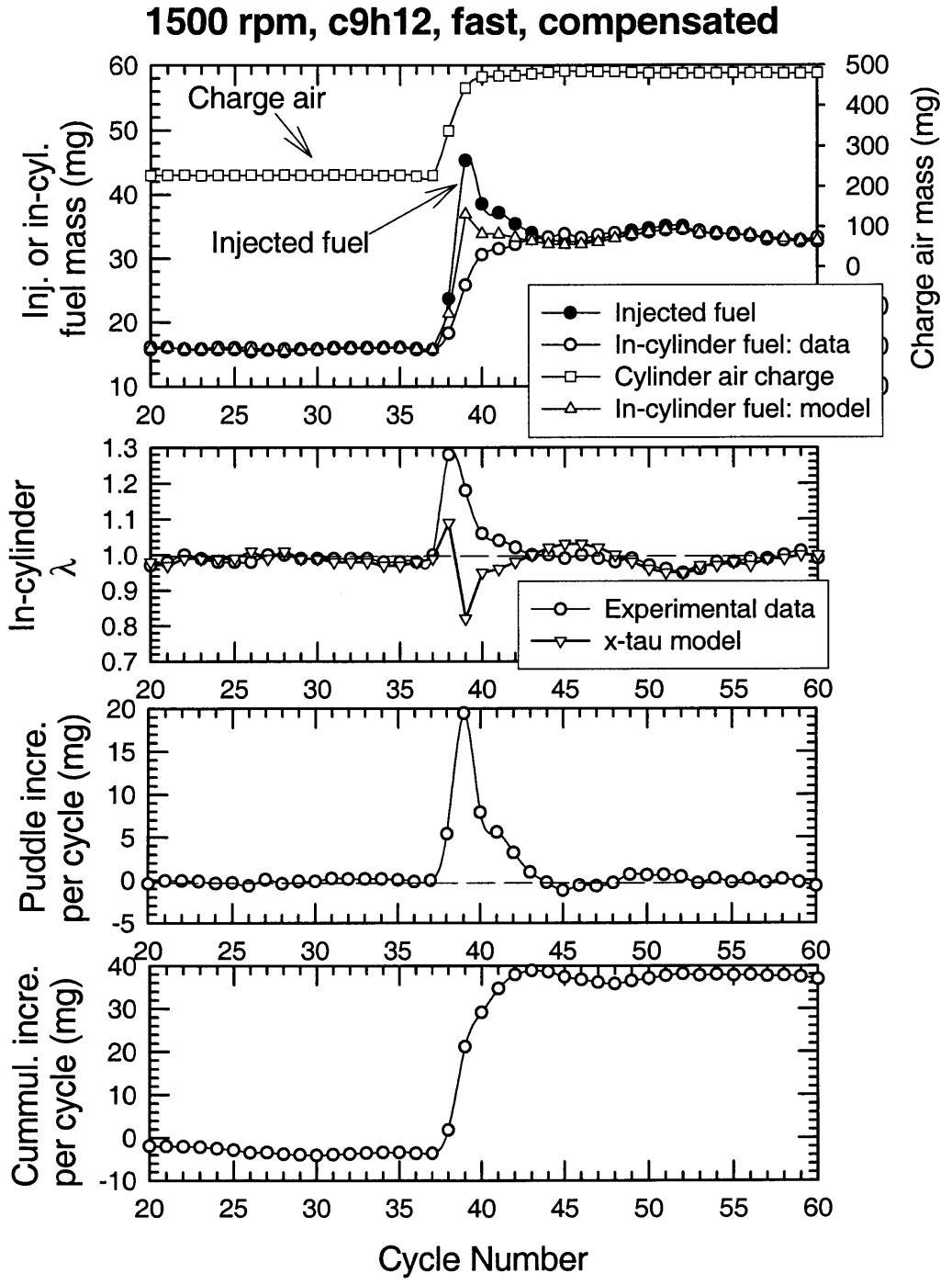

Figure 4.29: Fueling behavior for a fast throttle ramp (0.3 sec. ramp time). Engine operated at 1500 rpm; transient fuel compensation as controlled by the production EEC was applied. Cumene fuel.

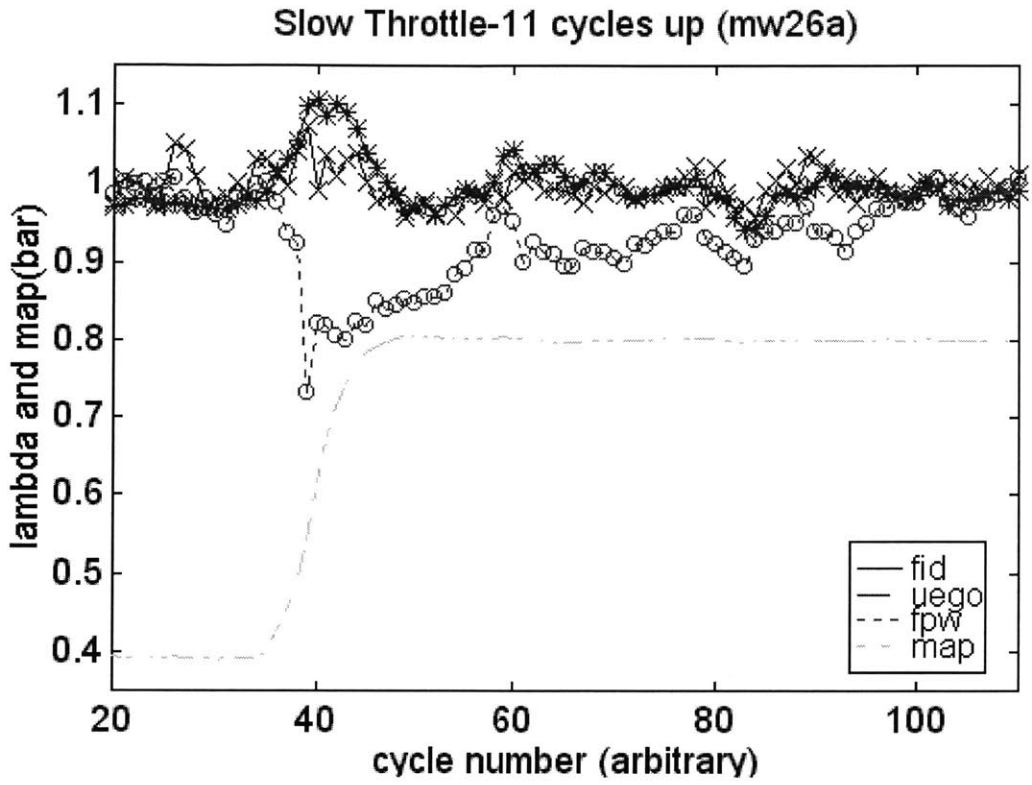

Figure 4.30: Cold Engine Slow Throttle Transient

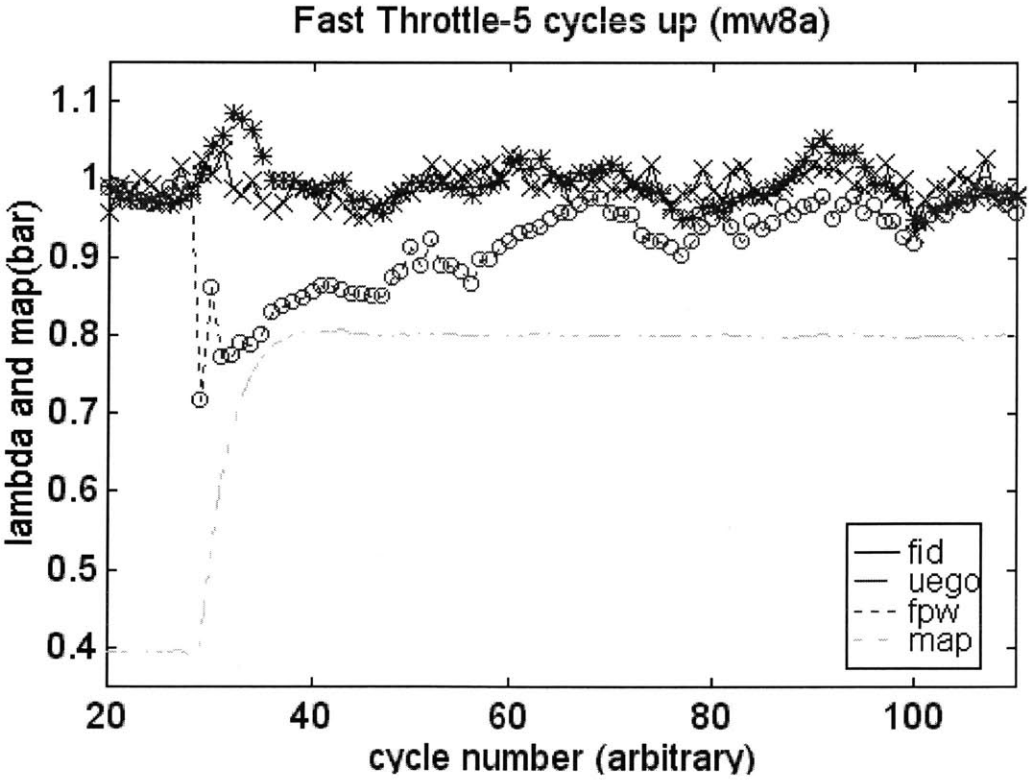

Figure 4.31: Cold Engine Fast Throttle Transient

(This page was intentionally left blank)

Chapter 5
Engine Cranking-Starting Overview

5.1 General Engine Behavior

5.1.1 Basic Physical Description

In general, the mixture preparation process described for throttle transients in **Section 3.1.1**. is also applicable to cranking-startup. There are however some important exceptions, which need to be considered in the study of cranking-startup behavior.

Engine starting generally begins with a 'dry' intake port. Visual intake port studies have shown this to be the case at various starting temperatures [5.1,5.2]. Additionally, engine shutdown experiments (similar to injector cut-off draining experiments, **Section 4.4**) indicate that residual port fuel is almost fully purged from the intake port during the decelerating engine cycles. The implications of such behavior requires that additional fuel needs to be injected on the first engine cycle to account for significant wall wetting. The second and following cycles will then already contain residual port fuel.

Due in part to wall wetting, large first cycle Fuel Pulse Widths (FPWs) are generally required to generate strong first fires. Fuel injection levels can often be many times more than required during stabilized engine operation. Thus, it is anticipated that much liquid fuel transport in-cylinder can result. Visual studies during crank have indeed shown that liquid fuel is allowed to collect on the combustion chamber walls as a result of Open Valve Injection (OVI) [5.3, 5.4]. Some of this liquid fuel persists through subsequent firing events. Closed Valve Injection (CVI) also leads to in-cylinder liquid fuel films, although the amount is less.

The amount of intake air and the fuel delivery process depend on the initial piston position. Unfortunately, engine position is generally not known when cranking begins, and production controllers start fuel injection immediately after the engine begins to

rotate. It is common for production engine controllers to use bank injector firing in which all of the cylinders on a given engine bank receive the same commanded FPW at the same time during the first few cycles. (The engine controller cannot begin to synchronize the individual fuel injectors until it detects the camshaft signal). As a result, some cylinder events during crank will receive OVI, which leads to high liquid fuel transport into the cylinder and to high exhaust HCs. The result of this effect was made apparent in a production engine study that observed the role of initial engine position before start on engine out HCs. Significantly higher HC levels were observed at initial positions corresponding to open intake valve fuel injection [5.5].

During crank, as with stabilized engine operation, it is the light fuel components that preferentially vaporize to provide a significant fraction of the vaporous fuel to start the engine. One study sampled combustion chamber gases before spark in order to determine the contribution of various fuel components to the mixture preparation [5.7]. The study was able to quantify the expected strong role of light fuel components during the cranking process.

Finally, during the engine cranking process, the engine operating conditions are unique. The engine is attempting to run at nearly wide-open Throttle (WOT) with a very low engine speed. With low crank speeds, intake port velocities and in-cylinder turbulence levels are significantly reduced compared to normal engine operation. Thus in-cylinder film flow of the puddle fuel mass, as well as strip atomization processes [5.8] will be significantly reduced in comparison to normal engine operation. Additionally, at the high engine load (high intake pressure) during the first few cycles, it is anticipated that minimal in-cylinder back flow occurs into the intake port since there is a small pressure difference between the in-cylinder gases and the intake manifold as the intake valve opens. The absence of significant intake valve opening back-flow would eliminate the effect of fuel redistribution into the upstream intake port.

The above mentioned effects will now be discussed in detail below.

5.1.2 Engine Stopping/Starting Positions

For a 4-cylinder 4-stroke engine, the engine tends to stop with one of the pistons at mid stroke (~90° from BDC) of compression. This is the point at the positive to negative transition of the sum of the individual cylinder gas load powers is equal to zero:

$$P_g = \sum_{\text{all cyliners}} p\dot{V} = 0 \qquad (5.1)$$

For a detailed analysis of this behavior see **Appendix B**. For this study, cylinder #4 piston starting positions A, B, C and E in **Figure 5.1** were used to replicate the typical configurations. (For position A, there were some technical difficulties with the PC fuel controller on hot starts so that the engine started with the piston at 160° from BDC in the compression stroke instead of at 90°. Since both intake and exhaust valves were closed, the later start should not lead to any material difference in engine behavior.) In addition, position D was added to examine the engine behavior with the piston starting from TDC of the intake stroke. **Figure 5.2** shows cylinder #4 timing relative to cylinders #1-3.

5.1.3 Representative Ambient Engine Start

A characteristic ambient (20° C) start behavior is shown in **Figure 5.3**. Prior to the start, the engine had come to rest at the mid-stroke of compression of cylinder #1. The firing order is 1-3-4-2. Cranking begins immediately after time zero on the abscissa. All the injectors were fired simultaneously at ~0.1 second after crank start. A substantial amount of fuel (~210 mg, λinj~0.15) was injected to cylinder #4 while the other three cylinders received the fuel metered from the Ford ECC. The dips in the MAP correspond to the air induction event of the individual cylinders. Cylinder #3 was the first cylinder to experience air intake (its starting position was at mid stroke intake). Cylinder #4 was the first to fire. The engine speed was cranked to ~200 rpm (the three dips in the rpm before engine firing were due to the compression gas loads of cylinders 1,3, and 4); then it accelerated with the power output of the firing cylinder. As the engine speeded up, the MAP decreased to ~0.45 bar at 1 second after cranking.

One of the distinct features of the first cycle of combustion is that it takes place at substantially lower rpm (~200) than normal engine operation. Furthermore the crank accelerates substantially during the heat release period. As such, the air flow velocities, the heat transfer characteristics, and the combustion phasing for MBT are substantially different then normal practice. The effects will become evident in the heat release analysis discussion in a later section.

5.1.4 Effect of Starting Position on Startup RPM

The instantaneous RPM for the first combustion cycle of cylinder #4 also depends very much on the starting position. The instantaneous hot start speeds at the time of ignition for cylinder #4 in the first cycle are shown in **Figure 5.4**. With starting position A, the crankshaft has been accelerated by two firing cycles (from cylinders #1 and #3), and thus the speed reaches ~680 rpm. With positions B, the crankshaft has been accelerated by 1 firing cycle (from cylinder #3); the speed reaches ~500 rpm. For positions C, D and E, there are no previous firing cycles; the speed is determined by the starter motor, and it is ~200 rpm.

The averaged intake valve open engine speeds (simple rpm average each cadeg during the intake event) are also shown in **Figure 5.4**. These speeds are important from the mixture preparation perspective, as they will be the force behind convective mass transfer and strip atomization processes. While the trends are generally expected, some exceptions exist. For example, position C posses a relatively high average engine speed during the intake event. As seen in **Figure 5.3**, both MAP and RPM have significant fluctuations. At initial position C, during intake, cylinder #4 is additionally experiencing the expansion of cylinder #3. This tends to raise the average engine speed during this period.

Ambient engine starting showed less engine speed sensitivity as a function of initial engine position. This was due to the production controller delivering insufficient fuel to

cylinders #1-3. Engine speed at spark for ambient starting was thus roughly constant at 200 rpm.

Finally, engine speed variations during cranking greatly affect the crank angle duration of the fuel injection event. **Figure 5.5** shows the necessary fuel injection duration versus injection mass and engine speed.

5.2 Approaches used in Production Controllers

As mentioned in the previous section, production controllers generally start fueling immediately upon the start of engine rotation from the starter motor. This approach is used to generate fast starts (an important customer requirement and perceived quality indicator). Some controllers will inject one fuel pulse per cylinder for each cranking cycle, while others will use multiple shorter pulses per cycle. These crank fueling strategies are often employed until engine speeds exceed approximately 700 rpm (above this speed the Mass AirFlow Sensor signal becomes stable). It takes upwards of two engine revolutions in order for the production engine controller to obtain the camshaft signal. After the camshaft signal is received, individual cylinder injection events must be 'moved' to their appropriately timed location. Various algorithms exist to do this, although they generally take many more cycles to fully synchronize. Thus, some engine cylinders may receive open valve injections until synchronization occurs.

Beyond injection timing exists the question of how much fuel to inject? This is commonly referred to as engine calibration. Unfortunately, a common diagnostic, the UEGO, is ineffective for the first few engine cycles due to its relatively slow response time, exhaust gas mixing and often cold temperatures at startup. While some internal industry efforts have used in-cylinder pressure or exhaust FFID analysis, these techniques are not widespread for production development. Thus the majority of engine calibration development to achieve acceptable startup performance is empirically based.

Extensive testing of engine starts at a variety of ambient and engine temperatures, ambient humidities, elevations and fuels is required in order to develop an acceptable calibration. Unfortunately, this process is very time consuming and expensive.

5.3 Practical Issues and Motivation

Current industry efforts are seeking to reduce engine calibration development time. However, as emission regulations are getting tighter, more effort is often employed to find 'optimum' fuel calibrations.

In the past, as looser emission regulations allowed, over-fueling during crank and warm-up allowed for acceptable startup performance, but at the expense of high engine out (and often tailpipe) emission levels. Over-fueling was often calibrated to account for low quality-low volatility fuels. But as over-fueling calibrations are reduced the possibility of under-fueling leading to misfires with very high levels of engine out HCs becomes very real. What is the optimum balance?

As discussed above, during crank, fuel injection occurs for all cylinders simultaneously in production controllers. The question arises as to the appropriateness of this approach. Do significant differences exist cylinder to cylinder during a given engine cranking cycle? This question is plausible due to the wide variation in engine speed observed in **Figure 5.4**.

Beyond fueling, spark control has often been fixed for cranking. Another significant unknown revolves are what spark timing is appropriate for crank. Engine controllers are starting to implement this flexibility, but little is known as to appropriate ignition calibration during startup.

5.4 The Direction of this Study

In light of the limited fundamental information regarding engine cranking-startup performance, this study will seek to characterize engine starting performance (IMEPg and in-cylinder fuel) versus injected fuel across a range of initial conditions (ECT, starting position, spark timing-were applicable) in cylinder #4 of the four cylinder production engine.

Chapter 5 References:

[5.1] Saito, K., Sekiguti, K.,Imatake, N., Takeda, K., Yaegashi, T.,"A New Method to Analyze Fuel Behavior in a SI Engine", SAE#950044, 1995.

[5.2] Shin, Y., Min, K.D. and Cheng, W.K., "Visualization of Mixture Preparation in a Port Fuel Injected Engine during Engine Warm-up", SAE#952481, 1995.

[5.3] Imatake, N., Saito, K., Morishima, S., Kudo, S., and Ohhata, A., "Quantitative Analysis of Fuel Behavior in Port-Injection Gasoline Engines", SAE#971639, 1997.

[5.4] Stanglmaier, R.H., Hall, M. J. and Mattews, R.D., "In-Cylinder Fuel Transport during the First Cranking Cycles in a Port Injected 4-Valve Engine", SAE Paper 970043, 1997.

[5.5] Henein N.A., Tagomori M.K., Yassine M.K., Asmus T.W., Thomas C.P., and Hartman P.G., "Cycle-by-Cycle Analysis of HC Emissions During Cold Start of Gasoline Engines", SAE Paper 952402, 1995.

[5.6] Koenig, M.H., Stanglmaier, R.H. Hall, M.J. and Matthews, R.D, "Mixture Preparation during Cranking in a Port-Injected 4-Valve SI Engine", SAE#972982, 1997.

[5.7] Shayler, P.J., Issacs, R.M. and Ma, T.H., "The Variation of In-Cylinder Ratio during Engine Cranking at Low Ambient Temperatures", Proc. Inst. Mech. Engrs. Vol.206, pgs.55-62., 1992

[5.8] Shin, Y., Cheng, W.K., and Heywood, J.B., "Liquid Gasoline Behavior in the Engine Cylinder of a SI Engine", SAE Paper 941872, 1994.

[5.9] Castaing, B.M.P., Cowart, J.S and Cheng, W.K., "Fuel Metering Effects on HC Emissions and Engine Stability during Cranking and Startup in a PFI SI Engine", SAE#00FL-0693, SAE Fall Fuels and Lubricants Meeting, Baltimore, 2000.

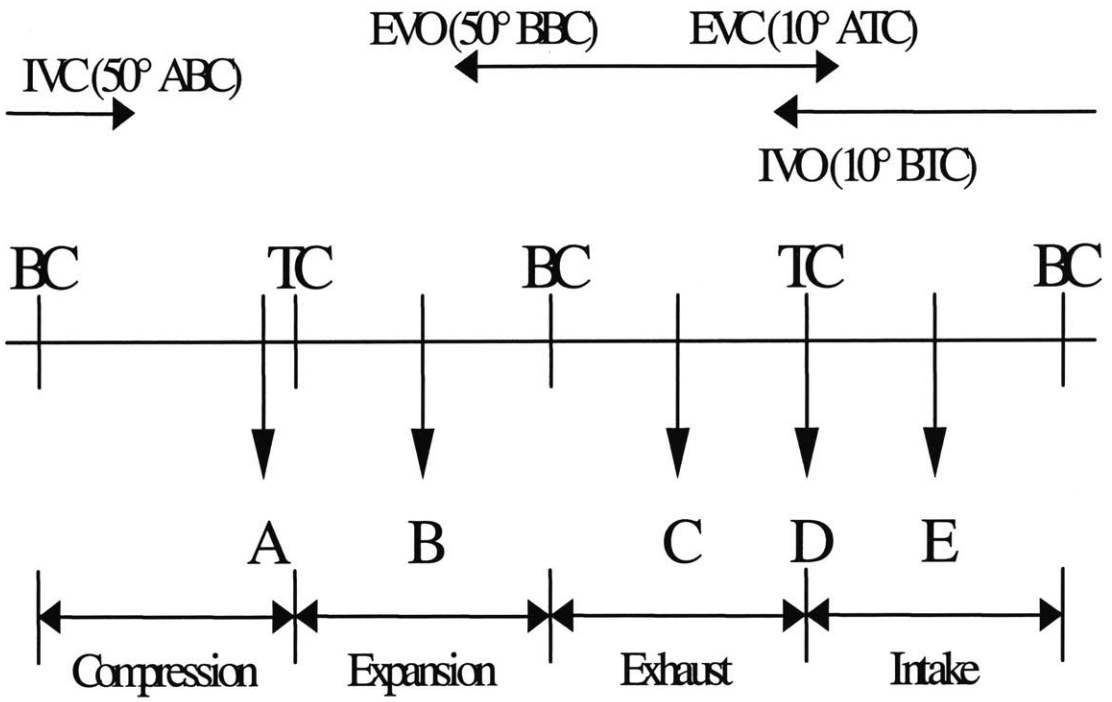

Figure 5.1: Engine starting positions for cylinder #4.

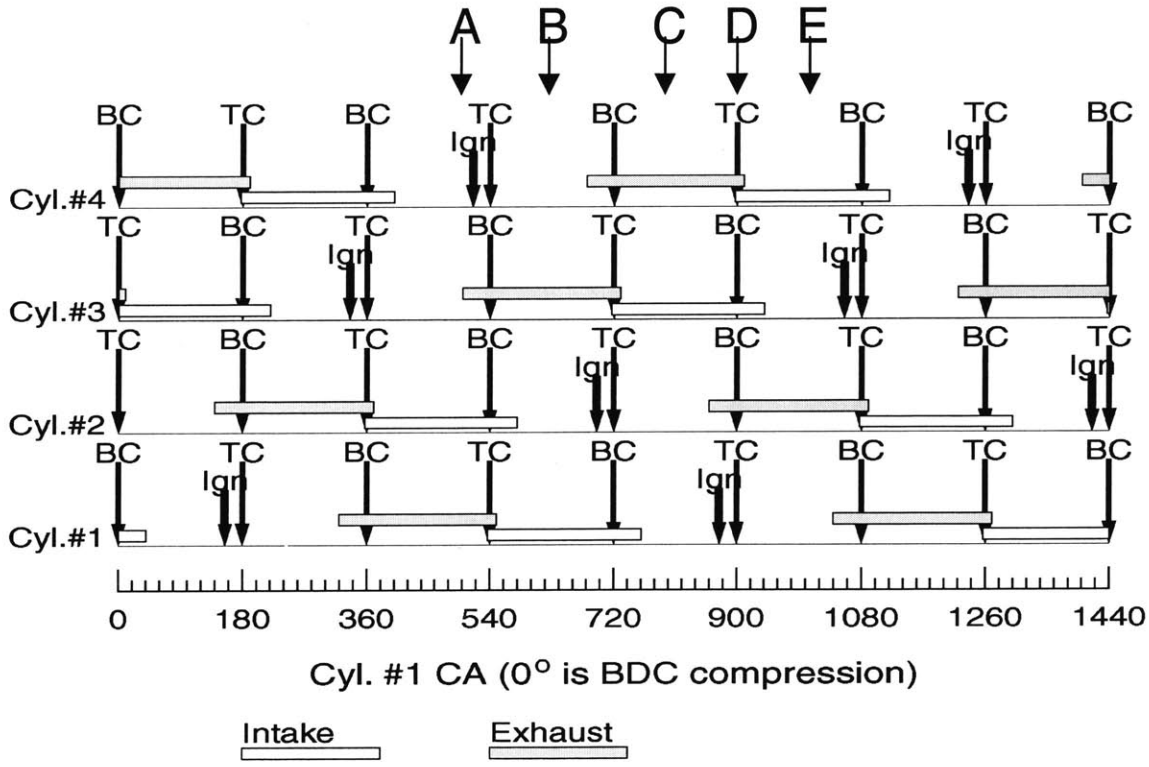

Figure 5.2: Zetec engine timing chart. Firing order: 1-3-4-2

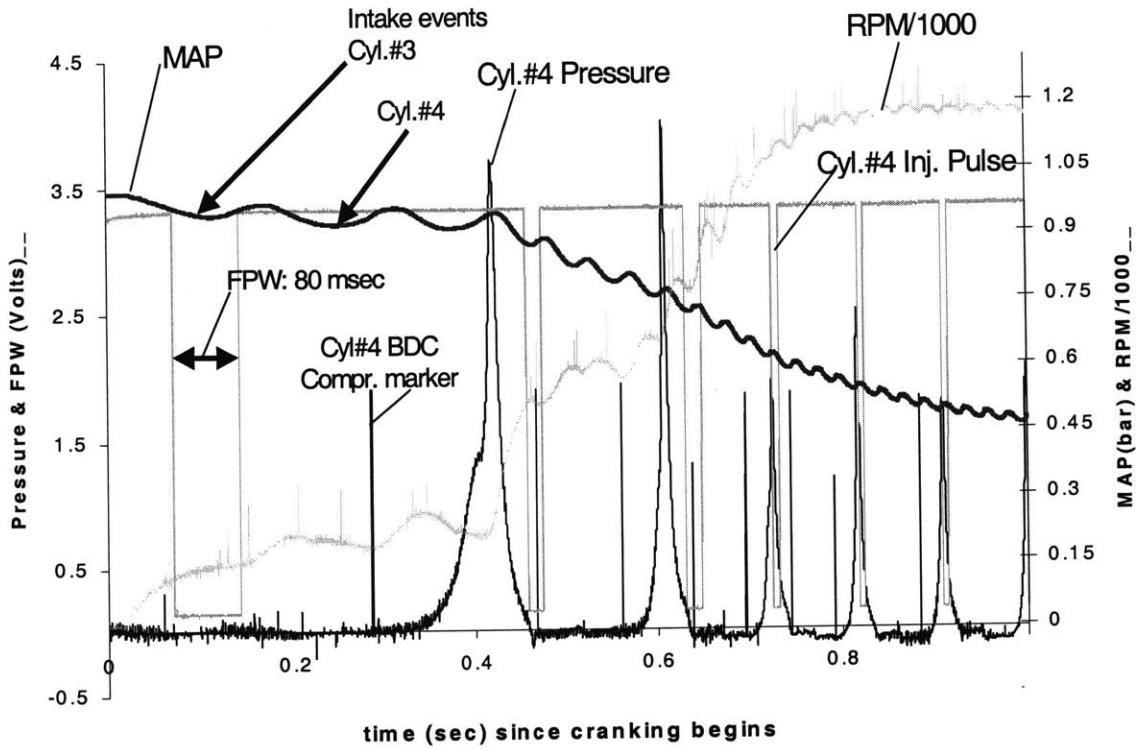

Figure 5.3: Characteristic ambient engine star from Position C.

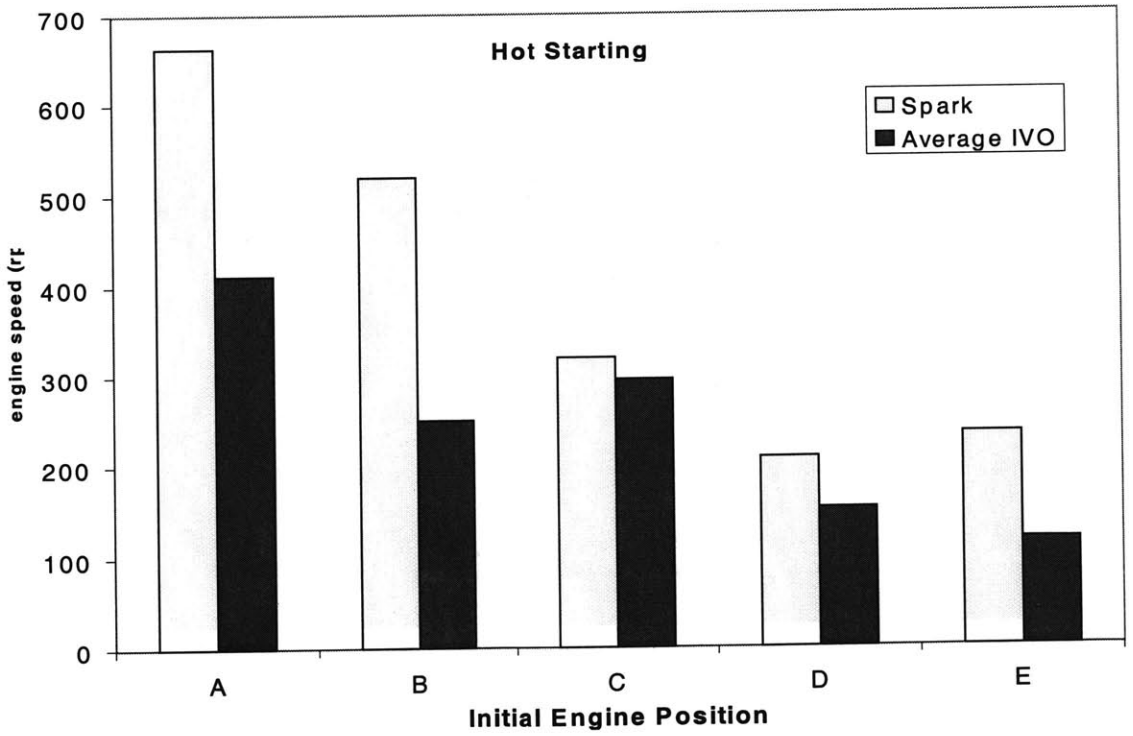

Figure 5.4: Hot starting 1st cycle engine speed versus starting position. Engine speed at spark, and average engine speed during intake are shown.

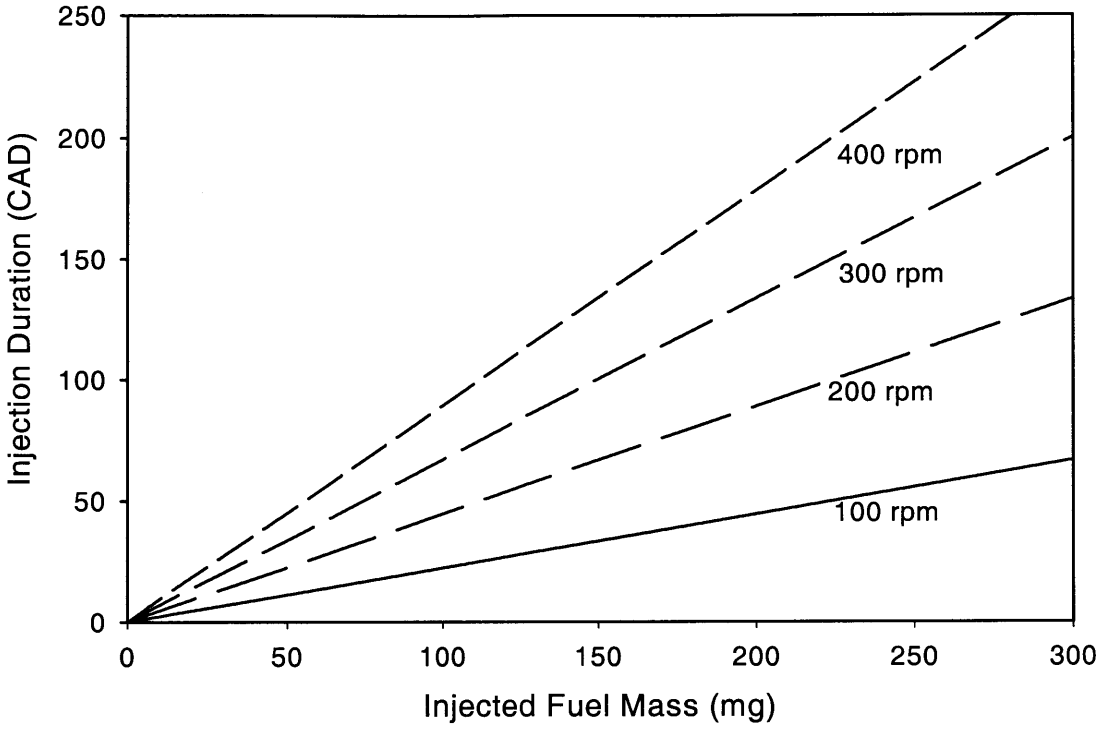

Figure 5.5: Injection duration (crank angle degrees) versus injection mass and engine speed

(This page was intentionally left blank)

Chapter 6

Engine Cranking Experimental Results

6.1 Introduction to the Experimental Work and Analysis

As discussed in **Chapter 5**, limited information exists as to the characteristics of engine starting behavior. Current industry practice relies heavily on empirical 'trail and error' approaches for cranking control algorithms and calibration. In an effort to improve and optimize cranking performance in order to meet future tightening of emission standards, a detailed study is thus pursued.

For this thesis, an experimental (**Chapter 6**) and modeling (**Chapter 7**) program was pursued to evaluate the role of initial engine starting position, engine temperature and fueling strategy upon the preparation of a combustible mixture and the resulting combustion stability for the first few engine cycles.

The approach used here was to perform conventional engine starts (using the production starter motor) on a production engine over a broad matrix of conditions (initial engine position, temperature, fueling). In-cylinder FFID and pressure data was used as the primary diagnostic (simultaneous exhaust HC data will be collected: B. M. Castaing, S.M. Thesis). Efforts to elucidate the injected fuel mass disposition over the first few engine cycles were pursued.

The organization of this cranking behavior portion of the thesis is as follows:

Hot starting experimental results for the first engine cycle are presented in **Section 6.2.1**. Hot starting experimental results for the second and third cycles of engine crank are presented in **Section 6.2.2**.

Ambient starting experimental behavior is discussed in **Section 6.3.1** for the first engine cycle, and **Section 6.3.2** for the second engine cycle.

Cold engine cranking experimental results are presented in **Section 6.4**.

Chapter 7 discusses the modeling of the first engine cycle. The model is described and simulations of the experimental conditions are performed. Study of the first engine cycle is performed due to the critical nature of getting excellent 'first fire'. Additionally, the nature of the first engine cycle allows for physically based modeling simplifications that allow for the complex engine environment to be made more tractable.

6.2 Hot Engine Experiments

6.2.1 Hot Start 1st Cycle

The hot start first cycle in-cylinder air/fuel equivalence ratios (λ) measured by the FFID as a function of the amount of injected fuel and initial piston positions are shown in **Figure 6.1**. While the data points shown are for individual engine starts, the experiments were repeated to ensure that the absolute levels and trends were repeatable. In all these cases, the end times of injection plus the transport delay from the injector to the valve (~5 ms) were before the BC of the intake stroke. The mixture becomes richer when more fuel is injected. With the same fueling, the λ values are relatively insensitive to the starting position, (except for Case E, which will be discussed later). There is, however, a small but definite difference when cases A and B are compared to cases C and D. (There are also some small but significant difference between cases C and D as will be shown shortly). The situation in Case C is geometrically not very different from that of A and B. All three cases are closed valve injections; most of the liquid fuel is deposited at the vicinity of the valve and is carried into the cylinder by the intake flow (there is negligible back flow in the first cycle). The port flow velocity during the intake determines how much fuel is left behind. (The concept of the 'left behind' fuel is more applicable than that of the amount going forward into the cylinder because the residence time for the fuel in the port in the three cases are different; thus there are different amounts of liquid and vapor in the port before the intake valve opens.) We therefore attribute the difference in λ values to the different intake airflow velocities: for Cases A and B, the crank rotation

speed is higher (see **Figure 5.4**), and therefore, less fuel is left behind and a richer mixture results than in Case C. Although Open-Valve-Injection (OVI) was used in Case D, the fuel was delivered in the early part of the intake stroke during which the port flow velocity was high. Therefore there is no substantial difference between Case C and Case D.

The λ values for starting position E appear to be higher than the other cases and to be somewhat irregular. When the raw FFID traces were examined, the signal indicated that there were substantial inhomogeneity in the charge, see **Figure 6.2**. The values of λ calculated in **Figure 6.1** were obtained by averaging the signal 'plateau'. For case E in which there are significant fluctuations in the 'plateau', this averaging may not be the correct weighting of the different parts of the signal and thus there is substantial uncertainty in these values. Therefore comparison between Case E and the rest of the cases is not appropriate. Nevertheless, the general trend that the λ values decrease with increase of fueling still holds.

From the λ values, the fuel mass may be computed. The charge is assumed to be a mixture of fuel vapor and air at intake pressure and temperature occupying the cylinder volume at IVC. The fractions of the injected fuel that goes into the combustible mixture for the different cases are shown in **Figure 6.3**. Because of the uncertainty in the measurements for starting position E, that set of data is omitted. Also because of measurement errors of the FFID, the fraction of injected fuel in the charge may be slightly larger than one in the low range of the measurement.

The fraction of the injected fuel that goes into the combustible mixture decreases almost linearly from unity when a small amount of fuel is injected. The slope is that for every 13 mg fuel increase, the fraction will decrease by 0.1. Thus as more fuel is injected, a proportionally larger amount will not be delivered into the charge. This retained fuel may either contribute to the charge of the next cycle (see next section), go to the sump [6.1], or escape as exhaust hydrocarbon [6.2,6.3].

Cylinder #4's IMEPg of the first cycle as a function of fueling and starting positions in hot starts are shown in **Figure 6.4**. Except for the case of very low fueling (13 mg injection), substantial IMEPg values were produced. To gain more insight into the first cycle performance, the IMEPg values are plotted in terms of the measured in-cylinder λ values for the different starting positions in **Figure 6.5.**

There are two noticeable features in **Figure 6.5**. (a) There is no substantial drop in the IMEPg values for a large range of λ values until the mixture is very rich (λ <0.65). (b) For the same λ values (e.g. at λ = 0.8) the IMEPg values for the different starting positions are substantially different.

Feature (a) will be discussed later in the ambient temperature start section. For feature (b), a heat release analysis of the pressure data [6.4] was carried out to understand the difference in IMEPg in the not-too-rich region. The calculation was done for starting positions A and C at the same amount of first cycle fueling (39 mg). There was some difference in the in-cylinder λ (0.8 and 0.9 respectively); the major difference between the two cases was the engine speed (see **Figure 5.4**). There was also substantial crank shaft acceleration from the combustion gas load during the cycle: for position A, the speed rose from 680 rpm at ignition to 790 rpm at EVO; for position C, the values were 220 and 550 rpm. The pressure trace and distribution of the combustion energy release for the two cases are shown in **Figures 6.6 and 6.7**. It should be noted that the energy values in these plots are referenced to the ignition point; thus the compression work before ignition is not included in the indicated work.

The heat release analysis shows that the heat release per crank angle in Case C is substantially faster than that of case A. This is primarily due to the difference in rpm for the two cases. The heat transfer is also substantially higher in Case C because of (a) the major part of the heat release is close to TDC so that the early burned gas temperature is higher, and to a lesser extent, (b) because of the low rpm, there is more time for heat

transfer[1]. Thus comparing the IMEPg values for starting positions A-D, differences are due to combustion phasing effects which affect both the gas load phasing and the heat transfer characteristics of the cycle.

In case E, the IMEPg values are lower. This fact may be due to the charge non-uniformity as a result of the late open-valve injection (see **Figure 6.2**), although there is no direct evidence.

In **Figure 6.8**, the first cycle IMEPg values are plotted against the crank shaft speed at the ignition point for two different fueling (data points within the 'plateau' region in **Figures 6.4 and 6.5**). Except for starting position E, for which the data are outliers as explained earlier, there is good correlation between the first cycle IMEPg and the engine speed at ignition of the cycle.

The Engine-Out Hydrocarbon (EOHC) for the first cycle are shown in **Figure 6.9** as a function of the injected fuel mass, and in **Figure 6.10** as a function of the measured in-cylinder λ. The lowest EOHC levels are only slightly higher than low speed high load stabilized EOHCs (~2250 ppm C1 @ 1500 rpm, 0.9 bar pi). The EOHC values behave similarly for all the starting positions except for position E; there the values were higher (**Figure 6.10**) plausibly due to mixture non-uniformity. Except for the non-firing cases for which the raw fuel was exhausted, the EOHC for all the starting position increase modestly with increase of fueling until fueling of ~80 mg. Then the mixture became very rich (λ below 0.65, see **Figure 6.10**), and partial burn occurred, which resulted in high EOHC values.

For the range of λ between 1.1 and 0.65, The EOHC values are modest (rises from ~3000 to ~6000 ppmC1). This behavior may be explained as follows. The EOHC values are influenced by λ in two ways [6.5]: charge quenching and oxidation of the parasitic HC (i.e., the HC that escapes the main combustion process; e.g. the HC in the crevices).

[1] Heat transfer rate ~ $rpm^{0.8}$ [12]; available time ~ rpm^{-1}; therefore the heat transfer is proportional to $rpm^{-0.2}$. Thus heat transfer increases with decrease of rpm, although the dependence is not strong and is relatively small compared to the temperature effect.

Because of the low RPM at the first cycle, end of combustion occurs early in the expansion process; so quenching is not a severe problem unless the charge is very rich. Oxidation of the parasitic HC is oxygen limited and it is therefore not sensitive to the value of λ in the rich range.

To study the effect of ignition timing on the first cycle engine behavior, a spark sweep was carried out at a fixed fueling of 39 mg and at starting position E. At this condition, the in-cylinder λ was approximately stoichiometric and the engine speed at ignition of the first cycle was at ~200 rpm. The result is shown in **Figure 6.11**. Because of the low RPM and that there is significant acceleration of crank shaft speed during the heat release process, the MBT timing at ~185° (5° ATDC) is substantially retarded from the usual practice. Furthermore, the nominal ignition timing of at 170° (10° BTDC) is much too advanced for good torque output.

6.2.2 Hot Start 2nd and 3rd Cycles

The second and third cycle IMEPg and EOHC behaviors were measured under the following fueling conditions. For each starting position, the first cycle was fueled at the various levels as described in the last section. The second cycle was fueled at a fixed 26 mg. In the third and subsequent cycles, the fueling was done via a speed/density calibration based on the intake manifold pressure to deliver a stoichiometric charge. The choice of the 26 mg fueling in the second cycle was based on empirical results showing this amount would give an approximately stoichiometric charge at typical values of the manifold pressure during the second cycle intake. For both the second and third cycles, the start of injection was at BDC of the expansion stroke.

The IMEPg and EOHC values for starting position A with the various first cycle fueling are shown in **Figure 6.12**. In this case, for the very low (13 mg) first injection, the second cycle had a misfire (very low IMEPg). For all other starting positions with this first cycle fueling, strong IMEPg values for the second cycle were obtained. This behavior is due to the higher rpm at the first cycle with position A so that much of the

first cycle fuel is carried forward to the cylinder by the strong port flow and not much of this small amount of injected fuel is left for the second cycle.

The general behavior of the 2nd cycle as a function of the residual fuel from the first cycle are shown in **Figures 6.13 to 6.16.** The latter quantity is the difference between the first cycle injected fuel and the amount that is in the first cycle charge as measured by the FFID. Note that a substantial amount of this residual fuel may not be going to the second cycle but it is lost to the sump [6.1].

The IMEPg and EOHC values for the second cycle are shown as a function of the first cycle residual fuel in **Figure 6.13**. Strong firings were obtained in all the cases. (The single misfired second cycle for the 13 mg first cycle fueling in case A has been omitted in the plot.) The second cycle EOHC values increase with increase of first cycle residual fuel.

The second cycle behavior may be explained by the augmentation of the 2nd cycle injected fuel by the residual fuel from the first cycle. This augmentation is shown in **Figure 6.14**, which shows that the 2nd cycle mixture is enriched by the residual fuel. The sensitivity is that λ decreases by 0.1 with every 22 mg increase in the residual fuel.

The second cycle IMEPg values are shown as a function of in-cylinder λ in **Figure 6.15**. The values drop off on the lean side, but similar to the first cycle behavior (**Figure 6.5**), they do not vary much over a wide range of rich equivalence ratios. This feature will be discussed in the next section.

The second cycle EOHC values are shown as a function of in-cylinder λ in **Figure 6.16**. As the mixture goes richer, the EOHC value increases. The rise of ~3000 to 6000 ppmC1 for λ in the range of 1.1 to 0.65 is approximately the same as that in the first cycle (except for case E, the late OVI case). Thus the HC mechanisms for the first and second cycle are likely to be similar.

The third cycle engine behavior is shown in **Figure 6.17**. By this time, the IMEPg values show little dependence on the first cycle setting. There is still some dependence. of the in-cylinder λ values on the left over fuel from the first cycle; the slope — a λ decrement of 0.1 with a residual fuel increase of 42 mg —is approximately half of that of the second cycle (see **Figure 6.14**). Because of this change in λ, the EOHC also increases moderately with the increase of first cycle residual fuel.

6.3 Ambient Engine Experiments

6.3.1 Ambient Start 1st Cycle

For ambient temperature starts (20° C coolant temperature), the Ford EEC unit did not provide enough first cycle fuel enrichment to cylinders 1-3 for consistent firing. Therefore the engine rpm and cylinder #4 behavior for starting positions A and B were erratic: they depended on how many previous firings were there. To compare the results consistently, only the data from runs without any prior firing are presented here. Thus for all the starting piston positions in the following discussion, cylinder #4 was the first one to fire. The engine speeds at ignition for all cases were at ~200 rpm.

The first cycle IMEPg values for cylinder #4 are shown in **Figure 6.18** as a function of the first cycle fueling. The results for starting position E (late Open-Valve Injection) are not shown. It was found that for this case, the engine failed to fire in the first cycle no matter how much fuel was injected. This was due to the significant liquid fuel present so that the spark plug was wetted by the fuel.

Compared to the hot start case, substantially larger amount of fuel was needed to achieve firing (~80 mg and above were needed, compared to the ~26 mg required for the hot start). Once firing was achieved, however, the IMEPg values were not sensitive to the amount of fueling.

The first cycle in-cylinder λ values are shown in **Figure 6.19.** The mixture became richer with increase of first cycle fueling. The change in λ, however, is far less than the

change in fueling; e.g., when the fueling is changed from 100 to 270 mg (factor of 2.7), the value of λ only changes from ~1.1 to 0.7 (factor of 1.6). Thus as more liquid fuel is injected, a proportionally lower fraction gets delivered into the combustible mixture; see the plot in **Figure 6.20**, which shows a positive curvature.

The first cycle IMEPg are shown as a function of the in-cylinder λ values in **Figure 6.21**. The engine does not fire until the mixture is richer than $\lambda \sim 1.1$. This criterion is almost the same as that of the hot start (90° C coolant temperature case (see **Figure 6.5**). Then over a range of λ values (~0.7 to 1.1), the IMEPg values do not change appreciably.

The insensitivity of the IMEPg values to λ until λ is very rich is also observed in the hot start. The observation may be explained as follows. The engine at cranking is running at such a low rpm (~200 rpm at ignition) that the heat release per crank angle is very high. Thus at the set ignition timing at 10° BTC, the combustion is too advanced. As the mixture is enriched (at fixed spark timing), the laminar flame speed lowers and the heat release schedule is more favorably phased. (Note that at the low cranking speeds, there is not much turbulence; whence the laminar flame speed has a substantial effect on the combustion rate. Also for normal engine speeds, the flame propagation rate at $\lambda<\sim0.6$ will be too slow for combustion completion. Such, however, is not the case at the cranking speed.) The gain in IMEPg due to the better phasing, however, is offset by the decrease in combustion efficiency due to enrichment. Note that there is a substantial drop in the combustion efficiency (to ~50%) when λ is enriched to 0.65, but because more fuel is burned the drop of the relative energy release is modest (to 83%), see **Figure 6.22**. The net result is that IMEPg values do not change appreciably until the mixture is very rich.

The first cycle EOHC are shown in **Figure 6.23** as a function of the first cycle in-cylinder λ values. Very high levels of EOHC were registered for the cycles that did not fire. For the firing cycles, however, the values for starting positions A, B and C are in the 4000 to 8000 ppmC1 range. These values are a few thousand PPM higher than those of the hot start; see **Figure 6.10**. For starting position D with fueling being injected at the early part

of the valve opening period, the EOHC values are significantly higher. This higher emission is a result of the direct liquid deposition into the cylinder by the injection process [6.1, 6.2, 6.6, and 6.7] – the liquid fuel film may survive the combustion process and then evaporate and exit the combustion chamber as EOHC. (In the hot start, because of the higher cylinder wall temperature, there is very little liquid fuel film that survives the cycle [6.2]; hence the EOHC behavior for Case C is the same as that of A and B, see **Figure 6.10**. In that figure, the high EOHC for Case E is due to mixture non-uniformity.)

6.3.2 Ambient Start 2nd Cycle

As mentioned before, because the Ford EEC unit did not provide sufficient enrichment for cylinders 1-3, the firing of these cylinders in the first 2 cycles were erratic. In the last section, only the data in which cylinder #4 was the first to fire was selected and reported. Within that data set, however, there could be one, two or three firings among cylinders 1-3 before the second cycle of cylinder #4. Thus the cylinder #4 - second cycle IMEPg data had large variations in them accordingly and no representative results can be extracted. Therefore, only the in-cylinder λ values for the second cycle of cylinder #4 are discussed in the following. (Again, cylinder #4 was the first one to fire in this set of data.) The results represent the behavior of the second cycle mixture preparation.

The second cycle in-cylinder λ are plotted against the residual fuel from the first cycle in **Figure 6.24**. The residual fuel is defined as the difference between the amount injected in the first cycle and that which appeared in the charge as measured by the in-cylinder FFID. The data were taken with the various starting piston positions (denote by the plotting symbols in the figure) and different first cycle fueling. The second cycle fueling was fixed at 26 mg. The in-cylinder λ values correlates well with the amount of the first cycle residual fuel, which augments the second cycle fueling. The value of λ decreases by 0.1 for every 74 mg of residual fuel increase. This slope is considerably less than that of the hot start (see **Figure 6.14**), which only requires a decrease of 22 mg of residual fuel for the same decrement of λ . The lower slope at the ambient temperature implies a much reduced delivery (factor of ~3.4) of the residual fuel to the second cycle due to the

lower rate of evaporation; thus the residual fuel may have a long residence time in the port and may affect the behavior of many subsequent cycles.

6.4 Cold Engine Experiments and Summary across Starting Temperatures

Engine cranking/startup experiments were performed at 0 degrees C. The entire engine was enclosed by insulating walls, and cooled by an industrial air-conditioning unit. These cold engine-starting experiments were performed only at initial engine position A. As with the ambient starts, the Ford EEC engine controller did not deliver enough fuel on the first engine cycle to cylinders #1-3. Thus, the engine speed at IVC for cylinder #4 was approximately that of the starter motor speed (~200 rpm).

The IMEPg behavior as a function of injected fuel is shown in **Figure 6.25** for all three starting temperatures. It is clear that as engine starting temperature drops, the level of injected fuel necessary for strong first-fire increases dramatically. Hot starting requires approximately 26 mg of injected fuel, while ambient starting and cold starting require fuel injection levels of approximately 100 mg and 300 mg, respectively. For all temperatures (except hot starting position A), additional injected fuel beyond the minimum for a positive first fire does not increase IMEPg. This effect was discussed in the previous section as a tradeoff between reduced combustion efficiency and improved combustion phasing. At 90 C starting, position A, maximum levels of IMEPg are seen due to its very high engine speed.

The in-cylinder λ behavior for the first cycle of crank across all three starting temperatures is shown in **Figure 6.26**. The trends are similar for all starting temperatures with in-cylinder λ decreasing towards an asymptote. The minimum λ (richest state) is approximately 0.5 λ for hot starting, and approximately 0.9 λ for ambient and cold starting. Additionally for hot starting, the slope with which λ approaches 1 is much steeper with increasing injected fuel as compared to ambient starting. Cold starting shows an even more gradual enrichment behavior across large increases in injected fuel.

Figure 6.27 shows the fraction of injected fuel into the combustion chamber as vapor plotted against injected fuel for the three starting temperatures. Again, the decreasing levels of injected fuel entering the combustion chamber with decreasing temperature are significant. At all temperatures, more fuel injection delivers a fractionally less amount of injected fuel to the combustion chamber. For cold starting approximately only 5% of the injected fuel contributes to in-cylinder fuel vapor. There is only a slight decline in this value as fuel injection is increased by many factors.

A compilation of IMEPg data plotted against in-cylinder λ is shown in **Figure 6.28**. For all temperatures and engine positions (positions A and D only shown in this figure), the transition from negative to positive IMEPg behavior occurs around ~1.1. In-cylinder fuel vapor concentrations below 1.1 result in strong first fires across all temperatures.

Finally, second cycle in-cylinder λ behavior is shown versus residual first cycle fuel in **Figure 6.29**. The second cycle injected fuel mass is constant at 190 mg for all of the starts. Significantly higher levels of residual fuel exist for cold starting as compared to ambient and hot starts. Additionally, the slope of decreasing 2^{nd} cycle λ with increasing residual fuel is approximately the same for cold and ambient starting.

Chapter 6 References:

[6.1] Takeda, K., Yaegashi, T., Sekiguchi, K., Sakito, K. and Imatake, N., "Mixture Preparation and HC Emissions of a 4-Valve Engine with PFI during Cold Starting and Warm-up", SAE Trans. 104, 3, pp. 88-94, Paper #950074, 1995.

[6.2] Shin, Y., Cheng, W. and Heywood, J., "Liquid Gasoline Behavior in the Engine Cylinder of a SI Engine", SAE#941872, 1994.

[6.3] Imatake, N., Saito, K., Morishima, S., Kudo, S., and Ohhata, A., "Quantitative Analysis of Fuel Behavior in a PFI Gasoline Engine", SAE Trans. 106, 3, pp. 1779-1789, aper 971639, 1997.

[6.4] Chun, K. M. and Heywood, J. B., "Estimating Heat Release and Mass of Mixture Burned from SI Engine Pressure Data", Combustion Science and Technology, Vol.54 pp. 134-143, 1987.

[6.5] Cheng, W.K., Hamrin, D., Heywood, J.B., Hochgreb, S. Min, K.D., Norris, M., "An Overview of HC Emissions Mechanisms in Spark-Ignition Engines", SAE Trans. 102, Paper 932708, pp. 1207-1220, 1993.
[6.6] Stanglmaier, R.H., Hall, M. J. and Matthews, R.D., "In-Cylinder Fuel Transport during the First Cranking Cycles in a PFI 4-Valve Engine", SAE #970043, 1997.
[6.7] Witze, P.O. and Green, R.M., "LIF and Flame-Emission Imaging of Liquid Fuel Films and Pool Fires in a SI Engine during a Simulated Cold Start", SAE Trans. 106, 3, Paper 970866, pp 1291-1305, 1997.

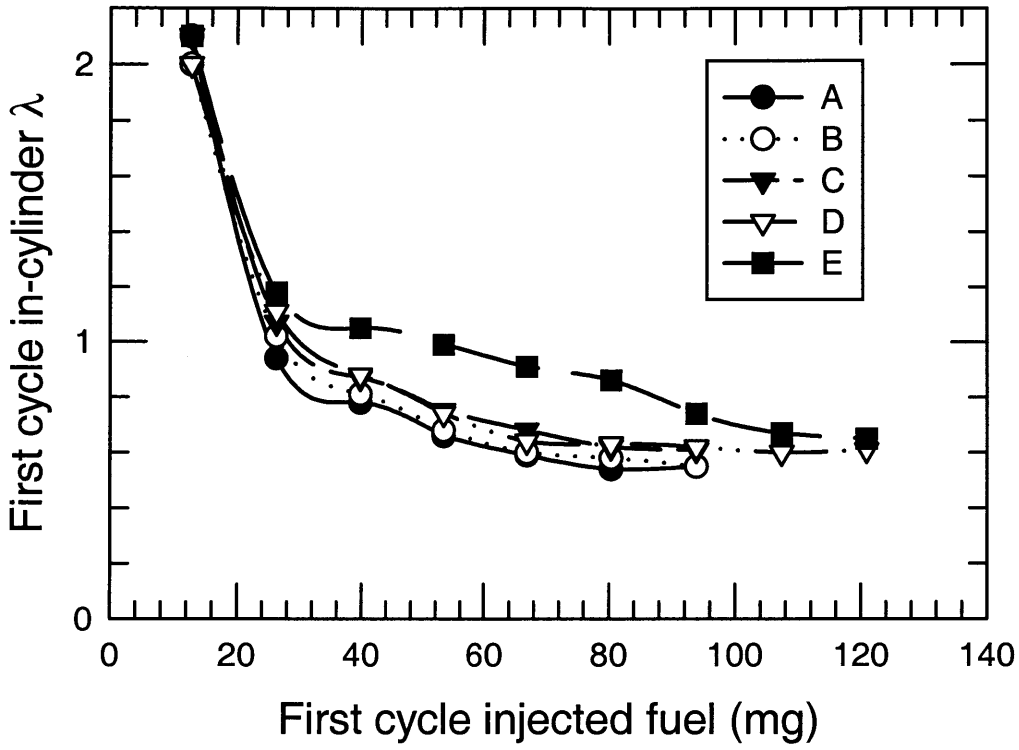

Figure 6.1: In-cyl. air/fuel equivalence ratio λ of first cycle as measured by the FFID for the different hot starting positions as a function of the injected fuel mass.

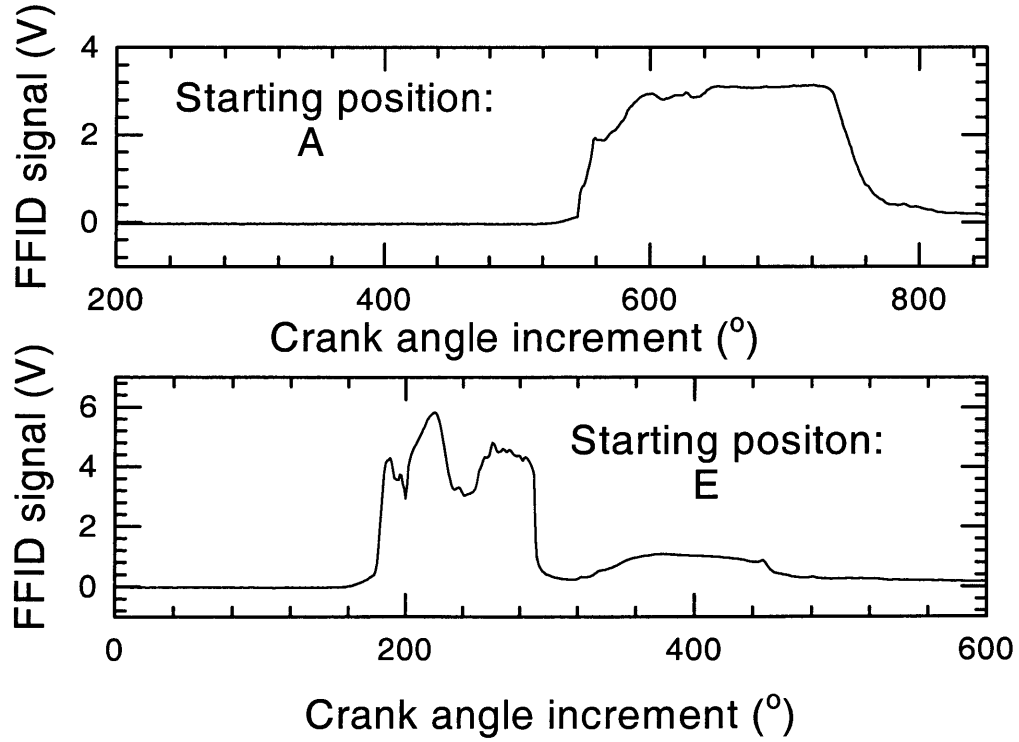

Figure 6.2: Top: FFID signal of in-cylinder HC measurement for a well mixed charge; Bottom: that for starting postioin E, for which the signal indicates substantial charge inhomogeneity. Hot start.

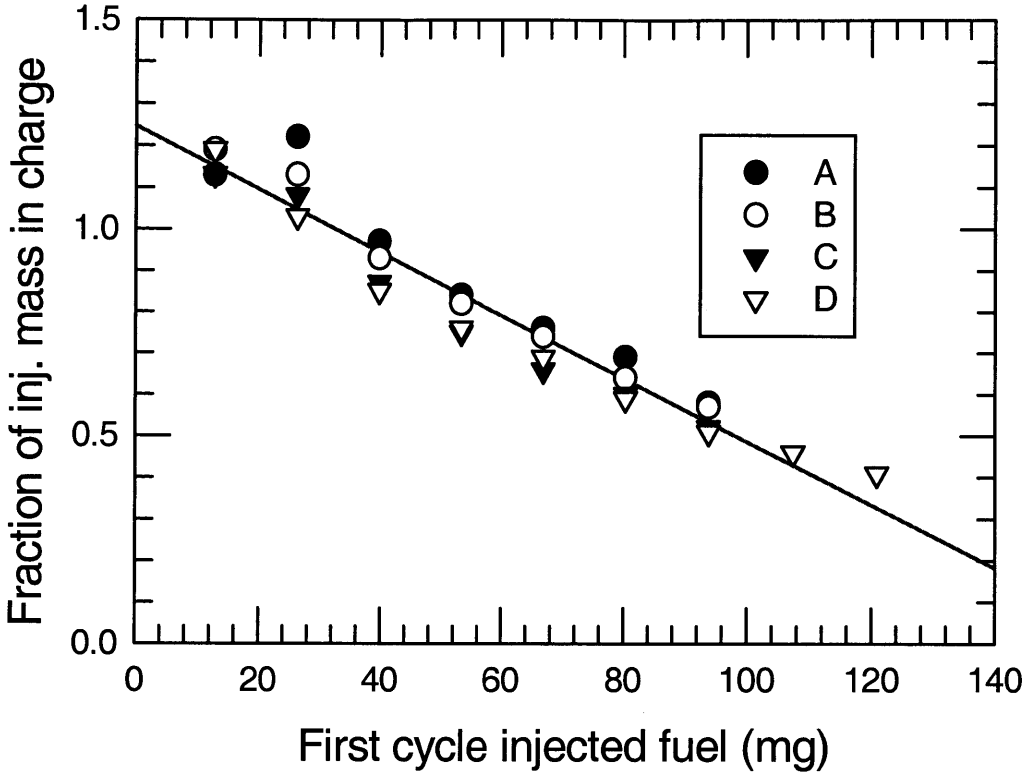

Figure 6.3: The fraction of the injected fuel that constitutes the combustible mixture in the first cycle in a hot start.

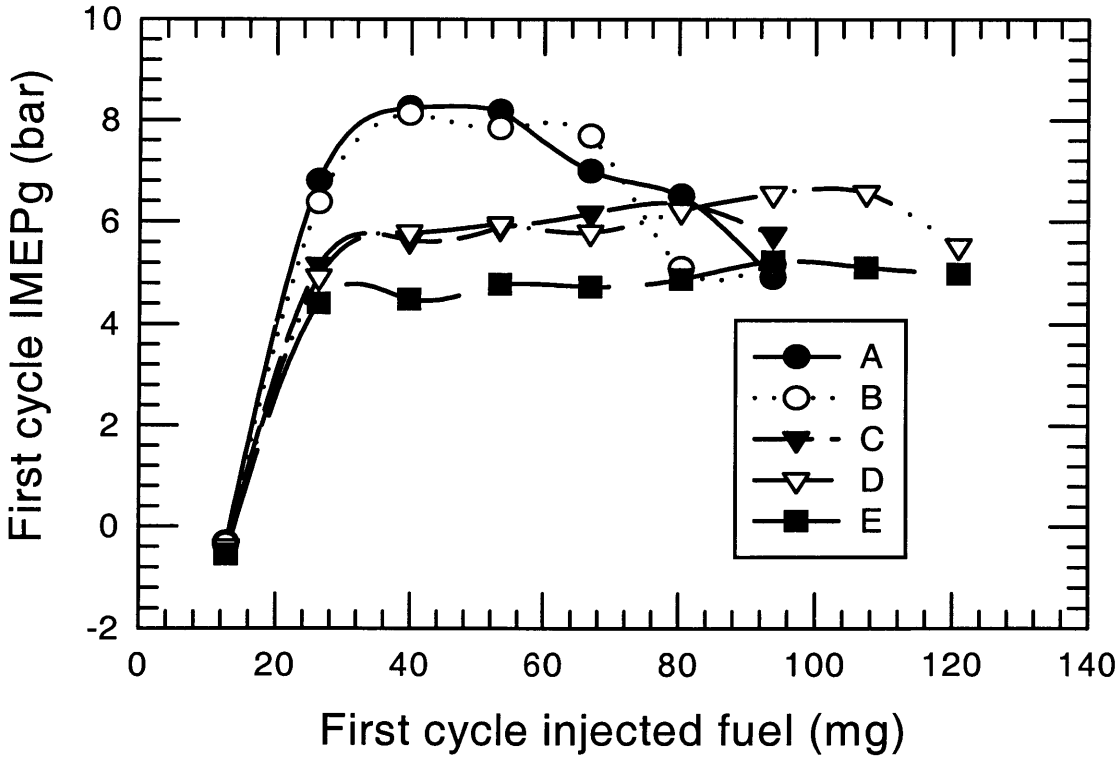

Figure 6.4: Gross IMEP of first cycle of cylinder #4 in hot start as a function of fueling and starting positions.

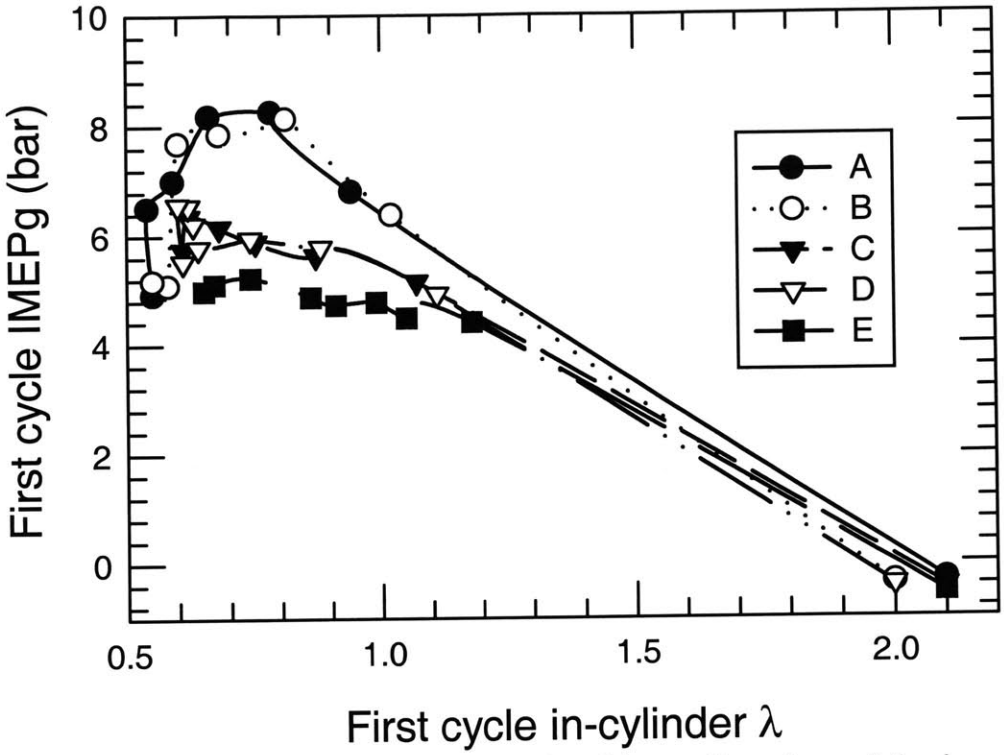

Figure 6.5 First cycle IMEPg of cylinder #4 as a function of the in-cylinder λ value for the different starting positions; hot start.

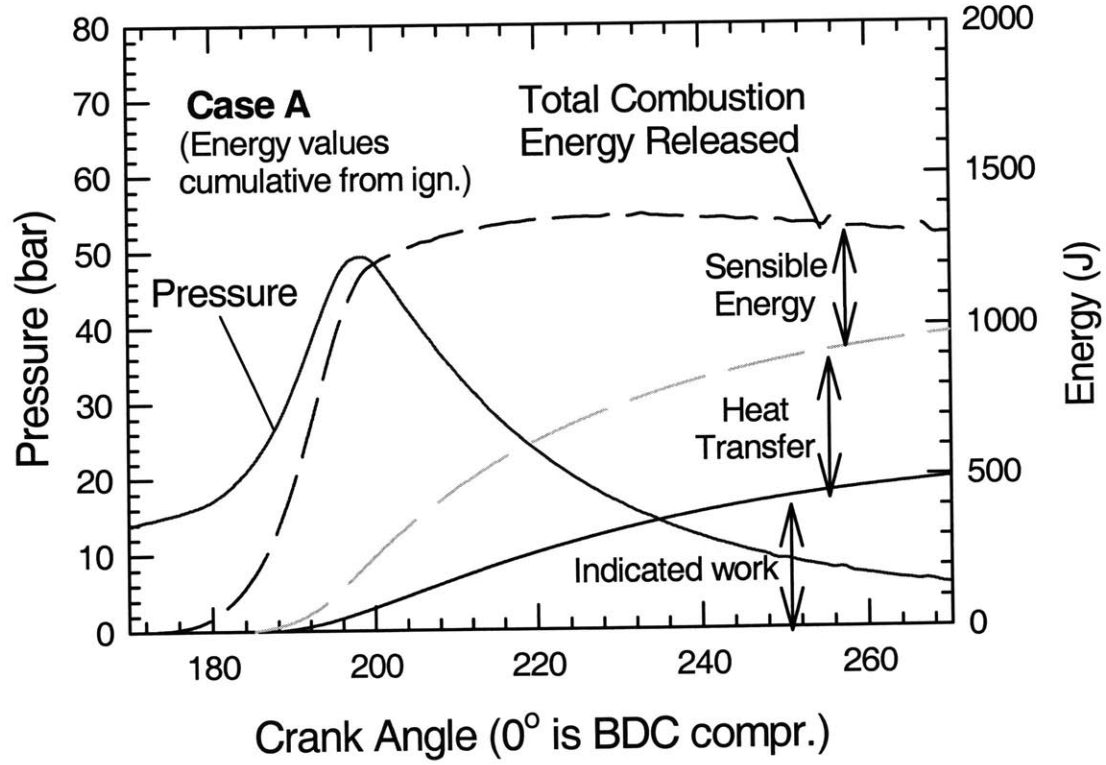

Figure 6.6: Heat release analysis for cylinder #4 first cycle combustion with starting position A; 39 mg fuel; ignition at 170° CA.

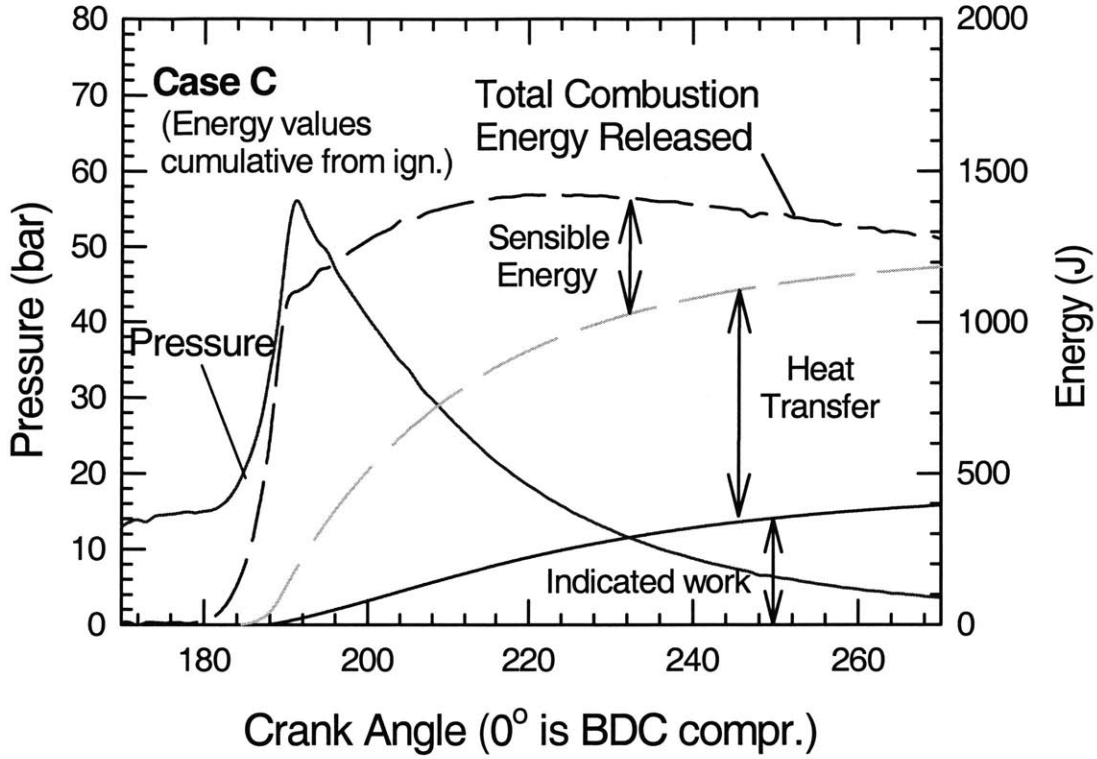

Figure 6.7: Heat release analysis for cylinder #4 first cycle combustion with starting position C; 39 mg fuel; ignition at 170° CA.

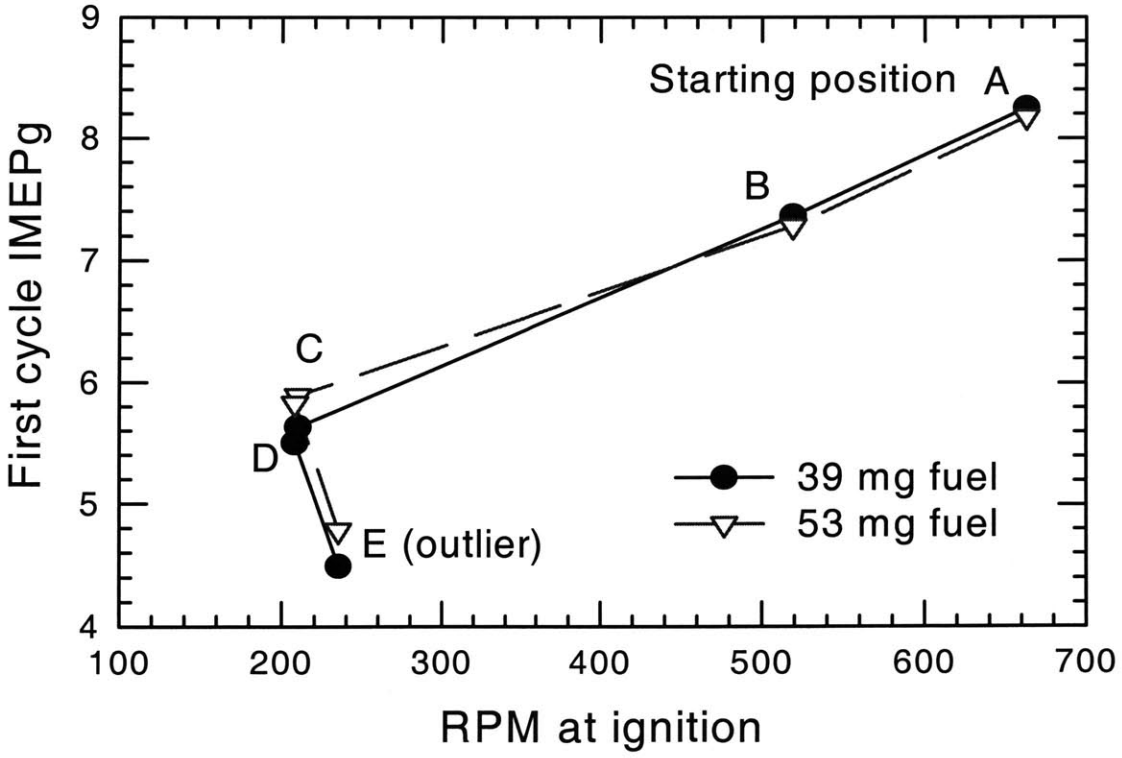

Figure 6.8: First cycle IMEPg versus instantaneous engine speed at ignition point. Ignition fixed at 10° BTC.

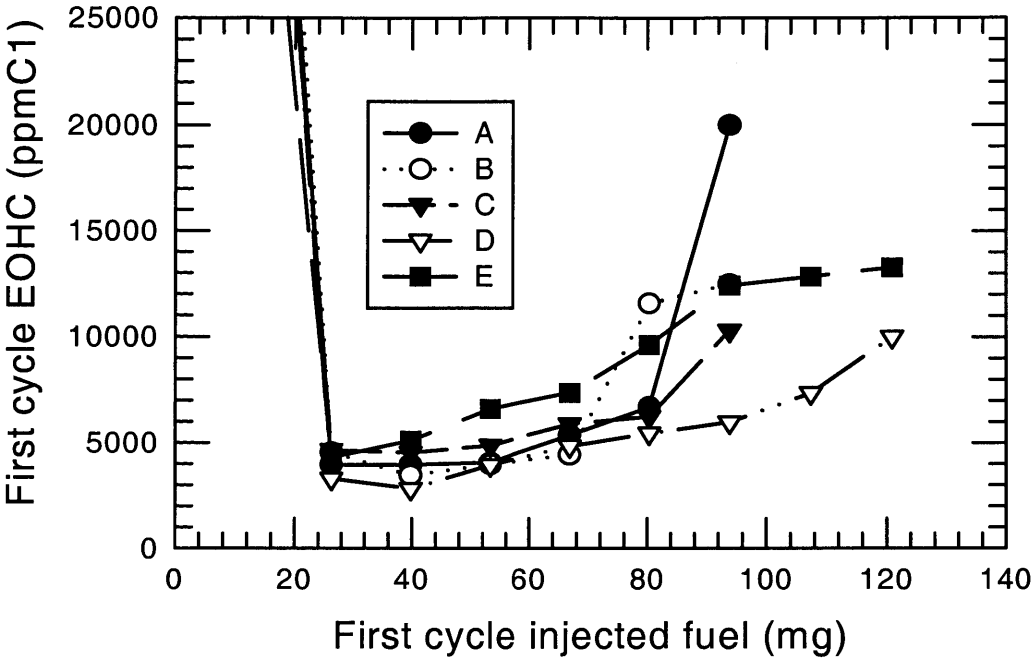

Figure 6.9: First cycle engine-out hydrocarbon for the different starting positions, as function of first cycle fuel.

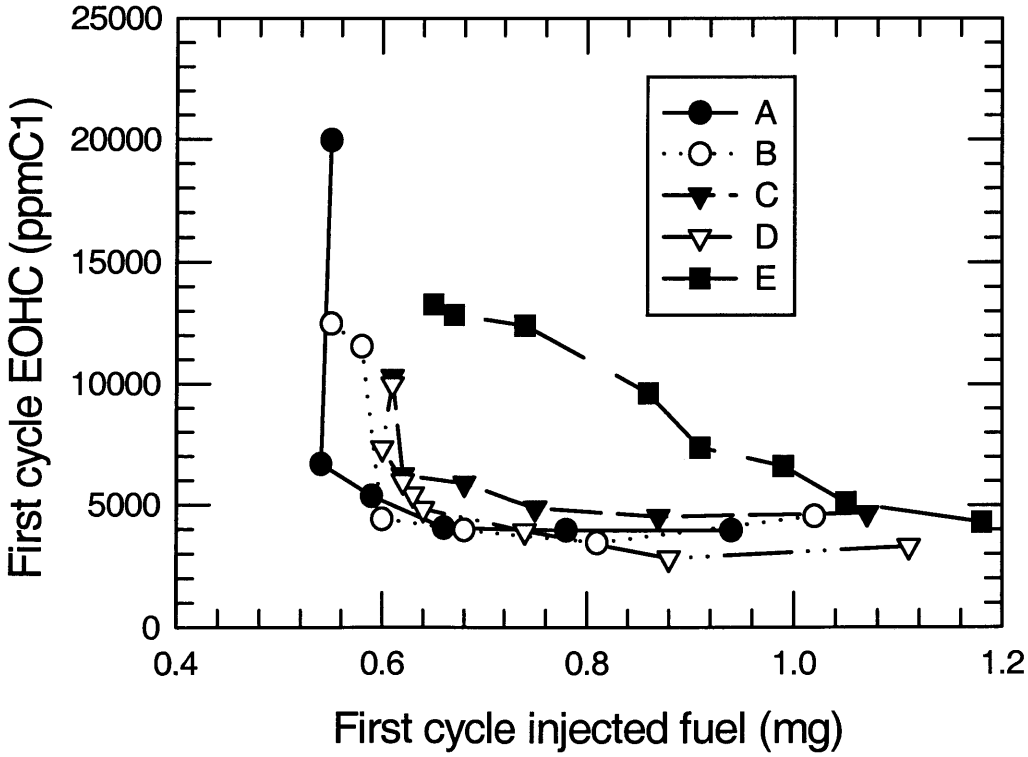

Figure 6.10: First cycle Engine-Out Hydrocarbon for the different starting positions, as function of in-cylinder λ.

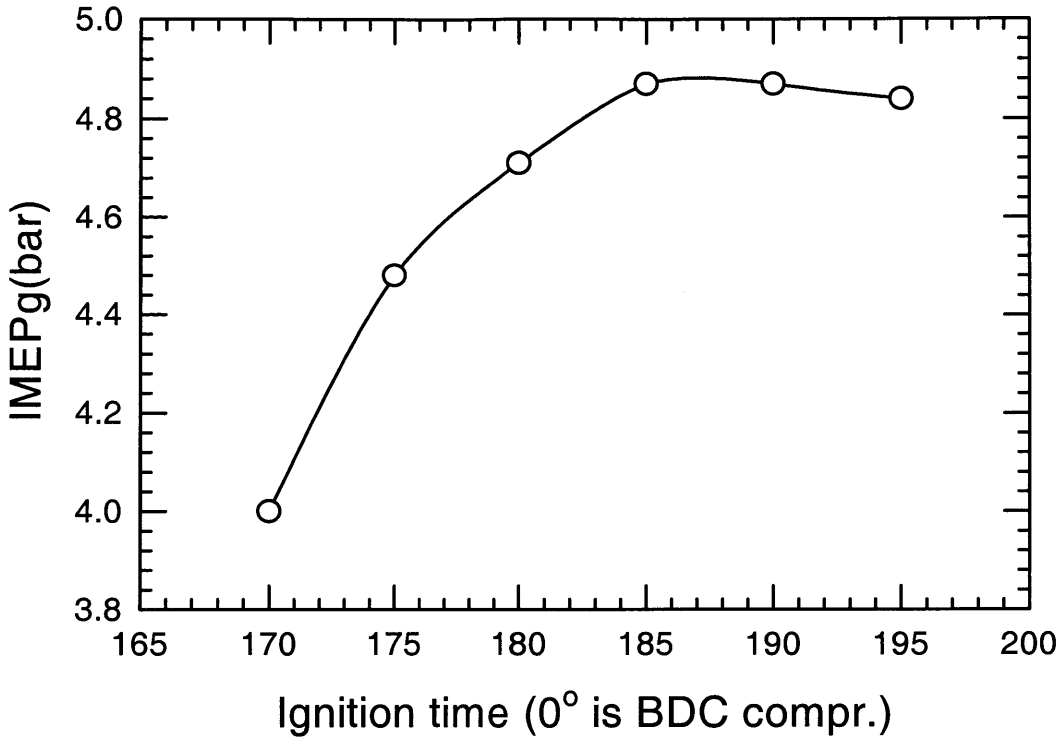

Figure 6.11: First cycle park sweep at 39 mg fuel; starting position E.

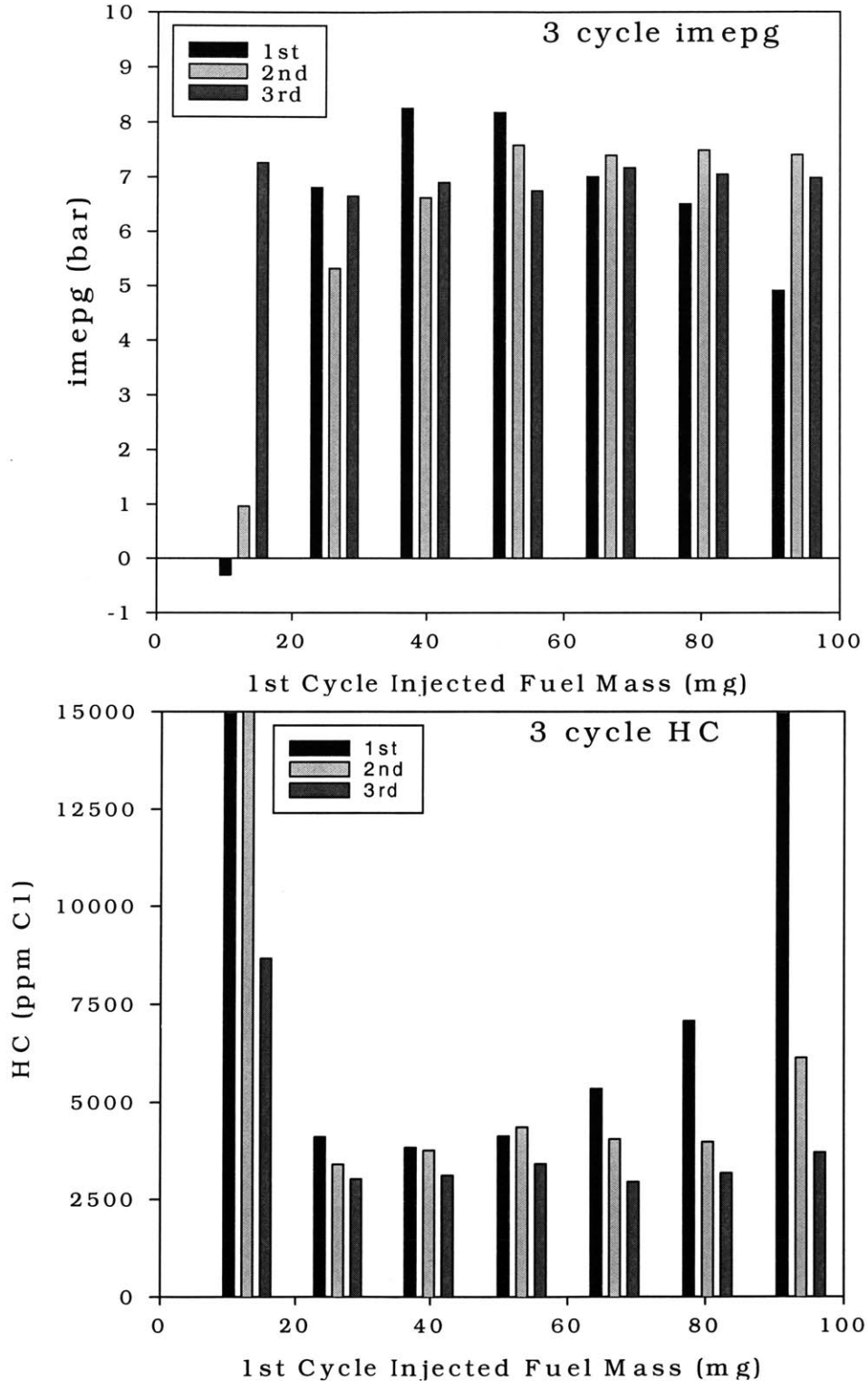

Figure 6.12: The first three cycles IMEPg and EOHC; piston starting position A. See text for fueling scheme.

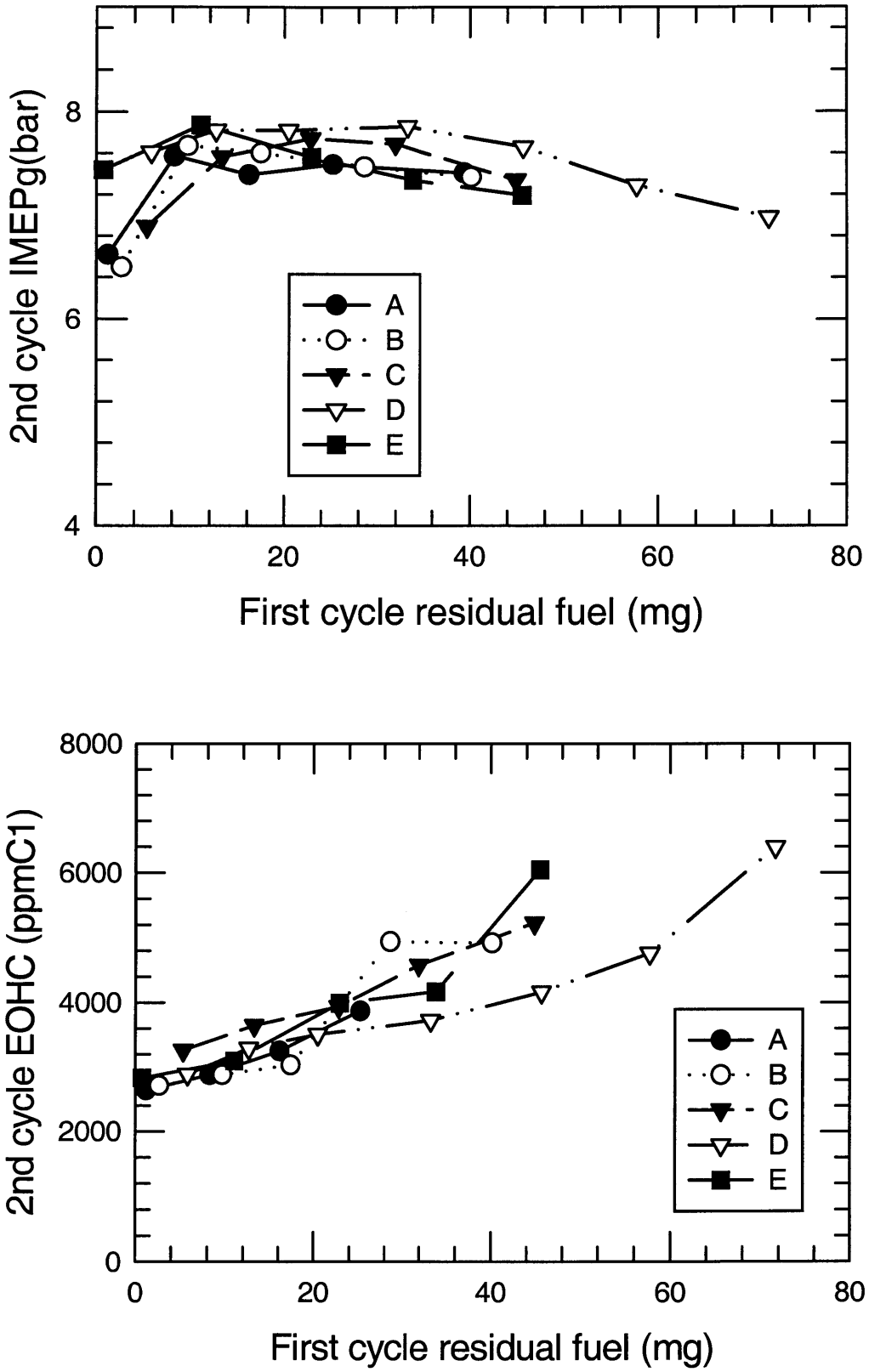

Figure 6.13: Second cycle IMEPg and EOHC as a function of the residual fuel from the first cycle; hot start.

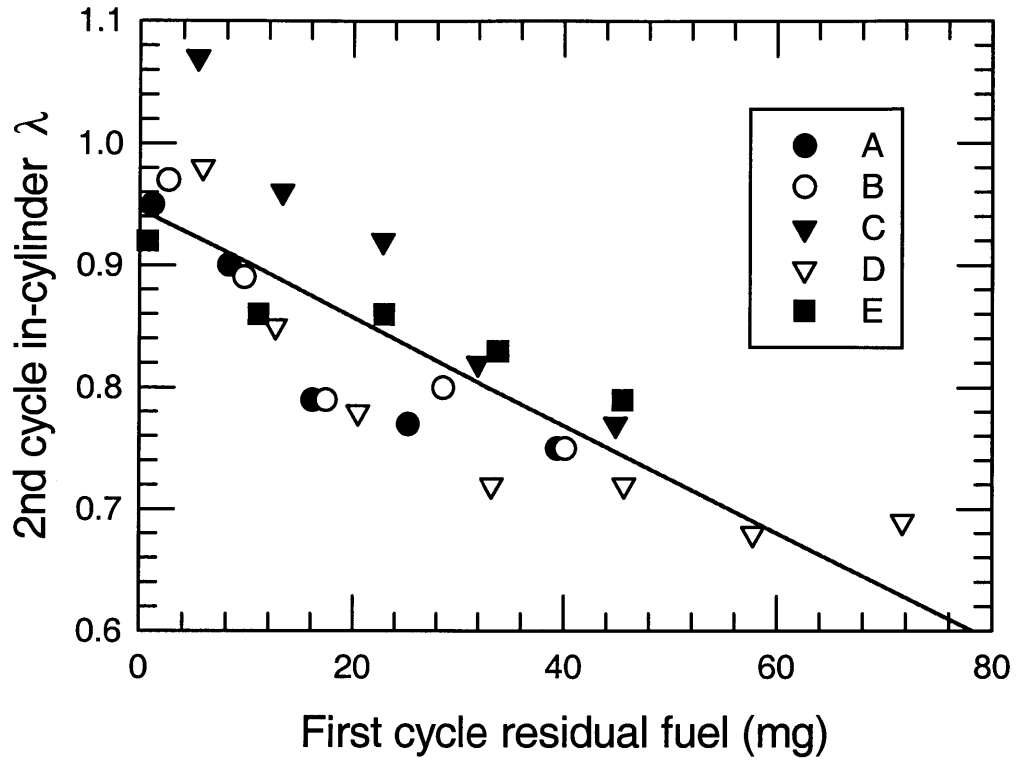

Figure 6.14: Second cycle in-cylinder λ values as a function of the residual fuel from the first cycle; hot start. Line is least square fit.

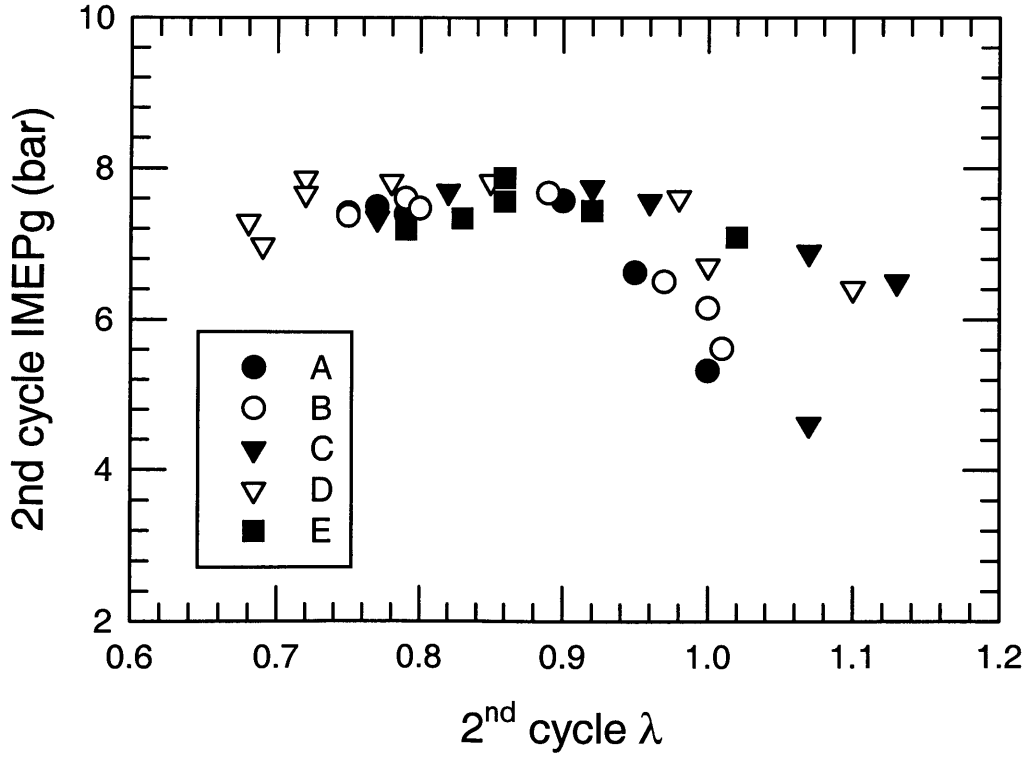

Figure 6.15: Second cycle IMEPg as a function of the second cycle in-cylinder λ; hot start.

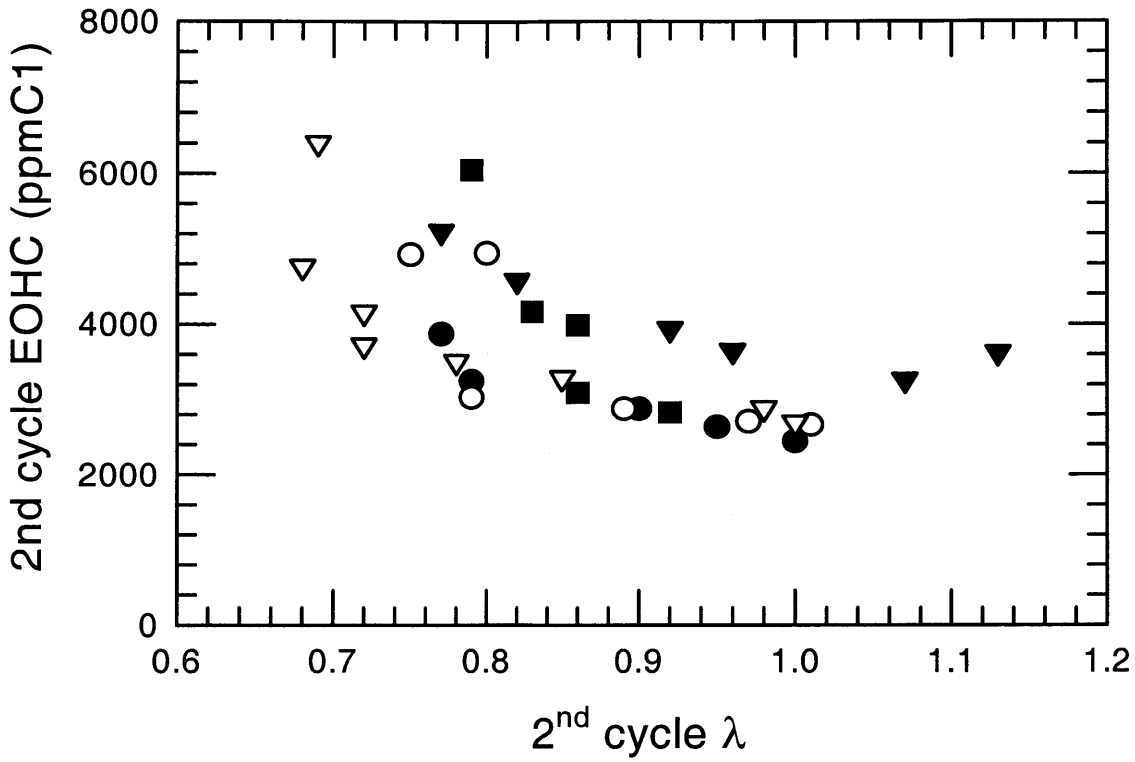

Figure 6.16: Second cycle EOHC as a function of the second cycle in-cylinder λ; hot start. Line is least square fit to the data

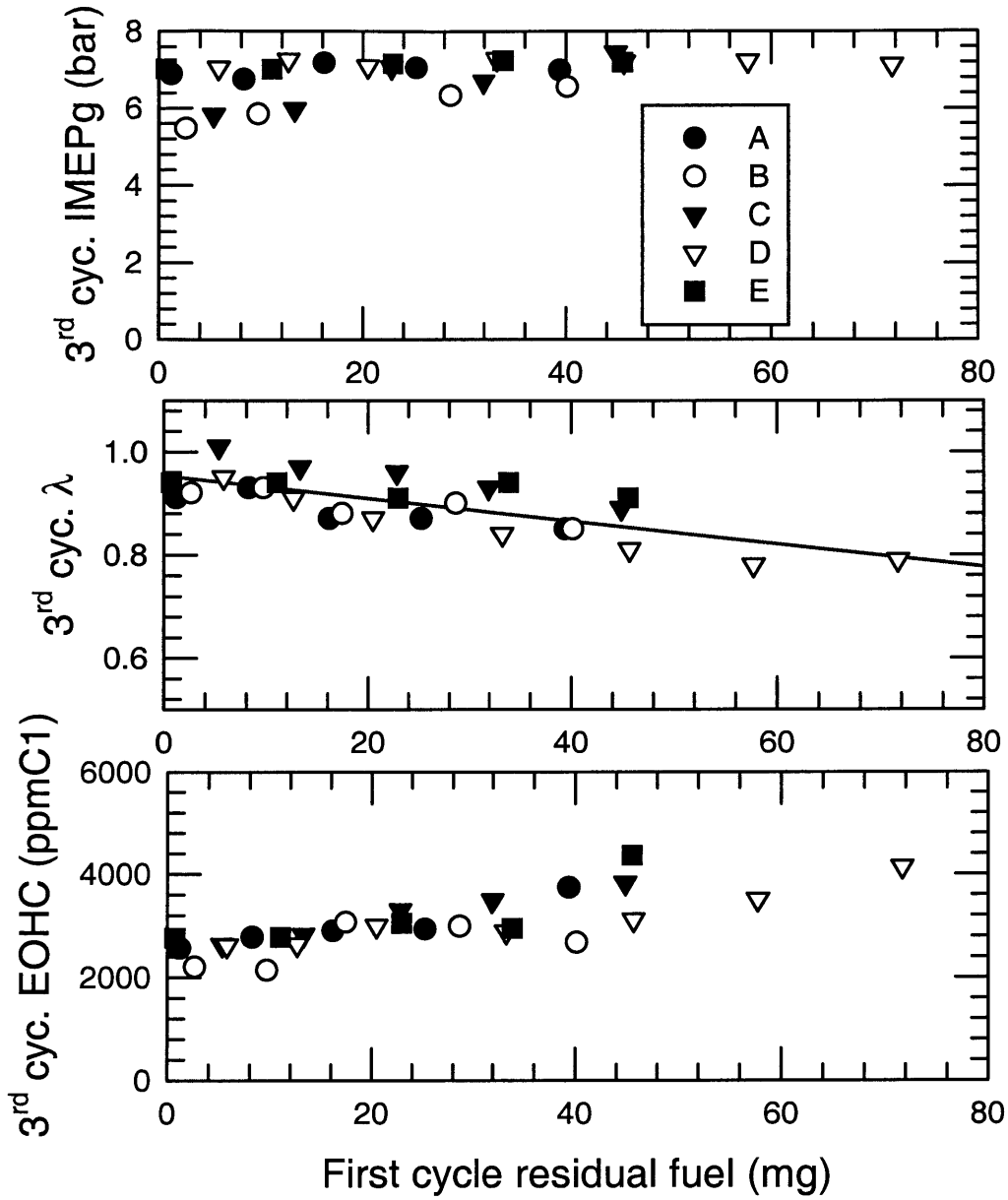

Figure 6.17: Third cycle engine behavior as a function of the residual fuel from the first cycle; hot start. Line is least square fit of 3rd cycle λ.

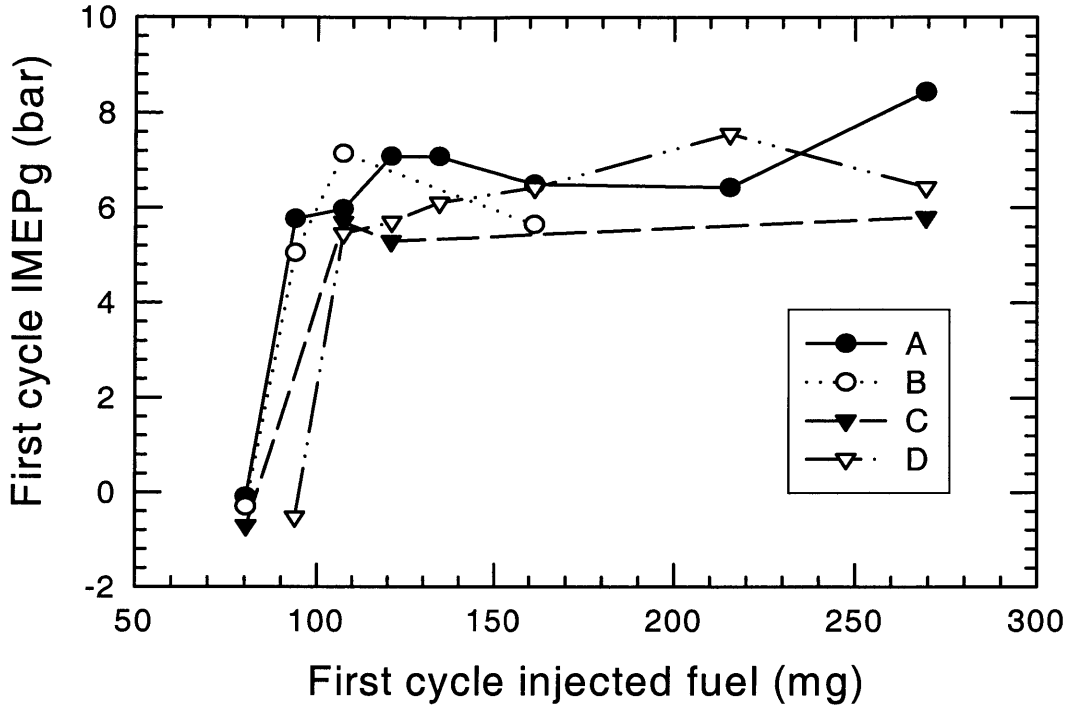

Figure 6.18: First cycle IMEPg versus injected fuel, ambient temperature start.

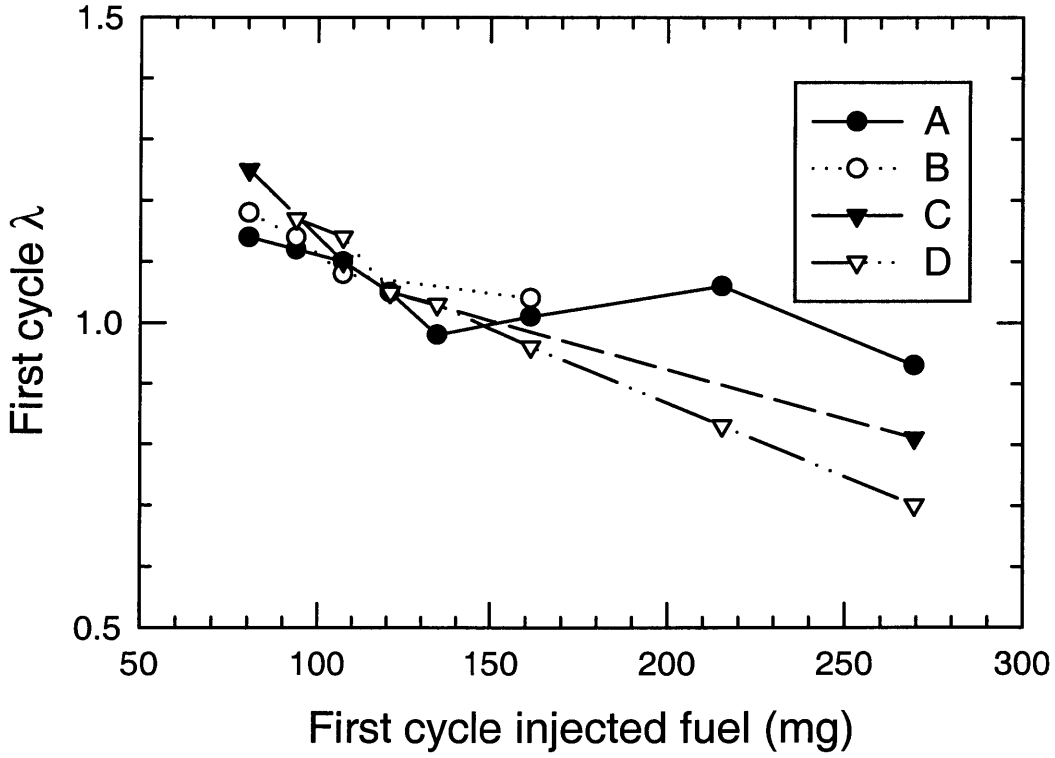

Figure 6.19: In-cylinder first cycle λ values versus first cycle fueling; ambient temperature start.

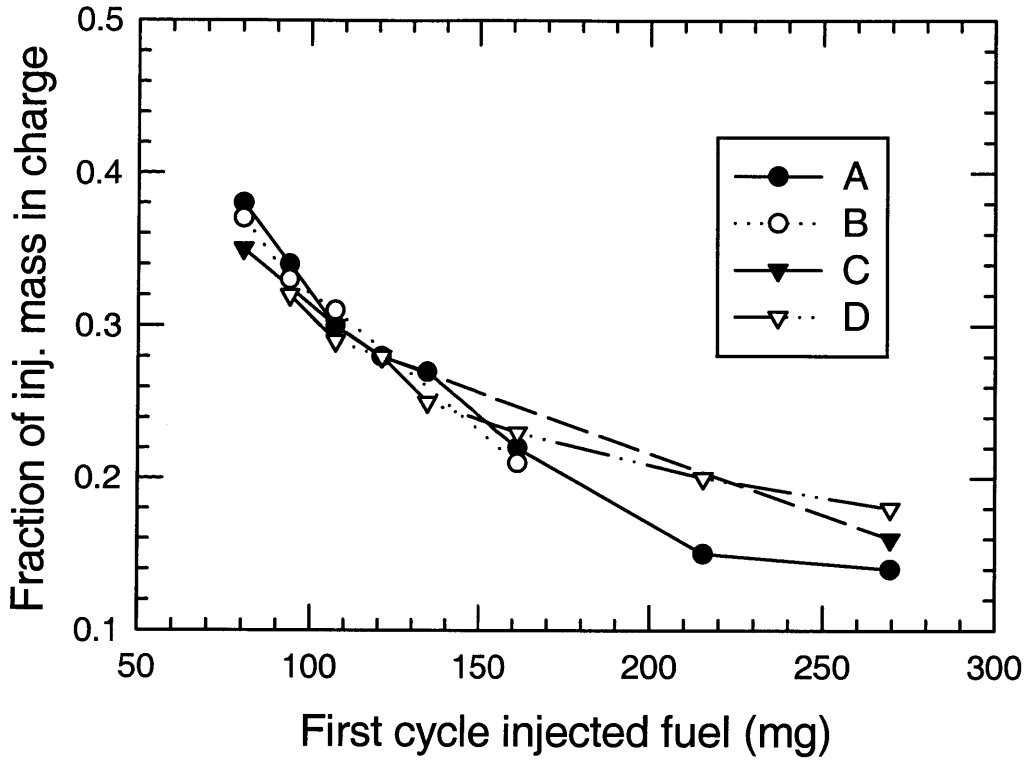

Figure 6.20: Fraction of the injected mass that gets delivered to the charge mixture in the first cycle as measured by the FFID; ambient temperature start.

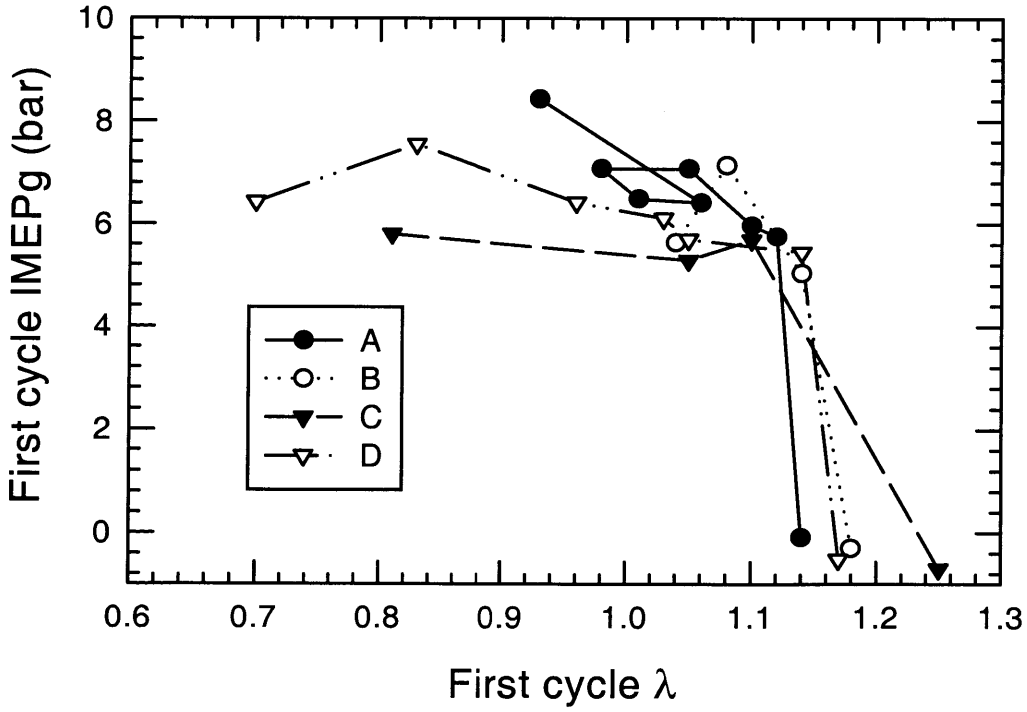

Figure 6.21: First cycle IMEPg as a function of the in-cylinder λ values; ambient temperature start.

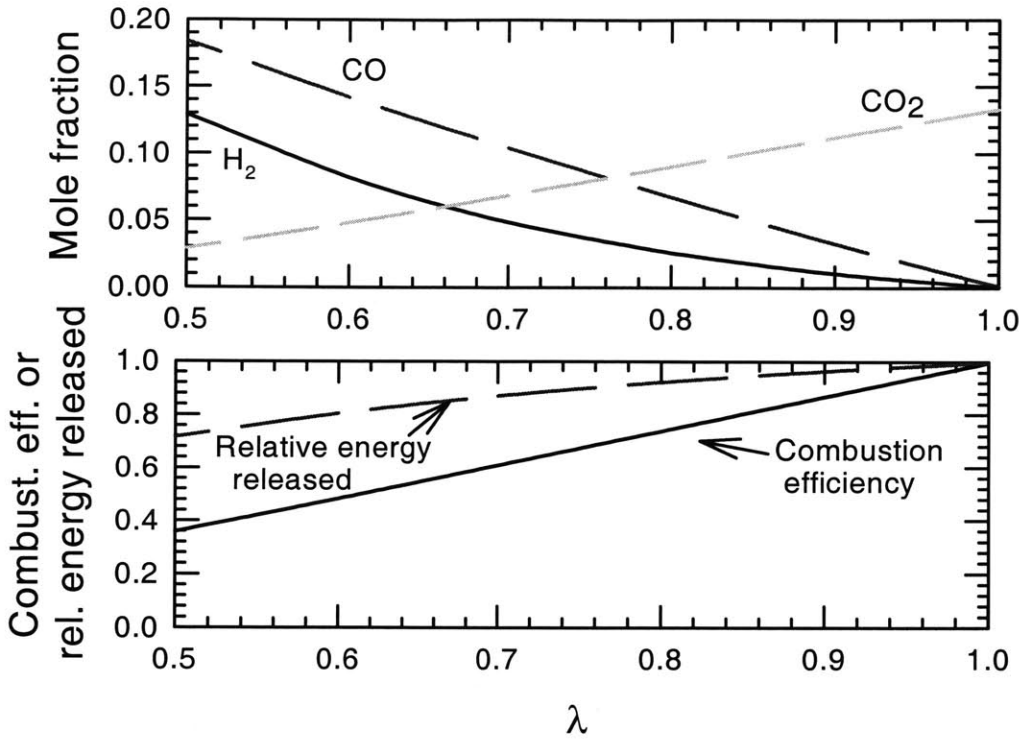

Figure 6.22: Gasoline combustion behavior as a function of λ; top: exhaust species; bottom: combustion efficiency and energy release relative to that at λ = 1.

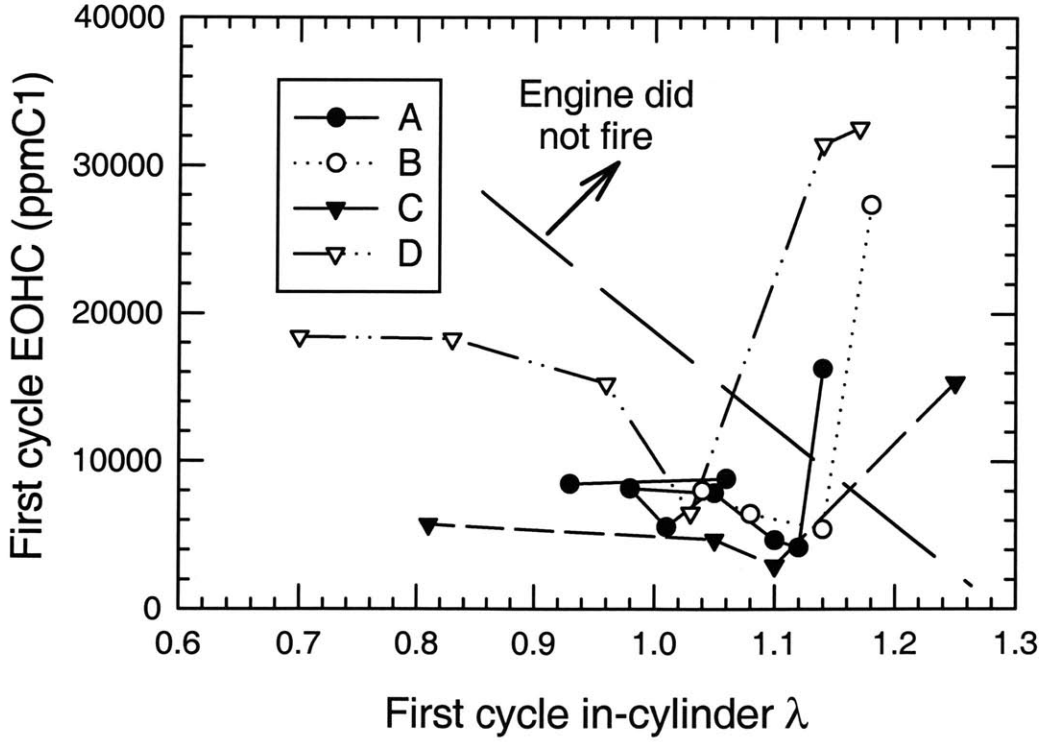

Figure 6.23: First cycle EOHC as a function of in-cylinder λ values; ambient temperature start.

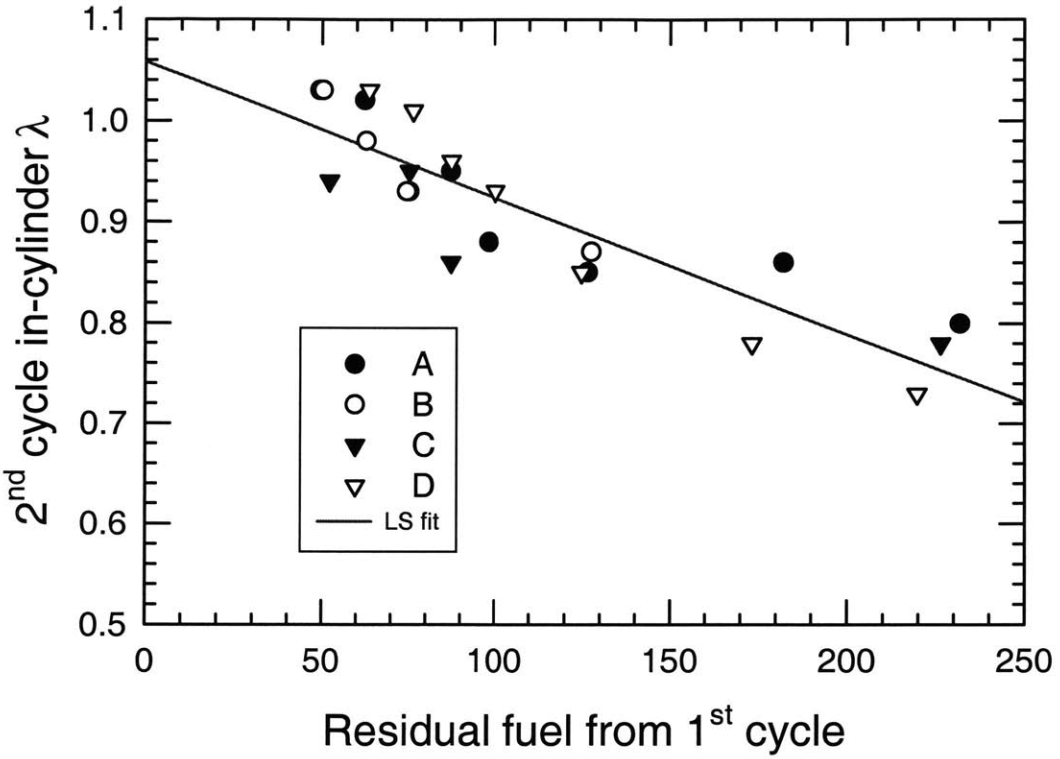

Figure 6.24: In-cylinder λ values as a function of the residual fuel from the first cycle, ambient temperature start. Line is least square fit.

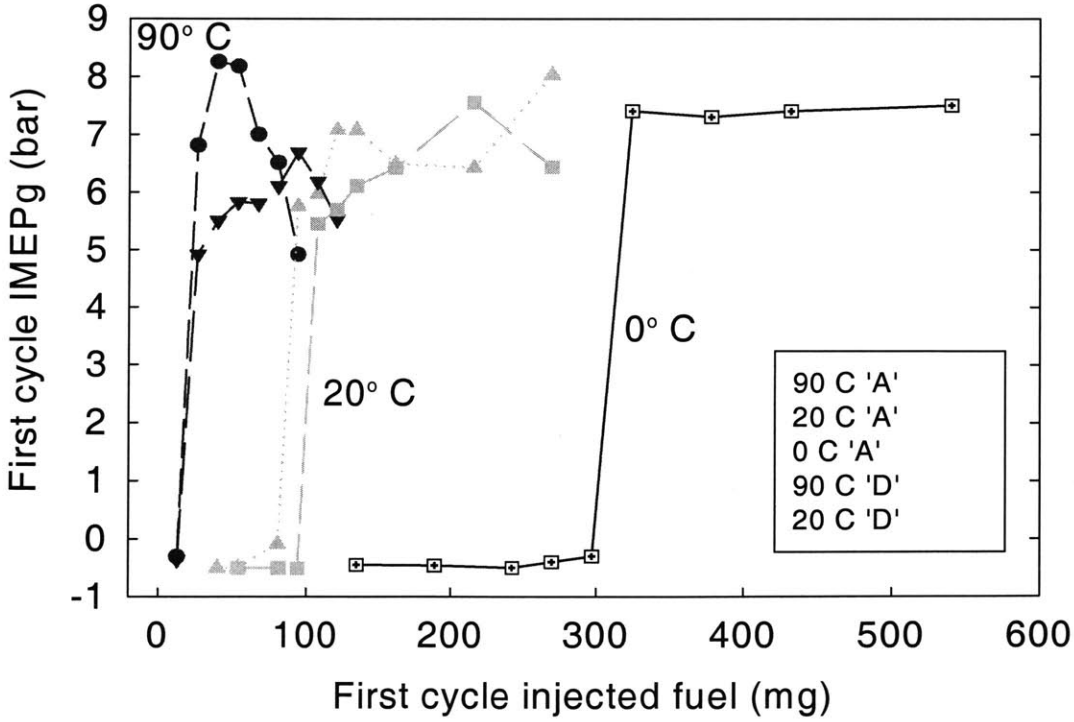

Figure 6.25: First cycle IMEPg as a function of injected fuel across all three temperatures

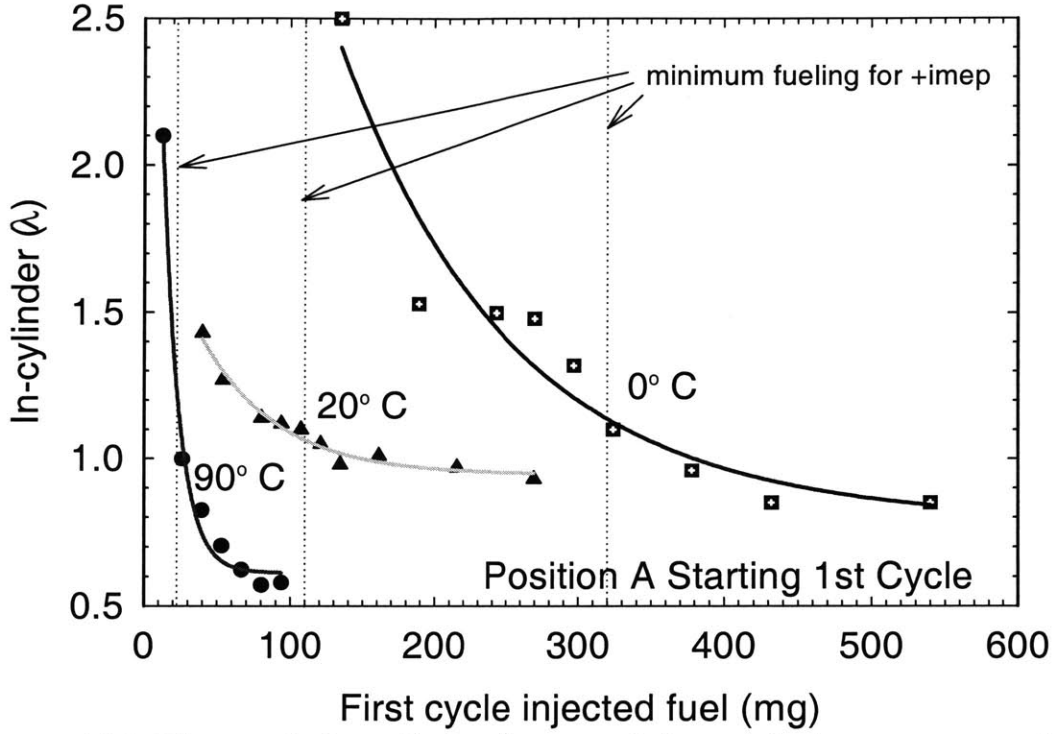

Figure 6.26: First cycle in-cylinder λ versus injected fuel mass across all three temperatures

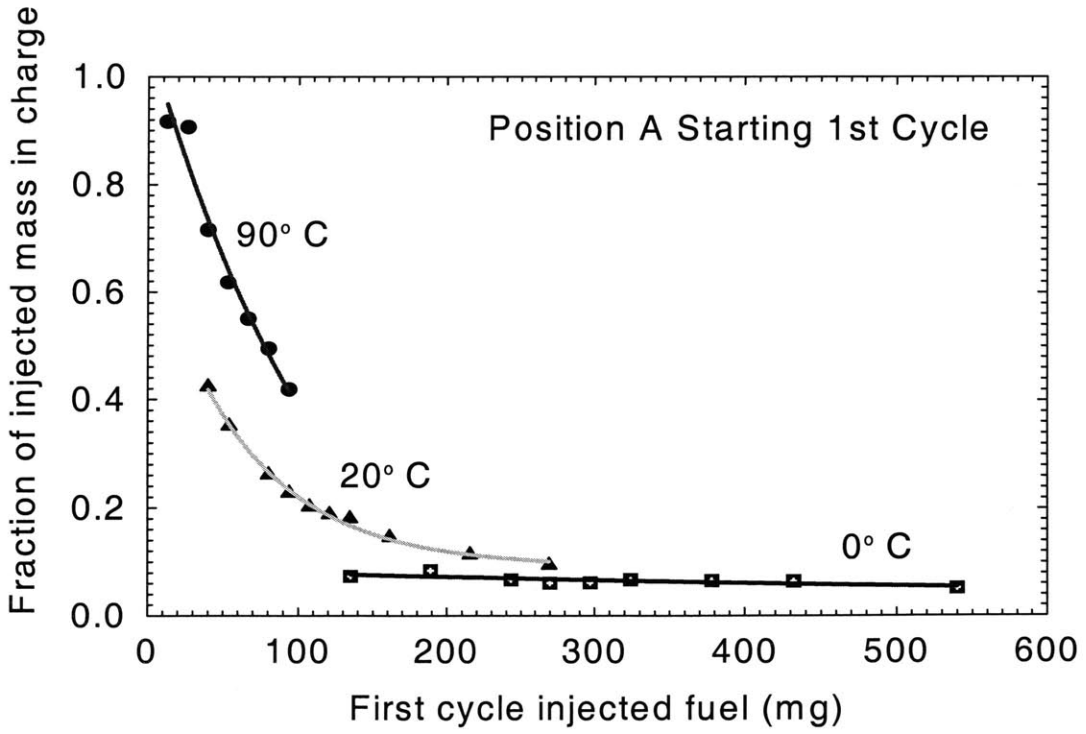

Figure 6.27: The fraction of injected fuel that constitutes the combustible mixture in the first cycle across all three temperatures

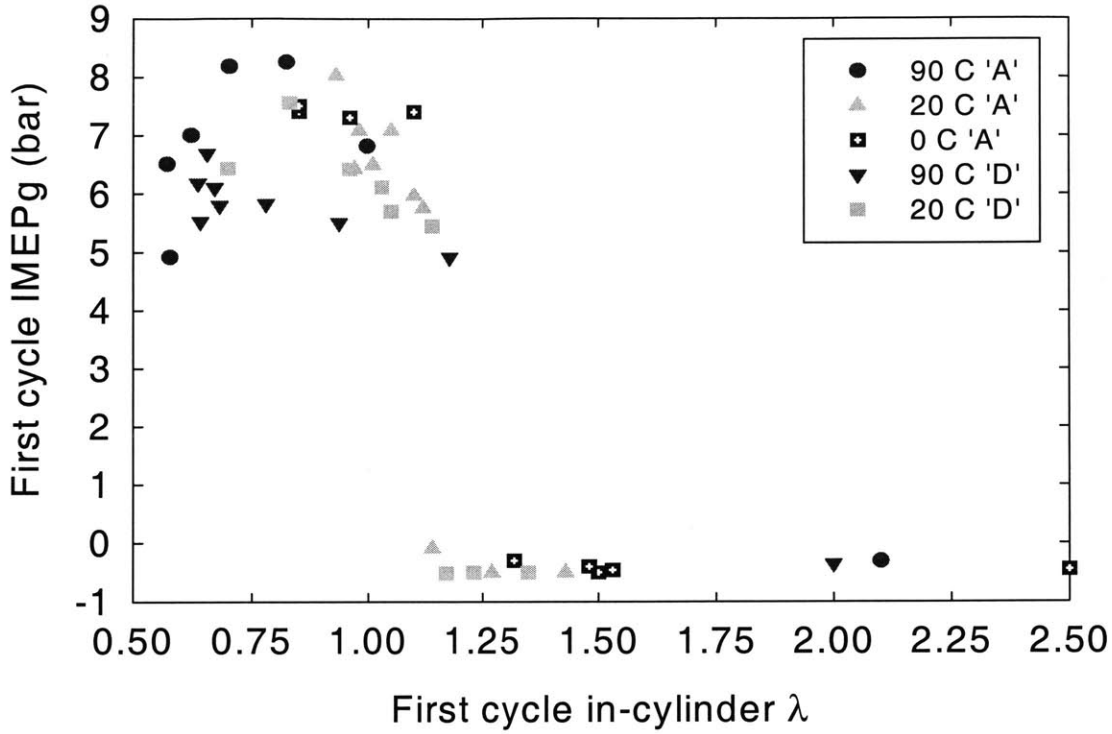

Figure 6.28: First cycle IMEPg versus first cycle in-cylinder λ across all three temperatures

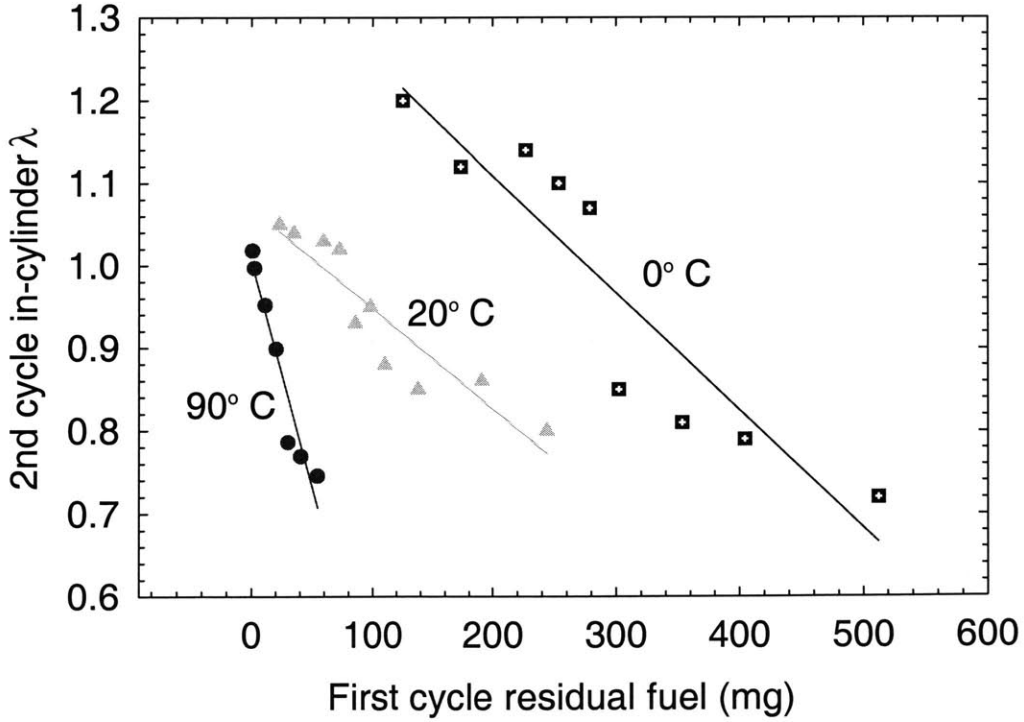

Figure 6.29: Second cycle in-cylinder λ as a function of residual fuel from the first cycle across all three temperatures (position A)

Chapter 7
1st Cycle of Crank Modeling

7.1 Introduction to the Modeling

In the previous chapter many interesting effects were observed in cranking mixture preparation. This chapter seeks to expound upon the experimental data with physically based modeling of the first engine cycle.

Obtaining a strong 'first-fire' will be imperative to meet future customer demands and reduced engine emissions. Towards this end, a first cycle of crank model was developed that seeks to both improve the physical description of the mechanisms leading to in-cylinder fuel vapor generation, and to lay the groundwork for a practical engine calibration tool.

7.2 Model Framework

7.2.1 Assumptions

The nature of the first cycle of crank lends itself to some physically based modeling simplifications.

Due to the high MAP (close to atmospheric) on the first engine cycle, backflow effects, often seen at intake valve opening due to subatmospheric intake conditions, will be neglected. As a result, it is believed that the intake port puddle on the first engine cycle will not experience the fuel redistribution (often to the upstream port region) that has been observed during steady-state operation. Thus, the puddle formed by the injector remains intact until the intake valve opens and forward intake flow acts upon it.

This fuel injector has relatively large fuel droplets (~350 μm SMD) [7.1]. It is believed that all of the injected fuel impacts the surfaces ('walls') of the intake port and valve first,

and immediately becomes part of the puddle. This behavior is assumed true even for OVI. In the case of engine starting position D, estimates of direct in-cylinder fuel transport due to the open valve are small, approximately 5%, and thus this approximation should still be valid. For position E, approximately ¼ of the injected fuel could enter the combustion chamber directly. (These estimates were based upon port/valve/injector geometry with solid cone injector behavior.) However, as discussed in **Chapter 6**, position E possesses some substantial fuel-air non-uniformity that make interpretation of the data difficult, thus for now this direct fuel contribution will be neglected. It is likely that this direct fuel contribution to the combustion chamber is impacting and coalescing on the combustion chamber wall across from the intake valve [7.2], and thus only minimally contributing to the fuel vapor process for the first engine cycle.

Knowledge of the intake system surface temperature ('wall') on which the intake port puddle is formed is necessary for evaluation of boiled-distilled fuel levels. It is known that the intake valve and intake port are at the same temperature for all starting conditions. In the case of ambient and cold engine starts, the entire engine has been allowed to cool to the starting temperature. Intake port and valve temperature measurements confirmed equality of temperature at the ambient state. In the case of hot starting, measurements were also made of various intake valve and intake port temperatures. It was observed that if the engine stopped at positions A, B or C, the intake valve quickly achieved the intake port temperature, within tens of seconds. However, if the engine stopped at position E (or was moved manually to D), measurements showed that intake valve cooling occurred primarily through conduction up the intake valve stem. Many minutes were necessary to achieve similar intake valve head temperatures to that of the intake port. This effect was the motivation for waiting approximately five minutes between all of the experimental hot starts. Thus, for all modeled starting engine temperatures the intake port and valve are assumed to be at the same temperature.

This temperature equality between the intake port and valve allows for the conceptualization of a single liquid fuel puddle mass, even though it may be distributed on both the lower intake port and valve. It has been shown that these thin fuel films

quickly (fraction of an engine cycle time) achieve the surface temperature to which they've been applied [7.3]. Knowledge of this wall and liquid film temperature will allow accurate estimates of puddle boiling/distillation as a function of intake wall temperature. Thus this model is alternatively called the 'one puddle model'.

In order to obtain reasonably accurate puddle boiling/distillation estimates, a multi-component fuel model was used. In this case, the experimental fuel (California Phase II Reformulated Gasoline) was represented by six fuel components. **Figure 7.1** shows the actual experimental distillation curve for the gasoline used, along with the six fuel components chosen for the modeling effort. The modeled fractions of the six fuel components are similar to that developed by Eric Curtis at Ford Motor Company. Curtis [7.4] developed the reduced multi-component fuel model specie fractions in order to simulate the evaporative characteristics of the real gasoline fuel. He then tested experimentally this reduced multi-component fuel and compared the evaporative behavior to that of the actual gasoline. Agreement during transient operation was described as very good [7.5].

7.2.2 Modeled Physical Processes

Once the puddle is formed by the injected fuel and defined to immediately reach the wall temperature, boiling/distillation of the lighter fuel components is allowed to immediately occur. The fuel vapor that forms from boiling/distillation is assumed to stay as vapor (no reverse processes allowed) and is all attributed to the in-cylinder fuel vapor mass once the intake valve opens.

Then, once the intake valve opens, the intake system airflow contributes to two more physical processes at work on the puddle. After the forward fresh airflow displaces the distilled vapor into the engine, there is further evaporative mass transfer from the liquid pool to the incoming fresh air. This transfer will be referred to as the convective mass transfer.

The second process during the intake event is that of shear driven (Couette type) flow in the fuel film. This film is then assumed to break up into droplets as it is being blown off the edge of the valve and valve seat. Estimates of their size will be made to determine if they contribute to the fuel vapor formation process. See **Figure 7.2** for a schematic of the above-described processes.

Finally, the contribution of the boiled/distilled fuel vapor, convected fuel vapor and liquid film small droplets (<10μm) are added to produce a modeled in-cylinder fuel vapor mass. A Conceptual picture of the model is shown in **Figures 7.3**.

7.3 Model Details

7.3.1 Mass Conservation Equations

At every crank angle degree after the start of engine rotation, equation 7.1 is evaluated for each fuel specie, 'i', in the puddle. Fuel injection is defined to occur over the same crank angle duration as the experimental data. However, for the model, injection occurs in a discrete amount each crank angle degree. Boiling/distillation is assumed to reach equilibrium each crank angle degree after additional injection mass is added to the puddle. Convection and liquid transport occur only during the intake event period. Thus,

$$\Delta m_{puddle,i} = m_{fuelinj,i} - (m_{distill,i} + m_{convection,i} + m_{liquid,i}) \qquad (7.1)$$

7.3.2 Puddle Aspect

While the conservation of mass equations only track fuel mass, many of the physical processes modeled require knowledge of the puddle area and height (e.g. aspect ratio) in order to estimate their specific behaviors. Thus, a simplified fluid mechanics solution was pursued to understand the relation between puddle mass or volume and its corresponding area and height. It is assumed that a single continuous puddle exists on a

flat surface. The puddle is circular with a radius of curvature (R_{arc}). **Figure 7.4** shows a side-view schematic of this idealized configuration. A vertical force balance was applied to the puddle as in equation 7.2, with a hydrostatic pressure distribution as in equation 7.3, and an inner puddle surface pressure as in equation 7.4.

$$\int_0^R 2\pi r P_{base} dr + 2\pi R\sigma \sin\alpha = g\rho \int_0^R 2\pi r h(r) dr \tag{7.2}$$

$$P_{base} = P_i + \rho g h(r) \tag{7.3}$$

$$P_i - P_{atm} = \sigma / R_{arc} \tag{7.4}$$

Then, solving numerically gives a puddle height of:

$$h_{\max} = c * \sqrt{V_{olume}} \tag{7.5}$$

This solution agrees very well with observations of puddle formation on a flat plate. For the complex geometry in the intake port, it is assumed that the $Volume^{0.5}$ dependence still holds approximately. Ford researchers saw experimentally that puddle height was proportional to the square root of puddle mass. The constant 'c' in equation 7.5 was set from the Ford puddle experiments. A puddle representative of one high load injection fuel mass (~30 mg) possessed a height of ~15 μm.

7.3.3 Distillation

Estimates of individual component boiling/distillation are made using Raoult's Rule of the Ideal Solution. Ideal Solution behavior is defined either for a dilute solution or for a mixture consisting of constituents of similar structure. It is the latter that we are assuming valid in the current context. In this case, the solution assumes that each molecule of a given component experiences the same interactions whether its nearest neighbors are of the same or of another constituent. For each specie, Raoult's rule states

that the vapor pressure of each individual fuel specie is independent of the other species and only a function of temperature. The following equation applies to each fuel specie:

$$x_{i,g} * P_{TOT} = x_{i,f} * P_{SAT,i}(T) \tag{7.6}$$

where the index 'i' refers to an individual fuel component. 'x' is the mole fraction of a given fuel specie in both 'g'-vapor form, and 'f'-liquid form. P_{TOT} is the total intake port pressure, and $P_{SAT,i}$ is the saturated vapor pressure of specie 'i' at temperature T. These six equations along with the associated conservation (mass and moles) equations in the liquid and vapor phases provide a solution for the vapor mass of each fuel specie at the given T and P each crank angle degree.

7.3.4 Convection

Convective vapor mass transport estimates from the puddle are made using the Reynolds Analogy for heat and mass transfer. Detailed studies of heat transfer in rough wall tubes are included in most heat transfer texts [e.g. references 7.6, 7.7]. The Gnielinski Equation (heat transfer relation) was converted to a mass transfer correlation by Reynolds Analogy.

$$Sh = \frac{h_m * D_{port}}{D_{fi,air}} = \frac{(f/8) * (\mathrm{Re} - 1000) * Sc}{1 + 12.7 * \sqrt{f/8} * (Sc^{0.67} - 1)} \tag{7.7}$$

Sc is the Schmidt number. The other parameters are described below. This Sherwood (Sh) number was then used in a rate of vapor mass transfer correlation as established by Spalding [7.8]. The friction factor, 'f', in equation 7.7 is used as the calibration for the model. It has a physical meaning, and can be connected to a pipe roughness with the use of a Moody Chart. Thus, the final convective fuel vapor mass transfer rate equation is as follows:

$$m_{convection,i} = \int_{IVO}^{IVC} (1 + Sh) * [\frac{A_{ls}}{D_{port}} \rho_{gm} D_{fi,air} \ln(1 + \frac{\Delta MFF,i}{1 - MMFs,i})] \cdot dt \tag{7.8}$$

MMFs,i is the mass fraction of fuel vapor at the surface of the puddle. ΔMFF,i is the difference between the fuel vapor mass fraction at the surface and the centerline free stream fuel vapor level (set to zero). A_{ls} is the area of the liquid surface, from the puddle aspect ratio submodel. The density of the gas-vapor mixture at the puddle surface is ρ_{gm}. D_{port} is the port diameter and $D_{fi,air}$ is the fuel-air diffusivity of fuel specie 'i'.

7.3.5 Liquid (Couette) Flow and Breakup

Numerous authors have modeled shear driven intake port puddle film flow. Servati assumed that the liquid flow was of the Couette type, with a linear velocity profile [7.9]. Curtis believed that a laminar boundary layer flow was in effect, and assumed the corresponding parabolic velocity profile [7.10]. By equating the shear stress at the top of the liquid puddle film with the shear stress generated at the puddle surface by the forward air flow into the cylinder, the liquid fuel film transport into the engine's cylinder can be estimated (7.9). The scalar m=1 is for Couette flow, and m=1/2 for a laminar boundary layer type flow. The estimated difference in mass flow between the two types of liquid flow is more than a factor of two, with boundary layer flow being greater. In this study, Couette type flow is assumed.

$$m_{liquid,i} = y_{,i} \cdot m_{liquid} = \int_{IVO}^{IVC} y_{,i} \cdot P_w \cdot \rho_f \cdot \left(\frac{c_f \cdot Vo^2 \cdot h^2}{2 \cdot \mu_l}\right) \cdot dt \qquad (7.9)$$

The liquid puddle mass fraction term, $y_{,i}$, is used to account for the predominately heavier fuel species that comprise the puddle. P_w is the wetted perimeter of the puddle. The liquid puddle density, viscosity and height are ρ_f, μ_l and h. The port centerline velocity is Vo, and the coefficient of friction between the air-flow and the liquid surface is c_f (c_f=f/4, f:friction factor from above).

Once the liquid flow mass is established, a wave breakup model is applied [7.11] to determine the SMD of the droplets formed from the liquid film flow sheet breakup. A droplet distribution [7.12] is then applied to determine the fraction of droplets that are below 10 μm. Droplets that are below this diameter are then assumed to remain

suspended as vapor and contribute to the in-cylinder vapor mass. See reference [7.4] for an application of these two models to the engine environment.

7.4 Base Model Results

7.4.1 Base Model Inputs and Calibration

This 'One Puddle' 1st cycle of crank model (base model) was run at simulated hot starts (ECT=90 C) with the appropriate engine cycle phasing (starting positions: A, B, C, D and E) and averaged 1st cycle engine speed as seen in the experimental data at the different engine positions. Thus position A started fuel injection at 180 degrees (Top Center Compression-TCC, 0 degrees=BCC), and had an average engine speed during intake of 450 rpm. Position D started injection at 568 degrees, and had an average speed during intake of 200 rpm.

Average engine speed was scaled to a mean piston speed, and then instantaneous piston speed as a function of engine crank angle position. Next, instantaneous intake port air speed (averaged across the port cross section) was determined by scaling instantaneous piston speed by the ratio of piston area to port cross sectional area.

The base model required that the friction factor be set to 0.06 for agreement between the model and the hot start experimental data for in-cylinder fueling near stoichiometric. A friction factor of 0.06 corresponds to a normalized port wall roughness of 3% ($\varepsilon = 0.03$ = roughness height/diameter). While the exact roughness of the Zetec port is not known, this value of ε is certainly reasonable (although possibly slightly high) due to the fairly coarse intake port surface caused by sand castings.

A comparison of model predictions with experimental data is shown in **Figure 7.5**. In each group of bars are shown injected fuel mass, experimental in-cylinder fuel mass and model predicted in-cylinder fuel mass. Injected fueling of 27 mg generally provides for

slightly lean of stoichiometric in-cylinder fueling. Injected fueling of 40 mg generally provides for slightly richer than stoichiometric in-cylinder fueling.

The model predicts well in-cylinder fuel vapor levels. The model predictions are within ten percent of the experimental data for positions A and D with fueling near stoichiometric levels. Additionally, the model reproduces the differences between positions A and D. Position A delivers an in-cylinder relative air-fuel ratio (λ) that is generally 0.1 λ richer than position D for the same injected fuel mass. This effect is a result of the higher engine speeds during the intake stroke experienced with position A, convectively drawing in more fuel vapor. Thus, higher engine speeds enhance the convective mass transport of fuel from the puddle to the combustion chamber.

Unfortunately, model agreement with the data at Position E is not good. As mentioned in **Chapter 6**, position E, late intake event fuel injection timing delivers an in-cylinder mixture that is inhomogeneous. Still, the model underpredicts in-cylinder fuel vapor levels by almost a factor of two. The low in-cylinder fuel mass levels predicted by the model at 'E' are a result both of the assumption that all injected fuel must first impact the port walls, and the shortened times of intake valve open period. These effects coupled with the reducing piston/port velocities during the later half of the intake stroke result in low model predictions. In reality, it is likely that direct fuel flow from the injector into the combustion chamber results. Estimates based on geometry show that approximately 1/4-1/3 of the injected fuel directly enters the combustion chamber from the fuel injector. With the large droplet size containing significant momentum, it is believed that this direct injector contribution to the cylinder will likely hit the bore wall. Evaporation of the light fuel ends will result. Convective mass transfer during compression will additionally vaporize more cylinder wall/piston liquid fuel.

While this OVI behavior could be modeled, it is extremely difficult to experimentally verify the different in-cylinder vaporization mechanism at work. Fortunately, position E is a poor engine position to develop a first fire, both due to its inhomogeneity and high engine out HCs. Thus, efforts to model its behavior are not essential. In practice, it

would be advisable to skip fueling to the second cycle if the engine starting position is at 'E'.

Next, the simulated engine coolant temperature (ECT) and intake system wall temperature is reduced to ambient condition (20 C). No other modification is made to the model.

The results for positions A and D are shown also in **Figure 7.5**. In this case, 135 mg of injected fuel is necessary to deliver a near stoichiometric fuel vapor mass to the engine's cylinder. Above, for the hot starts, only ~40mg of fuel were necessary. From the modeling results it is clear that the model is able to naturally adjust to the changing simulated temperature conditions. Much less fuel is predicted to boil/distill at the ambient conditions. This leads to a larger puddle with a broad surface area. Thus, convective mass transfer is greatly enhanced and becomes the dominant fuel vapor generation mechanism (this effect will be discussed in detail in the next section). As was the case for the hot starts, position A shows slightly higher in-cylinder fuel vapor levels due to the slightly higher engine speed during the intake event. The agreement between the model and data at the varied starting positions, temperatures and injected fuelings is excellent, differences of less than ten percent exist.

7.4.2 Physical Processes

In this section detailed results from the model reveal the physical mechanisms at work during the first cycle of crank. As described in the model description sections (Section 7.2 and 7.3), physical mechanisms that can generate in-cylinder vapor include boiling/distillation, convective mass transport and liquid film flow breakup into small droplets. The relative importance of these mechanisms is now discussed.

Figure 7.6 shows a 1st cycle of crank model simulation for a hot start at an initial engine position slightly advanced of 'A' with stoichiometric in-cylinder fueling. All six fuel species are shown as a function of engine crank angle during the first engine cycle. The

ordinate displays the fraction of injected fuel that remains in the puddle during the first crank cycle. Fuel injection occurs from 120 to 150 crank angle degrees. Next the quiescent period until the intake valve opens lasts until 530 crank angle degrees. Finally, the intake valve open period lasts until 50 degrees after bottom center (ABC).

During the fuel injection period most of the i-pentane boils. Pentane is the lightest fuel specie modeled in the multi-component fuel model. A few percent of the injected pentane is seen retained in the puddle at the start of injection, but quickly all of the pentane boils and remains in the port as vapor until drawn into the combustion chamber at IVO.

The next modeled specie heavier than pentane is hexane. As seen in **Figure 7.6**, approximately 55% percent of the injected hexane remains in the puddle after injection is complete, with the remainder boiled/distilled off as vapor in the intake port.

As the fuel species' molecular weight (MW) increases, so does the fraction of injected fuel that remains in the puddle as liquid after injection. At the upper end of the distillation curve due to its heavy nature, n-decane is seen to leave almost all of its injected mass in the puddle as liquid.

For these hot starts it is seen that a significant fraction of the injected fuel (especially lighter fuel components) immediately vaporizes in the port, creating fuel vapor that will enter the combustion chamber upon IVO.

During the intake event period **Figure 7.6** shows all fuel species being draw out of the puddle. This convective mass transfer phase is very strong, but how much of the puddle reduction is due to liquid fuel transport and how much is due to convective vapor mass transfer?

Figure 7.7 shows the distribution of the injected fuel on the first cycle of crank for a hot start with near stoichiometric fueling (~40 mg). Approximately 1/2 of the injected fuel

becomes fuel vapor due to intake event convection. Next, roughly ¼ to 1/3 of the injected fuel becomes fuel vapor due to boiling/distillation. Injected fuel that remains in the puddle past the first engine cycle comprises slightly less than ¼ of the injected fuel. Liquid fuel transport into the cylinder comprises only a few percent.

Of the approximately 2% of injected fuel that is drawn into the cylinder as a liquid film, the wave breakup and distribution models predicts less than ten percent of it will be of a small enough diameter (< 10 μm) to be entrained in the combustion chamber gases as fuel vapor. Thus, the vapor contribution from the liquid film flow –breakup is very small. Most of the liquid film drawn into the combustion chamber is likely residing on both the cylinder wall and piston surfaces as a liquid film.

When the starting temperature is then dropped to ambient conditions (20 C), **Figure 7.8** shows the injected fuel distribution, again for near stoichiometric in-cylinder fueling. Most of the fuel remains in the port. Convective mass transfer is the dominant vapor formation mechanism. Distillation and liquid flow breakup are negligible at this condition.

Thus, common to both hot and ambient starting (with in-cylinder fuel vapor levels near stoichiometric), both the diffusional and liquid film flow breakup mechanisms can be neglected with regards to their contribution towards generating in-cylinder fuel vapor. The model predicts that both effects are second order and not significant in the mixture preparation process. Convection and distillation are the dominant mixture preparation mechanisms that need to be considered.

The relative roles of convection and distillation are shown across the starting temperature range from ambient to hot in **Figure 7.9.** These simulations show injected fuel levels necessary to achieve a stoichiometric in-cylinder fuel mass level across the temperature range. For ambient starting, convective mass transport is the only mechanism to deliver fuel vapor to the combustion chamber. The temperatures are too low for vapor generation. As the engine starting temperature warms from 50 to 80 C the relative

importance of distillation vapor generation becomes important. Likewise, as fuel vapor is generated from boiling/distillation, the puddle size during intake valve open is reduced leading to the lessening importance of convective mass transfer at higher engine temperatures. At hot engine starting, convection and distillation are of comparable importance with convection still being slightly more important.

7.4.3 Comparison to Vehicle Data and Zetec Data

'One Puddle' 1st cycle of crank simulations across a range of temperatures and fuel injections were performed to estimate appropriate 1st cycle of crank required fueling. **Figure 7.10** shows the modeling results compared to three production vehicle calibrations and the Zetec data.

The series of dashed lines represent the model predictions for various in-cylinder air-fuel ratios. The lowest dashed line shows the injected fuel mass necessary in order to achieve a 10% lean of stoichiometric in-cylinder mixture. In **Chapter 6**, this 10% lean limit was seen across the range of starting temperatures in order to achieve a positive IMEP first cycle. The next three dashed lines (moving upwards in the figure) show the model predictions of injected fuel for stoichiometric, 10% rich and 20% rich in-cylinder fueling.

The diamond, triangle and square symbols show the required fueling in three production Ford vehicles as a function of ECT. The agreement between the model and production fueling levels is very good from ambient to hot start conditions. For cooler than ambient starts (ECT < 20 C), it is expected that strong liquid fuel effects become important, requiring high levels of actual fueling in order to achieve a combustible mixture.

Finally, the Zetec data is shown in the ovals at 0, 20 and 90 C. Agreement between the model and data is excellent around stoichiometric fueling at both ambient and hot starting. However, for ambient rich fueling and cold starting the model underpredicts the required 1st cycle fueling necessary. This behavior will be discussed in the next section.

7.5 Base+Fuel Crevice Model (Rich Fueling) Results

7.5.1 Model Improvements and Results

While the base model predicts well the required injected fuel behavior near stoichiometric fueling, it does not work well for rich to very rich in-cylinder fuelings. **Figure 7.11** shows the 1st cycle in-cylinder relative air-fuel ratio (λ) as a function of first cycle injected fuel for hot starting at position A. For this case, and at all temperatures and starting positions, the experimental data (from **Chapter 6**) shows that despite high fuel injection levels, the in-cylinder λ reaches a constant level despite even higher fuel injection amounts. Unfortunately, the base model predictions do not predict this behavior. As seen in **Figure 7.11**, the base model shows continued enrichment with increasing first cycle fuel injection mass. What is the cause of this discrepancy?

In looking at the detailed model results at high first cycle fuel injections, it is evident that the associated high levels of predicted in-cylinder fuel mass are a result of the strong convective mass transfer action across a wide puddle area. In fact, this predicted puddle area is very wide, more than ten times the associated footprint area of the injection spray. This modeled spreading of the initial injection spray is likely too broad. What else might be occurring?

Both the intake port and valve are angled towards each other creating a crevice that is likely containing a pool of liquid fuel. **Figure 7.4** shows the port centerline angled approximately 30 degrees off the horizontal. Likewise, the intake valve head is angled approximately 20 degrees off the horizontal towards the intake port. The hypothesized location of the crevice pool is also shown in the figure.

By assuming that fuel is collecting in the form of a crevice pool, the modeled puddle area then is greatly reduced. This also reduces the convected in-cylinder fuel vapor mass since the convected mass is proportional to puddle area. But how much fuel is pooling in the crevice? Or alternatively, what is the overall thin film puddle area/mass?

One approach to determine the thin film puddle area/mass is to assume that the base thin film puddle can only contain as much fuel as exists in the intake port during normal engine operation at high load and low engine speed. In **Chapter 4** experimental estimates of the residual intake port fuel levels were made using injector cut-off/disablement. For stabilized engine operation (90 C ECT), at 0.9 bar 1500 rpm the residual port fuel was seen to be approximately 30 mg of fuel. Stabilized ambient engine experiments were also performed showing roughly 200 mg of residual intake port fuel at 20 C ECT.

Thus, these values will be used to define the maximum liquid fuel mass that is contained in the thin film puddle. When the modeled thin film puddle is predicted to exceed 30 mg (hot starting) the remainder of the fuel is assumed to pool in the crevice (see **Figures 7.3 and 7.14** for location of crevice pool). It is additionally assumed that the crevice pool is not so thick as to restrict the conductive wall heat transfer to the crevice pool, such that the crevice pool is assumed to also reside at the wall temperature.

With this crevice pool model modification, the modeling predictions are then shown in both **Figures 7.11 and 7.12**. From 40 to 80 mg of injected fuel, the improved model follows the experimental trends well for in-cylinder fuel vapor. **Figure 7.12** also shows both the convective mass transfer levels and boiling/distillation contributions to the in-cylinder fuel vapor. It is seen that by assuming the occurrence of liquid crevice pooling, convective mass transfer is relatively constant with increased first cycle injected fuel mass.

While this crevice pool model works well for high fuel injection levels, at very high fuel injection levels one further model modification needs to be made. Since the data shows in-cylinder fuel mass remaining constant at very high injection levels, it is likely that the crevice pool becomes so thick that insufficient time exists to conduct wall heat through the crevice pool (this assumption will be validated in the next section). Thus, the model shows that for hot starting, once the puddle plus crevice mass exceeds 45 mg, a cool

upper pool is assumed to exist that doesn't reach the wall temperature, and thus does not distill/boil as with the thin film puddle and lower crevice pool. With this final model modification agreement across the entire range of injection levels is attained. The conceptual picture of crevice pooling and the deep 'cool' pool are shown in **Figures 7.13 and 7.14**.

This base plus crevice pool model was next applied to hot starting at engine positions D and E. The modeling and experimental results are shown in **Figure 7.15.** The model predicts the reduced in-cylinder fueling differences as engine starting position is changed from A to D to E. This effect being a result of faster engine speeds at more advanced starting engine positions. Additionally, the crevice pooling plus deep cool pool assumptions work well for positions D and E, predicting a constant in-cylinder fuel vapor level with increasingly high fuel injection levels.

Next, the model is applied to increasing fuel injection levels at ambient starting. Similar behavior is observed as with hot starting. At high-rich fuel injection levels, the in-cylinder fuel mass becomes constant. Using 200 mg as the stable ambient thin film puddle level, the results are shown in **Figure 7.16**. While the trends are correct, the 200 mg level need to be reduced to 150 mg for agreement with the data.

7.5.2 Deep Crevice Liquid Pooling

If the above described deep cool crevice explanation is to be plausible, then a heat transfer analysis should confirm that when a deep crevice pool is formed, insufficient time exists to conduct wall heat through the deep crevice pool to the upper liquid surface.

Figure 7.17 shows conduction penetration thickness on the ordinate into a hypothetical liquid fuel film (initially at 20 C) versus time for conduction from a wall at 90 C on the abscissa. Curves for 10%, 50% and 90% temperature changes are shown. These percentages at a given time and thickness reflect the temperature of the outer surface of the liquid film as a percentage of the hot wall temperature. These percentages correspond

to an outer surface liquid film temperature of 27 C, 55 C and 83 C. The calculation of these curves was based on the transient plane slab assumption of a liquid fuel film with the lower outer surface of the liquid film at the temperature of the hot engine wall (90 C). Additionally, the upper liquid surface is assumed adiabatic. While the analysis is only approximate, it nonetheless gives an indication of the physical problem.

If fuel injection occurs very early in the engine cycle (e.g. initial position 'A') the maximum time for conduction of wall heat through the liquid film exists until the intake valve opens. This 'soak' time is the time on the abscissa. Some corresponding engine speeds for this maximum soak time are shown below the abscissa labeling. Thus, position A engine starting corresponds to an approximate 200 msec soak time due to its ~450 rpm average speed during the intake period. Since the abscissa reflects the maximum possible soak time (from ~IVC to IVO) this time scale is not appropriate for the later engine starting positions C, D and E since only a fraction of an engine cycle exists for puddle/pool soak despite their lower engine speeds. Thus, the late initial engine positions actually have soak times less than A despite their lower speeds.

As seen in **Figure 7.17**, the 45 mg thin puddle plus crevice pool line (minimum residual intake port fuel mass for hot starting at which the deep cool pool is believed to be occurring) provides for a maximum pool height of ~350 μm. This height is based on the assumption that the crevice pool is triangular in cross section around ½ the valve circumference. At this point (450 rpm – 200 msec), the puddle outer surface temperature is approaching a level 90% of the wall temperature. So distillation/boiling should still be occurring. However, as the injected fuel and thus crevice pool grows, as represented by the 80 mg thin puddle plus crevice pool line, the 90% (83 C) temperature penetration is ~400 mm short of the approximate deep crevice pool height. This suggests that boiling/distillation is not occurring in the upper part of the deep cool crevice pool. Engine speeds would need to be reduced by 2 ½ times for the full deep crevice pool to fully reach the wall temperature. Thus it is very likely that the deep crevice cool pooling assumption is valid based upon heat transfer arguments.

Chapter 7 References

[7.1] Whelan, D.E., Kelly-Zion, P.L., Lee, C.F., Peters, J.E. and White, R.A., "Back-Flow Atomization in the Intake Port of Spark Ignition Engines", SAE#972988, 1997.

[7.2] Stanglmaier, R.H., Hall, M. J. and Mattews, R.D., "In-Cylinder Fuel Transport during the First Cranking Cycles in a Port Injected 4-Valve Engine", SAE Paper 970043, 1997.

[7.3] Servati, H.B. and Herman, E.W., "Spray/Wall Interactions Simulation", SAE#890566, 1989.

[7.4] Curtis, E.W., Aquino, C.F., Trumpy, D.K. and Davis, G.C.,"A New Port and Cylinder Wall Wetting Model to Predict Transient A/F Excursions in a PFI Engine", SAE#961186, 1996.

[7.5] Personal communications with Eric Curtis, summer 1999.

[7.6] Incropera and DeWitt

[7.7] Mills, A.F, Heat and Mass Transfer, 1996.

[7.8] Spalding, D.B., Combustion and Mass Transfer, Pergamon Press, 1979.

[7.9] Servati, H.B. and Herman, E.W., "Spray/Wall Interactions Simulation", SAE#890566, 1989.

[7.10] same as [7.4]

[7.11] Rosin, P. and Rammler, E., J.Inst. Fuel, 1933, 7, 29.

[7.12] Fraser, R.P., Dombrowski, N., and Routley, J. H., "The Atomization of a Liquid Sheet by an Impinging Air Stream", Chemical Engineering Science, 1963, Volume 18, pp 339-353, Pergamon Press Ltd, Oxford, UK.

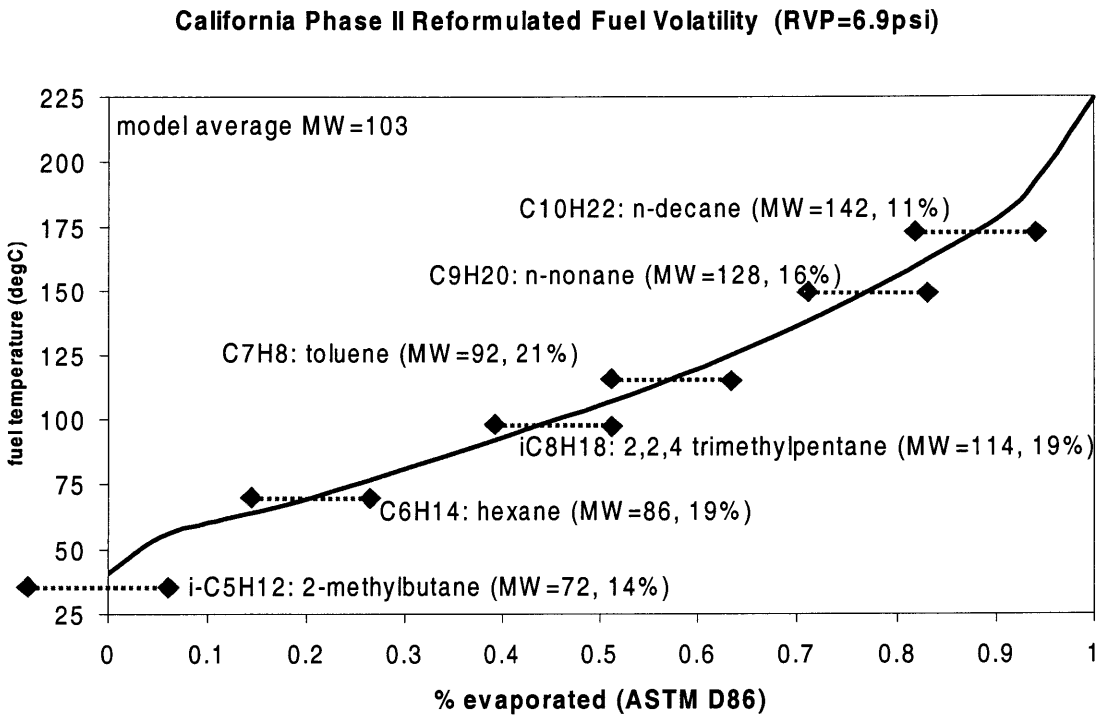

Figure 7.1: Reformulated gasoline distallation curve. Six species multi-component fuel model shown also.

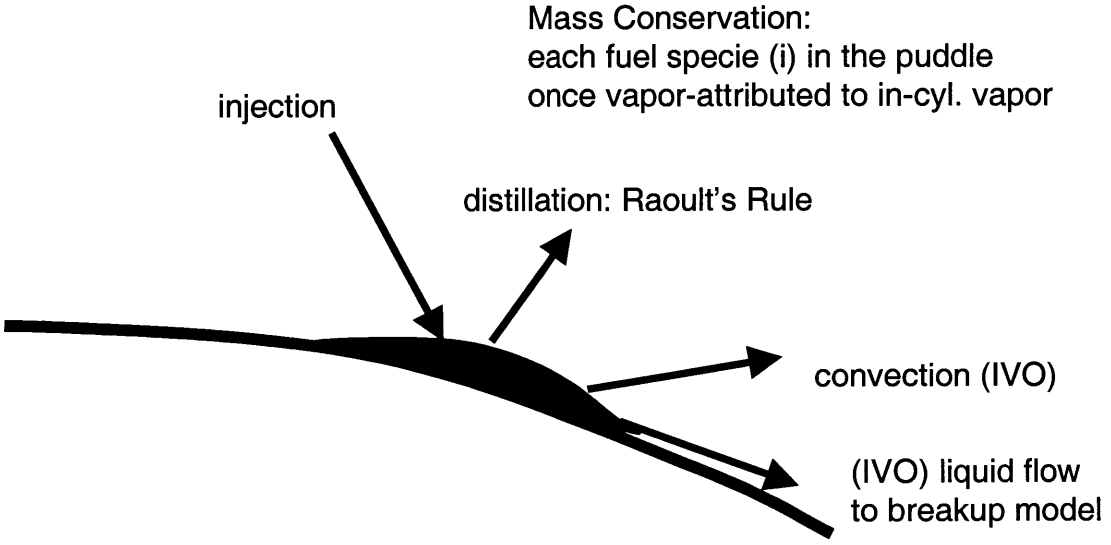

Figure 7.2: 1st cycle of crank modeled physical processes that contribute to in-cylinder fuel vapor.

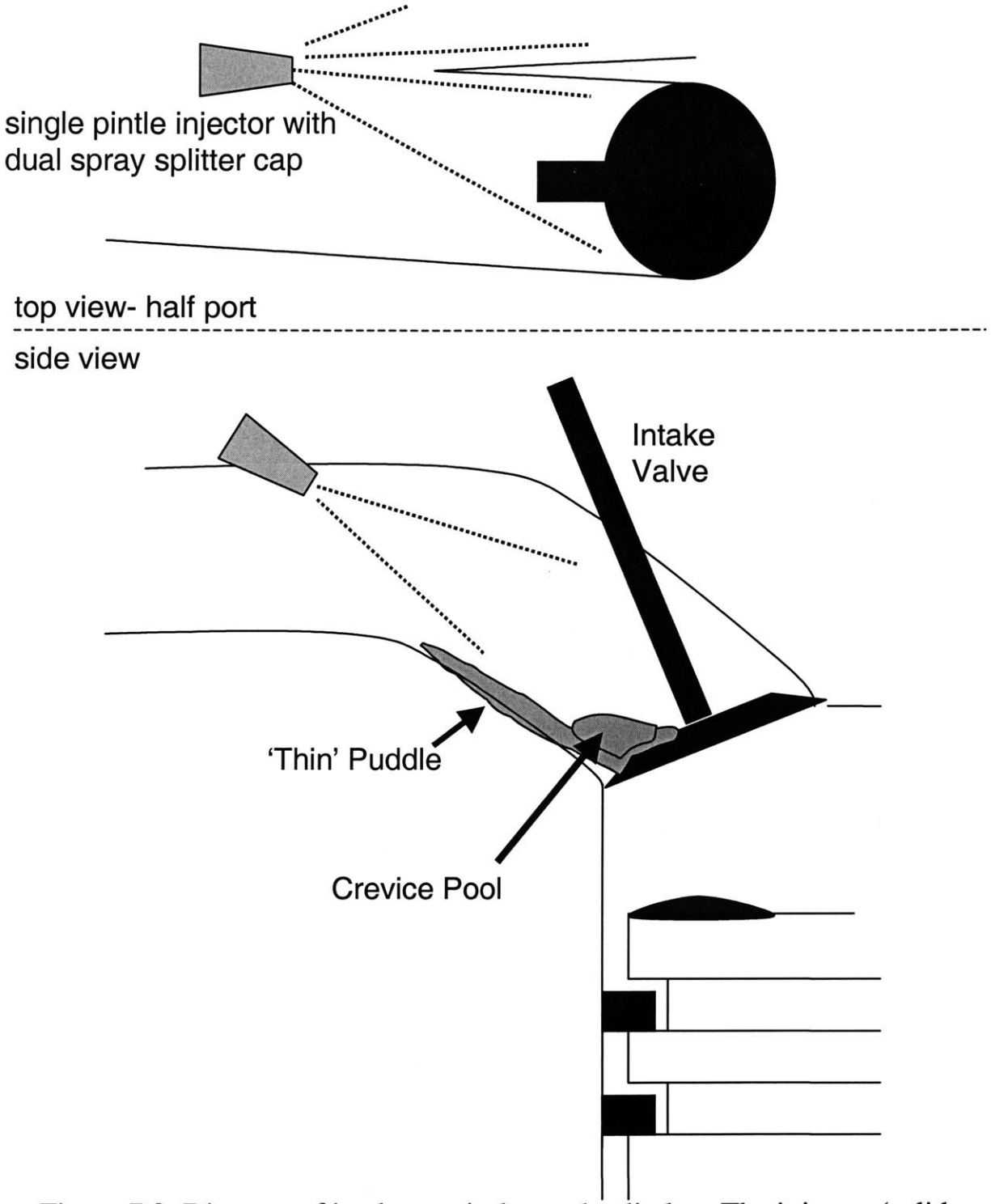

Figure 7.3: Diagram of intake port/valve and cylinder. The injector (solid cone spray is targeted at the base of the intake valve. The injector footprint is approximately the diameter of the intake valve head (~ 30 mm) [see reference 7.1]. The approximate location of the thin film liquid fuel puddle is shown. Crevice pooling (discussed in Section 7.5) is assumed to occur when the puddle mass gets large.

$$\int_0^R 2\pi r P_{base} dr + 2\pi R\sigma \sin\alpha = g\rho \int_0^R 2\pi r h(r) dr$$

$$P_{base} = P_i + \rho g h(r)$$

$$P_i - P_{atm} = \sigma / R_{arc}$$

Vertical Force Balance

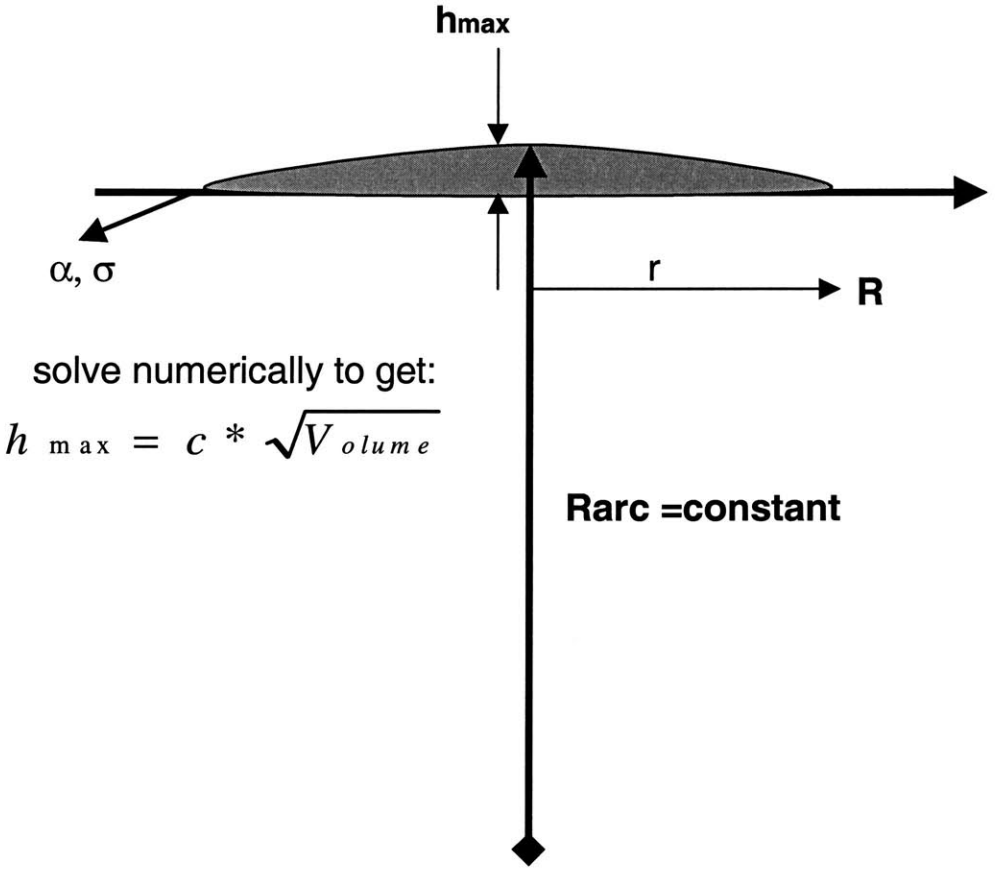

solve numerically to get:

$$h_{max} = c * \sqrt{Volume}$$

Figure 7.4: Analysis of a single puddle. Relationship between the puddle height and volume is determined.

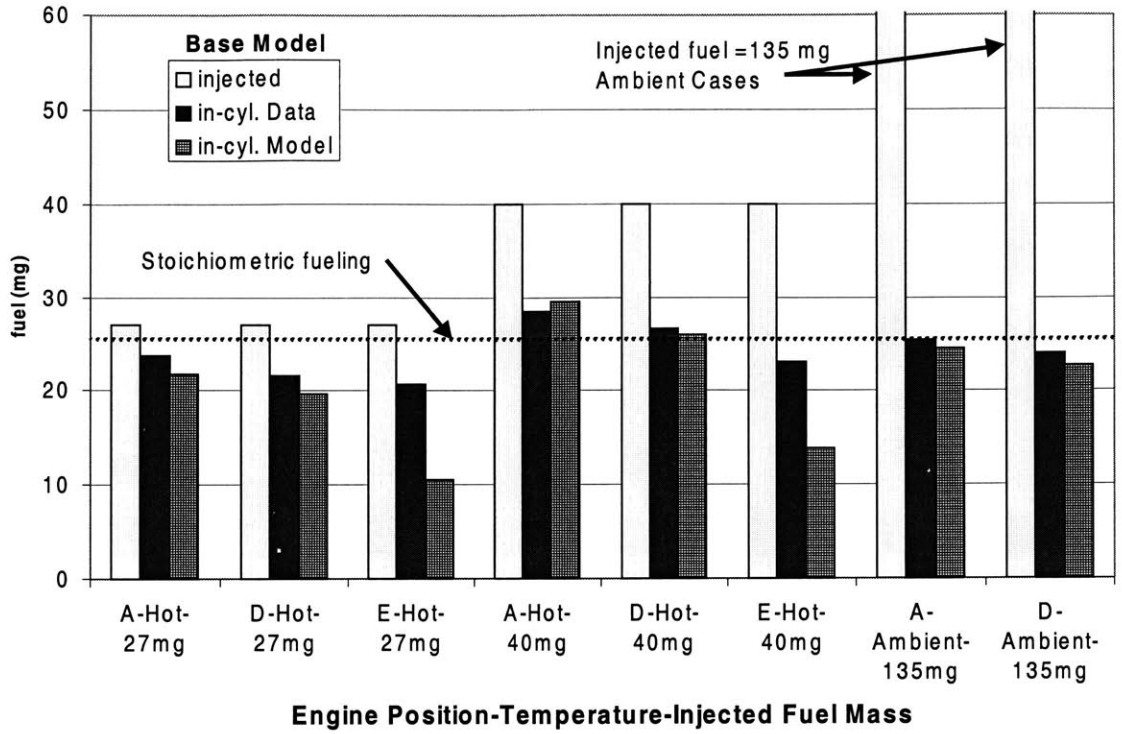

Figure 7.5: Base model comparison with experimental data at various starting positions. Hot start and Ambient start results are shown.

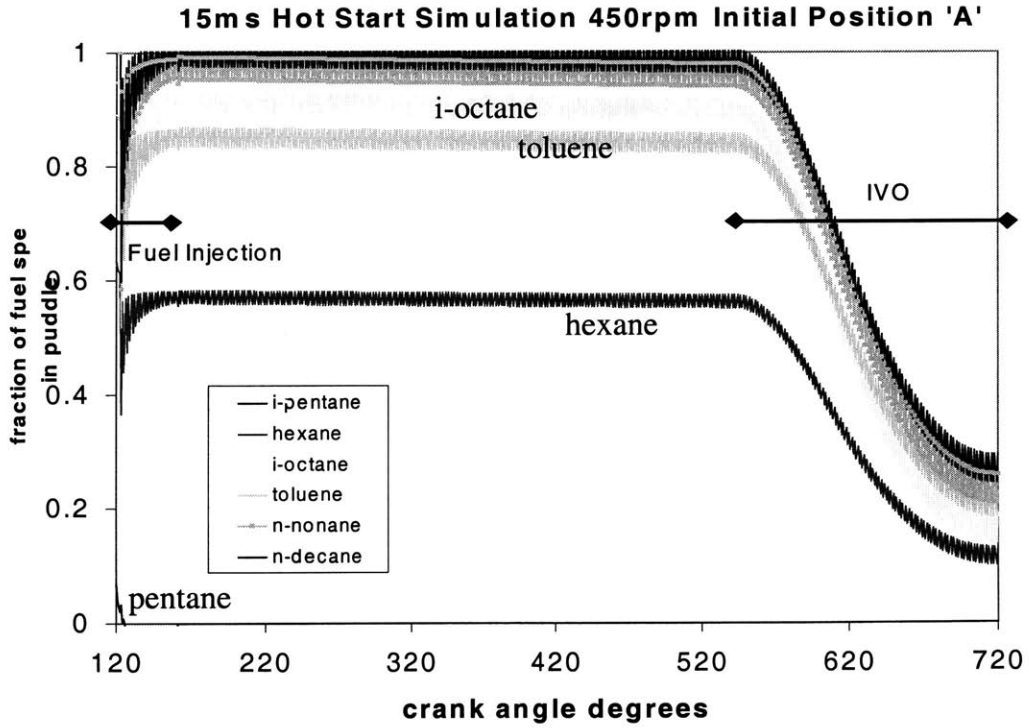

Figure 7.6: A simulated hot start at postion A. The fraction of each fuel specie that remains in the puddle during the first engine cycle is shown.

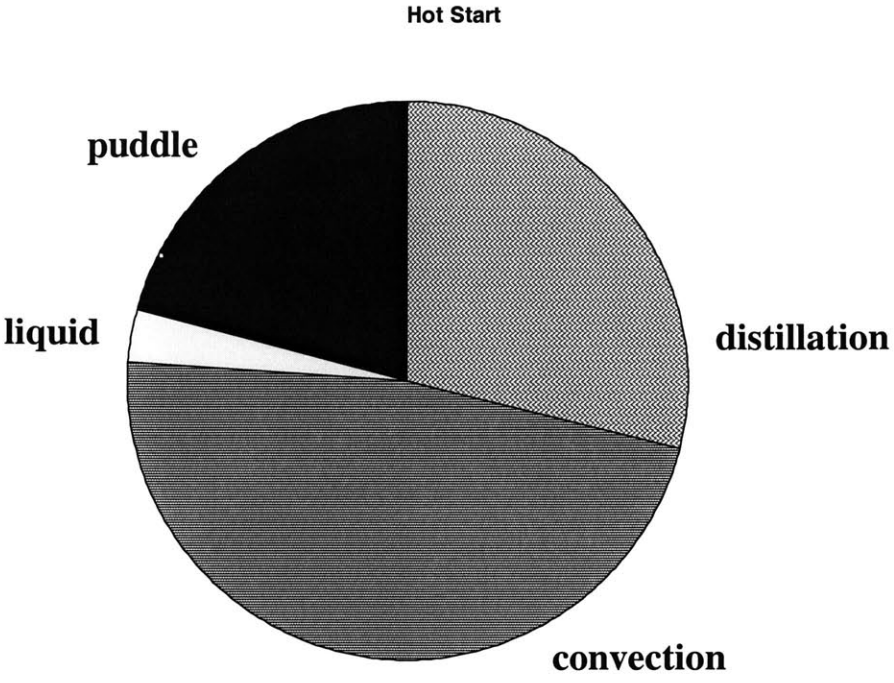

Figure 7.7: Distribution of injected fuel on the 1st cranking cycle-hot start

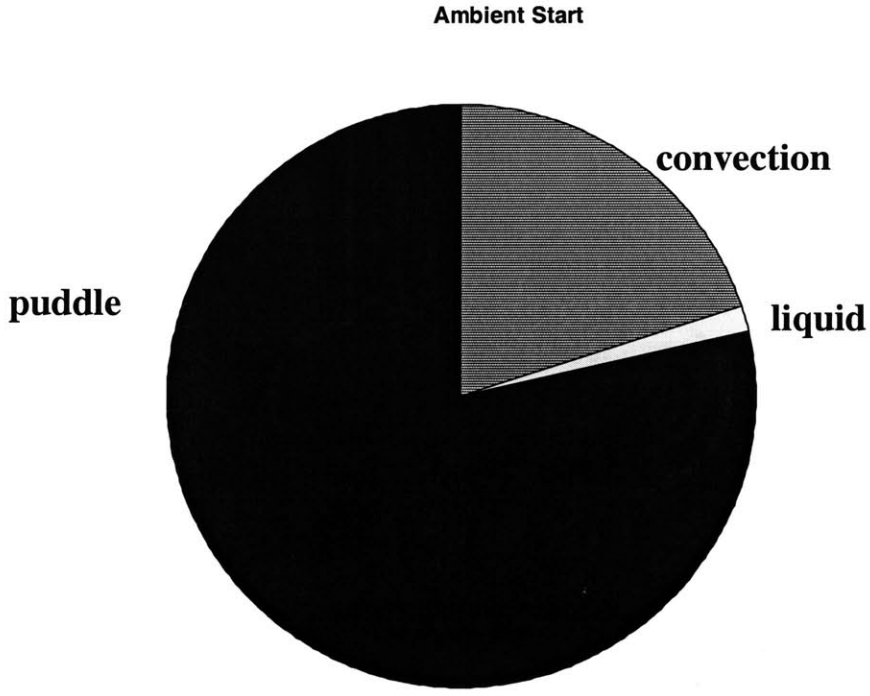

Figure 7.8: Distribution of injected fuel on the 1st cranking cycle-ambient start

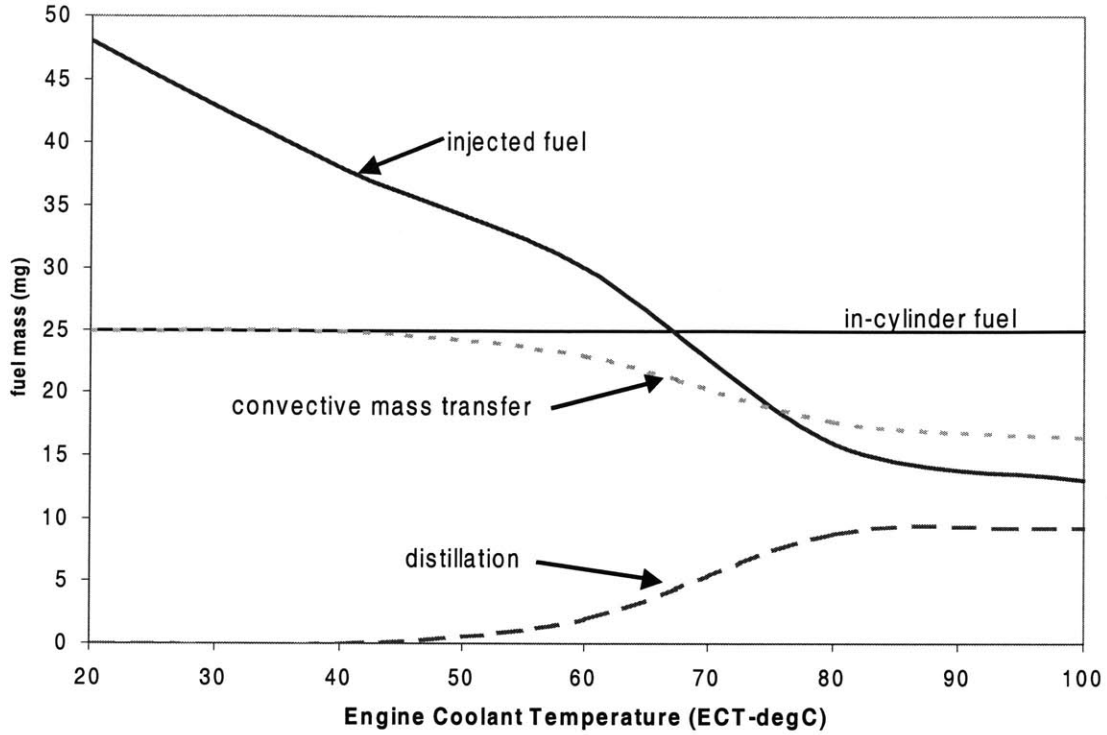

Figure 7.9: Model predicted injection mass necessary for stoichiometric in-cylinder fueling from 20-100 C starting temperature.

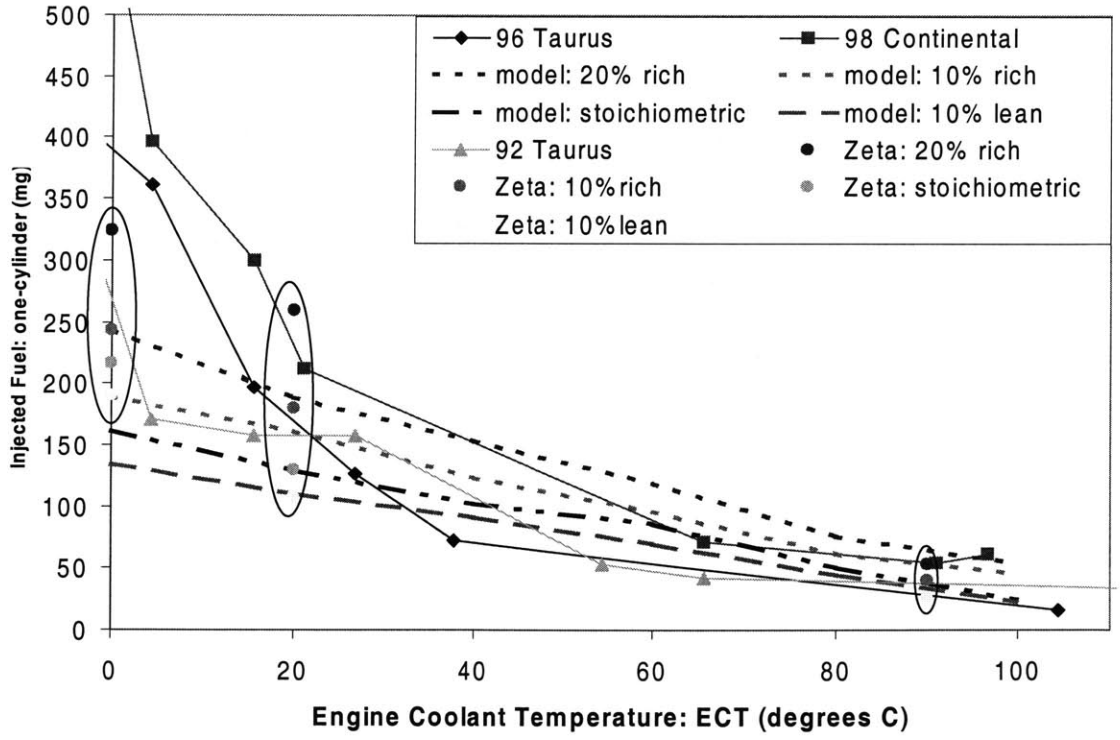

Figure 7.10: Comparison of model results to production engine calibrations and Zetec experimental results.

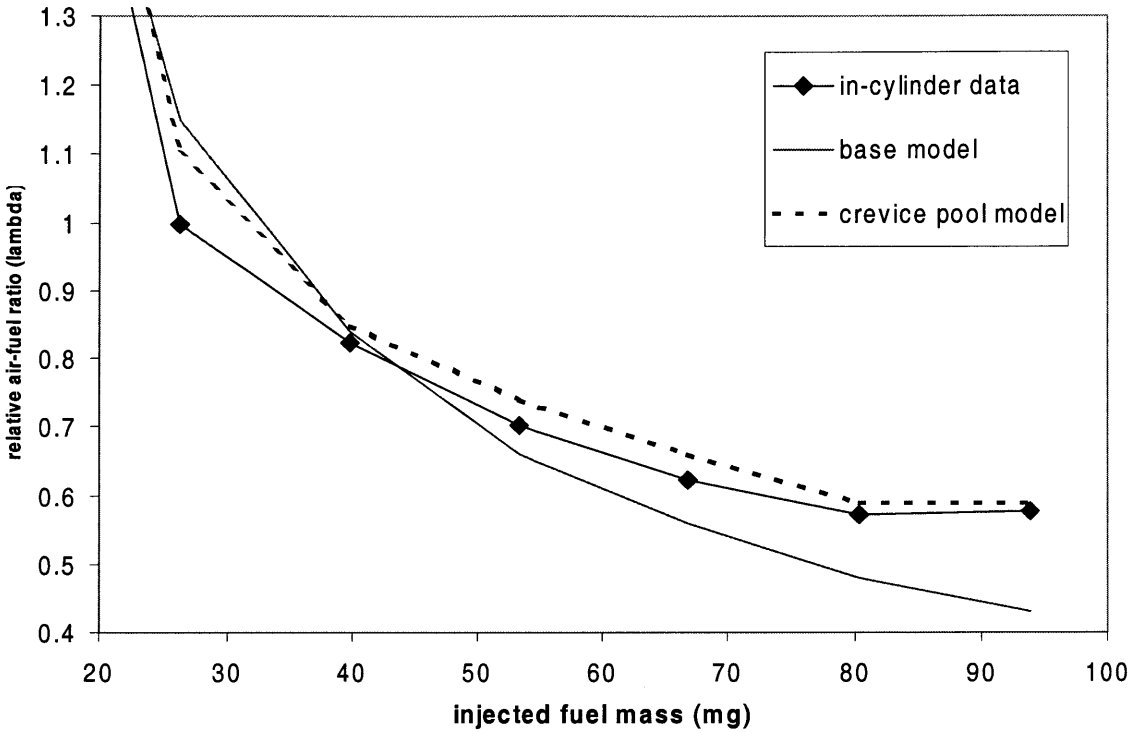

Figure 7.11: Position 'A' hot start data and modeling results.

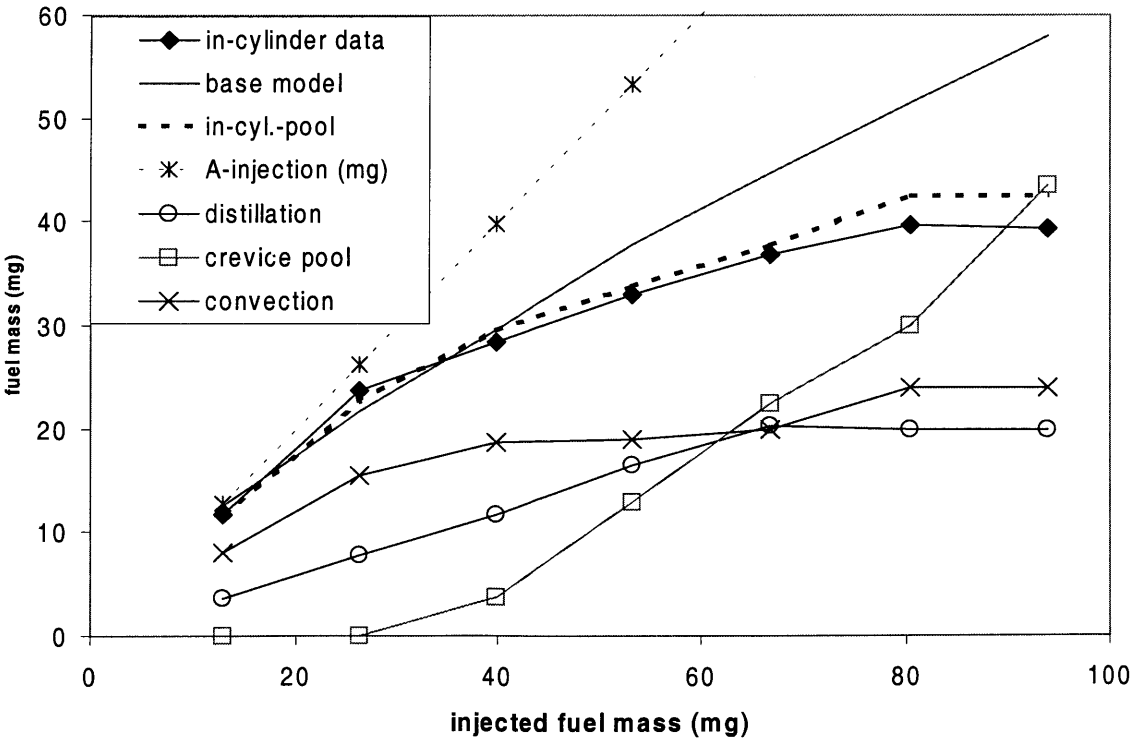

Figure 7.12: Position 'A' hot start modeling details with crevice pooling occurring at mid-high fuel injection levels.

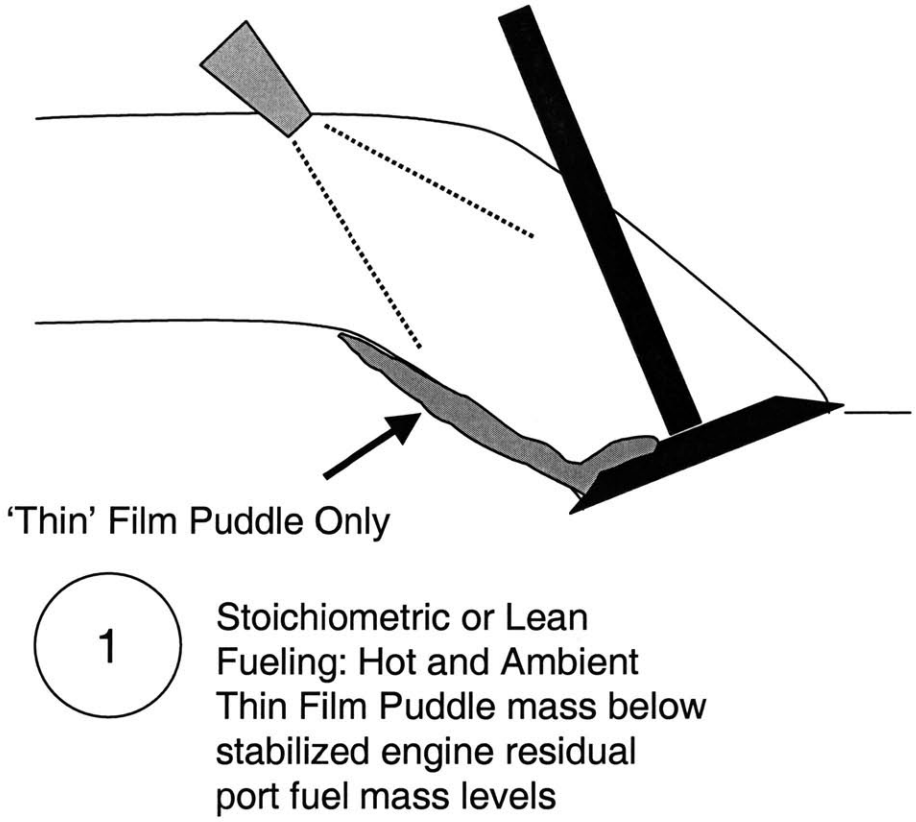

Figure 7.13: A schematic of the thin film puddle distribution as represented by the base model with in-cylinder fueling near stoichiometric.

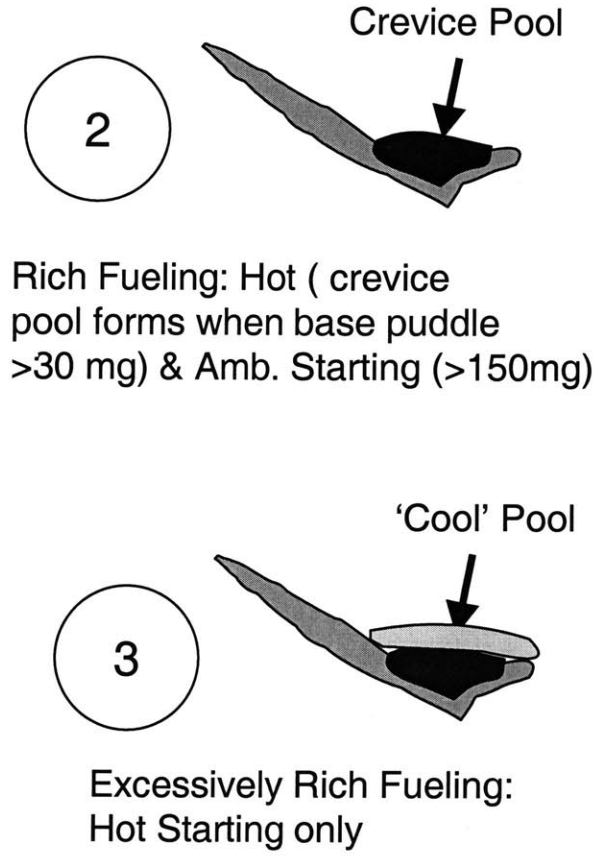

Figure 7.14: A schematic representing the pooling of liquid fuel in the crevice between the intake port and valve (2). This occurs when first cycle fuel injection mass becomes large. For very high first cycle fuel injection mass, the crevice pool becomes very deep (3). The upper part of the deep crevice pool remains relatively cool.

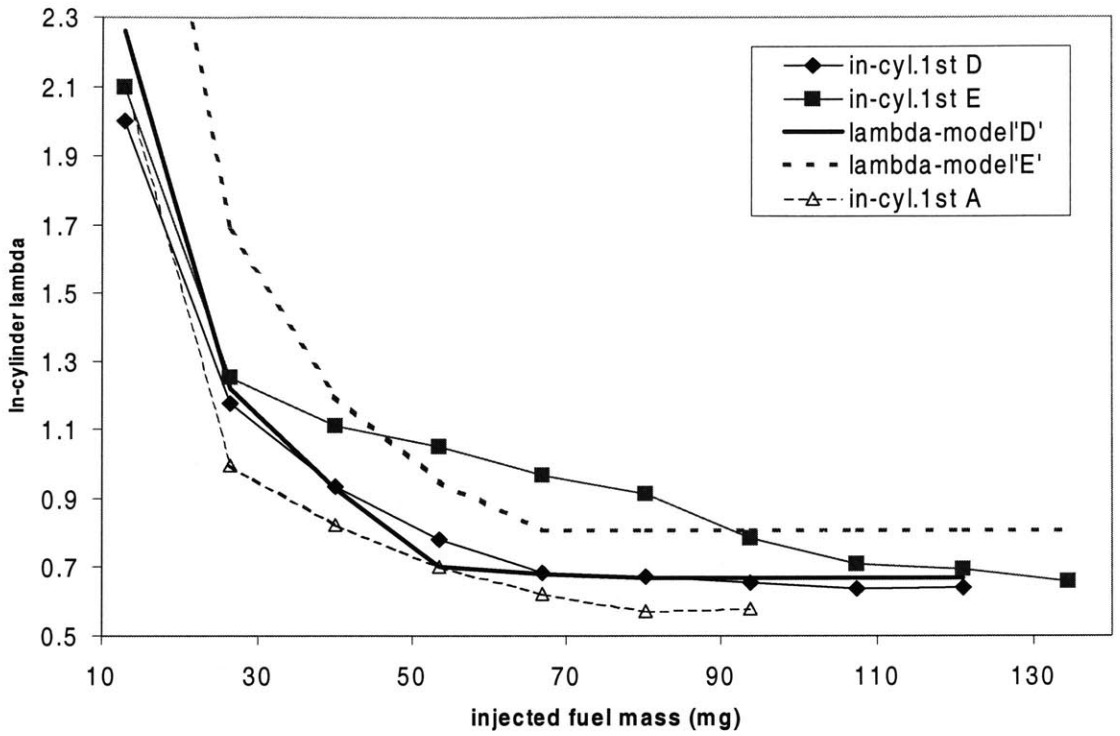

Figure 7.15: Hot start model comparison to data at positions D and E.

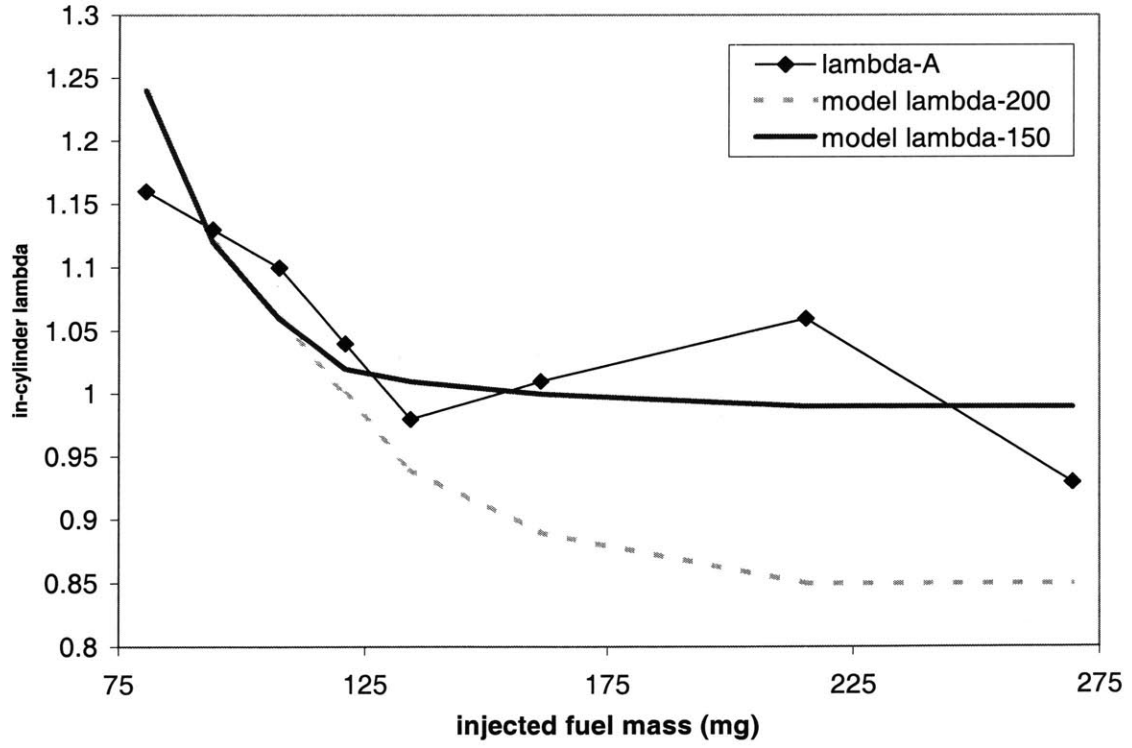

Figure 7.16: Ambient start model comparison to data at position A.

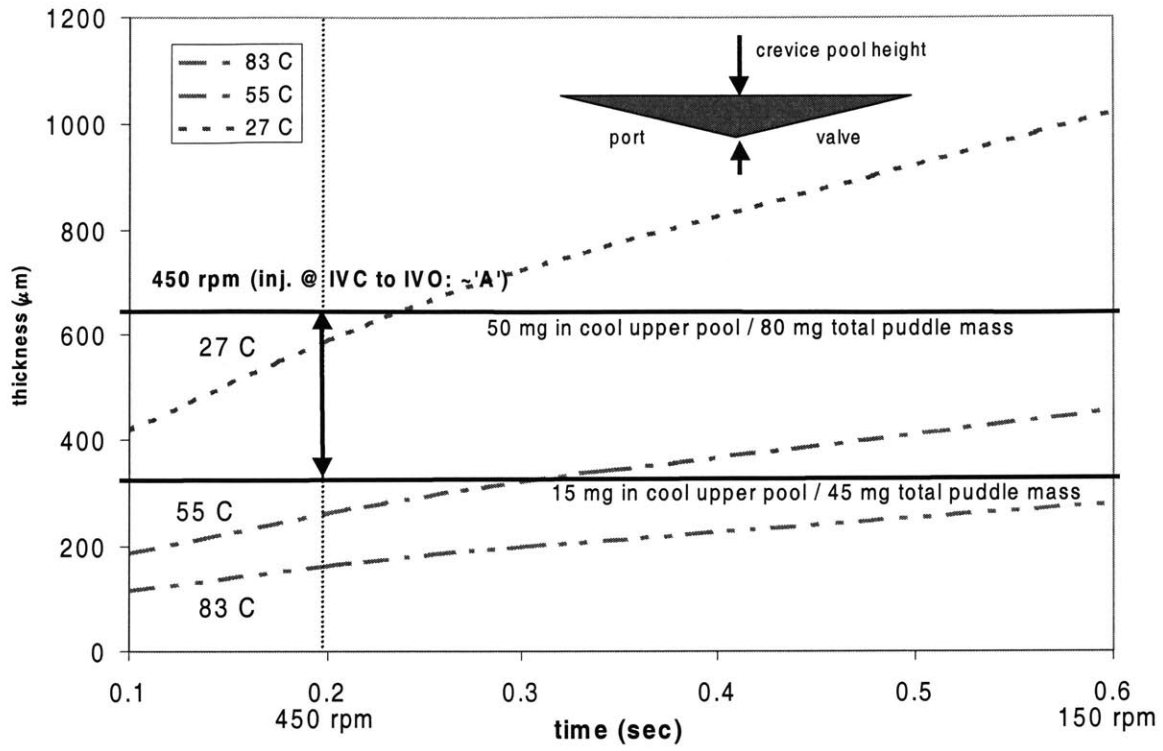

Figure 7.17: Conduction length into a liquid fuel film initially at 20 C from a wall at 90 C versus time. Estimated deep crevice depths are also shown.

(This page was intentionally left blank)

Chapter 8
Conclusions

8.1 Throttle Transients

8.1.1 A/F Measurement Techniques

1. Exhaust based UEGO measurements of in-cylinder A/F ratio are widely used for transient fueling calibration both in research and industry. Significant care must be employed, however, in experimental design and signal interpretation of the sensor due to the UEGO's relatively slow response time. This study showed the UEGO's response time to be approximately 200 msec under actual throttle transient conditions. At 1500 rpm, 2 ½ engine cycles occur during this time. Thus, the UEGO can miss significant fueling changes in an individual engine cycle during transient operation.

2. Using the FFID to sample in-cylinder gases was necessary to resolve cycle-by-cycle A/F ratio mixture changes during fast throttle transients and steady state step fuel experiments.

8.1.2 Characteristics of Mixture Preparation in Throttle Transients

1. Production Controller dynamic fuel pulses occurring in the middle to late portion of the intake valve open event do not enter the combustion chamber for the intended cycle. (This improper dynamic pulse timing was based upon transient injector timing experiments using a UEGO for feedback. The relatively slow UEGO response was responsible for this error.) While the fuel spray is believed to be reaching the lower intake port, due to the relatively late injection timing (640-670 cadeg, IVO: 530-770 cadeg), the dynamic pulse fuel mass does not experience the vigorous forward flow which carries fuel into the combustion chamber.

2. During throttle transients, independent of throttle rate or fuel control, the puddle increment per cycle normalized by the current cycles injected fuel mass showed approximately constant levels. For these stabilized engine experiments the normalized puddle increment was approximately 8%. On a absolute level, the puddle increment per cycle would increase roughly linearly with MAP increases during the transient.

3. For all stabilized engine throttle rates studied, the x-τ model (with constant coefficients calibrated from slow uncompensated throttle ramps at a specific engine rpm) describes remarkably well the puddle dynamics and in-cylinder fueling behavior both with and without Transient Fuel Control (TFC). This result also applied to various load changes at a given speed. When model coefficients applicable to another engine speed were used at that speed, similar excellent agreement was observed.

4. This excellent x-τ model behavior demonstrates that intake port puddle filling occurs in proportion to throttle rate during the transient. Faster throttle openings experience a quicker attainment of the final high load residual port fuel level as compared to slower throttle openings.

5. Comparison of throttle transients at all studied throttle rates shows that the intake port residual fuel-filling behavior is not dependent upon whether compensation is used. If Transient Fuel Compensation is used, the engine operates more closely to stoichiometric during the transient, than if fueling control is uncompensated.

6. On fast throttle openings a lean spike (λ~1.1 to1.2) was repeatedly observed. Based on the modeling analysis, it is believed that had the dynamic pulse been applied earlier in the intake process this effect could've been eliminated.

7. Intake Port 'Draining' Fuel Cut-off Experiments indicated that the change in residual intake port fuel is similar to that obtained by the throttle transient data. Thus if steady-state residual port fuel levels can be determined, appropriate x-τ model constants could be developed.

8. Both during steady-state operation and transient load increases, the physical basis for more retained fuel at higher engine loads is due to both temperature and pressure effects. At high engine loads with high fuel flow rates, the intake valve surface temperature in the area of fuel spray impacting is lowered significantly due to evaporative cooling. This same effect is responsible for lowering intake port surface temperatures at high engine loads in the vicinity of the fuel spray. These lower surface temperatures allow for more lighter fuel components to be retained in the puddle, thus increasing the puddle's mass. Additionally, as intake pressure increases, so does the saturated vapor pressure of individual fuel species. This effect tends to reduce the vaporization of fuel species, forcing some formerly vaporizing fuel species to remain in the liquid phase, tending to make the residual intake port fuel puddle larger also.

9. Throttle transient experiments with iso-pentane showed essentially no net change in residual intake port puddle mass with increasing load. This is due to its extremely volatile nature. Cumene, representative of the upper-middle portion of the distillation curve, showed slightly more residual intake port filling than gasoline. This is due to the molecular weight of cumene being larger than that of the gasoline average.

8.1.3 Practical Characterization Methods

1. One second (uncompensated) throttle ramps are an effective means to characterize x and τ at a given engine speed. The use of slow throttle ramps is essential in order to minimize air mass estimation errors. The resulting values of x and τ at a given engine speed are applicable to all load changes and throttle rates.

2. Step fuel characterization of x and τ produces model constants that are not representative of the dynamics involved in a real throttle transient. Using a UEGO with step fuel perturbations generates x's that are larger than obtained by the slow throttle transient characterization method. This is due to the slow UEGO response, which underestimates the in-cylinder response to the stepped fuel increase. Using a FFID in-

cylinder produces x's that are too small. These port fuel changes at a constant load are less than occurs when engine load is actually increased.

3. Fast throttle transients at 2000 rpm did not display the very rich cycles as was the case at 1500 rpm. Since only small differences exist in the x-τ model calibration between the two speeds, this effect is a result of more accurate air mass estimation during the transient at 2000 rpm. This difference in A/F performance during the transient demonstrates the need to carefully optimize manifold-filling characterization more precisely.

8.2 Cranking/Startup

8.2.1 Characterization of Mixture Preparation in Cranking/Startup

1. The most important effect of the piston starting position is on the engine instantaneous RPM values of the first cycle. These values depend on the crankshaft acceleration due to the firing of the other cylinders. The instantaneous RPM influences the IMEPg of the first cycle through its effect on combustion phasing, which affects both the work transfer schedule and the charge heat loss.

2. The first hot cranking cycle runs at typically ~200 to 600 rpm at ignition. There is also significant crankshaft acceleration during the combustion period. Therefore, the optimal heat release schedule is very different from normal practice. At these low speeds, combustion is very fast in terms of crank angles. Optimum ignition timing is typically after TDC; the usual practice of 10 degrees BTC ignition timing is thus too advanced. The IMEPg increases with RPM increase, which, in effect, slows down the heat release in terms of crank angles and benefits the phasing.

3. For all starting temperatures, the lean limit for robust first cycle firing is at an in-cylinder λ of ~1.1. Because of the much less favorable mixture preparation environment,

substantial amounts of injected fuel (>~300 mg) is needed to reach this condition in a cold start. Ambient and hot starting require greater than 100 mg and 26 mg, respectively.

4. The value of IMEPg during cranking is insensitive to the in-cylinder λ value in the range of 1.1 to ~0.65. This fact is a result of the slow engine speed so that the charge can burn to completion even at a very rich λ value. When the value of λ is decreased, the modest loss of relative energy released, which is the combined result of more fuel burned and lowered combustion efficiency, is offset by the slower combustion which results in a better heat release phasing. The net result is the insensitivity of the IMEPg to λ.

5. The following are observation for hot starts:

(a) The fraction of the injected fuel delivered to the charge mixture in the first cycle decreases linearly from unity as more fuel is injected. The net effect is that the mixture becomes richer with increase fueling, but with a diminishing return.

(b) The first cycle EOHC is at ~4000 to 8000 ppmC1, and is relatively insensitive to the first cycle in-cylinder λ until it is very rich (λ<0.65); then it rises sharply because of partial burn.

(c) The residual fuel (the part of the injected fuel which does not go into the charge mixture) from the first cycle enriches the second cycle mixture. The sensitivity is that λ decreases by 0.1 with every 22 mg increase in residual fuel.

6. The following are observation for ambient starts:

(a) A much lower fraction (compared to the hot start) of the injected fuel goes into the mixture. Again, the mixture becomes richer with increased fueling, but with a diminishing return.

(b) The first cycle EOHC value for the firing cases with closed valve injection are similar to the hot start case in both magnitude and sensitivity to in-cylinder λ value.

(c) Similar to the hot start, the second cycle in-cylinder λ is enriched by the presence of the residual fuel from the first cycle. The sensitivity, however, is approximately 3.4 times lower (λ decreases by 0.1 with every 74 mg increase in residual fuel.) This lower sensitivity is attributed to the slower rate of fuel evaporation.

7. The following are observations for cold starts:

(a) Only a very small fraction of the injected fuel enters the combustion chamber charge mixture, approximately 5%.

(b) EOHCs are approximately 2 to 3 times higher than for ambient and hot starting.

(c) The second cycle sensitivity to residual first cycle fuel has a similar slope to that of ambient starting, but occurs at much higher residual fuel levels.

8. In both hot start and ambient start, Open Valve Injection (OVI) is unfavorable to the mixture preparation process. It causes significant charge non-uniformity, directly deposits liquid fuel into the cylinder, which increases EOHC, and for the ambient and cold starts, wets the spark plug resulting in misfiring.

8.2.2 Modeling Insights

1. The relatively simple 'One Puddle' 1st cycle of crank model works remarkably well for predicting in-cylinder fuel vapor mass for near stoichiometric fueling across a broad range of temperatures (ambient to hot starting). A single calibration for the convective mass transfer relation at hot engine conditions is the only requirement. The model is capable of predicting the differences in in-cylinder fuel vapor that occur at different engine starting positions. This effect is a result of the increases in convective mass transfer from the puddle as initial engine position is advanced (and thus higher 1st cycle engine speeds).

2. Across the temperature range, for rich in-cylinder fueling, 'crevice pooling' is believed to be occurring. Model calibration is necessary based on steady-state residual intake port fuel levels (as a function of ECT). The crevice pool is still thin enough to achieve the port wall temperature before the intake valve opens. The crevice pool likely 'dumps' into the combustion chamber as large droplets and liquid film flows at IVO, and is not believed to be a factor in vapor generation on the first cycle.

3. With very high 1st cycle fuel injection levels during hot starting, the crevice pool is believed to be quite deep/thick, such that distillation/boiling is not occurring in the upper portion of the deep crevice pool.

4. For hot starting, the mixture preparation mechanisms of distillation/boiling and convective mass transfer are of comparable importance. Distillation produces fuel vapor that consists of primarily light-end fuel components, while convection draws in more of the heavy-end fuel components from the puddle. Liquid film flow from the thin puddle is of secondary importance and can be neglected.

5. For ambient and cold starting, convective mass transfer is the dominant fuel vapor generation mechanism. Once the crevice pool 'dumps' into the combustion chamber, thin film liquid flow is then only a few percent of the remaining puddle mass.

8.2.3 Implications for Practical Control

1. If engine position is known to be at position E for any temperature, it is best to delay fueling until the second cycle. Otherwise high EOHCs will result. Partial burns and misfires were frequently observed.

2. Cylinder specific spark during each cycle of crank is necessary to optimize IMEPg for each engine event. Engine speed-RPM should be evaluated prior to each spark event. In general, for the first cycle of crank, early cylinder events should receive ATC spark timing. As the engine speeds up, spark can be advanced.

3. Slight overfueling at all starting temperatures shows no increase in engine out HC emissions. This overfueling can be useful to protect against low volatility fuels which often lead to misfire, and the associated very high levels of EOHCs. It is believed, however, that overfueling will steadily raise engine out CO levels due to insufficient oxygen for complete mixture combustion.

```
/*  Appendix A: PC based fuel/spark controller
/*****************************************************************
**/
/*
 */
/*
 */
/*   The controller used is open loop.
 */
/*                                                    Jim Cowart
 */
/*                                          Last revised 6/1/00
 */
/*****************************************************************
**/
#include <stdio.h>
#include <stdlib.h>
#include <conio.h>
#include <math.h>
#include <dos.h>
#include "dasdecl.h"
#include "das1600.h"
#include "paramete.h"
#include "address.h"
#include "protos.h"

/* VARIABLES OF FCD */
   DWORD       hDrv;                                /* Driver Handle
 */
   DWORD       hDev;                                /* Device Handle
 */
   DWORD       hFrameAD;                          /* A/D Frame Handle
 */
   WORD far   *pDMABuf;          /* Pointer to allocated DMA buffer
 */
   WORD        hMem;                    /* allocated Memory Handle
 */
   short       nStatus;             /* Used to monitor DMA transfers
 */
   DWORD       dwTransfers;         /* Used to monitor DMA transfers
 */
   short       nErr;                   /* Function return error flag
 */
   DWORD       dwSamples = 2;        /* Number of samples to acquire
 */
   char far   *szErrMsg;                /* Pointer to error message
 */
   short       c,inj,soi,cycle,crk;
```

```
void DMA_setup(void);
void DisplayError(char *szFuncName, short nErr);
double AD_convert(int Chn);

long time(void);
short crank(void);
short absenc(void);


void main(void)
{
   float Pman,Tman,VM,Mth,lambda,mfs,pwca;
   float pswidth,N,mult;
   int i,strt,extra,initpos,moving,absecd,ginit;
   long injend;
   char buff[20];
   FILE *fpout;


   if((fpout=fopen("sensor.out","w"))==NULL){
      printf("cannot open file.\n");
      exit(1);
   }
   outp(B0_DIO,0X0);

   DMA_setup();
   counter_setup();
//   outp(B0_PIOPA,1);
   outp(B0_DIO,1);

   inj=0;
   soi=360;
   mult=1.0;
   extra=0;
   cycle=1;
   crk=0;
   N=0.;
   injend=0;
   ginit=0;

//   goto runmode;
//      initpos=absenc();
initpos=inp(B0_PIOPB);
moving=initpos-10;
        printf("init.pos.%d\n",initpos);
        printf("cycle no.%d\n",cycle);
```

```
// Start of infinite loop

//goto runmode;
//      while(cycle<6){
        while(crk==0){
//        if (N>=700)goto runmode;
                if (kbhit()) break;
                if (inj==0 && crk==0){
//                      if(absenc()>(initpos+20))crk=1;
                        if((inp(B0_PIOPB)) < moving){
                                crk=1;
                                printf("engine moving\n");
                                }
                }
}
//
        while(cycle==1){
        if(kbhit()) break;
        if (crk==1 && cycle==1 && inj==0){
                inj=1;
                outp(B0_DIO,0);
                injend=time()+90.*100.0;
//              printf("first cycle%ld,%ld\n",injend,time());
// was 25 for hot!
        }
//      printf("time%ld\n",time());
        if (crk==1 && cycle==1 && inj==1 && (time()>=injend)){
                inj=0;
                outp(B0_DIO,1);
                cycle=2;
                printf("eoi1\n");
        }
}
//goto finish;
  //      printf("time%ld\n",time());
        while (cycle==2){
        if(kbhit()) break;
        absecd=inp(B0_PIOPB);
        if (absecd > initpos && initpos > 25)ginit=1;
//      if (initpos<=25 && cycle==2)goto runmode;
        if (crk==1 && cycle==2 && inj==0 && ginit==1 && absecd<=140
){
//              printf("second cycle\n");
                inj=1;
                outp(B0_DIO,0);
                injend=time()+70.*100.0;
// was 1*
        }
```

```
        if (crk==1 && cycle==2 && inj==1 && (time()>=injend)){
                inj=0;
                outp(B0_DIO,1);
                printf("eoi2\n");
                cycle=3;
        }
}
//goto runmode;

        while (cycle==3){
        if(kbhit()) break;
        absecd=inp(B0_PIOPB);
//                      (initpos+80) for cold start pos.36 3rd
        if (( absecd > (initpos)) && initpos > 25)ginit=2;
//      if (initpos<=25 && cycle==3)goto runmode;
        if (crk==1 && cycle==3 && inj==0 && ginit==2 && absecd<=120
){
//              printf("second cycle\n");
                inj=1;
                outp(B0_DIO,0);
                injend=time()+50.*100.0;
// was 1*
        }
        if (crk==1 && cycle==3 && inj==1 && (time()>=injend)){
                inj=0;
                outp(B0_DIO,1);
                printf("eoi3\n");
                cycle=7;
        }

}
// end of while loop
runmode:
printf("runmode\n");
crk=0;

   for(;;){
      if (kbhit()) break;
        c=crank();
// start of measurement and injector on loop   was delta 10
        if((c>=soi) && (c<soi+20) && (inj==0) && (crk==0)){

                Pman=0.;
                N=0.;


                for(i=0 ; i<5 ; i++){
```

```
          if((nErr = K_DMAStart (hFrameAD) ) != 0){
             DisplayError("K_DMAStart", nErr);
             exit(1);
          }

          do{
             K_DMAStatus(hFrameAD, &nStatus, &dwTransfers);
          } while (nStatus & 1);

          if(nStatus & 2)
             printf("Overrun error during DMA transfer\n");


          Pman += AD_convert(Chn_Pman);
          N += AD_convert(Chn_N);
               }
//end measurement for loop


        Pman = 0.31947*Pman/5.-0.2827;
/*      Tman = 20.02*Tman/100.+269.19;*/
        Tman=293;
        N *= 200.;
//      printf("%f,%f\n",N,Pman);


        /* mass of stoich. fuel (mg), pswidth in msec  */
        mfs=1.5*mult*(Veff(N,Pman))*Pman*VD*FA_STOI/R/Tman;
//      printf("Veff,N,P%f,%f,%f\n",Veff(N,Pman),N,Pman);
        pswidth=.37*mfs+.27;
        pwca=pswidth*N*6./1000.;

        inj=1;
        outp(B0_DIO,0);
        injend=time()+pswidth*100.0;
//      strt=crank();

//      printf("%ld,%f,%f\n",time(),mult,pswidth);
//      printf("%ld\n",injend);
        }
// end of measurement and injector on loop

// start of injector off
/*       if(crank()>=(pwca+strt) && inj==1){
        inj=0;
        outp(B0_PIOPA,0);
        }
*/
```

```
        if(time()>=injend && extra==0 && inj==1 && crk==0){
         inj=0;
         outp(B0_DIO,1);
         }
//                      printf("%d\n",mult);
//              if(injend>=3000000)goto finish;
//              if(injend>=3008000)mult=1.0;
//              if(injend>=4500000)mult=0.78;


/*       c=crank();
         if ((c>=630) && (c<650) && (mult==2) && (inj==0)){
                 inj=1;
                 extra=1;
                 outp(B0_PIOPA,0);
                 }
         c=crank();
         if ( (c>=660) && (mult==2) && (inj==1)){
                 inj=0;
                 extra=0;
                 outp(B0_PIOPA,1);
                 }*/
//               printf("%ld\n",time());
//end of injector off

/* end of for ii loop*/
   }
/*   fclose(fpout);*/
finish:

//   outp(B0_PIOPA,1);
        outp(B0_DIO,1);
//   outp(B0_DIO,0X0);
   N=0.;
   mult=1;
   cycle=1;
//   portb=0;

   K_DMAFree (hMem);
   K_CloseDriver(hDrv);
   printf("done");

}
/*****************************************************************
**/
/*       Absolute Encoder decoding
 */
/*****************************************************************
```

```
**/
short absenc(void)
{
   int          portb;
   int          g[8],b[8],dec[3];
   int          j,k,m1,m2,rem,divi,tp,x,p;
//   long int   bin;
//portb=0;
                portb=inp(B0_PIOPB);
//                      fprintf(stderr,"portb is %d \n",portb);
                divi=portb;
//              printf("%d portb \n",portb);
                for(k=0 ; k<8 ; k++){
//                      printf("forloop %d\n",k);
                        g[k] = 0;
                        b[k] = 1;
//                      fprintf(stderr,"%d \t %d",g[k],b[k]);
//                      if (kbhit())goto finish;
                        }
                        j=0;
//                      bin=0;
                while(divi > 0)
                        {
//                      if (kbhit() )break;
//                      fprintf(stderr,"%d divi\n",divi);
                        rem=divi % 2;
                        divi=divi / 2;
                        g[j]=rem;
//                      fprintf(stderr,"%d \t %d \t %d\n",j,divi,g[
j]);
                        j++;
                        }
//                              fprintf(stderr,"%d\n",g[0]);
//                              *pts=g[7];
//                              fprintf(stderr,"%d\n",*pts);
//                              tp=*pts;
                              b[7]=g[7];
//              if(b[7] |= g[7]) b[7]=g[7];
//                              fprintf(stderr,"%d\n",g[0]);
                if(b[7]==g[6]) b[6]=0;
                if(b[6]==g[5]) b[5]=0;
                if(b[5]==g[4]) b[4]=0;
                if(b[4]==g[3]) b[3]=0;
                if(b[3]==g[2]) b[2]=0;
                if(b[2]==g[1]) b[1]=0;
                if(b[1]==g[0]) b[0]=0;
//              bin=b[0]+10*b[1]+100*b[2]+1000*b[3]+10000*b[4]+1000
00*b[5]+1000000*b[6]+10000000*b[7];
```

```
//              fprintf(stderr,"\n");

//               for (m1=0 ; m1<8 ; m1++)
//              fprintf(stderr,"%d",g[m1]);
//              fprintf(stderr,"\n");
//               for (m2=0 ; m2<8 ; m2++)
//              fprintf(stderr,"%d",b[m2]);
//              fprintf(stderr,"\n");
//              fprintf(stderr,"%ld\n",bin);
                p=b[0]+b[1]*2+b[2]*4+b[3]*8+b[4]*16+b[5]*32+b[6]*64+
b[7]*128;
/*              p=0;
                while( bin > 1){
                 x=bin % 10;
                 dec[p]=x;
                 bin = bin / 10;
                 p++;
                 }
                 portb=dec[0]+10*dec[1]+100*dec[2];*/
//               fprintf(stderr,"%d\n",p);
                 return (255-p);
}
/*****************************************************************
**/
/*   This function is to set up the free-run DMA data acquisition.
 */
/*****************************************************************
**/
void DMA_setup(void)
{
/* FIRST STEP IS TO INITIALIZE THE HARDWARE/SOFTWARE */
   if(( nErr = K_OpenDriver("DAS1600", "das1600.cfg", &hDrv)) != 0)
{
      putch (7); printf( "Error %X during K_OpenDriver", nErr);
      exit (1);
   }

/* ESTABLISH COMMUNICATION WITH THE DRIVER THROUGH A DEVICE HANDLE
*/
   if(( nErr = K_GetDevHandle(hDrv, 0, &hDev) ) != 0){
      putch (7); printf( "Error %X during K_GetDevHandle", nErr);
      exit(1);
   }

/* GET HANDLE TO AN A/D FRAME WITH THE DEVICE */
   if((nErr = K_GetADFrame( hDev, &hFrameAD )) != 0){
      DisplayError("K_GetADFrame", nErr);
```

```
      exit(1);
   }

/* ALLOCATE ENOUGH MEMORY BUFFER TO ACCOMODATE THE DESIRED NUMBER O
F SAMPLES */
   K_DMAAlloc (hFrameAD, dwSamples, (void far * far * )&pDMABuf, &h
Mem );
   if(pDMABuf == NULL){
      putch (7); printf( "Error; DMA buffer pointer is NULL!" );
      exit(1);
   }
/* ASSIGN DMA BUFFER AND NUMBER OF SAMPLES TO THE A/D FRAME. */
   if((nErr = K_SetDMABuf (hFrameAD, pDMABuf, dwSamples) ) != 0){
      DisplayError("K_SetDMABuf", nErr);
      exit(1);
   }

/* SPECIFY THE A/D SCAN CHANNELS AND GLOBAL GAIN CODE */
   if((nErr = K_SetStartStopChn (hFrameAD, 0, 5)) != 0){
      DisplayError("K_SetStartStopChn", nErr);
      exit(1);
   }
   if((nErr = K_SetADFreeRun (hFrameAD) ) != 0){
      DisplayError("K_SetADFreeRun", nErr);
      exit(1);
   }
}

/*****************************************************************
**/
/*   This function is to convert raw data into voltage.
 */
/*****************************************************************
**/
double AD_convert(int Chn)
{
   int count;

   count= (*(pDMABuf+Chn) >> 4) & 0x0FFF;
   return (count-2048.0)*span/4096.0+0.00122;
}
/*****************************************************************
**/
/*   This function is to display the error message.
 */
/*****************************************************************
**/
void DisplayError(char *szFuncName, short nErr)
```

```
{
   K_GetErrMsg(hDev, nErr, &szErrMsg);
   putch(7);
   printf("Error %X during %s operation: %Fs\n", nErr, szFuncName,
szErrMsg);
}
/*****************************************************************
***
   This function is to setup counters.
   Board 0:
        Counter 0 is used to read crank angle signal from the shaft
        encoder.  Gate0 (pin24) hi, CLK0 (pin21).
   Board 1;
        Counter 1 is used as a 0.01 msec clock out to counter 2.
        Counter 2 is used as a 0.1 sec clock out to counter 0.
        Counter 0 is used as a 1 hr clock.
        Pin 24 & 25 hi, CLK 2 out (pin 20) to CLK0 in (pin 21).
*****************************************************************
**/
void counter_setup(void)
{

   int cnten;
//   unsigned short hc;

/* Board 0: set counter 0 external clk */
   cnten = inp(B0_CNTEN);
   outp(B0_CNTEN, cnten&0XFD);

/* Board 0: set counter 0 mode 5, 0011 1010 */
   outp(B0_TIMERCTL, 0X3A);

/* Board 0: load counter 0 719 count = 0X02CF */
   outp(B0_TIMER0, 0XCF);
   outp(B0_TIMER0, 0X02);

/*   outp(B0_TIMERCTL, 0X76);
   outp(B0_TIMERCTL, 0XB4);
   outp(B0_TIMER1, 0X64);
   outp(B0_TIMER1, 0X00);
   outp(B0_TIMER2, 0X10);
   outp(B0_TIMER2, 0X27);
*/

/* Board 1: set counter 0 external clk, counter 1&2 disable */
   outp(B1_CNTEN, 0X01);

/* Board 1: set counter 1 mode 3, 0111 0110 */
```

```
   outp(B1_TIMERCTL, 0X76);

/* Board 1: set counter 2 mode 2, 1011 0100 */
   outp(B1_TIMERCTL, 0XB4);

/* Board 1: set counter 0 mode 4, 0011 1000 */
   outp(B1_TIMERCTL, 0X38);

/* Board 1: load counter 1 100 count = 0X0064, 0.01 msec clk out */
   outp(B1_TIMER1, 0X64);
   outp(B1_TIMER1, 0X00);

/* Board 1: load counter 2 10000 count = 0X2710, 0.1 sec clk out */
   outp(B1_TIMER2, 0X10);
   outp(B1_TIMER2, 0X27);

/* Board 1: load counter 0 36000 count = 0X8CA0, last for 1 hr */
   outp(B1_TIMER0, 0XA0);
   outp(B1_TIMER0, 0X8C);

/* Board 1: enable counter 1&2 */
   outp(B1_CNTEN, 0X00);


}

/*****************************************************************
***
  This function is used to read the crank angle from counter 0
  on board 0.
*****************************************************************
**/
short crank(void)
{
   int lo,hi;

/* latch allows reading contents 'on the fly' without w/out affecti
ng count
counter latch cmnd is like command word (CW) except written to CW T
imerCtl
Register
xx/xx/xxx/x 00/chl#     00/ctr.latch    xxx/pulse on term. count
 0/binary

/* Board 0: latch counter 0 */
   outp(B0_TIMERCTL, 0X00);

/* Board 0: read counter 0 LSB then MSB */
```

```
   lo = inp(B0_TIMER0);
   hi = inp(B0_TIMER0);

   return 719-(hi<<8)-lo;
}

/*****************************************************************
***
   This function is to read real time from timer/counter on
   board 1.  The time is in 0.01msec.
*****************************************************************
**/
long time(void)
{
   long int lo0,hi0,lo2,hi2;

/* Board 1: latch counter 0 and 2 */
   outp(B1_TIMERCTL,0X00);
// x80= 10 00 0000
   outp(B1_TIMERCTL,0X80);

/* Board 1: read counter 0 LSB then MSB */
   lo0 = inp(B1_TIMER0);
   hi0 = inp(B1_TIMER0);
//   h0=(hi0<<8);
//   printf("hi0, lo0 h0 %d,%d,%d10\n",hi0,lo0,h0);

/* Board 1: read counter 2 LSB then MSB */
   lo2 = inp(B1_TIMER2);
   hi2 = inp(B1_TIMER2);
//   h2=(hi2<<8);
//   printf("hi2, lo2 %d,%d\n",hi2,lo2);
/* time will count up from 0 to 360,0 00,000 in one hour
                                        /.01msec   */

   return (36000-(hi0<<8)-lo0)*10000+10000-((hi2<<8)+lo2);
}
/*****************************************************************
***
  This is the look-up table for finding the volumetric efficiency
  at a given intake manifold pressure, Pman, and engine speed, N.
  It is calibrated for Pman between 0.29 to 1.0bar; N between 1100r
pm
  to 2200rpm.  Extrapolation is used when the condition is outside
  this range.
********************* Last revised 12/05/96 ***********************
**/
double Veff(double N, double Pman)
```

```
{
   const static float P[19]={.20,.25,.29,.33,.37,.41,.45,.49,.53,.5
7,
      .61,.65,.69,.73,.77,.81,.85,.89,1.0};
   const static float RPM[12]={1104.,1206.,1307.,1407.,1507.,1606.,
      1706.,1805.,1904.,2004.,2103.,2204.};
   const static float veff[19][12]={
.5039,.5169,.5298,.5212,.5578,.5764,.5454,.5132,.5887,.5344,.5610,.
6010,
.5531,.5673,.5698,.5716,.6062,.6118,.5973,.5704,.6104,.5843,.6085,.
6350,
.5924,.6076,.6018,.6119,.6449,.6401,.6388,.6161,.6278,.6242,.6465,.
6622,
.6264,.6408,.6323,.6442,.6703,.6661,.6682,.6521,.6404,.6527,.6724,.
6853,
.6473,.6588,.6541,.6662,.6893,.6867,.6892,.6751,.6631,.6738,.6906,.
7035,
.6634,.6751,.6730,.6827,.7068,.7054,.7083,.6937,.6832,.6896,.7081,.
7178,
.6772,.6894,.6899,.6986,.7190,.7204,.7259,.7115,.6984,.7026,.7205,.
7306,
.6885,.7016,.7030,.7121,.7297,.7305,.7386,.7240,.7105,.7152,.7312,.
7405,
.6959,.7097,.7135,.7211,.7374,.7392,.7466,.7336,.7201,.7223,.7394,.
7471,
.7027,.7167,.7214,.7275,.7441,.7461,.7531,.7412,.7289,.7308,.7452,.
7528,
.7103,.7225,.7293,.7347,.7487,.7508,.7597,.7483,.7372,.7380,.7508,.
7584,
.7168,.7278,.7358,.7394,.7527,.7553,.7659,.7550,.7433,.7440,.7551,.
7632,
.7239,.7330,.7417,.7444,.7566,.7599,.7714,.7608,.7489,.7501,.7592,.
7668,
.7286,.7352,.7490,.7499,.7614,.7651,.7768,.7660,.7544,.7547,.7636,.
7717,
.7349,.7374,.7570,.7554,.7661,.7712,.7823,.7706,.7601,.7591,.7679,.
7769,
.7415,.7434,.7652,.7616,.7705,.7788,.7881,.7780,.7667,.7661,.7732,.
7834,
.7482,.7474,.7734,.7675,.7759,.7863,.7921,.7833,.7752,.7738,.7793,.
7882,
.7541,.7531,.7816,.7738,.7845,.7947,.7974,.7849,.7782,.7842,.7858,.
7933,
.7674,.7710,.8035,.7888,.8107,.8193,.8254,.7852,.7787,.8155,.8094,.
8095};
   double veff1,veff2;
   short i=1,j=1,i1,j1;
```

```
    if(Pman > 0.89)
       i = 18;
    else if(Pman < 0.25)
       i = 1;
    else
       while(Pman > P[++i]);
    i1=i-1;

    if(N > 2100.)
       j = 11;
    else if(N < 1200)
       j = 1;
    else
       while(N > RPM[++j]);
    j1 = j-1;

    veff1 = veff[i1][j1]+(veff[i][j1]-veff[i1][j1])
           *(Pman-P[i1])/(P[i]-P[i1]);
    veff2 = veff[i1][j]+(veff[i][j]-veff[i1][j])
           *(Pman-P[i1])/(P[i]-P[i1]);

    return veff1+(veff2-veff1)*(N-RPM[j1])/(RPM[j]-RPM[j1]);
}
```

Appendix B: Engine Stopping/Starting Locations

When an engine coasts to stop, the final piston position is determined by the gas load, inertia load and friction. The kinetic energy (KE) of the moving parts is governed by

$$\frac{d(KE)}{dt} = P_g - P_f \qquad \text{(B1)}$$

where P_f is the power dissipated by friction and P_g is the power produced by the gas load.

$$P_g = \sum_{\text{all cyliners}} p\dot{V} \qquad \text{(B2)}$$

Note that for each cylinder, the value of P_g is negative for the compression stroke and positive for the expansion stroke. When the pistons are close to stop, KE is small so d(KE)/dt cannot be very large. For simplicity, P_f is assumed to be small (to be justified later by comparing results with observations). Thus the engine will stop at the positions of the zeros of P_g. Furthermore, the zeros involving the negative to positive transition of P_g are unstable in the sense that the engine will accelerate once the zero is crossed. Therefore, the preferred stopping positions are the zeros associated with the positive to negative transitions of P_g.

The values of the individual cylinder P_g and the total are shown in Fig. A1. For this calculation, the engine geometry has a connecting rod to crank radius ratio of 3.1 (value of the Zetec engine). The pressure values were obtained from a cycle simulation of an engine operating at WOT motoring condition at 100 rpm (which approximates the engine condition before it stops). The piston stopping positions are marked. They are at the mid stroke (88° from BDC) of compression of one of the pistons. The results compared favorably with the observed stopping positions (~90° from BDC). Thus the friction term contribution in Eq.(A6) to the piston stopping position is indeed small.

To further check the validity of the analysis, the procedure was applied to a 6 cylinder engine. The result was that the stopping position should be at 118° from BDC of the compression stroke. This value agrees well with that of Reference [5.5] (at 110±15°).

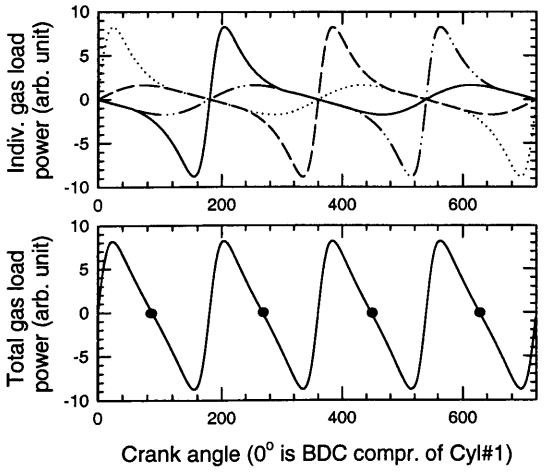

Figure B1: The gas load power ($p\dot{V}$) for the individual cylinders and the total value for a motoring 4 cylinder engine at WOT. The markers indicate the piston stops which are at the zeros of the positive to negative transitions of the total gas load power.

```
      program pudcrk      !Appendix C
c
c     written by Jim Cowart   MIT     3-19-00
c
c         for distill
      common /mixture1/W(15),ispec(15),nsp,nspf,nspo
      common /diffeqn/idiff,iinj,finjdeg,ftotinj(10),fmassfr(10),invopen
      common /diffeqn2/rpm,ica,isig,ff,ivfirst,yfg(10)
      common /opcond/temp,press,secprdeg
      real mgperdeg
c
      dimension pmass(10), dist_m(10),opmass(10),
     +vappr(10),pmole(10),xvap(10),opmole(10)
c         for fuelnum     ispec and W already specified
      dimension cn(21),hn(21),st(21),ww(21)
      dimension cnum(10),hnum(10),stoi(10)
c
      parameter (neq=8,npt=1000)   !six fuel species + vapor + in-cyl.liq.
      dimension y(neq,npt)
      dimension work(neq,3)
      character*3, rpmc,fpwc
      character*1, injsc,tempc
c
      external diffeq
c
      nspo=4
      nspf=6  !no. of fuel species
c
      ispec(1)=7
      ispec(2)=8
      ispec(3)=10
      ispec(4)=11
      ispec(5)=13
      ispec(6)=15
      ispec(7)=1
      ispec(8)=2
      ispec(9)=18
      ispec(10)=20
      ispec(11)=0
      ispec(12)=0
      ispec(13)=0
      ispec(14)=0
      ispec(15)=0
c
      call fuelnum(nspf,nspo,ispec,cnum,hnum,stoi,W)
c
ccccccccccccccccccc input parameters ccccccccccccccccccccccccccccc
      temp=373.
      tempc='h'   !h=hot g=hot w/sigmah
      press=.9*101325.
      rpm=450.       !@IVC
      rpmc='450'
c         hot: 'a'=183deg/450rpm
c         hot: 'd'=565deg/150rpm
      injstrt=183   !cadeg 0=BCC, TCC=180 'd'=540  'e'=650
      injsc='a'
      ipw=30  !msec
      fpwc='30'
      ff=0.06
      open(unit=26,name=fpwc//injsc//rpmc//tempc)
ccccccccccccccccccc
      iinj=1
      isig=0  !=1 use sigma for h determination
      idiff=0
      invopen=0
c     !for positions 'D' and 'E' set to 1 w/ iinj=1
      ivfirst=0   !for 1st entry into OV w/ CVI for mass conc. in port
ccccccccccccccccccc engine geometry/fixed parameters
      ivo=530 ! 10BTC
      ivc=720 ! BCC.....in reality ~770, but later period is backwards
ccccccccccccccccccc
      secprdeg=1.0/(rpm*6.)   !seconds per crank angle degree
      mgperdeg=secprdeg*1000./0.37    !mg of injected fuel per cadeg at rpm
      finjdeg=mgperdeg/1000000.       !kg of injected fuel per cadeg
      durinj=float(ipw)/(1000.*secprdeg)  !cadeg
      injdur=nint(durinj) !cadeg
```

```
      ftinj=durinj*finjdeg    !total injection mass(kg)
      print*,'injdur,totinjms,injdeg',durinj,ftinj,finjdeg
ccccccccccccccccccc
c         mass fraction of fuel species 'i'
      fmassfr(1)=.15  !was
      fmassfr(2)=.18  !was
      fmassfr(3)=.19  !was
      fmassfr(4)=.21  !was .3
      fmassfr(5)=.16  !
      fmassfr(6)=.11  !
      fmassfr(7)=0.0
      fmassfr(8)=0.0
      fmassfr(9)=0.0
      fmassfr(10)=0.0
ccccccccccccccccccc
c         calculate total injected fuel of each specie 'i'
      do jj=1,nspf
      ftotinj(jj)=float(ipw)*fmassfr(jj)/370000.  !units kg
      enddo
ccccccccccccccccccc
c         initial puddle condition
      do jj=1,nspf+2
          pmass(jj)=fmassfr(jj)*finjdeg
          y(jj,injstrt)=0.0       !zero initial puddle mass (or pmass(jj) )
          y(jj,injstrt-1)=0.0
          y(jj,injstrt-2)=0.0
      enddo
ccccccccccccccccccc
c         integrate over one crank angle
      dtheta=1.0    !one crank angle degree
ccccccccccccccccccc
      goto 454
c         start injection and flash evap.
c         y(i,ica):puddle mass of each fuel specie 'i'
ccccccccccccccccccc
c         start up calculations w/ runga-kutta
c         injection on! start-up
      do ica=injstrt,injstrt+2
          rcrkang=float(ica)
          call rk2(neq,rcrkang,dtheta,y(1,ica),
     +        y(1,ica+1),diffeq)
      write (26,910)float(ica),(y(j,ica+1)*1000000.,j=1,neq)
      enddo
ccccccccccccccccccc
c         injection on!
454   istart=0    !for wai's integrator- forward.for
      do ica=injstrt,injstrt+injdur       !+3
      call forward(
     +neq,rcrkang,dtheta,y(1,ica),y(1,ica-1),y(1,ica-2),
     +y(1,ica-3),y(1,ica+1),diffeq,istart,work)
c     print*,y(1,ica+1)*1000000.,y(4,ica+1)*1000000.,y(6,ica+1)*1000000.
      write (26,910)float(ica),(y(j,ica+1)*1000000.,j=1,neq)
      enddo
      iinj=0  !injector off
c
c         sum up puddle
      fuelsum=0.0
        do jj=1,nspf
          fuelsum=fuelsum+y(jj,injstrt+injdur+1)
        enddo
      print*,'inj/pudpostinj/vap',ftinj*1000000.,fuelsum*1000000.,
     +y(7,injstrt+injdur)*1000000.
ccccccccccccccccccc
c         quiescent port diffusion
      if(invopen.eq.1)goto 777    !for the case of 'D' and 'E' skip diffusion
c
      idiff=1     !diffusion allowed to occur until the IVOpens
      do ica=(injstrt+injdur+1),ivo
      call forward(
     +neq,rcrkang,dtheta,y(1,ica),y(1,ica-1),y(1,ica-2),
     +y(1,ica-3),y(1,ica+1),diffeq,istart,work)
c     print*,y(1,ica+1)*1000000.,y(4,ica+1)*1000000.,y(6,ica+1)*1000000.
      write (26,910)float(ica),(y(j,ica+1)*1000000.,j=1,neq)
      enddo
c
c
```

```
c      call distill(temp,press,pmass,dist_m,opmass)
c     do jj=1,nspf
c         print*,pmass(jj),dist_m(jj),y(jj,121),y(jj,122)
c     enddo
c
      fuelsum=0.0
      do jj=1,6
          fuelsum=fuelsum+y(jj,ivo)
      enddo
      print*,'pudpost-diff',fuelsum*1000000
c
      idiff=0
c
ccccccccccccccccccc
c         IVO.........
777   continue
      invopen=1
      is=ica
      do ica=is,ivc
      rcrkang=float(ica)
      call forward(
     +neq,rcrkang,dtheta,y(1,ica),y(1,ica-1),y(1,ica-2),
     +y(1,ica-3),y(1,ica+1),diffeq,istart,work)
c     print*,y(1,ica+1)*1000000.,y(4,ica+1)*1000000.,y(6,ica+1)*1000000.
      write (26,910)float(ica),(y(j,ica+1)*1000000.,j=1,neq)
      enddo
c
      fuelsum=0.0
      do jj=1,6
          fuelsum=fuelsum+y(jj,ivc)
      enddo
      print*,'pudpostconv/vapor',fuelsum*1000000.,y(7,ivc)*1000000.
c     print*,'vapor sum',y(7,ivc)*1000000.
      print*,'liq. sum',y(8,ivc)*1000000.
c
910   format(9(1x,1e12.5))
      end
```

```
      subroutine diffeq(neq,rcrkang,z,zp)
c
c     by Jim Cowart MIT   5-23-00
c
      dimension z(neq),zp(neq)
      dimension pmass(10),dist_m(10),opmass(10)
      dimension ymfl(10),fmevap(10)       !,yfg(10)
      common /diffeqn/idiff,iinj,finjdeg,ftotinj(10),fmassfr(10),invopen
      common /diffeqn2/rpm,ica,isig,ff,ivfirst,yfg(10)
      common /opcond/temp,press,secprdeg
      common /mixture1/W(15),ispec(15),nsp,nspf,nspo
      open(unit=22,file='diffout')
c
c         zp(1)=dm/dt puddle 1-cranking port puddle
c             1-1st fuel component
c         injected rate 2.7 gm/sec = .0027kg/sec
c
      pi=3.141592
      contac=.5
      vprt=0. !initally set port velocity to zero
      arpud=0.
      h=0.
      re=0.
      sc=0.
      sh=0.
      call density(temp,ispec,dens)
      rhof=dens
999   format(i4,1x,e12.4,1x,e12.4,1x,f12.4,1x,f10.4,1x,f10.4,1x,f10.6)
ccccccccccccccccccccccccccc
c             injection--add new fuel CVInjection Only!!!!!!!!
      if(iinj.eq.1.and.invopen.eq.0)then
      do jj=1,nspf
          pmass(jj)=z(jj)+fmassfr(jj)*finjdeg
      enddo
c
      call distill(temp,press,pmass,dist_m,opmass)
c
      dmi=finjdeg
c
      do jj=1,nspf
      zp(jj)=(finjdeg*fmassfr(jj)-dist_m(jj)) !change in fuel mass per DEGREE
      enddo
c
      write(22,999)ica,arpud,h,re,sc,sh,vfrac
c         zp(7) for total port + in-cylinder fuel vapor
      zp(7)=dist_m(1)+dist_m(2)+dist_m(3)+dist_m(4)+dist_m(5)+dist_m(6)
c
c         zp(8) for in-cylinder liquid
      zp(8)=0.0
c
      endif       ! end of iinj=1 path
ccccccccccccccccccccccccccccccccccccccccccccccccccccccccccccccccccc
      if(idiff.eq.1.and.invopen.eq.0)then !Closed Valve Diffusion Only
c         calculate total puddle mass
      pdmstot=0.0
      do jj=1,nspf
      pdmstot=pdmstot+z(jj)
      enddo
c
      do jj=1,nspf
      ymfl(jj)=z(jj)/pdmstot  !mass fraction of each liquid fuel component
      enddo
c
      rhoair=press/(287.*293)
      dia=0.05    !meter
      prtlen=.1   !meter HUGE UNKNOWN
      volprt=pi*(dia**2.)*prtlen/4.
      airmass=rhoair*volprt   !estimated air mass in port that interacts w/vap
c
      totprgas=airmass
      do jj=1,nspf
      fmevap(jj)=ftotinj(jj)-z(jj)    !mass of each fuel comp. 'i' in vapor form
      totprgas=totprgas+fmevap(jj)
      enddo
c
      do jj=1,nspf
```

```
      yfg(jj)=fmevap(jj)/totprgas
      enddo

          if(pdmstot.le.0.0)then
      sigma=0.0
      goto 565
      else
      call surface(temp,ispec,nspf,pmass,sigmaavg)
      sigma=sigmaavg
      endif
565   continue
c
      g=9.81  !m/s2...gravity
c     contac=3.5
      if(isig.eq.1)then
      h=( sigma*(1-cosd(contac))/(rhof*g))**.5
      else
      h=.000015*(pdmstot/0.000030)**.5    !h/href=(V/Vref)^.5  15micron and 30mg
      endif
c     rhof=.74*1000.
      diaprt=.05
      arpud=pdmstot/(h*rhof)
c
      zp(7)=0.0
c
      do jj=1,nspf
      call coefdiff(temp,press,ispec(jj),diff)
      zp(jj)=-1.*(arpud*rhoair*diff/diaprt)*
     +    log(1 + ymfl(jj)/(1-ymfl(jj)))
      zp(jj)=zp(jj)*secprdeg  ! convert from delta mass/sec to del.mass/cadeg
      zp(7)=zp(7)-zp(jj)
      enddo
      zp(8)=0.0
      write(22,999)ica,arpud,h,re,sc,sh,vfrac
      endif
c     print*,zp(1),zp(2),zp(6)
ccccccccccccccccccccccccccccc
c         Convection of Puddle
      if(invopen.eq.1)then
c     print*,'iinj=0 and ivopen=1'
c         calculate total puddle mass
      pdmstot=0.0
      do jj=1,nspf
      pdmstot=pdmstot+z(jj)
      pmass(jj)=z(jj)
      enddo
c
      do jj=1,nspf
      if (pdmstot.le.0.0)then
      ymfl(jj)=0.0
      else
      ymfl(jj)=z(jj)/pdmstot  !mass fraction of each liquid fuel component
      endif
      enddo
c
      rhoair=press/(287.*293.)
      dia=0.03    !meter
      prtlen=.05  !meter HUGE UNKNOWN
      volprt=pi*(dia**2.)*prtlen/4.
      airmass=rhoair*volprt   !estimated air mass in port that interacts w/vap
c
c         for CVI do once upon entering open IV
      if(ivfirst.eq.0)then
      ivfirst=1
c
      totprgas=airmass
      do jj=1,nspf
      fmevap(jj)=ftotinj(jj)-z(jj)    !mass of each fuel comp. 'i' in vapor form
      totprgas=totprgas+fmevap(jj)
      enddo
c
      do jj=1,nspf
      if (totprgas.le.0.0)then
      yfg(jj)=0.0
      else
      yfg(jj)=fmevap(jj)/totprgas
```

```
      endif       !mass fraction of each fuel comp. 'i'
      enddo                          !in the vapor stream
c
      endif   !end of ivfist 'if'
c
c         liquid breakup mechanism
      if(pdmstot.le.0.0)then
      sigma=0.0
      goto 569
      else
      call surface(temp,ispec,nspf,pmass,sigmaavg)
      sigma=sigmaavg
      endif
569   continue
c     print*,sigma
c     sigma=1.
c
c
      g=9.81  !m/s2...gravity
c     contac=3.5
      if(isig.eq.1)then
      h=( sigma*(1-cosd(contac))/(rhof*g))**.5
      else
      h=.000015*(pdmstot/0.000030)**.5    !h/href=(V/Vref)^.5  15micron and 30mg
      endif
c     rhof=.74*1000.
      diaprt=.05
      diaprtsq=diaprt**2.
      if (h.le.0.0)then
      arpud=0.0
      else
      arpud=pdmstot/(h*rhof)
      endif
      spbar=2.*.136*rpm/60.
      rsq=3.1**2.     !R=l/a  Heywood
      bsq=.085**2.    !cylinder bore squared
      sp=(spbar*pi*sind(float(ica)+180)/2.)*
     +(1.+ ( cosd(float(ica)+180.)/(rsq-(sind(float(ica)+180.))**2.) ) )
      if(sp.lt.0.0)sp=0.0
      vprt=(bsq/diaprtsq)*sp
      anu=0.00001566  !air dyn.viscosity at 300K
      re=diaprt*vprt/anu  !reynold's no. for air in port
c     print*,'re',re
c
      zp(7)=0.0
      zp(8)=0.0
c
      do jj=1,nspf            !$$$$$$$$$$$$$$$$$$$$
      call coefdiff(temp,press,ispec(jj),diff)
      if(diff.le.0.0)then
      sc=1.
      else
      sc=anu/diff     !schmidt no. for air
      endif
c     sh=0.023*(re**0.83)*(sc**0.33)  !low levels of convective MT
c
c     f=.07   !friction factor
      f=ff
      if(re.lt.1000.)re=1000.
      sh=(f/8.)*(re-1000.)*sc/(1.+12.7*((f/8.)**.5)*(sc**.67-1))
c
          do ii=1,10
              pmass(jj)=z(jj)
          enddo
c
c     call distill(temp,press,pmass,dist_m,opmass)
c
c         liquid flow rate.........
      cf=f/4. !internal flows only
c     fmu=0.000867    !h2o 300k mu=8.67e-4 kg/ms nu=.87e-6
      if(pdmstot.le.0.0)then
      fmdotl=0.0
      goto 567
      else
      call viscosity(temp,ispec,nspf,pmass,viscoavg)
      fmu=viscoavg
```

```
c     print*,fmu
      pw=(4.*pi*arpud)**.5     !wetted perimeter--circumference
      fmdotl=pw*rhof*cf*(h**2.)*(vprt**2.)/(2.*fmu)
c         2.*fmu for couette flow....use .75*fmu for laminar BL flow
      fmdotl=fmdotl*secprdeg  !TOTAL convert from kg/sec to kg/cadeg
      endif
c
567   continue
      zp(jj)=-1.*sh*(arpud*rhoair*diff/diaprt)*
     +    log(1 + (ymfl(jj)-yfg(jj))/(1.-ymfl(jj)))
      zp(jj)=zp(jj)*secprdeg  !-dist_m(jj)    !delta mass/sec to del.mass/cadeg
      zp(7)=zp(7)-zp(jj)
      zp(jj)=zp(jj)-fmdotl*ymfl(jj)   !for liquid flow puddle reduction
c     zp(7)=zp(7)-zp(jj)  !use - if want all liq. into vap.
      enddo   !$$$$$$$$$$$$$$$$$$$$$$$$$$$$$$$$
      zp(8)=fmdotl
c     print*,'re,sc,sh',re,sh,ica,zp(1)
c
      if(vprt.le.0.0)then
      dsmd=0.0
      else
      dsmd=4.*1.89*(h*sigma/(rhoair*(vprt**2.)))**0.5
      endif
      c1=3.064
      c2=.5
      if(dsmd.le.0.0)then
      vfrac=0.0
      else
      cnst=( 0.000010/(c2*dsmd))**c1
      vfrac=1.-exp(-1*cnst)  !volume fraction in vapor form
      endif
c     print*,vfrac
      zp(7)=zp(7)+vfrac*fmdotl    !vapor form
      zp(8)=(1.-vfrac)*fmdotl     !liquid in-cylinder
      write(22,999)ica,arpud,h,re,sc,sh,vfrac
c     print*,zp(1),zp(2),zp(6)
      endif   !final endif for convection section
ccccccccccccccccccccccccccc
c             injection-and IVO-add new fuel plus immed. convection
c
c         modify above to include injection.......
      if(iinj.eq.1.and.invopen.eq.1)then
      do jj=1,nspf
          pmass(jj)=z(jj)+fmassfr(jj)*finjdeg
      enddo
c
      call distill(temp,press,pmass,dist_m,opmass)
c
      dmi=finjdeg
c     deriv=fueladded/ca  -evap      -convection
      zp(1)=zp(1)+dmi*fmassfr(1)-dist_m(1)    !change in fuel mass per DEGREE
      zp(2)=zp(2)+dmi*fmassfr(2)-dist_m(2)
      zp(3)=zp(3)+dmi*fmassfr(3)-dist_m(3)
      zp(4)=zp(4)+dmi*fmassfr(4)-dist_m(4)
      zp(5)=zp(5)+dmi*fmassfr(5)-dist_m(5)
      zp(6)=zp(6)+dmi*fmassfr(6)-dist_m(6)
      zp(7)=zp(7)+dist_m(1)+dist_m(2)+dist_m(3)+
     +dist_m(4)+dist_m(5)+dist_m(6)
      write(22,999)ica,arpud,h,re,sc,sh,vfrac
c
      endif       ! end of iinj=1 path
ccccccccccccccccccccccccccccccccccccccccccccccccccccccccccccccccc

c
      end
```

```
viscosity(T,ix,nspf,pmass,viscoavg)
```

```
density(T,ix,dens)
```

```
      subroutine distill(temp,press,pmass,dist_m,opmass)

c     parameter(nspecies=21)
      common /mixture1/W(15),ispec(15),nsp,nspf,nspo
      dimension pmass(10), dist_m(10),opmass(10),
     +vappr(10),pmole(10),xvap(10),opmole(10)
      external vappress
c     write(*,*) 'start of distill'
      tvappr=0.
      tmass=0.
      tmole=0.
      do 10 i=1,nspf
      pmole(i)=pmass(i)/W(i)
      tmass=tmass+pmass(i)
      tmole=tmole+pmole(i)
10    continue
c     write(*,*) '#1 of distill'
      if(tmass.eq.0.) then
      do 100 i=1,nspf
      opmass(i)=pmass(i)
      dist_m(i)=0.
100   continue
      go to 200
      endif

c     write(*,*) '#2 of distill'
      do 20 i=1,nspf
      call vappress(ispec(i),temp,vappr(i))
      tvappr=tvappr+vappr(i)*pmole(i)/tmole
20    continue
      do 30 i=1,nspf
      xvap(i)=vappr(i)/press      !tvappr
30    continue
c     write(*,*) '#3 of distill'
      if(tvappr.gt.press) then
      vap_mol=0.
      do 40 i=1,nspf
      vap_mol=vap_mol+vappr(i)*pmole(i)
40    continue
      vap_xvap=0.
      do 50 i=1,nspf
      vap_xvap=vap_xvap+vappr(i)*xvap(i)
50    continue
c     write(*,*) '#4 of distill'
      delmol=(vap_mol-tmole*press)/(vap_xvap-press)
c     write(*,*) '#5 of distill'
      do 60 i=1,nspf
      opmole(i)=pmole(i)-delmol*xvap(i)
      opmass(i)=opmole(i)*W(i)
      dist_m(i)=pmass(i)-opmass(i)
60    continue
      else
      do 70 i=1,nspf
      opmass(i)=pmass(i)
      dist_m(i)=0.
70    continue
200   endif

c     write(*,*) 'end of distill'
      return
      end
```

```
ccccccccccccccccccccccccccccccccccccccccccccccccccccccccccccccccccccccc
      subroutine rk2(neq,t,dt,y,ynew,yprime)
c     second order Runge Kutta method for integration
c     input
c     neq = no. of differential equations (max=15; change the parameter statement if >15)
c     t   = starting value of independent variable
c     dt  = t increment
c     y   = starting value of dependent variable; dimension neq
c     output
c     ynew = value of dependent variable at t+dt; dimension neq
c     external function for evaluating derivative
c     yprime(neq,t,y,yp), where yp is the derivative array
c     -------------------------
      parameter (neqmax=20)
      dimension y(neq),ynew(neq)
      dimension yp(neqmax)
      external yprime
c     external vol
      call yprime(neq,t,y,yp)
      do i=1,neq
      ynew(i)=y(i)+0.5*dt*yp(i)
      enddo
      call yprime(neq,t+.5*dt,ynew,yp)
      do i=1,neq
      ynew(i)=y(i)+dt*yp(i)
      enddo
      return
      end
ccccccccccccccccccccccccccccccccccccccccccccccccccccccccccccccccccccccc
```

```
ccccccccccccccccccccccccccccccccccccccccccccccccccccccccccccccccccccccc
      subroutine forward(neq,t,dt,yn,yn_1,yn_2,yn_3,ynp1,yprime,
     +                   istart,work)
c     ---------------------------------------------------------------------
c     predictor corrector method (Milne's Method) for integrating forward
c     i.e., given values at yn,yn_1, yn_2 and yn_3; output ynp1
c     assume yn is at time t, ynp1 is at time t+dt, yn_1 is at time t-dt, etc.
c     ----------------------
c     the subroutine is set up for integrating a maximum of 15 equations
c     for more than 15 equation, change the value of neqmax in the parameter statement
c     ++++++++  input   ++++++++++++
c     neq = no. of equations to be integrated forward.  Note that in the calling routine,
c           the dimension of yn_3,yn_2,yn_1,yn, and ynp1 are all two dimensional arrays of dimensi
on (neq,..)
c           where the first index is the variable index, and the second dimension is the time inde
x
c     t   = current independent variable value
c     dt  = step size of independent variable
c     yn  = current value of dependent variable array
c     yn_1, yn_2 , yn_3= values of the dependent variable at time t-dt etc, assume known already
c     ++++++++  output  ++++++++++
c     ynp1 = value of dependent variable at time t+dt
c     ++++++++ yprime ++++++++++++
c     specification of the external function defining the derivatives
c     Have to specify the derivative through the external subroutine yprime(neq,t,y,yp) where
c     the inputs are: neq is the number of equations, t is the independent variable and
c     y the dependent variable; the output is yp
c     note that in this subroutine, y and yp are both dimension neq
c     ++++++++++++++++++++++++++++++++
c     istart = flag to indicate that this is the first time calling the subroutine,
c              should be initialized to 1 in the calling routine; FORWARD automatically reset
c              it to 0
c     ++++++++ working storage +++++++++
c     work is a storage array of dimension (neq,3)
c     When the subroutine is called the first time, istart=1
c     signals the routine to calculate the derivatives
c     which should have been evaluated in the previous steps; for subsequent steps,
c     these derivatives have been stored in work.
c     ---------------------------------------------------------------------
      parameter (neqmax=20)
      dimension yn(neq),yn_1(neq),yn_2(neq),yn_3(neq),ynp1(neq)
      dimension work(neq,3)
      dimension ypn(neqmax),ypn_1(neqmax),ypn_2(neqmax),ypnp1(neqmax)
      external yprime
c     external vol
c     predictor
c     evaluate the derivatives
      if (istart.eq.1) then !------------if loop-------------
c     first time calling this subroutine
          call yprime(neq,t,yn,ypn,vol)
          call yprime(neq,t-dt,yn_1,ypn_1,vol)
          call yprime(neq,t-2.*dt,yn_2,ypn_2,vol)
      istart=0
      else
c     subsequent calling of this subroutine
      do i=1,neq
      ypn(i)     =work(i,3)
      ypn_1(i)   =work(i,2)
      ypn_2(i)   =work(i,1)
      enddo
      endif                          !-----------end of if loop-------
c     predictor value
      do i=1,neq
      ynp1(i)=yn_3(i)+1.333333*dt* ( 2.*ypn(i)-ypn_1(i)+2.*ypn_2(i) )
      enddo
c     Corrector value
c     Evaluate the derivative at t+dt using predictor value of ynp1
          call yprime(neq,t+dt,ynp1,ypnp1,vol)
c     corrector value; recalcualte ynp1
      do i=1,neq
      ynp1(i)=yn_1(i)+0.3333333*dt* ( ypn_1(i)+4.*ypn(i)+ypnp1(i) )
      enddo
c     update the work array for next time
      do i=1,neq
      work(i,1)=ypn_1(i)
      work(i,2)=ypn(i)
```

```
c       work(i,3)=ypnp1(i)   !jim added
        enddo
            call yprime(neq,t+dt,ynp1,work(1,3),vol)
222     return
        end
```

```
      subroutine fuelnum(nspf,nspo,ispec,cnum,hnum,stoi,W)
      parameter (nsp=21)
      dimension cn(nsp),hn(nsp),st(nsp),ww(nsp)
      dimension  ispec(15),cnum(10),hnum(10),stoi(10),W(15)

c               1=oxygen        2=nitrogen       3=hydrogen        4=methane (CH4)
c               5=propane (C3H8)    6=n-butane (C4H10)      7=iso-pentane (C5H12)
c               8=iso-hexane (C6H14)    9=iso-heptane (C7H16)   10=toluene (C7H8)
c               11=iso-octane (C8H18)   12=m-Xylene (C8H10)   13=n-nonane (C9H20)
c               14=isopropylbenzene (C9H12) 15=n-decane (C10H22)  16=cyclo-hexane (C6H12)
c               17=CO   18=CO2      19=n-pentane    20=H2O      21=MTBE (CH3-O-C4H9)

c       molecular weights
      data ww /
     +    32.,        28.01,      2.016,      16.04,      44.10,
     +    58.123,     72.150,     86.177,     100.204,    92.141,
     +    114.231,    106.167,    128.258,    120.194,    142.285,
     +    84.16,      28.011,     44.01,      72.151,     18.016,
     +    88.15
     +      /

c       carbon number
      data cn/ 0.,  0.,  0.,  1.,  3.,  4.,  5.,  6.,  7.,  7.,
     +         8.,  8.,  9.,  9., 10.,  6.,  1.,  1.,  5.,  0.,
     +         5.
     +       /
c       hydrogen atom number
      data hn/ 0.,  0.,  2.,  4.,  8.,  10., 12., 14., 16., 8.,
     +         18., 10., 20., 12., 22., 12., 0.,  0.,  12., 2.,
     +         12.
     +       /
c       number of oxygen in stoichiometric mixture for one mole of fuel
      data st/ 0.,  0.,  .5,  2.,  5., 6.5, 8., 9.5, 11., 9.,
     +         12.5, 10.5, 14., 12., 15.5, 9., .5, 0., 8., 0.,
     +         7.5
     +       /

      do 10 i=1,nspf
      ix=ispec(i)
      w(i)=ww(ix)
      cnum(i)=cn(ix)
      hnum(i)=hn(ix)
      stoi(i)=st(ix)
10    continue
      do 20 i=1,nspo
      ix=ispec(nspf+i)
      w(nspf+i)=ww(ix)
20    continue

      return
      end
```

```
      subroutine vappress(ix,Tf,vappr)

      parameter(nsp=21,ncoef=5)
      dimension  coef(ncoef,nsp)

      data coef/
c       (1)  O2 :  gas phase, not applicable
     +  5*0.,
c       (2)  N2 :  gas phase, not applicable
     +  5*0.,
c       (3)  H2 :  gas phase, not applicable
     +  5*0.,
c       (4)  methane
     + 5*0.,
c       (5)  propane
     + 5*0.,
c       (6)  n-butane
     +      6.6343e1, -4.3632e3, -7.0460e0, 9.4509e-6, 2.0e0,
c       (7)  iso-Pentane
     +      7.2350e1, -5.0109e3, -7.8830e0, 8.9795e-6, 2.0e0,
c       (8)  iso-hexane(2M-Pentane)
     +      7.5692e1, -5.7307e3, -8.2295e0, 7.4608e-6, 2.0e0,
c       (9)  iso-heptane(2M-Hexane)
     +      5.9531e1, -5.8264e3, -5.4269e0, 1.4542e-17, 6.0e0,
c       (10) toluene
     +      7.6945e1, -6.7298e3, -8.1790e0, 5.3017e-6, 2.0e0,
c       (11) iso-octane
     +      1.2081e2, -7.5500e3, -1.6111e1, 1.7099e-2, 1.0e0,
c       (12) m-Xylene
     +      8.5099e1, -7.6159e3, -9.3072e0, 5.5643e-6, 2.0e0,
c       (13) n-Nonane
     +      1.0935e2, -9.0304e3, -1.2882e1, 7.8544e-6, 2.0e0,
c       (14) iso-Propyl Benzene
     +      1.0281e2, -8.6746e3, -1.1922e1, 7.0048e-6, 2.0e0,
c       (15) n-Dodecane
     +      1.1237e2, -9.7496e3, -1.3245e1, 7.1266e-6, 2.0e0,
c       (16) cyclo-hexane
     + 5*0.,
c       (17) Carbon monoxide   :  gas phase, not applicable
     +   5*0.,
c       (18) Carbon dioxide    :  gas phase, not applicable
     +   5*0.,
c       (19) n-pentane
     + 5*0.,
c       (20)H2O    :  gas phase, not applicable
     +   5*0.,
c       (21)MTBE
     + 5*0.
     +    /


      vappr=exp(coef(1,ix)+coef(2,ix)/Tf+coef(3,ix)*log(Tf)+
     +        coef(4,ix)*Tf**coef(5,ix))

      return
      end
```

```
      subroutine coefdiff(temp,press,ix,diff)

      parameter(nsp=21)
      dimension  coef(nsp)
c     ******************************
c       binary diffusion coefficients of fuel species in air.
c     ******************************
      data coef /
c        (1)  O2 :   not applicable
     +  0.,
c        (2)  N2 :   not applicable
     +  0.,
c        (3)  H2 :   not applicable
     +  0.,
c        (4)  methane
     + 0.,
c        (5)  propane
     + 0.,
c        (6)  n-butane
     +       1.9636e-4,
c        (7)  i-pentane
     +       1.6411e-4,
c        (8)  i-hexane
     +       1.4866e-4,
c        (9)  i-heptane
     +       1.3325e-4,
c        (10)  toluene
     +       1.5348e-4,
c        (11) iso-octane
     +       1.1918e-4,
c        (12) m-xylene
     +       1.3680e-4,
c        (13) n-nonane
     +       1.2280e-4,
c        (14) i-propylbenzene
     +       1.2291e-4,
c        (15) ndecane
     +       1.1572e-4,
c        (16) cyclo-hexane
     + 0.,
c        (17) Carbon monoxide    :   not applicable
     +   0.,
c        (18) Carbon dioxide     :   not applicable
     +   0.,
c        (19) n-pentane
     + 0.,
c        (20)H2O     :  gas phase, not applicable
     +   0.,
c        (21)MTBE
     + 0.
     +    /

      diff=coef(ix)*temp**1.7/press

      return
      end
```